Dissertation

Holistic Evaluation of Power-to-Liquid Processes Producing Methanol and Fischer-Tropsch Products

Carried out for the purpose of obtaining the degree of Doctor technicae (Dr. techn.)
submitted at TU Wien,
Faculty of Technical Chemistry by

Simon PRATSCHNER

Mat. No.: 01340505

under the supervision of

Univ. Prof. Dipl.-Ing. Dr. techn. Franz Winter

Institute of Chemical, Environmental and Bioscience Engineering

Vienna, March 2024

Reviewed by:

Gürkan Sin

Technical University of Denmark

Department of Chemical and Biochemical Engineering

Søltofts Plads, 227, 228

2800 Kgs. Lyngby, Denmark

Andreas Werner

TU Wien

Institute of Energy Systems and Thermodynamics

Getreidemarkt 9, E302

1060 Vienna, Austria

This work has received funding from the Mobility of the Future Program - a research, technology and innovation funding program of the Federal Ministry of Climate Action, Environment, Energy, Mobility, Innovation and Technology, Republic of Austria. The Austrian Research Promotion Agency (FFG) has been authorized to manage the program of the project “IFE - Innovation Flüssige Energie” (project number 884340).

I confirm that the printing of this thesis requires the approval of the examination board.

Affidavit

I declare in lieu of oath that I wrote this thesis and carried out the associated research myself, using only the literature cited in this volume. If text passages from sources are used literally, they are marked as such.

I confirm that this work is original and has not been submitted for examination elsewhere, nor is it currently under consideration for a thesis elsewhere.

I acknowledge that the submitted work will be checked electronically-technically using suitable and state-of-the-art means (plagiarism detection software). On the one hand, this ensures that the submitted work was prepared according to the high-quality standards within the applicable rules to ensure good scientific practice "Code of Conduct" at the TU Wien. On the other hand, a comparison with other student theses avoids violations of my personal copyright.

Place and Date	*Signature*

Table of Contents

Abstract

Defossilizing the chemical and plastics industry, as well as aviation and maritime transport, is a key stone in mitigating the climate crisis. Power-to-Liquid (PtL) processes, converting electricity, CO_2 and water into hydrocarbons, can reduce CO_2 emissions by substituting fossil feedstocks and fuels.

The presented thesis is founded on the process design of pilot and industrial-scale plants based on methanol and Fischer-Tropsch synthesis. Process modeling and static process simulation of the established plant configurations serve as a foundation to determine the processes' PtL and carbon efficiency for different CO_2 sources. The net production costs of green methanol and Fischer-Tropsch products were determined via techno-economic assessments. In addition, the CO_2 footprint of Fischer-Tropsch products was examined to ensure a holistic evaluation of PtL processes.

A maximum PtL efficiency of 63.8% and carbon efficiency of 88.6% were found for the high-temperature co-electrolysis and Fischer-Tropsch synthesis process route valorizing CO_2 emitted by a biogas upgrading plant. Maximum PtL efficiencies of 54.2% (air combustion) and 51.9% (oxy-fuel combustion) were determined to produce green methanol, including a low-temperature electrolyzer.

Applying wind or photovoltaic power to a PtL plant yielding Fischer-Tropsch products resulted in possible CO_2 footprint reductions of 95% and 65% compared with fossil fuels.

Green methanol net production costs of 569 to 785 €$_{2022}$/t were determined. The net production costs of Fischer-Tropsch products ranged from 2,420 to 4,560 €$_{2022}$/t based on grid electricity and 1,280 to 2,400 €$_{2022}$/t for the assumed off-grid scenarios. CO_2 prices of 220 to 310 €/t are required to make green methanol cost-competitive with methanol derived from natural gas. Substituting fossil jet fuel with Fischer-Tropsch-derived fuels can potentially become a business case for CO_2 prices exceeding 500 €/t.

A rapid expansion of renewable power sources is necessary to industrially implement PtL plants since the EU's 2022 grid electricity mix is not eligible for producing synthetic chemicals and fuels. Highly concentrated biogenic CO_2 sources should be prioritized for the first generation of PtL plants. The electricity costs and the plant availability are the major cost drivers. Thus, off-grid PtL plants based on hybrid power plants and storage technologies promise a significant economic potential.

Keywords:

Power-to-Liquid, process simulation, techno-economic assessment, green methanol, Fischer-Tropsch, solid-oxide co-electrolysis

Kurzfassung

Die Defossilisierung der Chemie- und Kunststoffindustrie, sowie von Luft- und Schifffahrt, stellt einen zentralen Baustein zur Bekämpfung der Klimakrise dar. Power-to-Liquid-Prozesse (PtL) ermöglichen die Substitution fossiler Einsatzstoffe mittels der Produktion von Kohlenwasserstoffen auf Basis von Elektrizität, CO_2 und Wasser.

Die vorliegende Dissertation basiert auf der Erstellung von Anlagenkonzepten im Pilot- und Industriemaßstab zur Synthese von grünem Methanol und Fischer-Tropsch-Produkten (FT). Die Modellierung und statische Prozesssimulation der entworfenen Prozessrouten dienen als Grundlage zur Ermittlung der PtL- und Kohlenstoffwirkungsgrade für verschiedene CO_2-Quellen. Mithilfe techno-ökonomischer Bewertungen wurden die Produktionskosten von grünem Methanol und FT-Produkten bestimmt. Zusätzlich wurde der CO_2-Fußabdruck der FT-Produkte in Abhängigkeit vom Emissionsfaktor verschiedener Stromquellen ermittelt.

Ein maximaler PtL-Wirkungsgrad von 63.8% und Kohlenstoffwirkungsgrad von 88.6% resultierten aus der Prozessroute mit Hochtemperatur-Elektrolyse, FT-Synthese und Biogas als CO_2-Quelle. Der Vergleich zweier auf Niedertemperatur-Elektrolyse und Methanol-Synthese basierenden Routen ergab maximale PtL-Wirkungsgrade von 54.2% (Luftverbrennung) und 51.9% (Oxy-Fuel-Verbrennung).

Die Versorgung von PtL-Anlagen mit Windenergie oder Photovoltaik führt zu einer potentiellen Verringerung des CO_2-Fußabdrucks um 95% und 65% verglichen mit fossilen Treibstoffen.

Grünes Methanol kann zu Produktionskosten von 569 bis 785 €$_{2022}$/t hergestellt werden. Die Produktionskosten von FT-Produkten lagen zwischen 2420 und 4560 €$_{2022}$/t, basierend auf Netzstrom, beziehungsweise 1280 und 2400 €$_{2022}$/t für autarke PtL-Systeme. CO_2-Preise von 220 bis 310 €/t sind notwendig, um grünes Methanol konkurrenzfähig zu aus Erdgas hergestelltem Methanol zu machen. Wirtschaftlich interessante Szenarien zur Substitution von fossilem Flugtreibstoff durch FT-Produkte ergeben sich ab CO_2-Preisen von 500 €/t.

Eine rasche Ausweitung erneuerbarer Energieträger ist für die industrielle Realisierung von PtL-Prozessen unabdingbar. Der durchschnittliche Strommix der EU im Jahr 2022 eignet sich nicht zur Produktion synthetischer Basischemikalien und Energieträger. Hochkonzentrierte, biogene CO_2-Quellen sollten für die erste Generation von PtL-Anlagen priorisiert werden. Die Stromkosten und jährlichen Betriebsstunden konnten als wesentliche Kostentreiber identifiziert werden. Autarke PtL-Anlagen ohne Netzanschluss, welche auf hybrider Stromversorgung und Speichertechnologien für Strom und Syngas basieren, weisen somit ein vielversprechendes ökonomisches Potential auf.

Schlagworte:

Power-to-Liquid, Prozesssimulation, techno-ökonomische Bewertung, grünes Methanol, Fischer-Tropsch, Festoxid-Elektrolyse

List of Publications

This thesis is founded on the following publications:

Journal Articles

I. Pratschner, S.; Skopec, P.; Hrdlicka, J.; Winter, F. Power-to-Green Methanol via CO_2 Hydrogenation—A Concept Study Including Oxyfuel Fluidized Bed Combustion of Biomass. *Energies* 2021, 14, 4638. https://doi.org/10.3390/en14154638.

II. Pratschner, S.; Hammerschmid, M.; Müller, F.J.; Müller, S.; Winter, F. Simulation of a Pilot Scale Power-to-Liquid Plant Producing Synthetic Fuel and Wax by Combining Fischer–Tropsch Synthesis and SOEC. *Energies* 2022, 15, 4134. https://doi.org/10.3390/en15114134.

III. Pratschner, S.; Hammerschmid, M.; Müller, S.; Winter, F. Evaluation of CO_2 Sources for Power-to-Liquid Plants Producing Fischer-Tropsch Products. *Journal of CO_2 Utilization* 2023, 72, 102508. https://doi.org/10.1016/j.jcou.2023.102508.

IV. Pratschner, S.; Radosits, F.; Ajanovic, A.; Winter, F. Techno-Economic Assessment of a Power-to-Green Methanol Plant. *Journal of CO_2 Utilization* 2023, 75, 102563. https://doi.org/10.1016/j.jcou.2023.102563.

V. Pratschner, S.; Hammerschmid, M.; Müller, S.; Winter, F. Off-grid vs. Grid-based: Techno-Economic Assessment of a Power-to-Liquid Plant combining Solid-Oxide Electrolysis and Fischer-Tropsch Synthesis. *Chemical Engineering Journal* 2024, 481, 148413. https://doi.org/10.1016/j.cej.2023.148413.

Peer-reviewed Conference Papers

I. Pratschner, S.; Hammerschmid, M.; Müller, S.; Winter, F. CO_2 Footprint of Fischer-Tropsch Products produced by a Power-to-Liquid Plant. 15th Mediterranean Congress of Chemical Engineering (MECCE 15), Barcelona, Spain. May 30 to June 2, 2023.

II. Pratschner, S.; Hammerschmid, M.; Müller, S.; Winter, F. Converting CO_2 and H_2O into Fischer-Tropsch Products: A Techno-Economic Assessment. 27th International Symposium for Chemical Reaction Engineering (ISCRE 27), Québec City, Canada. June 11 to June 14, 2023.

Simon Pratschner is the corresponding author of all listed **Journal Articles** (**I-V**) and **Conference Papers I** and **II**. He conducted the process modeling, economic modeling and process simulation and was responsible for writing and editing the manuscripts. Martin Hammerschmid contributed to **Journal Articles II, III** and **V** and **Conference Papers I** and **II** by providing the required software and basic process models. He was the first contact for feedback and gave valuable input on the technology's embedding into today's energy supply system. Stefan Müller contributed to **Journal Articles II, III** and **V** as well as **Conference Papers I** and **II** with project administration, providing the process simulation software, funding acquisition and discussion. Florian Müller contributed to **Journal Article II** with his

valuable and critical feedback on process design and the technology's comparison with alternative processes. Pavel Skopec and Jan Hrdlicka contributed to **Journal Article I** by sharing their expertise on modeling oxy-fuel combustion processes in fluidized bed reactors as well as editing and discussing the initial draft. Frank Radosits and Amela Ajanovic integrated their knowledge of the economic modeling of renewable power sources in **Journal Article IV**, thus having a significant impact on the obtained results and their economic evaluation. Franz Winter contributed his scientific expertise to all **Journal Articles** (**I-V**) as well as **Conference Papers I** and **II** by supervising and discussing the papers' technical and administrative features. In addition, he provided his experience in editing all manuscripts and by providing the scientific framework and organization.

Further publications

Journal Articles as Co-Author

- Hammerschmid, M.; Bartik, A.; Benedikt, F.; Marton, V.; Pratschner, S; Müller, S.; Hofbauer, H. Economic and Ecological Impacts on the Integration of Biomass-Based SNG and FT Diesel in the Austrian Energy System. *Energies* 2023, 16, 6097. https://doi.org/10.3390/en16166097.

- Müller, F.J.; Fuchs, J.; Cuesta, M.F.; Gutiérrez, A.O.; Pratschner, S.; Müller, S.; Winter, F. CO_2 Conversion to CO by Fluidized Bed Biomass Gasification: Analysis of Operational Parameters. *Journal of CO_2 Utilization* 2024, 81, 102706. https://doi.org/10.1016/j.jcou.2024.102706.

- Radosits, F.; Ajanovic, A.; Pratschner, S. Costs and Perspectives of Synthetic Methane and Methanol Production using Carbon Dioxide from Biomass-Based Processes. Journal of Sustainable Development of Energy, Water and Environment Systems 2024, 12, 2, 1120484. https://doi.org/10.13044/j.sdewes.d12.0484.

Additional Conference Contributions

- Simulation of a Pilot Scale Power-to-Liquid Plant. 19th Austrian Chemistry Days, Vienna, Austria. September 20 to September 22, 2022.

- Oxy-fuel- und Luftwirbelschichtverbrennung zur Herstellung von grünem Methanol. 12th Austrian IEA Fluidized Bed Meeting, St. Veit a. d. Glan, Austria. September 7 to September 9, 2022.

- Fluidized Bed in Air and Oxyfuel Combustion Mode for Green Methanol Production. 82nd IEA-FBC Meeting, Ottawa, Canada (Online). June 10 to June 11, 2021.

Acknowledgment

Der familiäre Rückhalt ist die absolute Basis, um seine kognitiven und emotionalen Fähigkeiten für die Absolvierung eines Studiums bündeln zu können. Seit meiner Kindheit genieße ich vollkommene Freiheit bezüglich der Gestaltung meiner Ausbildung und Freizeit bei gleichzeitig unerschüttbarem Vertrauen in meine Entscheidungen. Ich möchte meinen Eltern, Elisabeth und Thomas, für dieses Privileg danken. Hervorheben möchte ich weiters den Stolz und die Begeisterung, die mir meine Großeltern, Edith, Christine und Johnny, bei jedem meiner Schritte entgegenbringen. Ein gesundes Verhältnis zu seiner Arbeit beinhaltet auch den notwendigen Abstand zu dieser. Für die Schaffung der hierfür notwendigen emotionalen Rückzugsorte möchte ich meiner Partnerin Julia und meinen Geschwistern, Julian, Béla und Aurelia, danken.

Größter Dank gebührt meinem langjährigen Mentor und Betreuer Professor Franz Winter, der mir vollstes Vertrauen und absoluten Freiraum bei der wissenschaftlichen Bearbeitung meiner Projekte entgegengebracht hat und mir gleichzeitig in den entscheidenden Momenten mit seiner Erfahrung und Expertise zur Seite stand.

Mein Grundsatz war stets, meine Mitmenschen als Lehrmeisterinnen und Lehrmeister zu sehen und zu versuchen, deren positive Charaktereigenschaften in meine eigene Persönlichkeit zu integrieren. In dieser Hinsicht waren die vergangenen drei Jahre nicht nur fachlich, sondern auch persönlich unglaublich bereichernd für mich. Besonders hervorheben möchte ich meine Freundschaft mit Lena, Florian und Eugen. Die gemeinsame Zeit am Institut wird mir Dank euch stets in guter Erinnerung bleiben. Des Weiteren möchte ich mich bei allen Kolleginnen und Kollegen des Instituts für Verfahrenstechnik sowie des Doktoratskollegs CO_2Refinery für die gemeinsame Bearbeitung vieler Projekte und zahlreiche, lehrhafte Diskussionen bedanken. Unterstreichen möchte ich hier die intensive Zusammenarbeit mit meinen Kollegen Martin und Frank, welche die Basis für zahlreiche wissenschaftliche Publikationen darstellte.

Für ihren Einsatz und ihre exzellente Arbeit möchte ich mich bei Daniel, Julian und Aaron bedanken, deren Masterarbeiten ich im Rahmen meines Doktorats betreuen durfte.

Zu guter Letzte möchte ich Professor Gürkan Sin und Professor Andreas Werner für ihren Aufwand und ihre Unterstützung im Rahmen der Begutachtung dieser Dissertation danken.

Nomenclature

Abbreviations

AACE	… Association for the Advancement of Cost Estimating
AEL	… Alkaline electrolysis
ASF	… Anderson-Schulz-Flory
ASU	… Air separation unit
BEP	… Break-even point
BtL	… Biomass-to-Liquid
CAPEX	… Capital expenditure
CCS	… Carbon capture and storage
CEPCI	… Chemical Engineering Plant Cost Index
CHP	… Combined heat and power
CO_2eq	… CO_2 equivalents
CtL	… Coal-to-Liquid
DAC	… Direct air capture
DH	… District heating
DME	… Dimethyl ether
ETS	… Emission trading system
FBMR	… Fixed-bed multitubular reactor
FCI	… Fixed capital investment
FT	… Fischer-Tropsch
GHG	… Greenhouse gas
GtL	… Gas-to-Liquid
HT	… High-temperature
IEA	… International Energy Agency
IMPCA	… International Methanol Producer and Consumer Association
LCOE	… Levelized cost of electricity
LPG	… Liquified petroleum gas
LT	… Low-temperature
MCR	… Microchannel reactor
MEA	… Monoethanolamine
MeOH	… Methanol
MTBE	… Methyl tert-butyl ether
NPC	… Net production costs
NPV	… Net present value
OPEX	… Operational expenditure
PEMEL	… Proton exchange membrane electrolysis
PtL	… Power-to-Liquid
PtX	… Power-to-X
PVGIS	… Photovoltaic geographic information system
SAF	… Sustainable aviation fuel
SBCR	… Slurry bubble column reactor
SOEL	… Solid-oxide electrolysis
TEA	… Techno-economic assessment
TRL	… Technology readiness level
USGC	… U.S. Gulf Coast
WGS	… Water-gas shift

Parameters			Indices	
$\dot{m}$	[kg/s]	… Mass flow rate	i,j,k	… Chemical compounds
$\dot{n}$	[mol/s]	… Molar flow rate	Cat	… Catalyst
$\dot{Q}$	[$W_{th.}$]	… Heat flow rate	rec.	… Recirculated
$\dot{U}$	[$W_{ch.}$]	… Stream of chemical energy	El.	… Electricity
Availability	[h/a]	… Annual operating hours	el.	… Electric
COR	[-]	… Carbon oxide ratio	m.	… Mechanical
d	[-]	… Scaling exponent	s	… Isentropic
$EF_{El.}$	[$CO_2eq/kWh_{el.}$]	… Emission factor of electricity source	Base	… Base scale
EF_{FT}	[CO_2eq/kg_{FT}]	… Emission factor of FT products	Design	… Design scale
FCI	[€]	… Fixed capital investment	ch.	… Chemical
i	[-,%]	… Discount rate	th.	… Thermal
LCOE	[€/$kWh_{el.}$]	… Levelized cost of electricity		
m	[kg]	… Mass		
NPC	[€/$kg_{Product}$]	… Net production costs		
p	[Pa]	… Pressure		
P	[W]	… Power		
RR	[%]	… Recirculation ratio		
RU	[-,%]	… Reactant utilization		
S	[-,%]	… Selectivity		
S/C	[-]	… Steam-to-Carbon ratio		
SN	[-]	… Stoichiometric number		
SV	[$Nm^3/(s \cdot kg_{Cat})$]	… Space velocity		
T	[K,°C]	… Temperature		
t	[a]	… Depreciation period		
X	[-,%]	… Conversion		
x	[mol/mol]	… Molar fraction		
Y	[-,%]	… Yield		
ΔG_r	[J/mol]	… Gibbs free energy		
ΔH_r	[J/mol]	… Enthalpy of reaction		
ΔS_r	[J/(mol·K)]	… Entropy of reaction		
%pt.	[%]	… Percentage points		

Greek symbols

α_1	[-]	… Chain growth probability for low carbon numbers (eASF)
α_2	[-]	… Chain growth probability for high carbon numbers (eASF)
β	[-]	… Re-adsorption factor (eASF)
γ	[-]	… Enhancement factor (eASF)
$\mu_{1,2}$	[-]	… Fraction of first and second distribution function (eASF)
ν	[-]	… Stoichiometric factor
η	[%]	… Efficiency

1 Introduction

1.1 Aim of the Thesis

The central objective of this thesis is to provide a holistic assessment of Power-to-Liquid (PtL) processes based on their energetic efficiency, carbon efficiency, economic performance and the products' CO_2 footprint. Several intermediate steps are required to achieve these defined goals. The respective sub-processes must be modeled and connected based on the elaborated pilot and industrial scale Power-to-Liquid plant design. Secondly, the Power-to-Liquid and carbon efficiency are assessed based on the determined mass and energy balances for the respective process routes and different CO_2 sources. As a next step, the products' CO_2 footprint is determined for various electricity sources, i.e., renewables and national grid electricity mixes. Finally, techno-economic assessments (TEA) are conducted to evaluate the economic performance of process routes for grid-based and off-grid scenarios.

The following specific research questions are answered by the presented thesis:

1. What are the ideal plant designs for Power-to-Liquid plants producing green methanol and Fischer-Tropsch products at a pilot and an industrial scale?
2. Which influence do the process design and the utilized CO_2 source have on the Power-to-Liquid and carbon efficiency of Power-to-Liquid plants?
3. How does the applied electricity source influence the CO_2 footprint of Power-to-Liquid products?
4. Which factors have the highest leverage on the economic performance of Power-to-Liquid plants and which CO_2 prices are required to make them economically competitive with conventional fossil-based processes?

1.2 Thesis Outline

An overview of the presented thesis's structure is provided in Figure 1. The overall aim was a holistic evaluation of carbon capture and utilization-based Power-to-Liquid processes, i.e., methanol and Fischer-Tropsch (FT) synthesis. The first research question, comprising **Journal Articles I** and **II**, focused on the conceptualization and plant design of PtL processes.

Journal Article I, *Power-to-Green Methanol via CO_2 Hydrogenation – A Concept Study including Oxy-fuel Fluidized Bed Combustion of Biomass*, presents a plant concept based on a 20 $MW_{th.}$ biomass heating plant. Bringing together industries based on water electrolysis with oxygen consumers will be a central element of sector coupling in the near future. Assessing the synergy between PtL processes and oxy-fuel combustion of biomass was the main objective of **Journal Article I**. The Power-to-Liquid and overall energetic efficiency for the oxy-fuel-based process route was compared with an air combustion process route, including a monoethanolamine-based (MEA) absorption process.

The objective of **Journal Article II**, *Simulation of a Pilot Scale Power-to-Liquid Plant Producing Synthetic Fuel and Wax by Combining Fischer-Tropsch Synthesis and SOEC*, was to find a feasible plant configuration for a pilot-scale PtL plant combining solid-oxide co-electrolysis (co-SOEL) and Fischer-Tropsch synthesis at a rated electrolyzer power input of 1 $MW_{el.}$. Three process configurations, based on different approaches concerning the recirculation and reforming of tail gas as well as syncrude separation, were modeled and simulated to determine the respective PtL efficiencies. In addition, the synergy between the co-SOEL and Fischer-Tropsch unit to control the reactor's required H_2:CO ratio was analyzed.

Research questions 2 and 3 are founded on the findings and basic modeling work of **Journal Article II** and focus on the established process route, including solid-oxide electrolysis and Fischer-Tropsch synthesis. To answer those questions, the modeling of additional sub-processes, i.e., CO_2 capture, SOEL and tail gas reforming, as well as their interconnection in an extended process flow diagram, were established. The findings of **Journal Article III** and **Conference Paper I** were determined based on the created process simulation environment.

Journal article III, *Evaluation of CO_2 Sources for Power-to-Liquid Plants Producing Fischer-Tropsch Products*, aimed at determining the designed industrial-scale PtL plant's Power-to-Liquid and carbon efficiency for three analyzed CO_2 sources, i.e., cement, biogas upgrading and biomass heating plant. For this purpose, the process route established in **Journal Article II** was extended with SOEL, CO_2 capture and tail gas reforming units. The determined results highlighted the necessity of sector coupling in order to exploit waste heat potentials and unite CO_2-emitting industries with PtL plants.

Within **Conference Paper I**, *CO_2 Footprint of Fischer-Tropsch Products produced by a Power-to-Liquid Plant*, several electricity sources, decentral renewables and grid electricity mixes of European countries were evaluated based on their emission factor in kg CO_2 equivalents (CO_2eq) per kWh of electricity. The determined specific CO_2 footprint of Fischer-Tropsch products was subsequently compared to conventional, fossil-based products to find appropriate electricity sources for PtL plants by establishing a CO_2 emission break-even point (BEP).

Techno-economic assessments of the established Power-to-Liquid plant concepts producing green methanol and Fischer-Tropsch products are the central element of research question 4.

Techno-Economic Assessment of a Power-to-Green Methanol Plant, **Journal Article IV**, uses **Journal Article I**'s plant design as a foundation for economically evaluating CO_2 hydrogenation to green methanol. Different investment scenarios were considered based on the net present value (NPV) method. Furthermore, the allocation of green methanol net production costs (NPC), including capital expenditure (CAPEX), fixed and variable operational expenditure (OPEX), as well as electricity, were assessed. A hybrid power plant, consisting of a wind park, a photovoltaic farm and a connection to the electricity grid, was designed to maximize the plant's annual operating hours, a key element in maximizing the economic performance of PtL plants.

Journal Article V, *Off-grid vs. Grid-based: Techno-Economic Assessment of a Power-to-Liquid Plant Combining Solid-Oxide Electrolysis and Fischer-Tropsch Synthesis*, and **Conference Paper II**, *Converting CO_2 and H_2O into Fischer-Tropsch Products: A Techno-Economic Assessment*, evaluate the economic performance of the modeled PtL plant producing Fischer-Tropsch products with a particular focus on the question, whether decentralized off-grid solutions based on renewable power sources should be prioritized over the supply with grid electricity. The three process routes designed in **Journal Article III** serve as a basis for determining the net production costs of Fischer-Tropsch products. Finding a balance between low electricity costs and high plant availability is crucial to making Power-to-Liquid processes cost-competitive with conventional processes based on fossil carbon sources. Furthermore, implementing storage technologies, e.g., for electricity, syngas or H_2, will be a central challenge for future Power-to-Liquid projects.

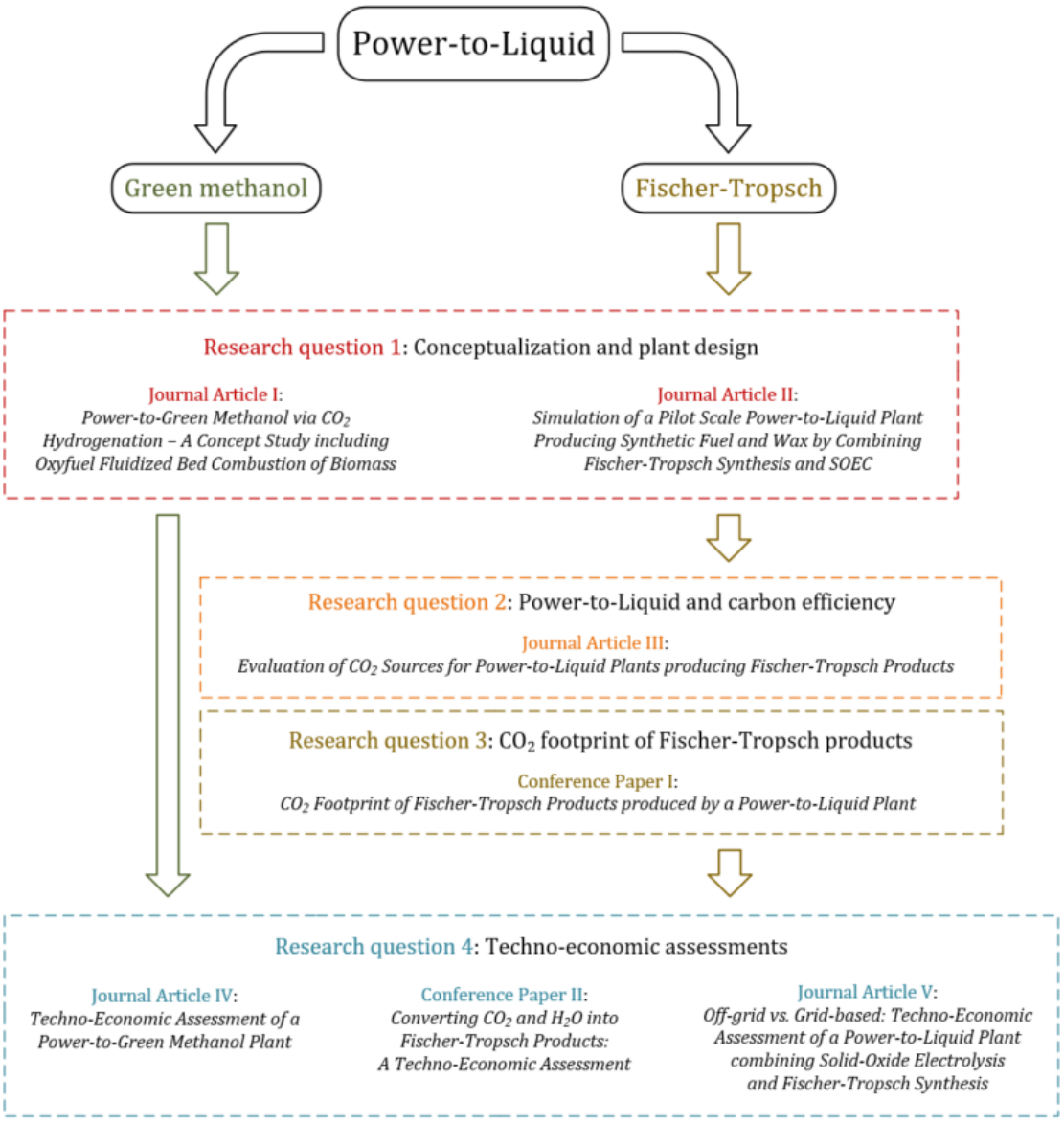

Figure 1: Overview of the presented thesis's underlying Journal Articles and Conference Papers.

1.3 The Need for Synthetic Platform Chemicals and Fuels

Averting the climate crisis poses humanity's primary challenge in the 21st century. According to the National Oceanic and Atmospheric Administration, the global mean surface temperature in 2022 rose by 1.06°C compared with pre-industrial levels [1]. The June-July-August 2023 season was the warmest on record, obtaining a mean temperature of 16.77°C, 0.66°C higher than the average. In addition, a startling frequency of global surface air temperature anomalies has been observed since 2010 [2]. The atmosphere's CO_2 level increased simultaneously, obtaining a peak of 419.51 ppm in June 2023 [3] and an average annual increase of almost 2.5 ppm from 2010 to 2020 [4].

The global annual CO_2 emissions amounted to 36 Gt in 2021, of which 2.4 Gt were directly emitted by the European Union's 27 member states [5]. The transport sector is the only EU sector with increasing CO_2 emissions. It is responsible for around 28%, with respective shares of 3.8%pt. for aviation and 4%pt. for marine navigation, of the EU's greenhouse gas emissions (GHG) [6]. The chemical sector was responsible for 3.2% of the EU's GHG emissions [7].

According to the IPCC's Sixth Assessment Report (AR6), the most significant GHG reduction potential lies within the expansion of renewable power sources, i.e., solar and wind, in combination with the electrification of the mobility and industry sector [8]. Power-to-Liquid processes and carbon capture and utilization technologies can potentially become building blocks of future energy systems by providing liquid platform chemicals and fuels for hard-to-electrify and hard-to-abate sectors. The foundation of those processes will be to establish a "Hydrogen Economy", which is projected to make up a $2.5 trillion industry by 2050 and, thus, become a cornerstone of the 21st century global economy [9].

Hydrogen can be divided into different categories based on its production process and applied energy [9]:

- Black – based on coal gasification.
- Grey – based on natural gas reforming.
- Blue – based on natural gas reforming combined with carbon capture and storage (CCS).
- Turquoise – based on methane pyrolysis.
- Pink – based on water electrolysis powered with nuclear power.
- Yellow – based on water electrolysis powered with grid electricity.
- Green – based on water electrolysis powered with renewable electricity.

Today's share of low-emission hydrogen accounts for only 0.7% of the overall hydrogen production. A global overview of announced hydrogen projects was provided by the International Energy Agency's (IEA) global hydrogen review. The annual production capacity of those newly announced projects is projected to reach 38 million tons in 2030, of which 73% will be based on electrolysis and low-emission electricity and 27% on fossil fuels in combination with carbon capture and storage [10].

In summary, Power-to-Liquid processes provide a possible approach to chemically store hydrogen as platform chemicals or fuels, e.g., methanol or Fischer-Tropsch products. The application of PtL products in the chemical industry should be prioritized to extend the period in which the carbon is bound inside the product. Electrifying the mobility and industry sectors is a linchpin in averting the climate crisis. Thus, fuel applications of PtL products should focus on hard-to-electrify and hard-to-abate sectors, e.g., aviation, marine navigation and decentralized industries.

1.4 Legal Framework in the European Union

The revised Directive (EU) 2023/2413, i.e., Renewable Energy Directive III, entered into force on 20 November 2023, demanding a renewable share of 42.5% of the EU's total energy consumption by 2030. The specific regulations concerning the EU's transport sector include a renewable energy percentage of 29% by 2030. As a secondary target, 5.5% of that renewable energy must be advanced biofuels or renewable fuels of non-biological origin [11].

The European Council works on two proposals for regulations to ensure a level playing field for aviation and maritime transportation in the EU, i.e., ReFuelEU aviation and FuelEU maritime. Both proposals are part of the Fit for 55 legislative package to ensure a 55% reduction in GHG emissions until 2030.

ReFuelEU aviation is designed to gradually increase the share of sustainable aviation fuel (SAF), i.e., synthetic fuels, biofuels and recycled carbon fuels, supplied by aircraft fuel suppliers at EU airports every five years from 2025 to 2050. The respective shares of SAF are planned to be 2% (2025), 6% (2030), 20% (2035), 34% (2040), 42% (2045) and 70% by 2050. In addition, EU airports must guarantee the necessary infrastructure to deliver, store and refuel aircraft with SAF [12].

The FuelEU maritime regulations are planned to include vessels above 5,000 gross tons, corresponding with 90% of maritime CO_2 emissions, at European ports. The GHG intensity of energy used on board must be reduced by 2% (2025), 6% (2030), 14.5% (2035), 31% (2040), 60% (2045) and 80% (2050) compared with the average in 2020 [12].

The minimum threshold of GHG emission savings of synthetic fuels is regulated by the Commission Regulation (EU) 2023/1185 of 10 February 2023. The total emissions of synthetic fuels, in g_{CO2eq}/MJ_{Fuel}, include inputs, processing, transport and distribution, combustion and potential emission savings from Carbon Capture and Storage. The emissions of machinery and equipment production are not considered. The emission savings compared with conventional carbon-based fuels must be at least 70% based on a fossil fuel comparator of 94 $g_{CO2eq}/MJ_{Fossil\ fuel}$. Captured emissions of non-sustainable fuels for producing electricity should be considered as avoided until 2035. In contrast, emissions of non-sustainable fuels for other uses should be regarded as avoided until 2040. The regulation's appendix provides tables that include emission factors of potential feedstocks and applied electricity. Renewable electricity sources complying with Article 27(3) of Directive (EU) 2018/2001 shall be factored in with zero GHG emissions [13].

1.5 Power-to-Liquid – An Overview

The following chapter aims to provide a brief overview of Power-to-Liquid synthesis routes, focusing on the processes elaborated in this thesis, i.e., Fischer-Tropsch and methanol synthesis. In addition, a short examination of alternative PtL process routes, i.e., ammonia and dimethyl ether, is given.

1.5.1 Fischer-Tropsch

The Fischer-Tropsch process has been industrialized for several decades as a synthesis route producing synthetic fuels through Coal-to-Liquid (CtL) and Gas-to-Liquid (GtL) processes. In addition, medium-scale Fischer-Tropsch plants serve as a viable process route for Biomass-to-Liquid (BtL) processes, whereas Power-to-Liquid plants were only established recently. A global overview of currently operating FT plants was provided by Advanced Energy Technology [14]. Summaries of ongoing and planned PtL projects based on FT synthesis were presented in published journal articles by the author of this thesis [15,16].

The process can be classified into high-temperature (HTFT), operated in circulating or bubbling fluidized bed reactors, and low-temperature Fischer-Tropsch synthesis (LTFT), operated in fixed-bed multi-tubular (FBMR), slurry bubble column (SBCR) or microchannel reactors (MCR). Fischer-Tropsch reactor technologies, including their advantages and disadvantages, have been extensively analyzed in numerous studies [17–23]. FBMR and SBCR are the preferred reactor technologies for industrial plants producing up to 160,000 barrels per day. In contrast, MCR technologies received increased interest for PtL applications within the past years due to the possibility of a modular scale-up [24] while obtaining high per-pass CO conversions of up to 79% with selectivities for C_{6+} hydrocarbons of 89% [25,26].

State-of-the-art catalyst systems are based on cobalt and SiO_2, Al_2O_3 or TiO_2 carriers, or iron, typically used as bulk catalysts [17]. The main advantages of cobalt-based catalysts over iron-based catalysts are their high activity, high selectivity for long-chained hydrocarbons and long lifetime. In contrast, the major downsides are an increased vulnerability to catalyst poisoning and no activity for the water-gas shift (WGS) reaction [27]. The critical properties of Fischer-Tropsch catalysts comprise hydrogenation activity, WGS activity, mechanical stability, resistance against catalyst poisons, economic factors and criticality of applied materials [17,28].

The FT synthesis underlies a highly complex reaction system with a critical sensitivity to the chosen process parameters and reactor technologies. De Klerk provided a comprehensive overview of the most significant parameters, i.e., temperature, pressure, H_2:CO ratio, overall gas composition and space velocity [17]. Gavrilovic et al. analyzed those parameters' influence on CO conversion and product composition [27]. A kinetic study on the effect of the H_2:CO ratio on the process has been conducted by Ostadi et al. [29].

Finding and optimizing catalyst systems being active for CO_2 should become a primary focus of future R&D projects. Guilera et al. aimed to exploit the high CO_2 share of biomass-derived syngas by

promoting a cobalt-based catalyst with lanthanum [30]. Corrao et al. obtained a CO_2 conversion of 40% and a selectivity for C_{6+} compounds of 57% by combining a Na-promoted Fe_3O_4 catalyst with zeolites [31].

FT syncrude can be processed into various products, e.g., liquified petroleum gas (LPG), gasoline, diesel, jet fuel, lubricants and high-end petrochemicals [17,28,32]. In addition, FT wax can potentially be upgraded to fine chemicals [33]. This wide array of potential products entails a multitude of refinery concepts to maximize the desired product's selectivity. FT refineries can be based on several sub-processes, e.g., distillation, oligomerization, alkylation, hydrogenation and hydrocracking [34–36]. Petersen et al. modeled and simulated refinery concepts for different products, obtaining an average refining efficiency of about 85% [34]. A further elaboration on refining catalysts was given by Busca et al. [37]. Detailed information on the upgrading of FT waxes was provided by Bouchy et al. [38].

Rahman et al. established an aqueous FT product phase treatment based on Malaysia's Bintulu, Sarawak GtL plant's composition [39]. Besides water, around 99 wt%, alcohols and aldehydes were the main impurities, with mass shares of 0.71 and 0.20 wt%, respectively. Other impurities were carboxylic acids, 0.09 wt% and dissolved CO_2, 0.02 wt%.

1.5.2 Methanol

Methanol, i.e., CH_3OH, a clear, colorless liquid at standard conditions, is the smallest molecule of the alcohol group [40]. The global daily methanol consumption amounts to around 200,000 metric tons, making methanol production a $55 billion turnover industry [41]. Over 90 methanol plants operate globally, with a total annual production capacity of 110 million metric tons. The methanol industry relies heavily on fossil feedstocks, i.e., natural gas and coal, with shares of 65% and 35%, respectively [42]. Aasberg-Petersen et al. gave a detailed process description of a methanol plant based on natural gas reforming [43]. An extensive economic review of the industrial production of methanol for various regions was provided by Roode-Gutzmer et al. [44].

Methanol has a wide field of applications, e.g., as a precursor in the chemical industry, as a fuel additive, in olefin production, or as a direct application as a fuel. Formaldehyde and acetic acid production amounts to 40% of methanol consumption. Applications as a fuel additive, i.e., dimethyl ether (DME) or methyl tert-butyl ether (MTBE), amount to 17% of the methanol demand. Methanol as a direct fuel is responsible for 12%, whereas processing to olefins amounts to 5% of the total consumption [44].

An excerpt of operating and planned PtL plants based on methanol synthesis was part of one of this thesis's journal articles [45]. Dieterich et al. provided an overview of PtL plants applying methanol synthesis in 2020 [46]. Green methanol has the potential to achieve a CO_2 emission reduction of 95% compared with the conventional, fossil-based process route. It is projected that 80 renewable methanol projects will realize an annual production capacity of more than 8 million metric tons of green methanol per year by 2027 [47].

State-of-the-art methanol processes operate at temperatures ranging from 230°C, lower limit due to reactor productivity, to 270°C, upper limit due to catalyst sintering [48]. Typical synthesis pressure levels range from 40 to 100 bar at a space velocity of 7,000 to 12,000 m^3/h gas flow per m^3 catalyst volume [48,49]. Feeding a mixture of CO, CO_2 and H_2 into the reactor benefits the process productivity, obtaining a maximum at a carbon oxide ratio (COR) between 0.1 and 0.2 [50,51]. A stoichiometric number (SN) between 2.02 and 2.10 is recommended for methanol processes based on CO and CO_2 hydrogenation [48]. Lower per-pass CO_2 conversions of around 20% are realized for methanol processes solely based on CO_2 hydrogenation [52]. Detailed information concerning CO_2 hydrogenation, including the technical differences compared with conventional CO hydrogenation to methanol, has been the focus of numerous past studies [53–55].

Different methanol reactor types are applied at an industrial level, with the majority being either quench reactor, e.g., by Imperial Chemical Industry, Mitsubishi Gas Chemicals and M.W. Kellogg, or isothermal, multi-tubular, boiling water reactor systems, e.g., by Lurgi and Linde AG. Alternative reactor concepts include a radial flow reactor concept in series established by Haldor Topsoe or a slurry bubble column reactor by Chem. Systems Inc [48,56].

$Cu/ZnO/Al_2O_3$ catalysts are state-of-the-art, with an increased interest in enhancing the catalyst system's CO_2 activity [53,57]. Alternative catalyst systems can, for example, be based on Cu/MgO [58], In_2O_3 [59] or MoS_2 [60].

Regardless of their feedstock, a crucial part of methanol plants is the distillation section subsequent to the methanol reactor. State-of-the-art distillation and purification processes for methanol include a gas/liquid separator to liquefy the crude methanol, a light ends column to remove volatile impurities and a refining column [48,61] to process the crude methanol into methanol complying with the International Methanol Producers and Consumers Association (IMPCA) purity standards of 99.85 wt% [62].

1.5.3 Alternative Liquid Energy Carriers produced by Power-to-Liquid Processes

An overview of alternative liquid energy carriers produced via Power-to-Liquid processes, i.e., ammonia and dimethyl ether, is presented in this chapter to put the assessed products into context.

Ammonia, i.e., NH_3, is a promising non-carbon-based energy carrier, mainly applied as a feedstock in the fertilizer industry. Additional applications are the utilization as a feedstock in the explosives industry, as a direct fuel for fuel cells or as an energy storage vector for hydrogen [63]. The main advantages of ammonia include its high energy density, excellent stability, feasible storage possibilities with negligible energy losses and non-explosive features [63,64].

The ammonia industry is responsible for around 2% of the global energy consumption and 1% of the worldwide greenhouse gas emissions. The global ammonia production capacity amounted to 185 million tons in 2020 and is projected to rise to 230 million tons annually in 2050 [64].

State-of-the-art ammonia plants are natural gas-based and operate at elevated pressures, i.e., 150 to 250 bar, and at high temperature levels, i.e., 400 to 450°C. Nitrogen is provided by air separation units (ASU), whereas hydrogen is provided by the reforming of natural gas, the primary source of CO_2 emissions of ammonia plants [63].

Green ammonia production uses green hydrogen, produced by an electrolyzer based on renewable power sources, as a feedstock instead of hydrogen based on natural gas [64]. A green ammonia plant based on a 26 $MW_{el.}$ electrolyzer for producing explosives for the mining industry is currently planned in Mejillones, Chile [65,66]. Other projects include a planned green ammonia plant based on four wind turbines (16 MWp) in Tarniki, New Zealand [67], a planned plant with an annual production capacity of 1.3 million tons in Odisha, India [68] and a green hydrogen and ammonia plant in Newfoundland, Canada [69].

Dimethyl ether, i.e., CH_3OCH_3, is a volatile chemical compound with a vapor pressure comparable to propane and butane, which thus needs to be liquefied for its transport and application. The total global annual production capacity amounts to 5 million tons. DME offers a wide range of applications, e.g., as a feedstock for the chemical industry, a blending agent for LPG fuels and a solvent for liquid extraction processes [70].

Green DME can be used as a building block for value-added chemicals, acetic acid as well as ethanol and is an intermediate product of Methanol-to-Chemicals and Methanol-to-Olefins routes [70]. The advantages of DME fuel applications are its high conversion efficiency compared with other PtL processes [71] and its clean combustion properties due to the molecule's lack of carbon-carbon bonds [72].

Conventional DME production is either based on the indirect route as established by Haldor Topsoe, Lurgi and Mitsubishi, including methanol synthesis and subsequent dehydration of methanol, or the direct route, combining methanol and DME synthesis in a single reactor [73]. Advantages of this process route include overcoming reaction thermodynamics, increased reactor productivity and reduced hydrogen demand. However, this process intensification comes at the price of a more complex product separation step [70]. Innovative process designs are, for example, based on a membrane reactor concept combining synthesis and distillation in a single step [74] or the direct synthesis of DME in slurry bubble column reactors [75].

1.6 State-of-the-Art of Water Electrolysis Technologies

Water electrolysis will be a cornerstone of the 21st century global hydrogen industry. Specifically, three electrolysis technologies, i.e., alkaline (AEL), proton exchange membrane (PEMEL) and solid-oxide electrolysis (SOEL), are going to be applied for the production of green, pink and yellow hydrogen. AEL units offer a consistent, stable and relatively cheap operation with up to ten years of stack lifetimes. PEM electrolyzers are well suited for intermittent power sources due to their high flexibility. SOEL, operating at high temperatures, has the lowest specific electricity demand and is suitable in industrial environments that offer waste heat or process steam [76]. Direct comparisons of water electrolysis technologies were provided by Nasser et al. [77], Schmidt et al. [78] and Kecebas et al. [79]. Lange et al. assessed the respective technology readiness levels (TRL) at 9 (AEL), 6-8 (PEMEL) and 4-6 (SOEL) [80].

AEL, based on OH^- ions in an aqueous NaOH or KOH solution, is the most mature of the stated options, obtaining lower CAPEX per installed kW compared with PEMEL and SOEL. The hydrogen stream's purity is 99.5 to 99.9 mol% [77]. Typical operating conditions include temperatures from 70 to 100°C and pressure levels between 1 and 40 bar [76]. Modern AEL systems are more flexible than generally perceived and show a specific electricity demand of 4.5 to 7 $kWh_{el.}/Nm^3$ hydrogen [80]. Kecebas et al. provided an overview of applied materials for electrodes, diaphragm and electrolytes [79]. Today's largest green hydrogen AEL plant, with a rated power of 150 $MW_{el.}$, operates in Ningxia, China [81].

The main advantages of PEM electrolyzers, based on the transfer of H^+ ions in Nafion electrolytes, are their fast responses and swift start-up times. In addition, highly pure hydrogen of up to 99.999 mol% can be provided [77]. PEMEL units typically operate at temperatures between 70 and 90°C and a pressure level below 80 bar [80]. The technology's major setbacks include its dependency on noble materials, i.e., platinum, iridium and ruthenium, and its lower stack lifetime than alkaline electrolyzers. Liu et al. provided a comprehensive overview of applied materials and electrocatalysts [82]. Large-scale PEMEL projects of up to 35 $MW_{el.}$ rated power were announced in 2022. Additionally, a large-scale PEM electrolyzer plant in Guangdong, China, with an annual production capacity of 1 GW, will be commissioned in 2023 [83].

SOEL units, based on the exchange of O^{2-} ions in a yttrium-stabilized zirconium electrolyte [84], operate at elevated temperatures ranging from 600 to 900°C and atmospheric pressure [80]. The technology's primary advantage is its lower specific power consumption, ranging from 3.2 to 3.7 $kWh_{el.}/Nm^3$ [78,80,85], utilizing waste heat or industrial steam streams. In addition, SOEL units can be operated in co-electrolysis mode, converting CO_2 and water into H_2 and CO, thus avoiding an additional rWGS reactor. Wang et al. assessed the conversion of CO_2 to CO by analyzing the cell's area specific resistance, observing a significant influence of the rWGS reaction over electrochemical CO_2 splitting [86]. The SOEL unit's H_2:CO ratio can be flexibly adjusted by adapting the feed stream's H_2O:CO_2 ratio [87]. The technology's primary challenge is its higher degradation rate of 0.6 to 1.5 %/kh compared with AEL and PEMEL. An overview of applied electrode, electrolyte and support materials has been provided by Wolf et al. [84]. Today's largest operating SOEL unit, with a rated power of 2.6 $MW_{el.}$, is located in Rotterdam, The Netherlands [88]. In addition, an industrial SOEL factory with an annual production capacity of 500 MW, located in Herning, Denmark, was announced in 2023 [89].

2 Methodology

This chapter provides a summary of the necessary steps to assess the performance, i.e., efficiency, ecological impact and economic feasibility, of Power-to-Liquid plants, including:

- Modeling the plants' sub-processes.
- Process simulation.
- Economic modeling.
- Definition of key performance indicators, i.e., PtL, energy and carbon efficiency.
- Determining the CO_2 footprint of Power-to-Liquid products based on various power sources.

2.1 Process Modeling

The following chapter presents an overview of the Power-to-Liquid plants' main sub-processes, i.e., Fischer-Tropsch synthesis, methanol synthesis, solid-oxide electrolysis and steam reforming of recirculated tail gas.

2.1.1 General Formulae and Assumptions

The following formulae are applied for various processes, enabling a basic assessment of chemical reactors and processes. The conversion X of a feed j is calculated by dividing the converted share of j by the total molar flow rate of component j fed into the reactor or process, as stated in equation (1).

$$X_j = \frac{\dot{n}_{j,in} - \dot{n}_{j,out}}{\dot{n}_{j,in}} \quad (1)$$

The yield Y, see equation (2), includes the stoichiometric matrix of a chemical process by implementing the stoichiometric factors ν_k and ν_i and is defined as the produced molar flow rate of product i compared with the feed of key component k.

$$Y_{ik} = \frac{\dot{n}_{i,out} - \dot{n}_{i,in}}{\dot{n}_{k,in}} \cdot \frac{\nu_k}{\nu_i} \tag{2}$$

The selectivity S referring to product i is defined as the produced molar flow rate of i divided by the total amount of converted key component k, as seen in equation (3).

$$S_{ik} = \frac{\dot{n}_{i,out} - \dot{n}_{i,in}}{\dot{n}_{k,in} - \dot{n}_{k,out}} \cdot \frac{\nu_k}{\nu_i} = \frac{Y_{ik}}{X_k} \tag{3}$$

The ratio between the gaseous feed into a reactor, mass or volume flow rate, and the amount of catalyst inside the reactor, mass or volume, is defined as the space velocity SV. Equation (4) displays the space velocity in its form based on the feed's volume flow rate and the catalyst's total mass.

$$SV_{Cat} = \frac{\dot{V}_{Feed}}{m_{Cat}} \tag{4}$$

Recirculating unreacted gases back to the reactor inlet is a critical element of Power-to-Liquid processes to maximize the plant's productivity and efficiency. The recirculation ratio of tail gas RR is defined as the share of recirculated tail gas based on the total amount of tail gas, see equation (5). A share of the tail gas stream must be removed from the system as a purge gas to avoid the accumulation of inert gases. In addition, combusting the purge gas stream is essential to meet the plant's internal demand for high-temperature heat.

$$RR = \frac{\dot{m}_{Tail\ gas,\ rec.}}{\dot{m}_{Tail\ gas,\ total}} \cdot 100\% \tag{5}$$

$$\dot{m}_{Purge\ gas} = \dot{m}_{Tail\ gas,\ total} - \dot{m}_{Tail\ gas,\ rec.} \tag{6}$$

The assumptions concerning the Power-to-Liquid plant's auxiliary equipment, i.e., compressors, pumps and electric motors, are summarized in Table 1.

Table 1: Assumed efficiencies for auxiliary equipment.

Efficiency	Electric motors	Compressors	Pumps
Electric efficiency $\eta_{el.}$	96%	-	-
Mechanical efficiency $\eta_{m.}$	99%	90%	95%
Isentropic efficiency η_s	-	90%	90%

2.1.2 Fischer-Tropsch Synthesis

The Fischer-Tropsch synthesis is a complex reaction network, converting syngas consisting of CO and H_2 into a wide range of hydrocarbons, i.e., alkanes, alkenes, alcohols, carbonyls and carboxylic acids. The main reactions are given in equations (7-11) [17,19].

Alkanes: $$n\,CO + (2n+1)H_2 \rightarrow H(CH_2)_nH + n\,H_2O \qquad \Delta H_r^0 = -166.4\,kJ/mol \qquad (7)$$

Alkenes: $$n\,CO + 2n\,H_2 \rightarrow (CH_2)_n + n\,H_2O \qquad (8)$$

Alcohols: $$n\,CO + 2n\,H_2 \rightarrow H(CH_2)_nOH + (n-1)\,H_2O \qquad (9)$$

Carbonyls: $$n\,CO + (2n-1)H_2 \rightarrow (CH_2)_nO + (n-1)\,H_2O \qquad (10)$$

Carb. acids: $$n\,CO + (2n-2)H_2 \rightarrow (CH_2)_nO_2 + (n-2)\,H_2O \qquad n > 1 \qquad (11)$$

A typical product composition of a low-temperature Fischer-Tropsch synthesis applying a Co-based catalyst consists mainly of alkanes. Typical by-products are alkenes, obtaining a share of at least 10 wt% and oxygenates, obtaining a total share of 5-15 wt%. Additional by-products include aromatics and cyclo-alkanes with shares below 1 wt% each [17].

An established method to describe the Fischer-Tropsch synthesis's product distribution is the Anderson-Schulz-Flory (ASF) model, based on the chain growth probability α, the synthesized hydrocarbons' respective chain length n and the respective molar fraction of product n x_n. The standard and logarithmic, preferred for determining α based on experimental data, models are provided in equations (12) and (13).

$$x_n = (1-\alpha)\cdot\alpha^{n-1} \qquad (12)$$

$$\log x_n = n\cdot\log\alpha + \log\left(\frac{1-\alpha}{\alpha}\right) \qquad (13)$$

Three main deviations from the standard ASF model can be observed for real Fischer-Tropsch product distributions [90]:

1. Underestimation of the methane selectivity S_{CH4}.
2. Overestimation of the selectivity of hydrocarbons with a chain length of two, i.e., ethane and ethene.
3. LTFT processes show two α-value distributions for hydrocarbons with a chain length below eight and above twelve, including a transitional regime.

Förtsch et al. tackled those inaccuracies by establishing an extended ASF (eASF) model based on five parameters and equations (14-16) [90].

- α_1: First independent chain growth probability dominating the overall chain growth probability at low carbon numbers ($0 \leq \alpha_1 \leq 1$).
- α_2: Second independent chain growth probability dominating the overall chain growth probability at high carbon numbers ($0 \leq \alpha_2 \leq 1$; $\alpha_1 \leq \alpha_2$).
- γ: Enhancement factor adapting the methane selectivity ($0 \leq \gamma \leq 1$).
- β: Re-adsorption probability adapting the selectivity for C_2 hydrocarbons ($0 \leq \beta \leq 1$).
- μ_2: Fraction of second distribution function describing the deviation at high carbon numbers ($\mu_1 = 1-\mu_2$).

$$x_{CH_4} = (1-\mu_2)\cdot[1-\alpha_1\cdot(1-\gamma)] + \mu_2\cdot(1-\alpha_2) \tag{14}$$

$$x_{C_2H_6} = (1-\mu_2)\cdot(1-\alpha_1)\cdot\alpha_1\cdot\frac{1-\beta}{1-\beta\cdot(1-\alpha_1)}\cdot(1-\gamma) + \mu_2\cdot(1-\alpha_2)\cdot\alpha_2 \tag{15}$$

$$x_{C_nH_{2n+2}} = (1-\mu_2)\cdot(1-\alpha_1)\cdot\alpha_1^{(n-1)}\cdot\frac{1-\gamma}{1-\beta\cdot(1-\alpha_1)}\cdot\mu_2\cdot(1-\alpha_2)\cdot\alpha_2^{(n-1)} \tag{16}$$

Table 2 displays the assumed eASF parameters within this thesis based on the experimental findings of Gruber et al. and Guilera et al. [30,91].

*Table 2: Assumed eASF parameters [**Journal Article II**].*

Parameter	Value
α_1	0.78
α_2	0.90
γ	0.48
β	0.75
μ_2	0.95

2.1.3 Methanol Synthesis

Producing methanol is either based on CO hydrogenation, equation (17), CO_2 hydrogenation, equation (18), or a combination of those processes with the reverse water-gas shift reaction occurring as the primary side reaction, equation (19).

$$CO_2 + 3H_2 \rightarrow CH_3OH + H_2O \qquad \Delta H_r^0 = -49.8\ kJ/mol \tag{17}$$

$$CO + 2H_2 \rightarrow CH_3OH \qquad \Delta H_r^0 = -91.0\ kJ/mol \tag{18}$$

$$CO_2 + H_2 \rightarrow CO + H_2O \qquad \Delta H_r^0 = 42.1\ kJ/mol \tag{19}$$

The conversion of CO and CO_2, as well as the total carbon conversion to methanol, are described by equation (20). The selectivity of CO_2 hydrogenation to methanol is stated in equation (21).

$$X_i = \frac{\dot{n}_{i,in} - \dot{n}_{i,out}}{\dot{n}_{i,in}} \qquad \text{i} = \text{CO, CO}_2\text{, CO} + \text{CO}_2 \qquad (20)$$

$$S_{MeOH} = \frac{\dot{n}_{MeOH,out} - \dot{n}_{MeOH,in}}{\dot{n}_{CO_2,in} - \dot{n}_{CO_2,out}} \qquad (21)$$

The stoichiometric number SN describes the stoichiometric ratio between carbon oxides, i.e., CO and CO_2, and hydrogen for the methanol synthesis, see equation (22). Supp recommends a stoichiometric number between 2.02 and 2.10 [48].

$$SN = \frac{\dot{n}_{H_2} - \dot{n}_{CO_2}}{\dot{n}_{CO} + \dot{n}_{CO_2}} \qquad (22)$$

The carbon oxide ratio COR is defined as the ratio of CO_2 to the sum of CO_2 and CO molecules in the syngas stream, as stated in equation (23). An optimum overall conversion of carbon oxides to methanol was observed for a carbon oxide ratio between 0.1 and 0.2 [50,51].

$$COR = \frac{\dot{n}_{CO_2}}{\dot{n}_{CO} + \dot{n}_{CO_2}} \qquad (23)$$

Recirculating the tail gas leaving the methanol synthesis unit is essential to maximize the process efficiency. Typical tail gas recirculation ratios, see equation (5), for industrial methanol synthesis applications are around 80% for processes based on CO hydrogenation [92] and up to 90% for processes based on CO_2 hydrogenation [93].

2.1.4 Solid-Oxide Electrolysis

Solid-oxide electrolyzers operate at atmospheric pressure and an elevated temperature of 600 to 900°C [86]. The required enthalpy of reaction (ΔH_r) of water splitting is defined as the sum of the Gibbs free energy (ΔG_r) and the entropy of reaction (ΔS_r), as stated in equation (24). Thus, high-temperature water electrolysis can utilize waste heat of adjacent industrial processes or exothermal chemical reactions to lower the unit's demand for electricity [94].

$$\Delta H_r = \Delta G_r + T \cdot \Delta S_r \qquad (24)$$

SOEL units operating in co-electrolysis mode, i.e., converting a feed stream of water and CO_2 to H_2 and CO, offer significant synergetic effects with synthesis processes based on CO hydrogenation, e.g., Fischer-Tropsch [87]. The outlet's H_2:CO ratio is primarily influenced by the inlet's H_2O:CO_2 ratio and does not depend on the applied current density, thus enabling great flexibility concerning required H_2:CO

ratios for various heterogeneous synthesis processes [95]. The occurring chemical reactions at the cathode and anode are stated in equations (25-27).

Cathode: $$H_2O + 2e^- \rightarrow H_2 + O^{2-} \quad (25)$$

Cathode: $$CO_2 + 2e^- \rightarrow CO + O^{2-} \quad (26)$$

Anode: $$O^{2-} \rightarrow \frac{1}{2}O_2 + 2e^- \quad (27)$$

Wang et al. found that the major share of CO_2 conversion at the cell's cathodic side is caused by the rWGS reaction, see equation (28) instead of direct CO_2 splitting [86].

$$CO_2 + H_2 \rightarrow CO + H_2 \quad (28)$$

The conversion of water and CO_2 is calculated according to equation (1) in chapter 2.1.1. The reactant utilization RU, directly proportional to the applied cell current, is defined as the unit's total conversion of water and CO_2 [95].

$$RU = \frac{(\dot{n}_{CO_2,in} + \dot{n}_{H_2O,in}) - (\dot{n}_{CO_2,out} + \dot{n}_{H_2O,out})}{(\dot{n}_{CO_2,in} + \dot{n}_{H_2O,in})} \quad (29)$$

An overview of the established SOEL model operating in co-electrolysis mode is given in Figure 2. Water is evaporated before being mixed with the CO_2 feed stream. The SOEL feed stream is subsequently heated to the required temperature level. The conversions of water and CO_2 are set within the stoichiometric model. In addition, the electricity needed for water splitting and reaction heat of the rWGS reaction is calculated based on the stoichiometric model. As a next step, oxygen is split from the gas stream and mixed with air, which is required to flush oxygen out of the cell's anode. The syngas, consisting of CO, H_2, CO_2 and H_2O, is drained from the cathode.

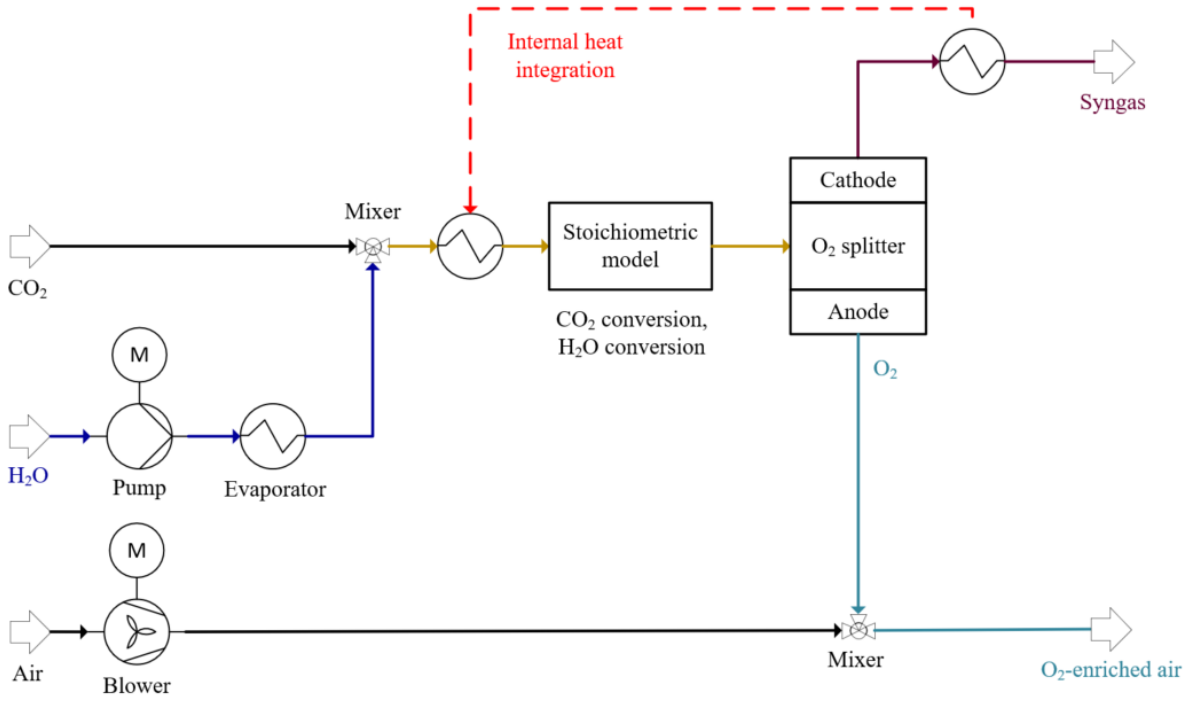

Figure 2: Overview of the designed SOEL model (co-electrolysis mode).

2.1.5 Steam Reforming of Tail Gas

Reforming recirculated tail gas is a linchpin of industrial PtL plants to increase process efficiency and productivity. Steam reforming reactors operate at temperatures ranging from 800 to 900°C. State-of-the-art catalysts are based on nickel on a $CaAl_{12}O_{19}$ or Al_2O_3 carrier [57]. A trade-off between hydrocarbon conversion and reactor productivity has to be found concerning applied pressure, typically ranging from 10 to 20 bar [96]. The established model of a steam tail gas reformer is based on the conversion of CH_4, C_2H_4, C_2H_6 and C_3H_8, according to equation (1), and the conversion of CO_2 via the rWGS reaction, see equation (28). Conversions between 90% (CH_4) and 99% (C_3H_8) are assumed for hydrocarbons. The conversion of CO_2 to CO is calculated via the chemical equilibrium at the chosen process conditions.

A central process parameter is the steam-to-carbon ratio S/C, defined in equation (30), based on the molar flow rate of carbon atoms in the feed stream's hydrocarbons. Typical S/C ratios range from 2 to 4 [97,98]. High S/C ratios decrease the risk of catalyst coking and increase the total conversion of hydrocarbons. In addition, the outlet's H_2:CO ratio can be adjusted by the applied S/C ratio [96].

$$S/C = \frac{\dot{n}_{H_2O}}{(\dot{n}_{CH_4} + 2 \cdot \dot{n}_{C_2H_4} + 2 \cdot \dot{n}_{C_2H_6} + 3 \cdot \dot{n}_{C_3H_8})} \quad (30)$$

2.2 Process Simulation

Determining a process's mass and energy balances is the linchpin of following projects, i.e., plant design, techno-economic assessments and ecological evaluations. IPSEpro version 8.0 was applied as a process simulation tool. IPSEpro is a stationary, equation-based process simulation software, thus providing steady-state calculations with no time dependency while solving all equations simultaneously.

Compared with modular-sequential alternatives, the advantages of equation-based process simulation programs include increased flexibility concerning the specification and input of process variables, shorter calculation run times and the possibility of extending the designed models to dynamic models feasibly. Disadvantages include increased CPU-intensive calculations, weaker traceability of calculations and increased difficulty locating errors and warnings. In addition, good initial values are required to avoid convergence issues.

The applied IPSEpro program modules included the model development kit MDK (model development), PSExcel (data reading) and PSOptimize (process optimization). The applied model library was based on the Pyrolysis and Gasification library extended with additional individually designed process models.

FactSageEdu was used to model the tail gas reformer within **Journal Article II** as a Gibbs minimization reactor. HSC Chemistry version 6 was applied to determine the reaction enthalpies at the chosen process conditions. In addition, COCO and ChemSep were used to elaborate the crude methanol distillation and purification process step based on a gas-liquid separator and two distillation columns.

2.3 Economic Modeling

Assessing the potential economic performance of newly designed chemical plants and processes is critical to facilitating decision-making on different process routes. As a first step, the investment's fixed capital investment (FCI) is determined based on existing cost data for equipment, factorial methods, and cost escalation. As stated in Table 3, five cost estimate classes have been defined by the Association for the Advancement of Cost Estimating (AACE) International.

Table 3: AACE International cost estimate classes [99].

Name (Class)	Benchmark	Application	Accuracy
Order of magnitude (5)	Similar processes	Initial feasibility studies	− 20% to − 50% + 30% to + 100%
Preliminary (4)	Basic process design	Decision on design alternatives	− 15% to − 30% + 20% to + 50%
Definitive (3)	P&I and sizes of major items	Budgeting decision	− 10% to − 20% + 10% to + 30%
Detailed (2)	Nearly complete design	Project cost control	− 5% to − 15% + 5% to + 20%
Check (1)	Completed design	Procurement negotiations	− 3% to − 10% + 3% to + 15%

In addition, the plant's fixed and variable operational expenditure, as well as its expected annual revenue, are required. As a final step, economic key performance indicators, e.g., net present value and net production costs, can be determined based on the CAPEX, OPEX, and revenue found.

2.3.1 Net Present Value and Net Production Costs

The net present value, as seen in equation (31), enables the comparison of different investment options and can be applied to determine the economic performance of chemical plants. It is defined as the sum of the cash flows', stated in equation (32), present values obtained within the chosen plant lifetime t, including the required FCI. The discount rate i is applied to consider the time value of money by discounting the cash flow of future years of operation.

$$NPV = FCI + \sum_{n=1}^{t} \frac{Cash\ flow_n}{(1+i)^n} \tag{31}$$

$$Cash\ flow_n = Revenue_n - OPEX_{Fixed,n} - OPEX_{Variable,n} \tag{32}$$

The NPC of a product are determined according to equation (33) based on the FCI's annuity, as defined in equation (34), the fixed and variable OPEX, the annual revenue and the plant's annual production capacity. In addition, corporate overhead charges, i.e., product distribution, R&D as well as selling and marketing, of 5% were assumed according to Towler and Sinnott [99]. Calculating the annuity of an investment is required to discount and allocate the plant's initial investment based on the discount rate i and the plant lifetime t.

$$NPC = \frac{Annuity + OPEX_{Fixed} + OPEX_{Variable} - Revenue}{Annual\ production\ capacity} \tag{33}$$

$$Annuity = FCI \cdot \frac{(1+i)^t \cdot i}{(1+i)^t - 1} \tag{34}$$

2.3.2 Equipment Costs and Fixed Capital Investment

Several steps are required to convert cost data to today's standards and economic status. As a first step, acquired equipment or process cost data must be converted to the designed plant or equipment specifications, as stated in equation (35). The economies of scale are considered by applying scaling exponent d, ranging from 0 to 1. Previous studies and textbooks provided detailed information concerning d for equipment, processes or whole plants [99–103].

$$Costs_{Design} = Costs_{Base} \cdot \left(\frac{Scale_{Design}}{Scale_{Base}}\right)^d \tag{35}$$

Inflation and purchase power are considered by the cost escalation of data according to equation (36). Several indices, such as the Chemical Engineering Plant Cost Index (CEPCI), can be applied. The CEPCI's development and an overview of its applied factors and their weighting are provided by the Chemical Engineering Magazine [104].

$$Costs_{Design\ year} = Costs_{Base\ year} \cdot \left(\frac{CEPCI_{Design\ year}}{CEPCI_{Base\ year}}\right) \quad (36)$$

In addition, location factors, as stated in equation (37), and currency exchange rates must be applied to consider regional differences in chemical industries and economic development. Lists of location factors were provided by Seider et al. and Towler and Sinnot [99,102].

$$Costs_{Location\ i} = Costs_{USGC} \cdot Location\ factor_{Location\ i} \quad (37)$$

As a last step, additional cost factors, engineering, process control and pipe installation, must be considered by applying an additional factor, e.g., Lang factor, on the determined major equipment costs, see equation (38) [99,101,102]. A detailed breakdown of the Lang factor was provided by Peters et al. [101]. Seider et al. recommended a Lang factor of 5.04 for fluid-processing plants based on modern industry standards [102].

$$FCI = Lang\ factor \cdot \sum Costs_{Equipment} \quad (38)$$

2.3.3 Fixed and Variable Operational Expenditure

A chemical plant's OPEX can be divided into fixed OPEX, e.g., labor, insurance, maintenance and renting of property, and variable OPEX for feedstocks and consumables, e.g., electricity, process water and catalysts. Fixed OPEX of chemical plants can be determined by applying factors for the respective cost centers based on the plant's FCI [105,106] or its annual production capacity [99,107]. Green and Southard proposed a factorial method to determine the plant's required shift operators based on equipment coefficients and detailed process flow charts [108]. Additional expenses for supervision are assumed to be 20% of the determined labor expenses. The necessary payroll charges are chosen to be 30% of the sum of operating and supervision expenses [108]. Counting in the costs for electrolyzer stack replacements is crucial for Power-to-X (PtX) applications [106,109]. Applying current and realistic electricity prices is a linchpin to determining the variable OPEX of PtX applications powered with grid electricity. An additional approach is to determine the levelized cost of electricity (LCOE), as seen in equation (39), if the designed plant is powered by adjacent renewable power sources. The LCOE, given in costs per kWh of produced electricity, is based on the investment's annuity, fixed capital investment, fixed costs, additional costs, variable costs and the power plant's full load hours. Geographical information systems, i.e., the Global Wind Atlas 3.0 provided by the Technical University of Danmark (DTU) [110] and the Photovoltaic Geographical Information System (PVGIS) provided by the European

Commission [111], were applied to determine the electricity yield of renewable power sources at the chosen plant locations.

$$LCOE = \frac{Annuity \cdot FCI + Costs_{Fixed} + Costs_{Additional}}{Full\ load\ hours} + Costs_{Variable} \quad (39)$$

2.4 Power-to-Liquid, Overall and Carbon Efficiency

The Power-to-Liquid efficiency η_{PtL}, stated in equation (40), is defined as the ratio between the chemical energy of products, i.e., naphtha, middle distillate, wax and methanol, and the plant's total electricity input.

$$\eta_{PtL} = \frac{\dot{U}_{Products}}{P_{Total,in}} \cdot 100\% \quad (40)$$

The PtL efficiency provides a proper key performance indicator for processes solely based on electricity as energy input and PtL products as energy output. The overall energy efficiency η_{Energy}, stated in equation (41), additionally includes fuel input streams as well as heat input and output streams.

$$\eta_{Energy} = \frac{\dot{U}_{Products} + \dot{Q}_{out}}{\dot{U}_{Fuel,in} + P_{Total,in} + \dot{Q}_{in}} \quad (41)$$

Determining the carbon efficiency η_{Carbon}, stated in equation (42), of chemical processes and plants is a cornerstone of state-of-the-art assessments. It is defined as the carbon stream bound in products, i.e., naphtha, middle distillate, wax and methanol, divided by the plant's sum of carbon feed streams.

$$\eta_{Carbon} = \frac{\dot{n}_{Carbon,\,Products}}{\dot{n}_{Carbon,\,Feed\ streams}} \quad (42)$$

2.5 Carbon Footprint of Power-to-Liquid Products

Conference Paper I's aim was to calculate the CO_2 footprint of Power-to-Liquid products based on the applied electricity's emission factor. The determined results were compared with emission factors of conventional fuels and biofuels. It must be highlighted that **Conference Paper I** solely considered the electricity input and excluded additional emissions caused by equipment and plant construction.

PtL plants can either be powered with off-grid renewable power sources or grid electricity. Table 4 provides an overview of electricity emission factors. Legally binding emission factors for calculating GHG emission savings were provided by the European Commission in 2023 [13]. Detailed information concerning the emission factor of electricity in Austria, i.e., certified green electricity, national production and overall, was provided by the Austrian Environment Agency [112]. The GHG intensity development from 1990 to 2021 of electricity production in the EU member states was analyzed by the European Environment Agency [113].

Table 4: Emission factors of renewable electricity sources, Austrian electricity and the EU 27 grid average.

Electricity source	Emission factor [kg CO_2eq/kWh$_{el.}$]	Source
Hydropower	0.003	[114]
Offshore wind	0.006	[114]
Onshore wind	0.010	[114]
Photovoltaic	0.067	[114]
Austria green electricity	0.014	[112]
Austria production	0.143	[13]
Austria incl. imports	0.202	[112]
EU 27 average	0.265	[113]

The emission factor of PtL products $EF_{Product}$ in kg CO_2eq/kg$_{Product}$ is determined according to equation (43) based on the electricity sources emission factor $EF_{El.}$, the plant's total power input P_{Total} and the produced mass flow rate $\dot{m}_{Product}$. The CO_2 break-even point compared with fossil-based products or biofuels, see Table 5, is determined according to equation (44).

$$EF_{Product} = \frac{EF_{El.} + P_{Total}}{\dot{m}_{Product}} \quad (43)$$

$$CO_2\ break\text{-}even\ point = \frac{EF_i + \dot{m}_{Product}}{P_{Total}} \quad \text{i … comparison} \quad (44)$$

Table 5: Emission factors of fossil-based fuels, methanol and biodiesel.

Product	Emission factor [kg CO_2eq/kWh$_{ch.}$]	Source
Biodiesel	0.171	[112]
Diesel	0.321	[112]
Gasoline	0.341	[112]
Methanol (natural gas)	0.342	[115,116]
Methanol (coal)	0.569	[115,116]

3 Results and Discussion

The most important results based on **Journal Articles I-V** and **Conference Papers I** and **II** as well as additional findings based on those are presented in the following chapter. The journal articles' overlaps and their comparison to existing studies are discussed after every subchapter. In addition, all subchapters are summed up by intermediate conclusion sections, which serve as a foundation for this thesis's overall conclusion.

3.1 Process Design for Power-to-Liquid Plants

3.1.1 Power-to-Green Methanol based on Oxy-fuel or Air Combustion

Journal Article I provided a simulation study of a Power-to-Green methanol plant based on stationary fluidized bed combustion with a 20 $MW_{th.}$ wood chips fuel input. The main objective was to determine possible synergies between alkaline electrolysis, producing oxygen as a by-product, and oxy-fuel combustion systems, requiring a mixture of oxygen and recirculated flue gas as a fluidization agent. In doing so, two PtL process routes have been designed, i.e., oxy-fuel combustion in combination with a DeOxo reactor and a conventional route based on air combustion and MEA-based CO_2 capture. Table 6 summarizes the sub-processes' design parameters.

Table 6: Design parameters of the Power-to-Green methanol plant.

Oxy-fuel route				Air combustion route			
Sub-process	Parameter	Value	Unit	Sub-process	Parameter	Value	Unit
Oxy-fuel comb.	$\dot{Q}_{Fuel,in}$	20	$MW_{th.}$	Air comb.	$\dot{Q}_{Fuel,in}$	20	$MW_{th.}$
DeOxo reactor	$\dot{V}_{in}$	4,333	Nm^3/h	CO_2 capture	$\dot{V}_{in}$	27,000	Nm^3/h
AEL	P_{AEL}	57	$MW_{el.}$	AEL	P_{AEL}	54	$MW_{el.}$
MeOH synthesis	$\dot{V}_{in}$ [1)]	16,000	Nm^3/h	MeOH synthesis	$\dot{V}_{in}$ [1)]	16,850	Nm^3/h
Distillation	$\dot{m}_{Crude}$	8.5	t/h	Distillation	$\dot{m}_{Crude}$	7.7	t/h

1) Fresh syngas, excluding recirculated tail gas.

The respective process routes primary input and output streams are listed in Table 7.

Table 7: Main input and output streams of the Power-to-Green methanol plant.

Oxy-fuel route				Air combustion route			
Inputs		Outputs		Inputs		Outputs	
Wood chips	6.1 t/h	Methanol	5.5 t/h	Wood chips	6.1 t/h	Methanol	4.9 t/h
Air	-	Oxygen	2.9 t/h	Air	29.3 t/h	Oxygen	7.8 t/h
Water	2.3 t/h	Off-gas	-	Water	1.9 t/h	Off-gas	24.6 t/h
Electricity	55.2 $MW_{el.}$	DH	10 $MW_{th.}$	Electricity	58.3 $MW_{el.}$	DH	2.8 $MW_{th.}$

The AEL unit's rated power input is a central design parameter of the proposed plant layout. A power input of 57 $MW_{el.}$, 54 $MW_{el.}$ for the methanol synthesis and 3 $MW_{el.}$ to provide the DeOxo reactor with hydrogen, is required to utilize the total amount of CO_2 emitted by the combustor. Minimum power input of 39 $MW_{el.}$ is necessary to provide the oxy-fuel combustor with sufficient oxygen, i.e., 6.2 t/h. A 6.1 t/h wood chips input is required to produce 5.5 t/h methanol with the oxy-fuel and 4.9 t/h methanol with the conventional air combustion route.

The respective routes' main differences are their oxygen and district heating outputs. Almost five additional tons of oxygen per hour could be sold as a by-product for the air combustion route. However, only 2.8 $MW_{th.}$ can be transferred to a district heating network, compared with 10 $MW_{th.}$ for the oxy-fuel route due to the CO_2 capture unit's heat demand.

3.1.2 Fischer-Tropsch Synthesis at a Pilot-Scale

Establishing a feasible process route for a PtL plant combining Fischer-Tropsch synthesis and solid-oxide electrolysis at a scale of 1 $MW_{el.}$ rated electrolyzer power was the objective of **Journal Article II**. This study's mass and energy balances could serve as a design foundation for subsequent basic and detail engineering studies. Figure 3 displays the determined pilot-scale plant design.

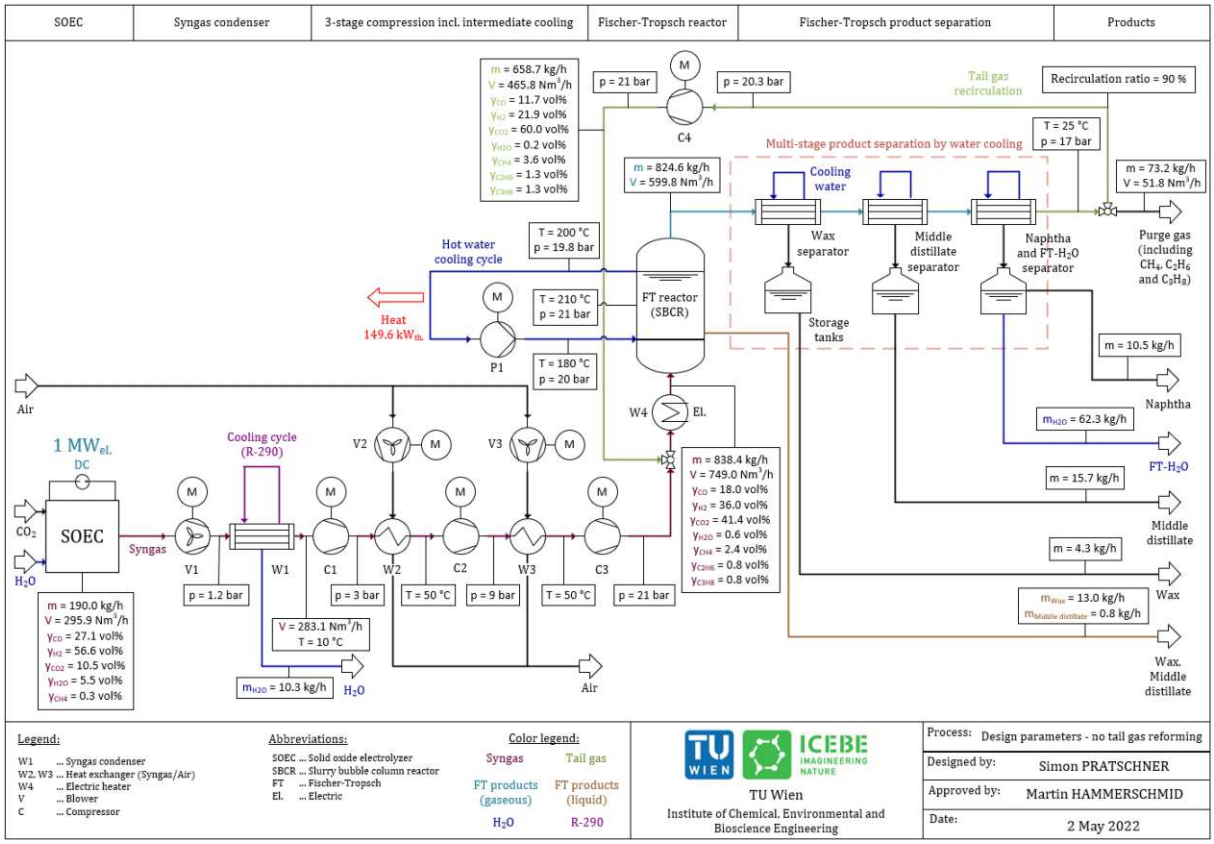

*Figure 3: Process flow diagram and design parameters of a pilot-scale PtL plant [**Journal Article II**].*

CO_2 and water are converted into syngas, consisting of H_2, CO and unconverted educts, by a 1 $MW_{el.}$ SOEL unit. Excess water is condensed from the syngas stream before being pressurized to 21 bar by a three-stage compressor, including intermediate cooling with air. The pressurized syngas is mixed with the recirculated tail gas and is fed into the FT reactor at a temperature of 210°C. The product separation section comprises three water-cooled separators, separating the FT syncrude into the product fractions wax, middle distillate and naphtha. A share of the unconverted gases and gaseous FT products, i.e., methane, ethane and propane, are recirculated to the FT reactor's inlet with an additional compression step to compensate the pressure drop caused by the reactor and product separation step. The non-recirculated share of tail gas is drained from the system to avoid the accumulation of inert gases, e.g., CO_2, and products, e.g., CH_4. In addition, combusting the purge gas is necessary to supply the PtL plant with high-temperature heat.

Several process simplifications were realized compared with industrial plants to ensure the pilot-scale plant's feasibility and affordability:

- No separate CO_2 capture unit is considered.
- Intermediate syngas cooling with air instead of water.
- Simplified multi-stage product separation by water cooling instead of an intricate syncrude refinery concept.
- Exclusion of a reformer within the tail gas recycle loop to avoid an additional high-temperature and high-pressure apparatus.

A total mass flow rate of Fischer-Tropsch products of 44.3 kg/h, 39 wt% wax, 37 wt% middle distillate and 24 wt% naphtha, are produced based on a syngas input of 190 kg/h. In addition, 62.3 kg/h of FT product water is produced and 73.2 kg/h of purge gas is purged out of the system.

3.1.3 Fischer-Tropsch Synthesis at an Industrial Scale

Extending **Journal Article II**'s process design to an extensive PtL plant concept was a central outcome of **Journal Article III**. A process flow diagram is depicted in Figure 4. Maximizing the PtL plant's productivity and efficiency is vital to ensure an economical operation. The following extensions have been added to the pilot-scale concept:

- Implementation of an MEA-based CO_2 capture unit model.
- Implementation of an SOEL model operating in co-electrolysis mode.
- Intermediate syngas cooling with water instead of air.
- Improvement of the Fischer-Tropsch product refinery concept.
- Implementation of a steam tail gas reformer in the tail gas recycle loop.
- Basic heat integration.

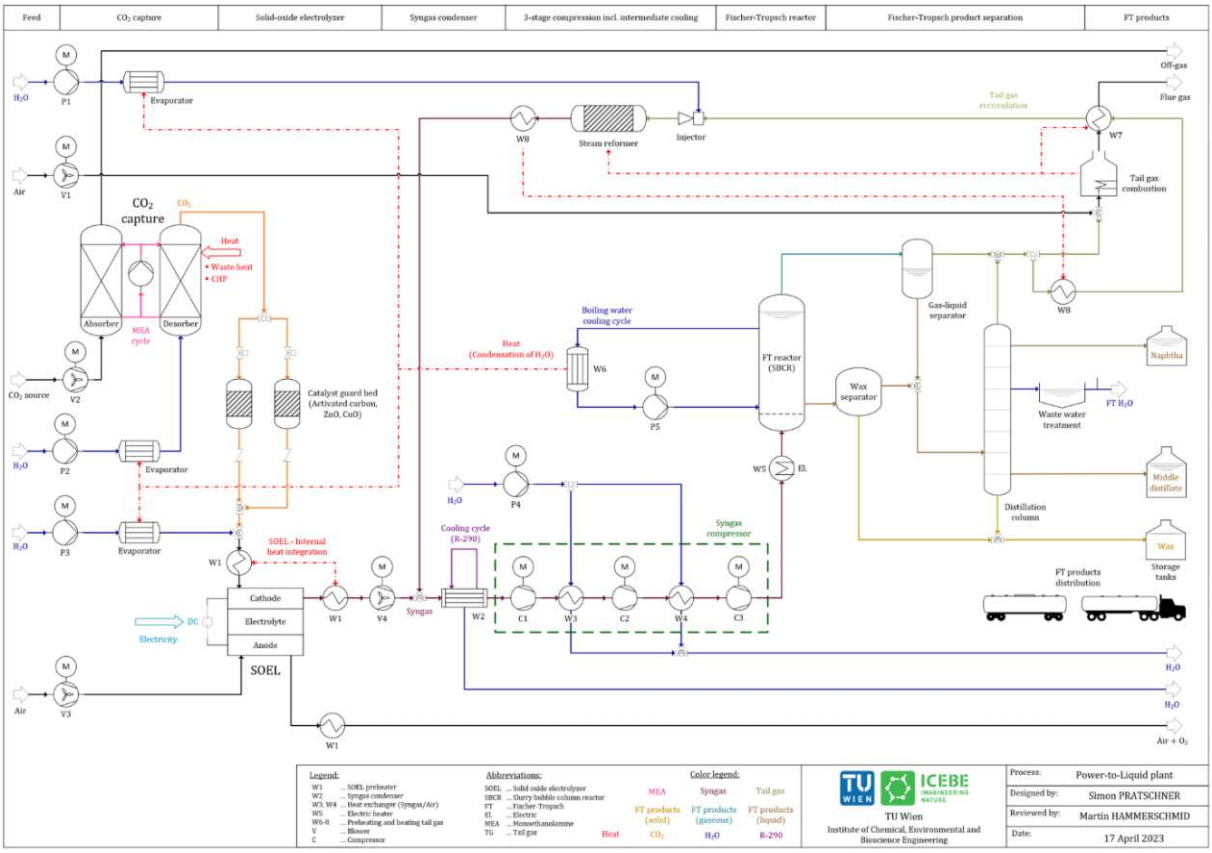

*Figure 4: Process flow diagram of a Power-to-Liquid plant at an industrial scale [**Journal Article III**].*

PtL plants can be based on point CO_2 sources, e.g., biogas upgrading, ethanol, cement, steel or combined heat and power (CHP) plants or combined with direct air capture (DAC) technology. Different CO_2 capture technologies must be applied depending on the CO_2 stream's concentration.

3.1.4 Discussion of Chapter "Process Design for Power-to-Liquid Plants"

Journal Article I compared two process routes based on oxy-fuel or air combustion of wood chips. Large electrolyzers with a rated power of around 55 $MW_{el.}$ are required to utilize the flue gas stream of a 20 $MW_{th.}$ CHP plant, thus making the synthesis process itself the plant's primary process. The oxy-fuel route is based on the assumption that oxygen, a by-product of the alkaline electrolyzer, is utilized in the combustion reactor to provide a CO_2-rich stream to the subsequent methanol synthesis. A minimum electrolyzer electricity input of 38.5 $MW_{el.}$ is necessary to provide the oxy-fuel combustor with sufficient oxygen. A major setback of this variant is that additional H_2 is required to remove the CO_2 stream's excess oxygen. In addition, only 2.9 t/h oxygen can potentially be sold as a by-product compared with 7.8 t/h for the air combustion route. The advantages of the oxy-fuel route are its 12% increase in produced methanol and a significantly larger heat output of 10 $MW_{th.}$, compared with 2.8 $MW_{th.}$ for the air combustion route.

The desired plant location is the most significant decision-making parameter between the proposed process routes. The oxy-fuel configuration is advantageous for plant locations with adjacent consumers of heat, e.g., villages located at higher latitudes or industries with a high demand for process steam. Existing district heating networks would significantly lower the required fixed capital investment. Process routes based on air combustion are more flexible concerning the share of valorized CO_2 and, thus, are better suited for locations with a fluctuating yield of renewable power sources. In addition, coupling the air combustion-based route with adjacent oxygen-consuming industries can significantly improve the plant's profitability.

The Fischer-Tropsch process routes of **Journal Articles II** and **III** are based on a solid-oxide instead of an alkaline electrolyzer. Cobalt-based FT processes require syngas consisting of CO and H_2 with an H_2:CO ratio of 2. Adapting the H_2O:CO_2 ratio at the solid-oxide electrolyzer's inlet allows flexible control of the outlet stream's H_2:CO ratio [86,95], thus ensuring a vital synergy with Fischer-Tropsch processes, including tail gas reforming. High-temperature electrolyzers have lower TRL and stack lifetimes than AEL and PEMEL units but can potentially decrease electricity consumption by 20% [78]. Alternative process routes for Fischer-Tropsch plants applying a cobalt-based catalyst combine AEL or PEMEL units with an rWGS reactor to convert CO_2 to CO and adjust the required H_2:CO ratio [117,118]. These concepts profit from a higher process maturity and, thus, could be deployed faster than plants based on SOEL units. However, implementing an additional rWGS reactor entails a more complicated system integration and energy losses due to an additional conversion step.

3.1.5 Conclusions of Chapter "Process Design for Power-to-Liquid Plants"

Large electrolyzers, at a rated power of 2.5 times larger than the plant's thermal input, are required to utilize the entire CO_2 stream emitted by biomass-based CHP processes. Implementing oxy-fuel combustion can potentially increase the methanol output but requires additional H_2 to remove the flue gas stream's O_2 content. The technology's initial purpose was to provide a highly concentrated CO_2 stream for enhanced oil recovery or carbon capture and storage applications. Implementing the technology in carbon capture and utilization processes entails a major challenge, i.e., missing a feasible solution for removing excess O_2 in the flue gas stream. Preferable plant locations for the oxy-fuel process route are sites with a high demand for heating or process steam, e.g., by adjacent villages or industries, due to a heat output of 10 $MW_{th.}$. Implementing a Power-to-Green methanol plant based on air combustion is more beneficial when coupled with oxygen-consuming industries, as it increases the plant's overall profitability.

Simplified process designs are required to increase the deployment speed and feasibility of pilot-scale Power-to-Liquid plants. In addition, pilot plants should focus more on evaluating the process's behavior in different environments and under changing circumstances. Assessing the synergy between the SOEL and the FT unit is projected to be a vital outcome of the pilot plant's operation. The following simplifications for pilot plants compared to industrial plants have been implemented in **Journal Articles II** and **III**.

- A CO_2 capture unit and a feed gas cleaning section have been excluded.
- A simple multi-stage product separation based on water-cooling instead of an intricate refinery concept was realized.
- The tail gas reformer has been excluded to avoid an additional high-temperature and pressure reactor.

Future research efforts concerning the design of PtL plants should focus on integrating sub-processes and heat exchangers. In addition, elaborate designs of the product separation and refining process sections are required. A tangible decision regarding the desired product of PtL plants based on FT synthesis is the first step toward designing a tailor-made refinery concept. Detailing the crude methanol separation and refining process step should be oriented after existing concepts for PtL plants producing methanol based on CO or CO_2 hydrogenation.

3.2 Power-to-Liquid Efficiency and Carbon Efficiency

The Power-to-Liquid efficiency, indicating the share of applied electricity being stored chemically as liquid products, and the carbon efficiency, indicating the share of carbon stored in products, are key performance indicators for PtL plants. A detailed definition is provided in Chapter 2.4.

3.2.1 PtL Efficiency of Green Methanol Based on Oxy-Fuel and Air Combustion

Designing and assessing a Power-to-Green methanol plant, based on a CHP plant with a thermal input of 20 $MW_{th.}$, was the main objective of **Journal Article I**. As stated in Chapter 3.1.1, a minimum electricity input of 38.5 $MW_{el.}$ into the electrolyzer is required to supply the oxy-fuel CHP plant with sufficient oxygen. Thus, additional oxygen, e.g., produced by an air separation unit, is necessary for operation periods obtaining a lower electricity supply. Table 8 summarizes the plant's determined PtL efficiencies in oxy-fuel and air combustion mode.

Table 8: Determined Power-to-Liquid efficiencies of the designed Power-to-Green methanol plant.

	Power-to-Liquid efficiency [%]	
Process route	Wind speed = 4 m/s	Wind speed > 12 m/s
Oxy-fuel	21.0	51.9
Air combustion	54.2	54.2

The significant variation in the oxy-fuel combustion route's PtL efficiency is caused by the assumed electricity supply by an adjacent wind park. The chosen wind turbine model starts to operate at a wind velocity of 4 m/s at hub height, hence providing insufficient electricity to the AEL unit for low wind velocities. Thus, additional oxygen has to be provided by an ASU powered with grid electricity. An inferior PtL efficiency of only 21.0% is achieved at the wind velocity's lower limit of 4 m/s. The maximum PtL efficiency of 51.9% was observed for operating points in which the wind park was operating at its maximum capacity at wind speeds exceeding 12 m/s. The air combustion mode's PtL efficiency of 54.2% does not depend on the wind velocity since the share of utilized CO_2 is adapted to the current power input into the electrolyzer.

3.2.2 Power-to-Liquid Efficiency - Solid-Oxide Electrolysis and Fischer-Tropsch

Journal Article II evaluated the Power-to-Liquid efficiency, including the product fractions naphtha, middle distillate and wax, of a pilot-scale plant based on SOEL and FT synthesis, excluding a CO_2 capture unit. A simple multi-stage product separation step based on water-cooling was implemented to keep the plant's complexity at a moderate level. The obtained PtL efficiencies of three analyzed process routes, i.e., once-through, without a tail gas reformer and with a tail gas reformer, are summarized in Table 9.

Table 9: Determined Power-to-Liquid efficiencies for a pilot-scale PtL plant.

Process configuration	Power-to-Liquid efficiency [%]
Once-through	30.8
Without a tail gas reformer	50.8
With a tail gas reformer [1)]	62.7

1) Modeled as a Gibbs minimization reactor in FactSage.

Within **Journal Article III**, the PtL efficiency of an industrial PtL plant combining SOEL and FT synthesis was evaluated based on different CO_2 sources. Additional process models were established to realize an industrial process route, i.e., a detailed SOEL model, an MEA-based CO_2 capture unit model and a stoichiometric tail gas steam reformer. The respective CO_2 sources' PtL efficiencies are stated in Table 10. PtL efficiencies ranging from 54.7% to 63.8% were determined for tail gas recirculation ratios between 75% and 90%. The sub-processes' relative power consumption is provided in Table 11. The most significant share of electricity, 89.1%, is consumed by the electrolyzer.

Table 10: Determined Power-to-Liquid efficiencies for different CO_2 sources.

CO_2 source	η_{PtL} [%]	Tail gas recirculation ratio [%]
Cement plant	58.8	85
Biogas upgrading plant	63.8	90
Biomass-based CHP plant	54.7	75

Table 11: Relative power consumption based on a cement plant as a CO_2 source.

Sub-process	Share of power consumption [%]
SOEL unit	89.1
Syngas compression	7.1
Syngas condenser	0.8
CO_2 capture	2.0
Auxiliaries	1.0

3.2.3 Discussion Concerning Power-to-Liquid Efficiency

The oxy-fuel plant route's low PtL efficiency of 21.0% at low wind velocities makes the proposed concept unfeasible for locations obtaining low annual average wind speeds and projects based on small-scale electrolyzers. In addition, the concept's significant dependability on grid electricity increases its vulnerability to fluctuating electricity market prices and high emission factors of specific local grid electricity mixes. Applying air combustion results in a potential PtL efficiency of 54.2%, independent of the electrolyzer's scale or power input. In addition, no ASU, powered with grid electricity, is required for this process route.

Comparable studies analyzing the efficiency of PtL processes combining low-temperature electrolysis and methanol synthesis determined PtL efficiencies ranging from 46.0% to 58.0%, as summarized in Table 12.

Table 12: Determined Power-to-Liquid efficiencies of comparable studies producing methanol.

	[46]	[46]	[118]	[94]	**Journal Article I**
η_{PtL} [%]	46.0 [1)]	58.0 [2)]	50.0	47.0-51.0	54.2

1) Lower limit.
2) Upper limit with an assumed electrolyzer efficiency of 70%.

The determined PtL efficiency of 54.2% for a green methanol plant based on the air combustion of wood chips and an alkaline electrolyzer lies in the upper range of comparable evaluations. One reason for that observation is that no methanol losses were considered in the product separation and purification step. In addition, a specific power consumption of 4.45 $kWh_{el.}/Nm^3$ hydrogen was assumed for the AEL unit, corresponding with an electrolyzer efficiency of 67%. Thus, the focus of potential future studies should be detailing the distillation unit's design and varying the electrolyzer's power consumption.

To the author's best knowledge, no comparable studies combining oxy-fuel combustion and PtL plants were available at the time of this writing. The best-case scenario of 51.9% lies within the range of studies based on air combustion. However, the lowest obtained PtL efficiency of 21.0%, obtained at low wind speeds, is not competitive.

PtL plants based on high-temperature electrolyzers have the highest potential concerning their PtL efficiency. Overall, pilot-scale PtL plants are projected to achieve a lower PtL efficiency than industrial plants due to a simplified process design, less sophisticated heat integration and a higher weighting of auxiliary equipment for process control and supervision. The limiting factors of **Journal Article II** include the absence of a CO_2 capture unit and the lack of an elaborate SOEL model.

A more holistic assessment was realized within **Journal Article III** by establishing IPSEpro process models for the CO_2 capture, the SOEL and the tail gas reforming unit. The most significant factor influencing the PtL efficiency is the available heat supply for the CO_2 capture step. Exploiting industrial waste heat is crucial in making PtL plant concepts feasible and efficient. Less tail gas must be combusted if enough heat is provided to the CO_2 capture unit, thus increasing process productivity and efficiency. Hence, sector coupling is a cornerstone of future industrial sites including PtL plants.

Utilizing highly concentrated CO_2 sources, e.g., biogas upgrading plants, is an additional lever to quickly deploy decentralized PtL plants at scales of around 20 $MW_{el.}$ rated electrolyzer power. The obtained best-case scenario of **Journal Article III** valorizes CO_2 emitted by a biogas upgrading plant, achieving a PtL efficiency of 63.8%. No additional CO_2 capture unit is required, enabling a tail gas recirculation ratio of 90%.

Detailed refinery concepts, specifically designed for a clearly defined product, are required based on the presented plant configuration. Typical FT refinery processes result in additional chemical energy losses ranging from 10% to 20% [34]. Establishing a refinery concept converting FT syncrude into drop-in fuels was part of an associated journal article within this thesis's framework [119]. In addition, future studies should integrate a detailed method estimating the additional power demand of auxiliary units for industrial PtL plants.

Table 13 contextualizes the obtained results in **Journal Article III** with previously conducted studies combining FT synthesis and SOEL.

Table 13: Determined Power-to-Liquid efficiencies of comparable studies based on SOEL and FT.

	[120]	[121]	[94]	[122]	**Journal Article III**
$\eta_{PtL,min}$ [%]	51.0	50.0	45.0	56.6	54.7
$\eta_{PtL,max}$ [%]		53.9	63.0	75.8	63.8

A comparison with alternative process routes, i.e., FT and PEMEL, FT based on direct air capture, Biomass-to-Liquid as well as Power and Biogas-to-Liquid via a plasma Boudouard reactor, is provided in Table 14. PtL plants based on low-temperature electrolyzers obtain similar energy efficiency rates, around 50%, as Biomass-to-Liquid processes. Power and Biogas-to-Liquid processes, based on CO_2, CH_4, water and power as feedstocks, can potentially reach energy efficiencies of 56% based on an overall plasma Boudouard reactor efficiency of 86%. PtL processes based on direct air capture obtain inferior energy efficiencies below 35%. Thus, projects commissioned within the next years should exploit concentrated CO_2 point sources.

Table 14: Comparison with maximum efficiencies of alternative process routes.

Process route	Max. energy efficiency [%]	Source
DAC, PEMEL and FT	36.3	[123]
Low-temperature electrolyzer and FT	53.0	[94]
Biomass-to-Liquid	51.0	[119]
Power and Biogas-to-Liquid	56.0	[124]

3.2.4 Conclusions Concerning Power-to-Liquid Efficiency

The determined PtL efficiencies in **Journal Article I**, based on low-temperature electrolysis and methanol synthesis, were 54.2% for the air combustion route and ranged from 21.0% to 51.9% for the oxy-fuel combustion route. Combining oxy-fuel combustion and PtL processes can be feasible when implemented at locations with adjacent heat or process steam consumers. Large-scale electrolyzers exceeding 39 $MW_{el.}$ and high yields of renewable power sources are required to avoid an additional air separation unit.

Journal Articles II and **III** evaluated the PtL efficiency of a plant concept combining a high-temperature electrolyzer and Fischer-Tropsch synthesis. PtL efficiencies ranging from 30.8 to 62.7% were determined for different process configurations of a pilot-scale plant. Three CO_2 sources, i.e., cement, biogas upgrading and biomass CHP plant, were assessed within **Journal Article III**. The obtained PtL efficiencies were 54.7% (biomass CHP plant), 58.8% (cement plant) and 63.8% (biogas upgrading plant). Valorizing biogenic and highly concentrated CO_2 sources should be prioritized for the first generation of PtL plants. Furthermore, CO_2 point sources provided by the process industry should be utilized before implementing DAC-based PtL plants.

3.2.5 Carbon Efficiency of Green Methanol Based on Oxy-Fuel and Air Combustion

Determining the processes' carbon efficiency was not initially included in the scope of **Journal Article I** but has been amended within the presented thesis. The oxy-fuel combustion route obtained a superior maximum carbon efficiency of 98.1%, whereas a carbon efficiency of 88.2% was obtained for the air combustion process route. The essential difference between those routes was the necessary CO_2 capture unit, MEA-based absorption, for the configuration based on air combustion.

3.2.6 Carbon Efficiency - Solid-Oxide Electrolysis and Fischer-Tropsch Synthesis

Finding the carbon efficiencies of a PtL plant at an industrial scale based on three CO_2 sources was a central objective of **Journal Article III**. The obtained efficiencies and shares of carbon streams are stated in Table 15. A maximum carbon efficiency of 88.6% was realized by a PtL plant based on a biogas upgrading unit. Utilizing CO_2 emitted by a cement plant resulted in a carbon efficiency of 75.7%, whereas a carbon efficiency of 68.4% was found when valorizing CO_2 emitted by a biomass-based CHP plant.

Table 15: Determined carbon efficiencies and carbon losses of a PtL plant combining SOEL and FT synthesis.

CO_2 source	Carbon efficiency [%]	MEA off-gas [%]	Purge gas [%]
Cement plant	75.7	10.0	14.3
Biogas upgrading plant	88.6	-	11.4
Biomass-based CHP plant	68.4	10.0	21.6

3.2.7 Discussion Concerning Carbon Efficiency

Oxy-fuel combustion-based PtL routes have the highest potential concerning carbon efficiency, obtaining a maximum value of 98.1% due to their complete combustion process to CO_2 and H_2O, thus not requiring an additional CO_2 capture unit. The major difference in comparison with conventional air combustion routes, obtaining a maximum carbon efficiency of 88.2%, is caused by the MEA absorber's CO_2 slip. The found carbon efficiencies within **Journal Article I** should be evaluated critically and serve as a best-case scenario's upper threshold due to the following limitations. The obtained mass balances are based on optimistic assumptions regarding the synthesis loop's CO_2 conversion to methanol without an additional rWGS reactor adjusting the syngas's carbon oxide ratio. In addition, no methanol losses caused by the gas-liquid separator and the following distillation process were considered.

Biogas upgrading plants must comply with local grid feed-in regulations, thus providing highly concentrated CO_2 streams. Prioritizing PtL plants valorizing CO_2 streams emitted by biogas upgrading plants, resulting in a carbon efficiency of 88.6%, is vital in maximizing the positive impact on climate change of PtL plants on a short-term basis. Cement plants have the potential to cover a part of the CO_2 capture unit's heat demand, resulting in a carbon efficiency of 75.7%. The lowest efficiency was found for the configuration based on a biomass-based CHP plant since 25% of the tail gas stream had to be combusted to supply the CO_2 capture process with heat.

Table 16 contextualizes this thesis's findings with comparable studies. The central factors affecting the carbon efficiency of PtL plants are the CO_2 source's concentration, the applied CO_2 capture technology, the synthesis reactor's per-pass conversion and the share of recirculated tail gas, i.e., the synthesis loop's overall conversion.

Table 16: Carbon efficiencies of comparable studies.

	[117]	[118]	[118]	[123] [4)]	**Journal article I**	**Journal article III**
$\eta_{Carbon,min}$ [%]	54.0 [1)]	85.0 [1)]	87.0 [3)]	58.1	88.2	68.4
$\eta_{Carbon,max}$ [%]	64.0 [2)]			73.8	98.1	88.6

1) PEMEL + FT; 2) SOEL + FT; 3) SOEL + MeOH; 4) DAC + FT.

3.2.8 Conclusions Concerning Carbon Efficiency

The carbon efficiencies determined within **Journal Articles I** and **II** are summarized in Table 17. The found carbon efficiencies in **Journal Article I** are based on optimistic assumptions concerning the synthesis loop's overall carbon conversion to methanol and thus should be seen as an upper threshold for PtL processes. The oxy-fuel process route can obtain a higher carbon efficiency since there are no CO_2 losses caused by the CO_2 capture technology. **Journal Article III** is based on improved sub-process models and provides a realistic assessment concerning the achievable carbon efficiency of Power-to-Liquid plants for different CO_2 sources. The highest carbon efficiency of 88.6% was achieved by the route based on a biogas upgrading plant as a CO_2 source since a tail gas share of only 10% had to be combusted for internal heat supply.

Table 17: Summary of determined carbon efficiencies of Power-to-Liquid plant concepts.

Process route / CO_2 source	Description	Carbon efficiency [%]
Oxy-fuel route	Oxy, AEL, MeOH	98.1
Air combustion route	Air, AEL, MeOH	88.2
Cement plant	SOEL, FT	75.7
Biogas upgrading plant	SOEL, FT	88.6
Biomass-based CHP plant	SOEL, FT	68.4

3.3 CO_2 Footprint of Fischer-Tropsch Products

Conference Paper I focused on determining the CO_2 footprint of Fischer-Tropsch products for different electricity sources based on the process modeling and plant design of **Journal Articles II** and **III**. The ecological evaluation considered solely the electricity's emission factor $EF_{El.}$ and excluded the plant equipment's CO_2 footprint. Figure 5 displays the Fischer-Tropsch products' emission factor EF_{FT} as a function of the electricity source's emission factor. The horizontal lines indicate the comparison to the direct and indirect GHG emissions of fossil gasoline and diesel. Applying wind power has the highest GHG savings potential with an obtained EF_{FT} of only 0.12 kg CO_2eq/kg$_{FT}$. Using certified green Austrian electricity, mainly hydropower and wind power, yields a low emission factor of 0.29 kg CO_2eq/kg$_{FT}$. Producing FT products based on photovoltaic power results in an emission factor of FT products of 1.38 kg CO_2eq/kg$_{FT}$.

A different picture emerges when utilizing 2022 EU grid electricity mixes for Power-to-Liquid plants. Applying electricity produced in Austria, excluding imports, results in an emission factor of 2.95 kg CO_2eq/kg$_{FT}$, showing only minor improvements compared with fossil diesel. FT products based on the EU's average grid electricity emission factor show a detrimental effect on climate change with an emission factor of 5.47 kg CO_2eq/kg$_{FT}$, an increase of 46% compared with fossil diesel.

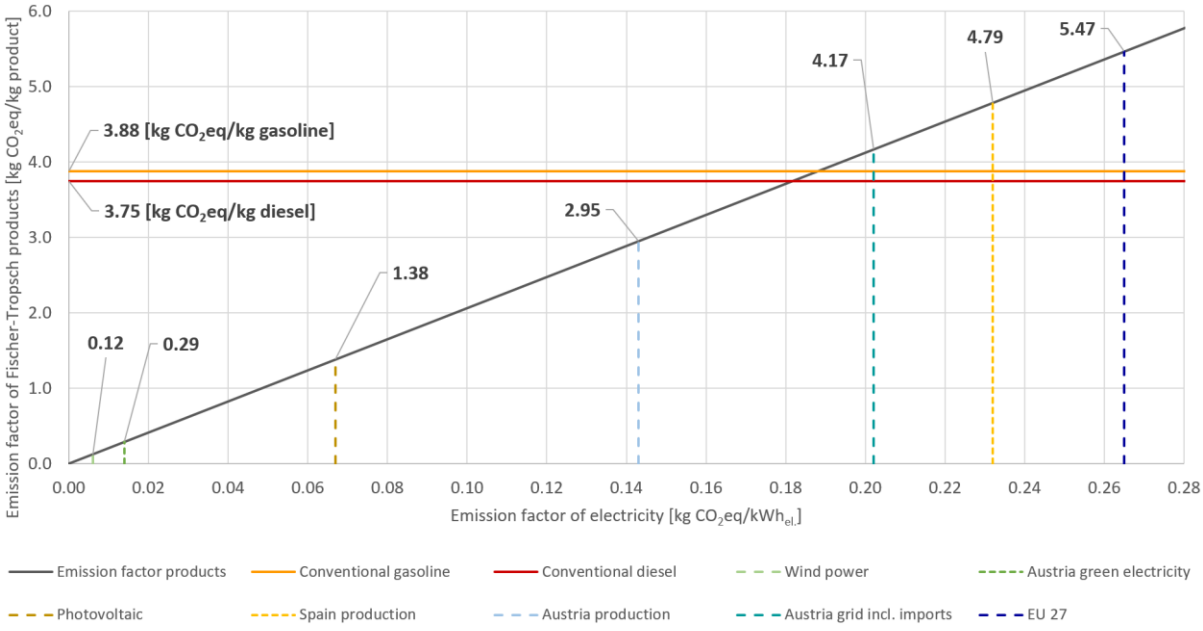

*Figure 5: FT products' emission factor depending on the electricity's emission factor [**Conference Paper I**].*

The CO_2 break-even points of FT products compared with rapeseed biodiesel, fossil diesel and fossil gasoline are depicted in Figure 6. An electricity source with an emission factor below 0.085 kg CO_2eq/kWh$_{el.}$ is required to obtain superior results compared to biodiesel based on rapeseed. Electricity emission factors below 0.188 kg CO_2eq/kWh$_{el.}$ are needed to achieve lower emission factors than fossil-derived fuels.

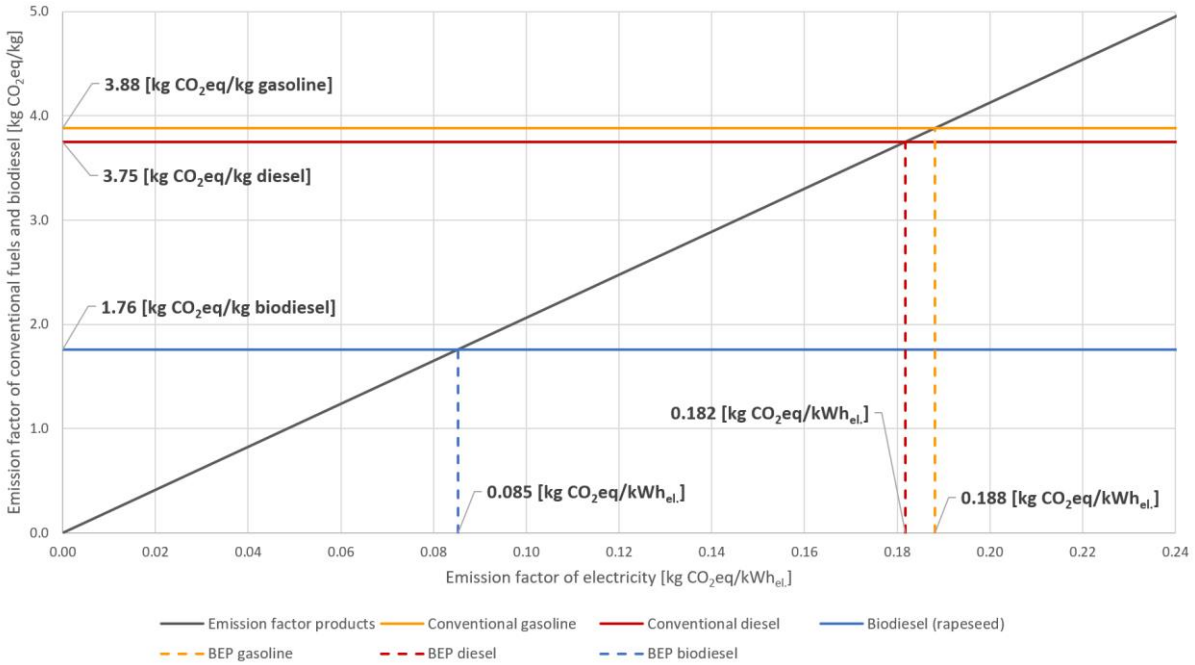

*Figure 6: CO_2 break-even points of FT products compared with biodiesel and fossil fuels [**Conference Paper I**].*

Conference Paper I's outcomes highlight that powering Power-to-Liquid plants with renewable power sources is necessary to ensure their benign effect on curbing the climate crisis. Applying wind power results in a potential reduction in GHG emissions of over 95% compared with fossil diesel. Lower emission factors than biodiesel can be obtained by utilizing photovoltaic power. Overall, a decrease in GHG emissions of about 65% compared with fossil diesel can potentially be achieved by FT products based on photovoltaic power. Applying today's EU average grid electricity mix entails an increase in GHG emissions of 46% compared with fossil diesel. Thus, increasing the share of renewables is a linchpin to deploying Power-to-Liquid plants at a large scale. As of 2022, only four national grid electricity mixes are suited for Power-to-Liquid applications in the European Union, i.e., Sweden, Denmark, Finland and France. The emission factors of national grid electricity mixes underlie daily and seasonal fluctuations depending on the mix's respective share of renewable power sources. Thus, grid electricity can potentially have a benign impact in periods with a high yield of renewable power sources.

The CO_2 source has not been defined within **Conference Paper I**. Ongoing research could assess the emission factor of Fischer-Tropsch products for different CO_2 sources. In addition, a clear definition of the products' application is required. This study has not considered the additional CO_2 footprint caused by potential downstream refining processes. The emission factor of national grid electricity mixes underlies significant daily and seasonal variations. Hence, dynamic process simulation can detail the presented study's time resolution.

3.4 Techno-Economic Assessments

This chapter summarizes and analyzes the economic findings of **Journal Article IV**, analyzing a Power-to-Green methanol plant, and **Journal Article V**, assessing off-grid and grid-based scenarios of a plant combining SOEL and FT synthesis.

3.4.1 Power-to-Green Methanol

Conducting an economic evaluation of **Journal Article I**'s plant concept was realized in **Journal Article IV**. The primary objectives were to determine the net production costs of green methanol possibly realized by the suggested plant layout and the necessary CO_2 price to make green methanol cost-competitive with fossil-based methanol. A hybrid power plant model, comprising a wind park, photovoltaic farm, CHP process and grid connection, was established based on the Global Wind Atlas 3.0, provided by the Danish Technical University (DTU) [110] and the Photovoltaic Geographic Information System (PVGIS), provided by the European Commission [111].

The total required FCI of the base scenario, based on a 50 $MW_{el.}$ alkaline electrolyzer, is 118.6 million $€_{2022}$, excluding the wind park and photovoltaic plant. The respective revenue shares are 71% methanol, 17% oxygen and 12% district heating. Table 18 lists the required methanol prices for varying amortization periods and plant scales. CO_2 prices ranging from 223 to 308 €/t are required to make the non-profit scenarios, i.e., based on an amortization period of 25 years, cost-competitive with fossil-based methanol prices in Germany as of 2022 [125].

*Table 18: Required green methanol prices for amortization periods of 5, 15 and 25 years [**Journal Article IV**].*

	Required methanol price for an amortization period of		
Electrolyzer scale	5 years	15 years	25 years
50 $MW_{el.}$	1,107 $€_{2022}$/t	833 $€_{2022}$/t	782 $€_{2022}$/t
100 $MW_{el.}$	995 $€_{2022}$/t	761 $€_{2022}$/t	717 $€_{2022}$/t

Assumptions: Discount rate of 8%, plant lifetime of 25 years and plant availability of 8,000 h/a.

The green methanol net production costs obtained in **Journal Article IV** are displayed in Figure 7. The cost centers' shares, i.e., CAPEX, fixed OPEX, variable OPEX, stack replacement and catalysts were analyzed for varying plant scales from 50 to 1,000 $MW_{el.}$. NPC of 785 $€_{2022}$/t were obtained for the base scenario with an electrolyzer scale of 50 $MW_{el.}$. Scaling up the plant to 1 $GW_{el.}$ entails a reduction in NPC to 569 $€_{2022}$/t. The share of variable OPEX, mainly electricity costs, rises from 54.8% to 69.8% since the electricity costs are directly proportional to the plant's methanol output and, thus, do not benefit from the economies of scale's effect.

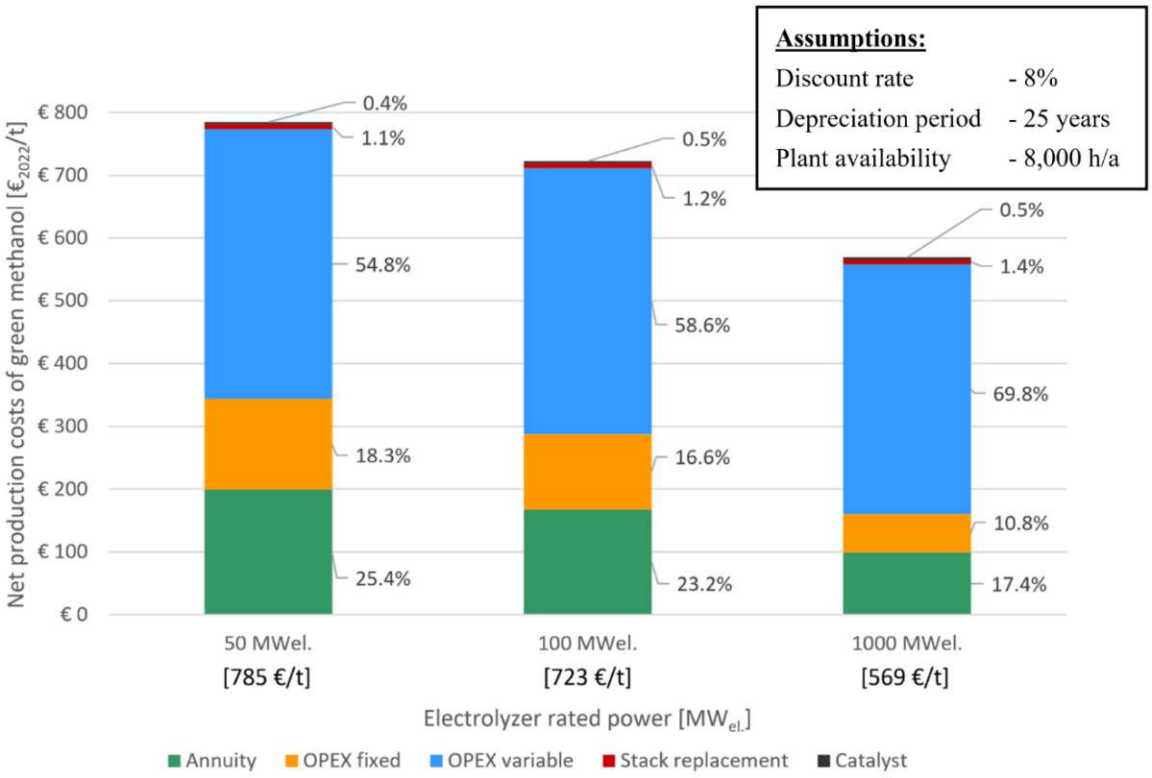

*Figure 7: Net production costs and cost centers of a Power-to-Green methanol plant [**Journal Article IV**].*

The sensitivity analysis results are depicted in Figure 8. The influence of grid electricity prices on NPC could be curbed by establishing a hybrid power plant, including the feed-in of surplus electricity. Doubling the grid electricity price from 0.2 to 0.4 €$_{2022}$/kWh$_{el.}$ results in an increase in NPC of only 3%. The plant availability has a significant influence on the PtL plant's economic performance. Reducing the annual operating hours from 8,000 to 2,000 entails an increase in NPC of 168%, whereas a reduction to 4,000 yearly operating hours leads to an increase of only 56%.

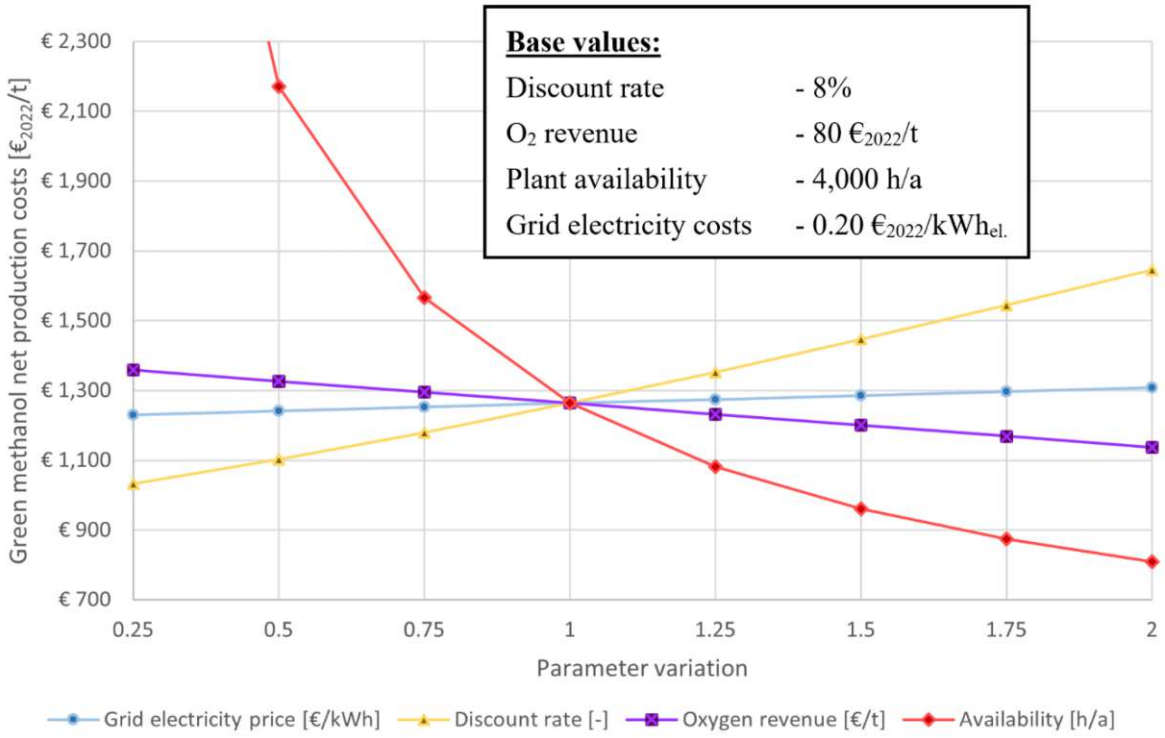

*Figure 8: Sensitivity analysis - Power-to-Green methanol plant [**Journal Article IV**].*

3.4.2 Fischer-Tropsch Products - Off-Grid vs. Grid-Based PtL Plants

The techno-economic assessment of a PtL plant, based on a solid-oxide electrolyzer and Fischer-Tropsch synthesis, conducted within **Journal Article V**, is based on the process design and modeling of **Journal Articles II** and **III**. The article's primary objective was to compare the economic performance of off-grid and grid-based PtL plants. In addition, a sensitivity analysis was conducted to evaluate the central economic parameters' influence on the net production costs of FT products.

The base scenario's required fixed capital investment, fixed and variable OPEX, as well as expected by-product revenue, are listed in Table 19. A total investment of 157.6 million € is required to realize the presented plant concept. The most significant cost factor is the variable OPEX, mainly electricity, with annual costs of 177.7 million €. The fixed OPEX, e.g., labor, maintenance and insurance, amount to yearly expenses of 10.9 million €.

*Table 19: FCI, OPEX and revenue for a 100 $MW_{el.}$ rated electrolyzer power PtL plant [**Journal Article V**].*

Parameter	Costs
Fixed capital investment	157.6 million €
$OPEX_{Fixed}$	10.9 million €/a
$OPEX_{Variable}$	179.3 million €/a
O_2 revenue	−13.9 million €/a

The cost allocation of Fischer-Tropsch products, i.e., CAPEX, OPEX excluding electricity and electricity, for 1, 10 and 100 $MW_{el.}$ rated electrolyzer power, based on electricity costs of 0.2 $€_{2022}/kWh_{el}$, is depicted in Figure 9. The CAPEX and electricity costs obtain shares of 21% and 66%, respectively, for plants at a pilot scale. CAPEX and fixed OPEX benefit from economies of scale, obtaining a combined share of only 12% of the total NPC at a scale of 100 $MW_{el.}$. The electricity demand is directly proportional to the produced FT products. Thus, scaling up the PtL plant significantly increases the relative share of electricity costs to up to 88%.

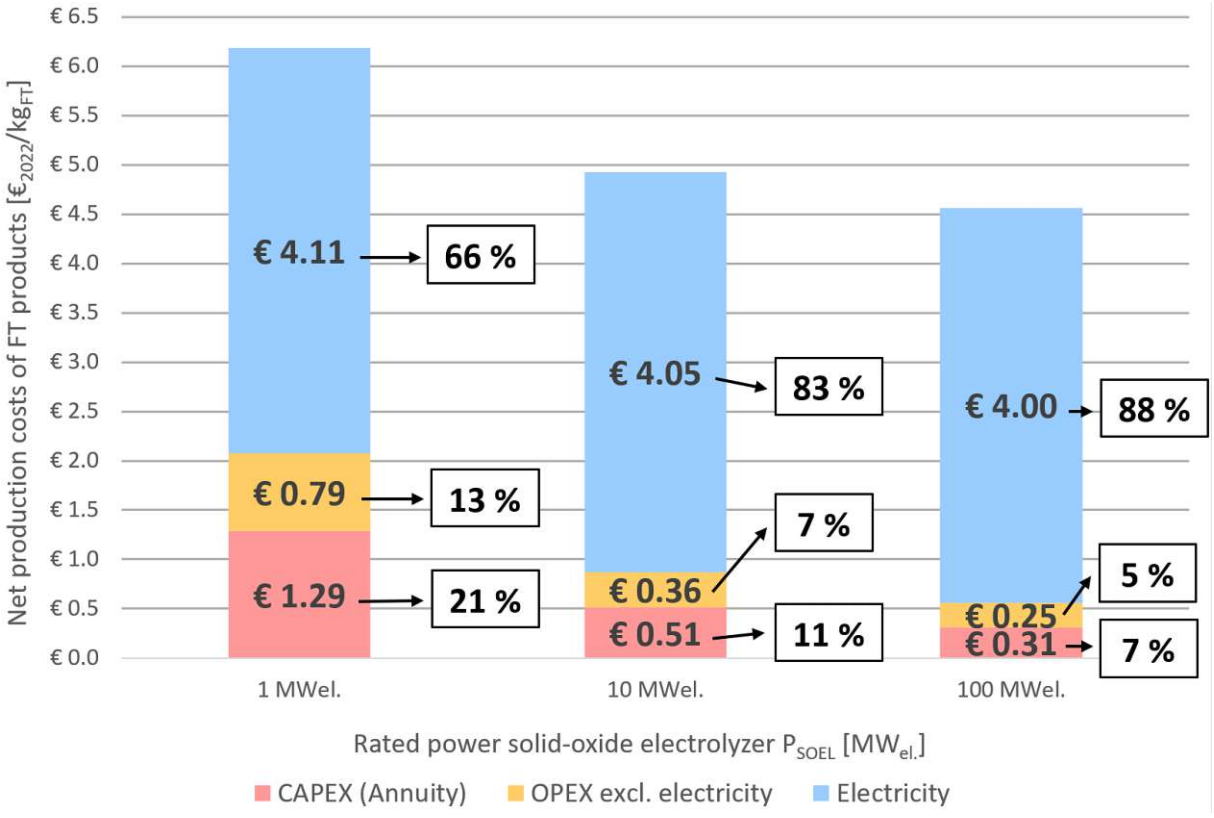

*Figure 9: Cost allocation of FT products based on plant scales from 1 to 100 $MW_{el.}$ [**Journal Article V**].*

A comparison between the economic performance of grid-based and off-grid scenarios is provided in Figure 10. Net production costs ranging from 2.42 to 4.56 €$_{2022}$/kg$_{FT}$ were obtained for the grid electricity scenario based on electricity costs between 0.1 and 0.2 €$_{2022}$/kWh$_{el.}$. Off-grid configurations solely based on a single renewable power source, e.g., onshore wind power, show an improved economic potential due to the significantly lower electricity costs. Even more promising results ranging from 1.08 to 1.28 €$_{2022}$/kg$_{FT}$ can be obtained by off-grid scenarios based on hybrid power plants and storage technologies due to cheap electricity provided by renewable power sources in combination with availabilities exceeding 6,000 hours per year.

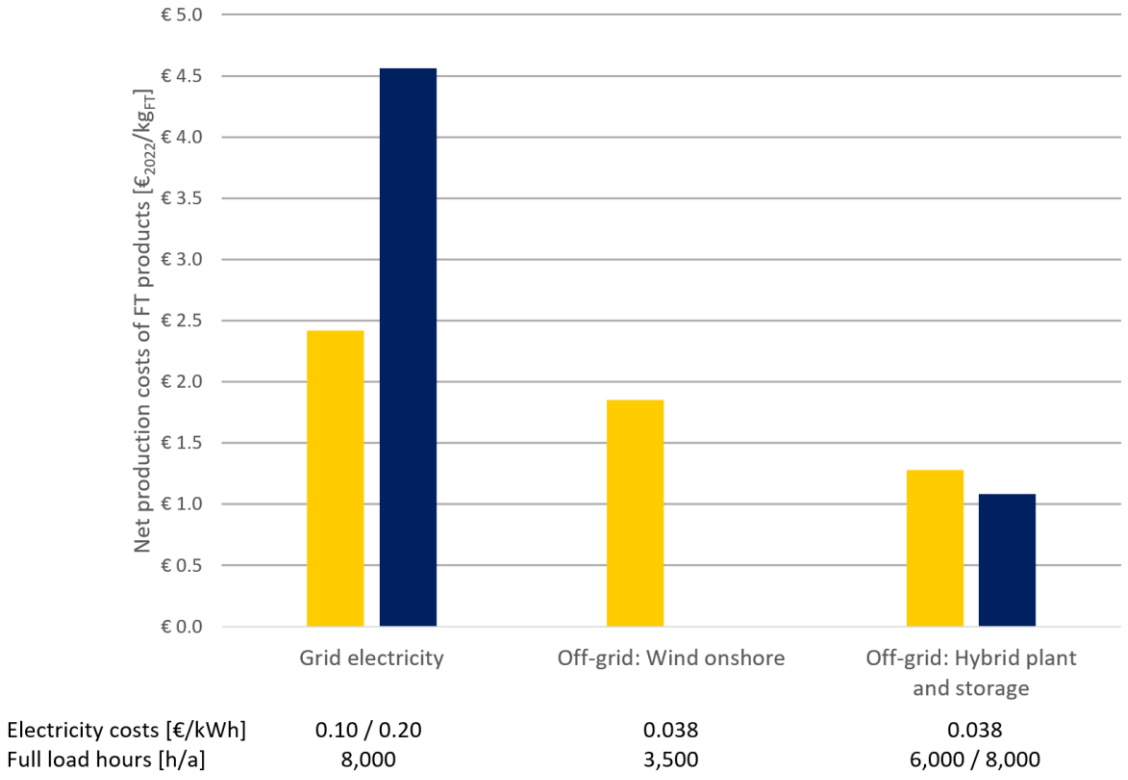

*Figure 10: Net production costs of FT products for grid-based and off-grid scenarios [**Journal Article V**].*

Table 20 displays the required CO_2 prices to make FT products cost-competitive with comparable fossil products and commodities, i.e., crude oil, aviation fuel and paraffin wax. A surcharge of 5% for corporate overhead charges was added to the determined NPC as proposed by Towler and Sinnott [99]. In addition, a 20% value-added tax surcharge was added for the comparison with crude oil and wax. The determined NPC of FT products produced with cheap grid electricity or hybrid plants are lower than the market price of paraffin wax. Substituting aviation fuel with FT products is unrealistic under current market conditions, with a required CO_2 price of 500 €/t and higher. Nonetheless, this scenario can potentially become viable if the market price of fossil jet fuel continues to rise and emitting CO_2 becomes more expensive. Substituting crude oil with FT products has no economic potential due to necessary CO_2 prices above 2,600 €/t.

*Table 20: Required CO_2 prices to make FT products cost-competitive with crude oil, aviation fuel and paraffin wax for three scenarios [**Journal Article V**].*

			Required CO_2 price [€/t]		
Reference [4)]	Market price	Source	Grid electricity [1)]	Wind onshore [2)]	Hybrid plant [3)]
Crude oil	600 €/t	[126]	8,445 - 17,743	5,969	2,623 - 3,492
Aviation fuel	900 €/t	[127,128,129]	3,491 - 8,272	2,218	498 - 945
Paraffin wax	2,032 €/t	[130]	1,256 - 4,585	369	−839 - −518

1) Electricity costs: 0.1−0.2 €/$kWh_{el.}$; Plant availability: 8,000 h/a.
2) Electricity costs: 0.038 €/$kWh_{el.}$; Plant availability: 3,500 h/a.
3) Electricity costs: 0.038 €/$kWh_{el.}$; Plant availability: 6,000-8,000 h/a.
4) Indirect emission factors: EF_{Crude} = 0.29 t_{CO2}/t [131,132], $EF_{Aviation}$ = 0.47 t_{CO2}/t [133], EF_{Wax} = 0.81 t_{CO2}/t [134].

The central economic parameters', i.e., electricity costs, availability, discount rate, depreciation period and fixed capital investment, influence on the net production costs of FT products is depicted in Figure 11. PtL plants should aim for annual operating hours of at least 3,000 to avoid a soaring increase in NPC below that threshold. Generally, availabilities exceeding 4,000 h/a are recommended for industrial PtL plants to ensure economical operation. The electricity costs are the most significant parameter influencing the NPC of FT products. An increase of 0.05 €/$kWh_{el.}$ results in a rise in NPC of 1.07 $€_{2022}/kg_{FT}$. Doubling the required fixed capital investment from 160 to 320 million € entails an increase in NPC of 20%. The other parameters, i.e., discount rate and depreciation period, mainly depend on the economic and political framework as well as the chosen plant location and can only partly be influenced.

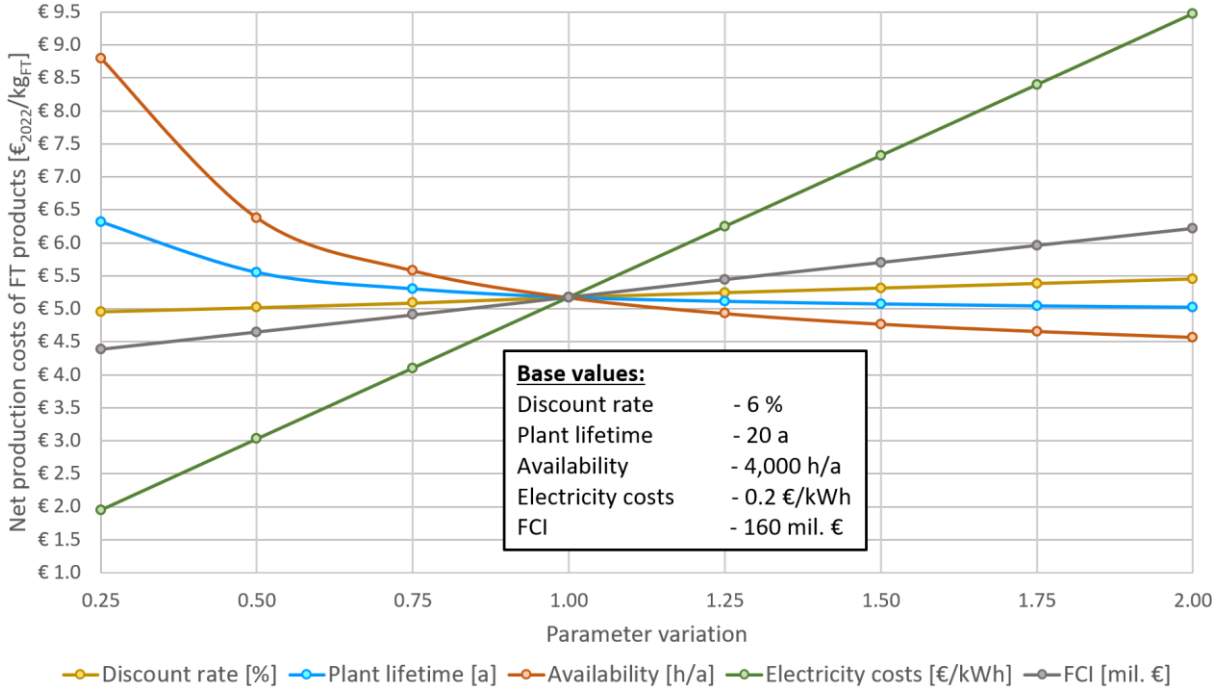

*Figure 11: Sensitivity analysis - Power-to-Liquid plant based on SOEL and FT synthesis [**Journal Article V**].*

3.4.3 Discussion of Chapter "Techno-Economic Assessments"

CO_2 prices of 220 to 310 €/t are required to make the proposed non-profit scenario of a Power-to-Green methanol plant, based on an amortization period of 25 years, cost-competitive with fossil-based methanol for German market prices in 2022 [125]. CO_2 prices in the EU in 2023 were significantly lower, i.e., 80-100 €/t for the European emission trading system (ETS) [135], 55 €/t for non-ETS sectors in Austria until 2025 [136] and 122 €/t in Sweden [137].

Further reductions in NPC and a substantial increase in CO_2 prices to at least 500 €/t are required to make Fischer-Tropsch processes cost-competitive compared with aviation fuel. However, substituting paraffin wax with FT wax can already be cost-competitive due to significantly lower NPC realized by PtL processes based on hybrid power plants.

The economies of scale's effect lowers the Power-to-Green methanol plant's cost shares of annuity and fixed OPEX from 43.7% to 28.2% for a scale-up from 50 to 1,000 $MW_{el.}$ rated electrolyzer power. However, the scale-up's overall beneficial effect is limited due to the direct proportionality of consumed power and produced green methanol. Scaling up the plant by a factor of 20 leads to a decrease in NPC of 27.5%.

A similar picture emerges for PtL plants based on Fischer-Tropsch and SOEL technology. Scaling up the plant from 1 to 100 $MW_{el.}$ entails a reduction in NPC of 20%. Nonetheless, this effect diminishes at scales exceeding 100 $MW_{el.}$ due to relative electricity costs of 80% and higher, depending on the assumed specific electricity costs per $kWh_{el.}$. The conducted TEAs aimed to provide class 4 studies, i.e., preliminary estimate studies, complying with the Association for the Advancement of Cost Engineering International classification. Thus, uncertainties concerning the fixed capital investment of -30% to +50% are anticipated, possibly entailing alternating results concerning the economies of scale's positive effect.

A crucial weakness of PtL plants, i.e., their dependency on the electricity market, can be negated by implementing hybrid power plants, including grid connection and the feed-in of surplus electricity. Selling O_2 as a by-product accounts for 17% of the plant's total revenue. Thus, coupling PtL plants with potential O_2-consuming industries is critical in making PtL processes economically viable. However, oxygen prices are predicted to drop if a significant number of O_2-selling PtL plants are established in the future. Thus, oxygen revenues are expected to be below 15% of the total revenue for industrial PtL plants. Another decisive factor is the realized plant availability. Connecting PtL plants with hybrid power plants and electricity and hydrogen storage technologies is a potential keystone to boost their economic performance. Annual operating hours of at least 3,000 are recommended based on the findings of **Journal Articles IV** and **V**.

Expanding the applied static process models to dynamic models offers the potential to specify the obtained results for different plant locations. Furthermore, implementing electricity and H_2 storage technologies can lower the dependency on grid electricity of PtL plants. In addition, future research should be based on a detailed P&ID to reduce the TEA's level of uncertainty.

A comparison of economic studies based on CO_2 hydrogenation to methanol is presented in Table 21. **Journal Article IV**'s promising results can be explained by three reasons. Firstly, realizing an industrial plant availability of 8,000 h/a entails a significant reduction in NPC. Decoupling the plant's economic performance from electricity market prices reduces investment risk. Furthermore, selling by-products, i.e., oxygen and district heating, results in an additional reduction in NPC.

*Table 21: Comparison of methanol net production costs based on CO_2 hydrogenation [**Journal Article IV**].*

NPC [€$_{2022}$/t]	[138]	[139]	[106]	[140]	[75]	[141]	**Journal Article IV**
NPC_{min}	1,685	958	1,159	1,612	1,421	665	569
NPC_{max}			1,562	1,905		950	785

Table 22 summarizes the findings of **Journal Article V** and contextualizes them with previously conducted techno-economic studies. The NPC of FT products substantially depend on the applied electricity costs. Hence, studies solely based on grid electricity obtain wider intervals of NPC compared with off-grid scenarios and Biomass-to-Liquid plants. PtL plants based on SOEL instead of PEMEL technology can achieve significantly lower NPC by reducing the overall electricity costs by 25%. Off-grid Power-to-Liquid plants based on hybrid power plants and storage technologies combine the advantages of cheap electricity and high availabilities and thus have the potential to achieve lower NPC than grid-based plants.

*Table 22: Fischer-Tropsch NPC comparison with previous PtL and BtL studies [**Journal Article V**].*

[€$_{2022}$/kg]	**Journal Article V**	[142] [4]	[143] [4]	[144] [4]	[145] [4]	[121] [4),5]	[143] [5]	[146] [6]	[147] [7]	[105] [7]
NPC_{min} [1]	2.42 [2]	1.28 [3]	1.38	3.40	1.26	2.24	8.40	4.39	2.59	3.09	1.42
NPC_{max} [1]	4.56 [2]	2.40 [3]	2.72	7.70	1.61	5.38	10.60	7.26	2.84	4.65	3.85

1) All values converted to 2022 levels (CEPCI = 816.0).
2) Grid-based scenario. Electricity costs = 0.1-0.2 €/$kWh_{el.}$.
3) Off-grid scenario.
4) SOEL + FT.
5) PEMEL + FT.
6) rWGS + FT.
7) Biomass-to-Liquid.

The net production costs of green methanol and Fischer-Tropsch products obtained in **Journal Articles IV** and **V** must be converted to energy-specific NPC to make them comparable. Green methanol NPC ranging from 0.103 to 0.142 €$_{2022}$/kWh_{MeOH} were found in **Journal Article IV,** whereas Fischer-Tropsch NPC in the range of 0.107 to 0.382 €$_{2022}$/kWh_{FT} were obtained in **Journal Article V**. It must be stated that the refining and conditioning of FT products were not considered in **Journal Article V**, thus higher NPC have to be expected for different final products. In addition, a significantly narrower interval has been found for the NPC of green methanol due to the modeled hybrid power plant, which concluded in an almost negligible influence of the electricity costs on the NPC, as can be seen when comparing the electricity costs' respective impact in Figure 8 and Figure 11.

3.4.4 Conclusions of Chapter "Techno-Economic Assessments"

Journal Article IV economically evaluates a green methanol plant based on **Journal Article I**'s findings. The reference scenario, based on 20 $MW_{th.}$ thermal input into the CHP plant and 50 $MW_{el.}$ rated electrolyzer power, requires a fixed capital investment of around 120 million €$_{2022}$. CO_2 prices ranging from 220 to 310 €$_{2022}$/t are needed to make green methanol cost-competitive to methanol derived from natural gas based on German market levels in 2022. Green methanol net production costs between 569 and 785 €$_{2022}$/t were determined. Combining a hybrid power plant, comprising a wind park, a photovoltaic farm, a CHP process and grid electricity, with the designed green methanol plant resulted in two major improvements, i.e., independence of volatile grid electricity markets and a significant increase in annual operating hours.

Journal Article V assesses and compares the economic performance of grid-based and off-grid Power-to-Liquid processes combining Fischer-Tropsch synthesis and solid-oxide electrolysis. The reference scenario is based on the process design of **Journal Article III**, including tail gas recirculation and steam reforming of tail gas for a rated electrolyzer power of 100 $MW_{el.}$. A fixed capital investment of 157.6 million € and an annual operational expenditure of 190.2 million € are necessary to realize the designed plant for a grid-based scenario. Off-grid power plants provide low electricity costs, which comes at the expense of detrimental annual full load hours. Thus, increasing the annual operating hours of off-grid Power-to-Liquid plants by implementing hybrid power plants and storage technologies, i.e.,

electricity and syngas, is vital in reducing the net production costs of Fischer-Tropsch products. Net production costs ranging from 2.42 to 4.56 €/kg_{FT}, based on grid electricity, and 1.28 to 2.40 €/kg_{FT}, based on off-grid scenarios, were obtained within **Journal Article V**. Increased CO_2 emitting penalties of around 500 €/t are required to make Power-to-Liquid plants producing Fischer-Tropsch products cost-competitive with fossil aviation fuel. Substituting paraffin wax with Fischer-Tropsch wax is cost-competitive under today's economic framework. However, replacing crude oil with Fischer-Tropsch syncrude has no economic potential.

3.5 The Necessity of Sector Coupling

Embedding Power-to-Liquid processes into industrial systems is a cornerstone of increasing their feasibility, efficiency and economic performance. Coupling PtL plants with CO_2-emitting and oxygen-consuming processes avoids additional infrastructure costs for pipelines and compressor stations. In addition, the utilization of industrial waste heat results in an increase in process and carbon efficiency.

Selling oxygen, a by-product of water splitting, can enhance the plant's economic performance. The oxygen revenue accounted for 17% of the Power-to-Green methanol plant's total income in **Journal Article IV**, resulting in a 7% reduction in the net production costs of green methanol. The findings of **Journal Article V** indicate that the revenue generated by selling oxygen results in an 8.5% reduction in annual OPEX. **Journal Article I** evaluated the utilization of generated oxygen in an oxy-fuel combustor and compared the determined efficiencies with a conventional air combustion route. Utilizing oxygen resulted in a detrimental Power-to-Liquid efficiency of 51.9% compared with a value of 54.2% realized by the air combustion route. The oxy-fuel route's overall energetic efficiency, including district heating, obtained a value of 57.0% compared with an efficiency of 54.4% for the air combustion route.

Another substantial element is the utilization of highly concentrated CO_2 sources. As a best-case scenario, PtL plants should be directly adjacent to industries emitting highly concentrated CO_2 streams to avoid additional gas conditioning and transportation expenses. **Journal Article III**'s findings state that a maximum PtL efficiency of 63.8% can be achieved based on a biogas upgrading plant as a CO_2 source, corresponding with an increase of almost 20 percentage points compared with a comparable process route based on direct air capture.

Supplying the CO_2 capture unit with heat is a central obstacle to PtL processes. Additional tail gas must be combusted as a heat source if no waste heat is provided by adjacent processes, thus reducing the PtL plant's efficiency and economic performance. Table 23 summarizes the PtL and carbon efficiencies achieved for different tail gas recirculation ratios.

*Table 23: PtL and carbon efficiency as a function of the tail gas recirculation ratio [**Journal Article III**].*

	CO_2 source		
Parameter	Biogas upgrading [1)]	Cement [2)]	Biomass CHP [3)]
Recirculation ratio	90%	85%	75%
PtL efficiency	63.8%	58.8%	54.7%
Carbon efficiency	88.6%	75.7%	68.4%

1) No additional CO_2 capture required.
2) Exploitation of the cement plant's waste heat potential.
3) The CO_2 capture unit's heat demand is fully covered by tail gas combustion.

3.6 Covering the European Demand for Methanol, Jet Fuel and Maritime Fuel with PtL

Defossilizing the chemical and plastics industry, as well as aviation and maritime transport, is a central step in achieving the EU's goal of becoming climate-neutral by 2050. The European annual methanol demand amounted to 10.8 million tons in 2023 [148]. The pre-COVID-19 jet fuel demand amounted to 47.5 million tons in 2019 [149]. A total of 35 million tons of fuel oil was used as maritime fuel in 2019, corresponding with 32 million tons of Fischer-Tropsch fuels [150]. A contextualization of the designed PtL plants' capacities with the European demand for methanol, jet fuel and maritime fuel is provided in Table 24.

Table 24: Plant capacities of the designed PtL plants compared with the annual European demand for methanol, jet fuel and maritime navigation fuel.

		Comparison with the European demand for:		
Process route	Capacity	Methanol [1)]	Jet fuel [2)]	Maritime fuel [3)]
Green methanol	44,000 t/a	0.41%	-	-
FT + SOEL (cement)	216,800 t/a	-	0.39%	0.58%
FT + SOEL (biogas)	10,400 t/a	-	0.02%	0.03%
FT + SOEL (CHP)	15,200 t/a	-	0.03%	0.04%

1) Annual demand of 10.8 million tons [148].
2) Annual demand of 47.5 million tons [149] and a refinery efficiency of 86% [34].
3) Fuel oil demand converted to 32 million tons of FT products [150] and a refinery efficiency of 86% [34].

About 250 Power-to-Green methanol plants, based on a rated electrolyzer power of 54 $MW_{el.}$, as proposed in **Journal Article I,** are required to substitute the total European consumption of fossil-based methanol. The realization of 425 PtL plants at a scale of 504 $MW_{el.}$ rated SOEL power input, according to the process route based on a cement plant as a CO_2 source in **Journal Article III**, is necessary to cover the EU's demand for aviation and maritime fuels. Providing the same amount of aviation and

maritime fuels based on biogas upgrading plants as CO_2 sources requires 8,900 PtL plants with a rated SOEL power input of 23.1 $MW_{el.}$.

As stated in **Journal Article III**, exploiting the total CO_2 stream emitted by the EU's cement industry with PtL plants combining SOEL and FT synthesis can provide 19.5 million t/a FT products. Thus, potentially covering 41% of the European jet fuel or 61% of the marine navigation fuel demand. Realizing Europe's full potential for biogas and biogas upgrading plants [151] can potentially provide an annual FT product stream of 47 million tons, corresponding to 98.9% of the jet fuel or 146.9% of the total marine navigation fuel demand.

4 Conclusion

Evaluating the efficiency, economic and ecological performance of Power-to-Liquid plants is essential to bring the technology closer to industrial realization. In addition, feasible process configurations were provided for producing green methanol and Fischer-Tropsch products at a pilot and an industrial scale. The following conclusions are drawn based on this thesis's scope and assumptions.

Research question 1: *What are the ideal plant designs for Power-to-Liquid plants producing green methanol and Fischer-Tropsch products at a pilot and an industrial scale?*

The decision on the applied combustion technology for Power-to-Green methanol plants should primarily be based on its location. Oxy-fuel routes offer an increased heat output compared to the air combustion-based route. It thus should be favored at sites with a demand for heat or process steam, e.g., by adjacent villages or industries, and if the required infrastructure is available, e.g., a district heating or steam supply network. Implementing the air-based process configuration is recommended when coupled with adjacent oxygen-consuming industries and for regions with a lower yield of renewable power sources since it is possible to adapt the share of valorized CO_2 to green methanol. Electrolyzers with a rated power of around 50 $MW_{el.}$ are required to process the flue gas stream of a CHP process with a thermal wood chip input of 20 $MW_{th.}$.

A simplified process design is recommended for pilot-scale PtL plants combining solid-oxide electrolysis and Fischer-Tropsch synthesis to ensure their feasibility and quick deployment. Pilot-scale plants should focus on the synergy and interaction between the high-temperature co-electrolysis and the Fischer-Tropsch process. In contrast, industrial-scale plants must operate as efficiently and cost-effectively as possible. Thus, additional process steps, e.g., tail gas reforming and CO_2 capture, as well as an intricate refinery concept based on the defined product specifications, should be implemented.

Research question 2: *Which influence do the process design and the utilized CO_2 source have on the Power-to-Liquid and carbon efficiency of Power-to-Liquid plants?*

The achieved PtL efficiency of the designed Power-to-Green methanol plant ranged from 21.0% to 51.9% for the oxy-fuel and was constant at 54.2% for the air combustion process route. Coupling oxy-fuel combustion with PtL plants has the potential to reach a carbon efficiency above 95% due to no losses at the CO_2 capture stage.

The effect of three CO_2 sources on the PtL and carbon efficiency of a plant combining high-temperature electrolysis and Fischer-Tropsch synthesis were assessed. The highest efficiencies, $\eta_{PtL,Biogas} = 63.8\%$ and $\eta_{Carbon,Biogas} = 88.6\%$, can be achieved by utilizing CO_2 emitted by a biogas upgrading plant. The obtained efficiencies in combination with a cement plant were $\eta_{PtL,Cement} = 58.8\%$ and $\eta_{Carbon,Cement} = 75.7\%$. Less promising results, $\eta_{PtL,CHP} = 54.7\%$ and $\eta_{Carbon,CHP} = 68.4\%$, were obtained for the scenario based on a biomass heating plant as a CO_2 source. Thus, highly concentrated biogenic CO_2 sources are recommended to be exploited for the first generation of PtL plants. Furthermore, industrial

waste heat potential should be utilized by PtL plants to minimize tail gas combustion for internal heat supply.

Research question 3: *How does the applied electricity source influence the CO_2 footprint of Power-to-Liquid products?*

Evaluating the greenhouse gas savings potential of PtL products is critical to ensure their positive effect on curbing the climate crisis. Applying wind power has the most benign impact, with a possible reduction in CO_2 emissions of 96% compared with fossil diesel. Products based on photovoltaic electricity can potentially achieve a 65% reduction in CO_2 emissions. However, powering PtL plants with the average EU27 grid electricity mix in 2022 results in a 46% larger carbon footprint than conventional fuels. Only four national grid electricity mixes of EU member states, i.e., Sweden, Denmark, Finland and France, were eligible for PtL applications in 2022. Expanding the overall share of renewable electricity is a cornerstone of ensuring a positive effect of PtL plants.

Research question 4: *Which factors have the highest leverage on the economic performance of Power-to-Liquid plants and which CO_2 prices are required to make Power-to-Liquid plants economically competitive with conventional fossil-based processes?*

Green methanol net production costs of 0.57 to 0.78 €/kg were determined. Fischer-Tropsch products can be provided at costs of 2.42 to 4.56 €/kg by grid-based and 1.28 to 2.40 €/kg by off-grid PtL plants. The electricity costs of the analyzed process routes account for 59% (green methanol) and more than 80% (Fischer-Tropsch) of the net production costs for plants at a scale of 100 $MW_{el.}$ rated electrolyzer power. Increasing the electricity costs by 0.05 €/$kWh_{el.}$ results in an increase in Fischer-Tropsch net production costs of 1.07 €/kg_{FT}. Expenses for electricity are the main cost driver of PtL plants and, hence, must be minimized to ensure an economical operation.

The second most important factor is the plant availability. Off-grid Power-to-Liquid plants based solely on one power source realize lower annual operating hours, consequently increasing net production costs. Implementing hybrid power plants and storage technologies, i.e., for electricity and syngas, is essential to benefit from cheap renewable electricity. Based on the presented findings, plant availabilities of at least 3,000 annual operating hours are recommended. Industrial PtL plants should aim for 6,000 yearly operating hours in the long run.

CO_2 prices ranging from 220 to 310 €/t are required to make green methanol cost-competitive with fossil methanol derived from natural gas based on the assessed non-profit scenario with an amortization period of 25 years. Substituting crude oil with Fischer-Tropsch syncrude is economically unfeasible. Fischer-Tropsch products can potentially become cost-competitive to 2023 jet fuel market prices for a CO_2 price of at least 500 €/t. Replacing fossil paraffin wax with Fischer-Tropsch wax produced by off-grid plants is cost-competitive under current market conditions, regardless of additional surcharges for CO_2 emissions.

5 Outlook

The first pillar of facilitating Power-to-Liquid processes is to improve process modeling and simulation as a foundation for future projects. Advancing the applied sub-process models' level of detail by implementing kinetic models based on experimental data is a possible first step. The steam reforming of tail gas holds a significant uncertainty factor due to alternating tail gas compositions and the influence of the rWGS reaction compared with conventional reforming of natural gas. In addition, implementing dynamic process models and simulation is an essential next step in analyzing the behavior of off-grid Power-to-Liquid plants based on renewable power sources for different locations.

The second pillar comprises process design and the conducted techno-economic assessments. The conducted evaluations are based on AACE class 4 studies. Elaborating on the plant design and establishing P&I flowcharts is necessary to further increase the studies' accuracy. Assessing the impact of storage technologies on efficiency and economic performance is vital to enhancing the annual operating hours of off-grid Power-to-Liquid plants. Furthermore, intricate control engineering systems are essential to facilitate the complex interactions of sub-processes, e.g., between the solid-oxide electrolyzer and the Fischer-Tropsch reactor.

Managing the industrialization of Power-to-Liquid processes requires the following steps. Rapidly expanding renewable power sources is critical to ensure a benign impact on society and climate. Biogenic and highly concentrated CO_2 sources should be prioritized for the first generation of Power-to-Liquid plants. As a next step, industrial and hard-to-abate sectors should be targeted. The use of fossil CO_2 sources needs to be avoided to prevent a carbon lock-in of fossil energy sources. Power-to-Liquid products are recommended for use as a material resource in the chemical and plastics industry and as fuels for aviation and maritime transport. However, they should not be used as fuel for individual mobility. Off-grid plants based on renewable power sources should be prioritized to ensure stable electricity prices, thus facilitating long-term investment scenarios. Furthermore, Power-to-Liquid processes can potentially make the EU's economy less dependent on crude oil and natural gas imports, reducing the susceptibility to energy and resource crises.

References

1. Lindsey, R.; Dahlman, L. Climate Change: Global Temperature. National Oceanic & Atmospheric Administration, U.S. Department of Commerce. 2024. Available at: https://www.climate.gov/news-features/understanding-climate/climate-change-global-temperature. [Accessed: 7.12.2023].
2. Copernicus. Summer 2023: The Hottest on Record. European Commission. 2023. Available at: https://climate.copernicus.eu/summer-2023-hottest-record. [Accessed: 6.10.2023].
3. Global Monitoring Laboratory. Global Monthly Mean CO2. National Oceanic & Atmospheric Administration, U.S. Department of Commerce. 2023. Available at: https://gml.noaa.gov/ccgg/trends/global.html. [Accessed: 6.10.2023].
4. Global Monitoring Laboratory. Annual Mean Global Carbon Dioxide Growth Rates. National Oceanic & Atmospheric Administration, U.S. Department of Commerce. 2023. Available at: https://gml.noaa.gov/ccgg/trends/gl_gr.html. [Accessed: 6.10.2023].
5. IEA. Global Energy Review 2021. IEA - International Energy Agency. France. 2021. Available at: https://www.iea.org/reports/global-energy-review-2021. [Accessed: 15.2.2024].
6. European Parliament. Emissions from Planes and Ships: Facts and Figures. 2022. Available at: https://www.europarl.europa.eu/news/en/headlines/society/20191129STO67756/emissions-from-planes-and-ships-facts-and-figures-infographic. [Accessed: 6.10.2023].
7. European Environment Agency. Managing the Systemic Use of Chemicals in Europe. Publications Office: LU. 2023. Available at: https://data.europa.eu/doi/10.2800/104101. [Accessed: 15.2.2024].
8. IPCC. Synthesis Report of the IPCC Sixth Assessment Report (AR6) - Summary for Policymakers. Intergovernmental Panel on Climate Change. Geneva, Switzerland. 2023. Available at: https://www.ipcc.ch/report/sixth-assessment-report-cycle/. [Accessed: 4.3.2024].
9. H2greensteel. The Colors of Hydrogen. 2022. Available at: https://www.consilium.europa.eu/en/infographics/fit-for-55-refueleu-and-fueleu/. [Accessed: 28.11.2023].
10. IEA. Global Hydrogen Review 2023. International Energy Agency. Paris, France. 2023. Available at: https://www.iea.org/reports/global-hydrogen-review-2023. [Accessed: 15.2.2024].
11. Directive (EU) 2023/2413 of the European Parliament and of the Council of 18 October 2023 Amending Directive (EU) 2018/2001, Regulation (EU) 2018/1999 and Directive 98/70/EC as Regards the Promotion of Energy from Renewable Sources, and Repealing Council Directive (EU) 2015/652. Official Journal of the European Union L, 31.10.2023.
12. European Council. Infographic – Fit for 55: Increasing the Uptake of Greener Fuels in the Aviation and Maritime Sectors. 2023. Available at: https://www.consilium.europa.eu/en/infographics/fit-for-55-refueleu-and-fueleu/. [Accessed: 28.11.2023].
13. Commission Delegated Regulation (EU) 2023/1185 of 10 February 2023 Supplementing Directive (EU) 2018/2001 of the European Parliament and of the Council by Establishing a Minimum Threshold for Greenhouse Gas Emissions Savings of Recycled Carbon Fuels and by Specifying a Methodology for Assessing Greenhouse Gas Emissions Savings from Renewable Liquid and Gaseous Transport Fuels of Non-Biological Origin and from Recycled Carbon Fuels. L 157/20, 20.6.2023.
14. Advanced Energy Technology. Advanced CtL, GtL and BtL Facilities With Fischer-Tropsch System, and Patenting Activity in the World. 2020. Available at: https://aenert.com/fileadmin/default/templates/images/Technologies/Unconventional_fossil_fuels/Synthetic_fuels/2021_Overview/22_fischer-tropsch-plants-map-2020__font_update.pdf. [Accessed: 7.8.2023].

15. Pratschner, S.; Hammerschmid, M.; Müller, F.J.; Müller, S.; Winter, F. Simulation of a Pilot Scale Power-to-Liquid Plant Producing Synthetic Fuel and Wax by Combining Fischer–Tropsch Synthesis and SOEC. *Energies* 2022, *15*, 4134, doi:10.3390/en15114134.

16. Pratschner, S.; Hammerschmid, M.; Müller, S.; Winter, F. Evaluation of CO2 Sources for Power-to-Liquid Plants Producing Fischer-Tropsch Products. *Journal of CO2 Utilization* 2023, *72*, 102508, doi:10.1016/j.jcou.2023.102508.

17. Klerk, A. de Fischer-Tropsch Refining; 1st. ed.; Wiley-VCH: Weinheim, Germany, 2011. ISBN 978-3-527-63560-3.

18. Makhura, E.; Rakereng, J.; Rapoo, O.; Danha, G. Effect of the Operation Parameters on the Fischer Tropsch Synthesis Process Using Different Reactors. *Procedia Manufacturing* 2019, *35*, 349–355, doi:10.1016/j.promfg.2019.05.051.

19. Martinelli, M.; Gnanamani, M.K.; LeViness, S.; Jacobs, G.; Shafer, W.D. An Overview of Fischer-Tropsch Synthesis: XtL Processes, Catalysts and Reactors. *Applied Catalysis A: General* 2020, *608*, 117740, doi:10.1016/j.apcata.2020.117740.

20. Guettel, R.; Kunz, U.; Turek, T. Reactors for Fischer-Tropsch Synthesis. *Chem. Eng. Technol.* 2008, *31*, 746–754, doi:10.1002/ceat.200800023.

21. Thomas, J.M.; Thomas, W.J. Principles and Practice of Heterogeneous Catalysis; Second, revised edition.; Wiley-VCH, Verlag GmbH & Co. KGaA: Weinheim, 2015. ISBN 978-3-527-68380-2.

22. Eilers, H. Flexibler Betrieb Der Fischer-Tropsch-Synthese - Katalysator- Und Reaktorverhalten Mit Co in Der 3-Phasen-Blasensäule. Dissertation, Fakultät für Chemieingenieurwesen und Verfahrenstechnik. Karlsruher Institut für Technologie. 2018.

23. Eilers, H.; González, M.I.; Schaub, G. Lab-Scale Experimental Studies of Fischer–Tropsch Kinetics in a Three-Phase Slurry Reactor under Transient Reaction Conditions. *Catalysis Today* 2016, *275*, 164–171, doi:10.1016/j.cattod.2015.11.011.

24. Pfeifer, P.; Schmidt, S.; Betzner, F.; Kollmann, M.; Loewert, M.; Böltken, T.; Piermartini, P. Scale-up of Microstructured Fischer–Tropsch Reactors – Status and Perspectives. *Current Opinion in Chemical Engineering* 2022, *36*, 100776, doi:10.1016/j.coche.2021.100776.

25. Ying, X.; Zhang, L.; Xu, H.; Ren, Y.; Xuan, J. An Experimental Study on a Microchannel Reactor for Fischer-Tropsch Synthesis. *Energy Procedia* 2014, *61*, 1394–1397, doi:10.1016/j.egypro.2014.12.134.

26. Cao, H.; Xu, R.; Tang, X.; Yang, T.; Hou, S.; Hou, C. Microchannel Reactors for Fischer-Tropsch Synthesis: Experimental Investigation and Mathematical Modeling. *Chinese Journal of Chemical Engineering* 2023, *64*, 224-240, doi:10.1016/j.cjche.2023.04.027.

27. Gavrilović, L.; Jørgensen, E.A.; Pandey, U.; Putta, K.R.; Rout, K.R.; Rytter, E.; Hillestad, M.; Blekkan, E.A. Fischer-Tropsch Synthesis over an Alumina-Supported Cobalt Catalyst in a Fixed Bed Reactor – Effect of Process Parameters. *Catalysis Today* 2020, *369*, 150-157, doi:10.1016/j.cattod.2020.07.055.

28. Maitlis, P.M., Klerk, A. de, Greener Fischer-Tropsch Processes for Fuels and Feedstocks. Eds.; Wiley-VCH: Weinheim, 2013. ISBN 978-3-527-32945-8.

29. Ostadi, M.; Rytter, E.; Hillestad, M. Boosting Carbon Efficiency of the Biomass to Liquid Process with Hydrogen from Power: The Effect of H2/CO Ratio to the Fischer-Tropsch Reactors on the Production and Power Consumption. *Biomass and Bioenergy* 2019, *127*, 105282, doi:10.1016/j.biombioe.2019.105282.

30. Guilera, J.; Díaz-López, J.A.; Berenguer, A.; Biset-Peiró, M.; Andreu, T. Fischer-Tropsch Synthesis: Towards a Highly-Selective Catalyst by Lanthanide Promotion under Relevant CO2 Syngas Mixtures. *Applied Catalysis A: General* 2022, *629*, 118423, doi:10.1016/j.apcata.2021.118423.

31. Corrao, E.; Salomone, F.; Giglio, E.; Castellino, M.; Ronchetti, S.M.; Armandi, M.; Pirone, R.; Bensaid, S. CO2 Conversion into Hydrocarbons via Modified Fischer-Tropsch Synthesis by Using Bulk Iron Catalysts Combined with Zeolites. *Chemical Engineering Research and Design* 2023, *197*, 449–465, doi:10.1016/j.cherd.2023.07.052.

32. de Klerk, A. Can Fischer−Tropsch Syncrude Be Refined to On-Specification Diesel Fuel? *Energy Fuels* 2009 *23*, 4593–4604, doi:10.1021/ef9005884.

33. Gruber, H. Synthesis and Refining of Biomass-Derived Fischer-Tropsch Paraffin Waxes. Dissertation, Institute of Chemical, Environmental and Bioscience Engineering. TU Wien, 2020.

34. Petersen, A.M.; Chireshe, F.; Okoro, O.; Gorgens, J.; Van Dyk, J. Evaluating Refinery Configurations for Deriving Sustainable Aviation Fuel from Ethanol or Syncrude. *Fuel Processing Technology* 2021, *219*, 106879, doi:10.1016/j.fuproc.2021.106879.

35. Fahim, M.A.; Alsahhaf, T.A.; Elkilani, A. Hydroconversion. In *Fundamentals of Petroleum Refining*; Elsevier, 2010. pp. 153–198 ISBN 978-0-444-52785-1.

36. Kang, J.; Ma, W.; Keogh, R.A.; Shafer, W.D.; Jacobs, G.; Davis, B.H. Hydrocracking and Hydroisomerization of N-Hexadecane, n-Octacosane and Fischer–Tropsch Wax Over a Pt/SiO2–Al2O3 Catalyst. *Catal Lett* 2012, *142*, 1295–1305, doi:10.1007/s10562-012-0910-5.

37. Busca, G. Catalysts for Hydrogenations, Dehydrogenations and Metathesis. In *Heterogeneous Catalytic Materials*; Elsevier, 2014. pp. 345–374 ISBN 978-0-444-59524-9.

38. Bouchy, C.; Hastoy, G.; Guillon, E.; Martens, J.A. Fischer-Tropsch Waxes Upgrading *via* Hydrocracking and Selective Hydroisomerization. *Oil & Gas Science and Technology - Rev. IFP* 2009, *64*, 91–112, doi:10.2516/ogst/2008047.

39. Rahman, N.A.; Jose Jol, C.; Linus, A.A.; Rozellia Kamel Sharif, D.S.; Ismail, V. Fischer Tropsch Water Composition Study from Distillation Process in Gas to Liquid Technology with ASPEN Simulation. *Case Studies in Chemical and Environmental Engineering* 2021, *3*, 100106, doi:10.1016/j.cscee.2021.100106.

40. Bertau, M., Offermanns, H., Plass, L., Schmidt, F., Wernicke, H.-J. Methanol: The Basic Chemical and Energy Feedstock of the Future*:* Asinger's Vision Today. Eds.; Springer Berlin Heidelberg: Berlin, Heidelberg, 2014. ISBN 978-3-642-39708-0.

41. Methanol Institute. The Methanol Industry. 2023. Available at: https://www.methanol.org/the-methanol-industry/. [Accessed: 2.10.2023].

42. Sollai, S.; Porcu, A.; Tola, V.; Ferrara, F.; Pettinau, A. Renewable Methanol Production from Green Hydrogen and Captured CO2: A Techno-Economic Assessment. *Journal of CO2 Utilization* 2023, *68*, 102345, doi:10.1016/j.jcou.2022.102345.

43. Aasberg-Petersen, K.; Nielsen Stub, C.; Dybkjaer, I.; Perregaard, J. Large Scale Methanol Production from Natural Gas; Haldor Topsoe, 2022.

44. Roode-Gutzmer, Q.I.; Kaiser, D.; Bertau, M. Renewable Methanol Synthesis. *ChemBioEng Reviews* 2019, *6*, 209–236, doi:10.1002/cben.201900012.

45. Pratschner, S.; Radosits, F.; Ajanovic, A.; Winter, F. Techno-Economic Assessment of a Power-to-Green Methanol Plant. *Journal of CO2 Utilization* 2023, *75*, 102563, doi:10.1016/j.jcou.2023.102563.

46. Dieterich, V.; Buttler, A.; Hanel, A.; Spliethoff, H.; Fendt, S. Power-to-Liquid via Synthesis of Methanol, DME or Fischer–Tropsch-Fuels: A Review. *Energy Environ. Sci.* 2020, *13*, 3207–3252, doi:10.1039/D0EE01187H.

47. Methanol Institute. Renewable Methanol. 2023. Renewable Methanol. Methanol Institute. Available at: https://www.methanol.org/renewable/. [Accessed: 2.10.2023].

48. Supp, E. How to Purify and Condition Methanol Synthesis Gas. In How to Produce Methanol from Coal; Springer Berlin Heidelberg: Berlin, Heidelberg, 1990. pp. 44–101 ISBN 978-3-662-00897-3.

49. Lee, J.S.; Han, S.H.; Kim, H.G.; Lee, K.H.; Kim, Y.G. Effects of Space Velocity on Methanol Synthesis from Co2/Co/H2 over Cu/ZnO/Al2O3 Catalyst. *Korean J. Chem. Eng.* 2000, *17*, 332–336, doi:10.1007/BF02699049.

50. Bussche, K.M.V.; Froment, G.F. A Steady-State Kinetic Model for Methanol Synthesis and the Water Gas Shift Reaction on a Commercial Cu/ZnO/Al2O3Catalyst. *Journal of Catalysis* 1996, *161*, 1–10, doi:10.1006/jcat.1996.0156.

51. Nestler, F.; Schütze, A.R.; Ouda, M.; Hadrich, M.J.; Schaadt, A.; Bajohr, S.; Kolb, T. Kinetic Modelling of Methanol Synthesis over Commercial Catalysts: A Critical Assessment. *Chemical Engineering Journal* 2020, *394*, 124881, doi:10.1016/j.cej.2020.124881.

52. Meunier, N.; Chauvy, R.; Mouhoubi, S.; Thomas, D.; De Weireld, G. Alternative Production of Methanol from Industrial CO2. *Renewable Energy* 2020, *146*, 1192–1203, doi:10.1016/j.renene.2019.07.010.

53. Ruland, H.; Song, H.; Laudenschleger, D.; Stürmer, S.; Schmidt, S.; He, J.; Kähler, K.; Muhler, M.; Schlögl, R. CO_2 Hydrogenation with Cu/ZnO/Al_2O_3 : A Benchmark Study. *ChemCatChem* 2020, *12*, 3216–3222, doi:10.1002/cctc.202000195.

54. Marlin, D.S.; Sarron, E.; Sigurbjörnsson, Ó. Process Advantages of Direct CO2 to Methanol Synthesis. *Frontiers in Chemistry* 2018, *6*, doi:10.3389/fchem.2018.00446.

55. Leonzio, G. Methanol Synthesis: Optimal Solution for a Better Efficiency of the Process. *Processes* 2018, *6*, 20, doi:10.3390/pr6030020.

56. Schühle, P. Methanolsynthese Aus CO2 an In2O3-Basierten Katalysatoren in Slurry- Und Festbettreaktoren. Dissertation, Friedrich-Alexander-Universität Erlangen Nürnberg, Technische Fakultät: Erlangen, 2021.

57. Clariant Catalysts. Catalysts for Methanol Synthesis. 2017. Available at: https://www.clariant.com/de/Solutions/Products/2022/12/12/09/57/MegaMax-900. [Accessed: 10.1.2024].

58. Kleiber, S.; Pallua, M.; Siebenhofer, M.; Lux, S. Catalytic Hydrogenation of CO2 to Methanol over Cu/MgO Catalysts in a Semi-Continuous Reactor. *Energies* 2021, *14*, 4319, doi:10.3390/en14144319.

59. Schühle, P.; Reichenberger, S.; Marzun, G.; Albert, J. Slurry Phase Hydrogenation of CO2 to Methanol Using Supported In2O3 Catalysts as Promising Approach for Chemical Energy Storage. *Chemie Ingenieur Technik* 2020, *93*, 585–593, doi:10.1002/cite.202000109.

60. Pacholik, G.; Enzlberger, L.; Benzer, A.; Rameshan, R.; Latschka, M.; Rameshan, C.; Föttinger, K. In Situ XPS Studies of MoS_2 -Based CO_2 Hydrogenation Catalysts. *J. Phys. D: Appl. Phys.* 2021, *54*, 324002, doi:10.1088/1361-6463/ac006f.

61. Wang, D.; Meng, W.; Zhou, H.; Yang, Y.; Xie, J.; Yang, S.; Li, G. Novel Coal-to-Methanol Process with near-Zero Carbon Emission: Pulverized Coal Gasification-Integrated Green Hydrogen Process. *Journal of Cleaner Production* 2022, *339*, 130500, doi:10.1016/j.jclepro.2022.130500.

62. IMPCA. IMPCA Methanol Reference Specifications. 2021. Available at: https://www.impca.eu/IMPCA/Technical/IMPCA-Documents. [Accessed: 2.10.2023].

63. Ojelade, O.A.; Zaman, S.F.; Ni, B.-J. Green Ammonia Production Technologies: A Review of Practical Progress. *Journal of Environmental Management* 2023, *342*, 118348, doi:10.1016/j.jenvman.2023.118348.

64. Mayer, P.; Ramirez, A.; Pezzella, G.; Winter, B.; Sarathy, S.M.; Gascon, J.; Bardow, A. Blue and Green Ammonia Production: A Techno-Economic and Life Cycle Assessment Perspective. *iScience* 2023, *26*, 107389, doi:10.1016/j.isci.2023.107389.

65. Enaex. Enaex Submits Green Ammonia Processing Plant Construction Project for Environmental Assessment. 2021. Available at: https://www.enaex.com/era/en/green-ammonia/. [Accessed: 4.10.2023].

66. Enaex and Engie. HyEx: Green Ammonia. Ammonia Energy Association. 2023. Available at: https://www.ammoniaenergy.org/articles/hyex-ammonia-from-the-chilean-desert/. [Accessed: 4.10.2023].

67. Brown, T. Green Ammonia Plants in Chile, Australia and New Zealand. Ammonia Energy Association. 2019. Available at: https://www.ammoniaenergy.org/articles/green-ammonia-plants-in-chile-australia-new-zealand/. [Accessed: 4.10.2023].

68. Atchinson, J. ACME & IHI: New Ammonia Mega-Project in Odisha. Ammonia Energy Association. 2023. Available at: https://www.ammoniaenergy.org/articles/acme-ihi-new-ammonia-mega-project-in-odisha/. [Accessed: 12.9.2023].

69. Njovu, G. More Progress for Canada-Based Project Nujio´qonik. Ammonia Energy Association, 2023. Available at: https://www.ammoniaenergy.org/articles/more-progress-for-canada-based-project-nujioqonik/. [Accessed: 12.9.2023].

70. Semmel, M.; Ali, R.E.; Ouda, M.; Schaadt, A.; Sauer, J.; Hebling, C. Power-to-DME: A Cornerstone towards a Sustainable Energy System. In *Power to Fuel*; Elsevier, 2021. pp. 123–151 ISBN 978-0-12-822813-5.

71. Schemme, S.; Breuer, J.L.; Köller, M.; Meschede, S.; Walman, F.; Samsun, R.C.; Peters, R.; Stolten, D. H2-Based Synthetic Fuels: A Techno-Economic Comparison of Alcohol, Ether and Hydrocarbon Production. *International Journal of Hydrogen Energy* 2020, *45*, 5395–5414, doi:10.1016/j.ijhydene.2019.05.028.

72. Matzen, M.; Demirel, Y. Methanol and Dimethyl Ether from Renewable Hydrogen and Carbon Dioxide: Alternative Fuels Production and Life-Cycle Assessment. *Journal of Cleaner Production* 2016, *139*, 1068–1077, doi:10.1016/j.jclepro.2016.08.163.

73. Maus, W. Zukünftige Kraftstoffe: Energiewende des Transports als ein weltweites Klimaziel. Ed.; Springer Berlin Heidelberg: Berlin, Heidelberg, 2019. ISBN 978-3-662-58005-9.

74. Kiss, A.A. Novel Catalytic Reactive Distillation Processes for a Sustainable Chemical Industry. *Top Catal* 2019, *62*, 1132–1148, doi:10.1007/s11244-018-1052-9.

75. Schemme, S. Techno-Economic Assessment of Processes for the Production of Fuels from H2 and CO2, Rheinisch-Westfälische Technische Hochschule Aachen, Institut für Energie- und Klimaforschung, 2020.

76. Ehlers, J.C.; Feidenhans'l, A.A.; Therkildsen, K.T.; Larrazábal, G.O. Affordable Green Hydrogen from Alkaline Water Electrolysis: Key Research Needs from an Industrial Perspective. *ACS Energy Lett.* 2023, *8*, 1502–1509, doi:10.1021/acsenergylett.2c02897.

77. Nasser, M.; Megahed, T.F.; Ookawara, S.; Hassan, H. A Review of Water Electrolysis–Based Systems for Hydrogen Production Using Hybrid/Solar/Wind Energy Systems. *Environ Sci Pollut Res* 2022, *29*, 86994–87018, doi:10.1007/s11356-022-23323-y.

78. Schmidt, O.; Gambhir, A.; Staffell, I.; Hawkes, A.; Nelson, J.; Few, S. Future Cost and Performance of Water Electrolysis: An Expert Elicitation Study. *International Journal of Hydrogen Energy* 2017, *42*, 30470–30492, doi:10.1016/j.ijhydene.2017.10.045.

79. Kecebas, A.; Kayfeci, M.; Bayat, M. Electrochemical Hydrogen Generation. In *Solar Hydrogen Production - Processes, Systems and Technologies*. 2019. ISBN 978-0-12-814853-2.

80. Lange, H.; Klose, A.; Lippmann, W.; Urbas, L. Technical Evaluation of the Flexibility of Water Electrolysis Systems to Increase Energy Flexibility: A Review. *International Journal of Hydrogen Energy* 2023, *48*, 15771–15783, doi:10.1016/j.ijhydene.2023.01.044.

81. Collins, L. Record Breaker - World's Largest Green Hydrogen Project, with 150MW Electrolyser Brought on Line in China. 2022. Available at: https://www.rechargenews.com/energy-transition/record-breaker-world-s-largest-green-hydrogen-project-with-150mw-electrolyser-brought-on-line-in-china/2-1-1160799. [Accessed: 12.10.2023].

82. Liu, R.-T.; Xu, Z.-L.; Li, F.-M.; Chen, F.-Y.; Yu, J.-Y.; Yan, Y.; Chen, Y.; Xia, B.Y. Recent Advances in Proton Exchange Membrane Water Electrolysis. *Chem. Soc. Rev.* 2023, *52*, 5652–5683, doi:10.1039/D2CS00681B.

83. Collins, L. US-Based Cummins to Build 1GW Hydrogen Electrolyzer Factory in China with State-Owned Oil Giant Sinopec. 2022. Available at: https://www.rechargenews.com/energy-transition/us-based-cummins-to-build-1gw-hydrogen-electrolyser-factory-in-china-with-state-owned-oil-giant-sinopec/2-1-1139138. [Accessed: 12.10.2023].

84. Wolf, S.E.; Winterhalder, F.E.; Vibhu, V.; De Haart, L.G.J. (Bert); Guillon, O.; Eichel, R.-A.; Menzler, N.H. Solid Oxide Electrolysis Cells – Current Material Development and Industrial Application. *J. Mater. Chem. A* 2023, *11*, 17977–18028, doi:10.1039/D3TA02161K.

85. Stoots, C.M.; O'Brien, J.E.; Herring, J.S.; Hartvigsen, J.J. Syngas Production via High-Temperature Coelectrolysis of Steam and Carbon Dioxide. *Journal of Fuel Cell Science and Technology* 2009, *6*, 011014, doi:10.1115/1.2971061.

86. Wang, Y.; Liu, T.; Lei, L.; Chen, F. High Temperature Solid Oxide H2O/CO2 Co-Electrolysis for Syngas Production. *Fuel Processing Technology* 2017, *161*, 248–258, doi:10.1016/j.fuproc.2016.08.009.

87. Cinti, G.; Baldinelli, A.; Di Michele, A.; Desideri, U. Integration of Solid Oxide Electrolyzer and Fischer-Tropsch: A Sustainable Pathway for Synthetic Fuel. *Applied Energy* 2016, *162*, 308–320, doi:10.1016/j.apenergy.2015.10.053.

88. Sunfire. Renewable Hydrogen Project "Multiplhy": World's Largest High-Temperature Electrolyzer from Sunfire Successfully Installed. 2023. Available at: https://www.sunfire.de/en/news/detail/renewable-hydrogen-project-multiplhy-worlds-largest-high-temperature-electrolyzer-from-sunfire-successfully-installed. [Accessed: 12.10.2023].

89. Topsoe. Press Release - Topsoe Celebrates Milestone in Construction of World's First Industrial Scale SOEC Electrolyzer Facility. 2023. Available at: https://www.arctictoday.com/arctic_business/topsoe-celebrates-milestone-in-construction-of-worlds-first-industrial-scale-soec-electrolyzer-facility/. [Accessed: 12.10.2023].

90. Förtsch, D.; Pabst, K.; Groß-Hardt, E. The Product Distribution in Fischer–Tropsch Synthesis: An Extension of the ASF Model to Describe Common Deviations. *Chemical Engineering Science* 2015, *138*, 333–346, doi:10.1016/j.ces.2015.07.005.

91. Gruber, H.; Groß, P.; Rauch, R.; Reichhold, A.; Zweiler, R.; Aichernig, C.; Müller, S.; Ataimisch, N.; Hofbauer, H. Fischer-Tropsch Products from Biomass-Derived Syngas and Renewable Hydrogen. *Biomass Conv. Bioref.* 2019, doi:10.1007/s13399-019-00459-5.

92. de Klerk, A. Transport Fuel. In *Future Energy*; Elsevier, 2020. pp. 199–226 ISBN 978-0-08-102886-5.

93. Leonzio, G.; Zondervan, E.; Foscolo, P.U. Methanol Production by CO2 Hydrogenation: Analysis and Simulation of Reactor Performance. *International Journal of Hydrogen Energy* 2019, *44*, 7915–7933, doi:10.1016/j.ijhydene.2019.02.056.

94. Schmidt, P.; Weindorf, W. Power-to-Liquids: Potential and Perspectives for the Future Supply of Renewable Aviation Fuel. German Environment Agency. 2016.

95. Cinti, G.; Discepoli, G.; Bidini, G.; Lanzini, A.; Santarelli, M. Co-Electrolysis of Water and CO_2 in a Solid Oxide Electrolyzer (SOE) Stack: Study of High-Temperature Co-Electrolysis Reactions in SOEC. *Int. J. Energy Res.* 2016, *40*, 207–215, doi:10.1002/er.3450.

96. Klerk, A. de Fischer-Tropsch Refining; 1st. ed.; Wiley-VCH: Weinheim, Germany, 2011. ISBN 978-3-527-63560-3.

97. Ali, S.; Sørensen, K.; Nielsen, M.P. Modeling a Novel Combined Solid Oxide Electrolysis Cell (SOEC) - Biomass Gasification Renewable Methanol Production System. *Renewable Energy* 2020, *154*, 1025–1034, doi:10.1016/j.renene.2019.12.108.

98. Schädel, B.T.; Duisberg, M.; Deutschmann, O. Steam Reforming of Methane, Ethane, Propane, Butane, and Natural Gas over a Rhodium-Based Catalyst. *Catalysis Today* 2009, *142*, 42–51, doi:10.1016/j.cattod.2009.01.008.

99. Towler, G.P.; Sinnott, R.K. Chemical Engineering Design: Principles, Practice and Economics of Plant and Process Design; Third edition.; Butterworth-Heinemann: Oxford [England]; Cambridge, MA, 2022. ISBN 978-0-12-821179-3.

100. Kunysz, D.O. Kostenschätzung im chemischen Anlagenbau: Cost Estimation Basics; essentials; Springer Fachmedien Wiesbaden: Wiesbaden, 2020. ISBN 978-3-658-29250-8.

101. Peters, M.S.; Timmerhaus, K.D.; West, R.E. Plant Design and Economics for Chemical Engineers; McGraw-Hill chemical engineering series; 5th ed.; McGraw-Hill: New York, 2003. ISBN 978-0-07-239266-1.

102. Seider, W.D.; Lewin, D.R.; Seader, J.D.; Widagdo, S.; Gani, R.; Ng, K.M. Product and Process Design Principles: Synthesis, Analysis, and Evaluation; Fourth edition.; John Wiley & Sons Inc.: New York, 2017. ISBN 978-1-119-26129-2.

103. Turton, R. Analysis, Synthesis, and Design of Chemical Processes; Ed.; 4th ed.; Prentice Hall: Upper Saddle River, NJ, 2012. ISBN 978-0-13-261812-0.

104. Chemical Engineering Magazine. Access Intelligence. Volume 130 (4). LLC April 2023. 2023.

105. Neuling, U.; Kaltschmitt, M. Techno-Economic and Environmental Analysis of Aviation Biofuels. *Fuel Processing Technology* 2018, *171*, 54–69, doi:10.1016/j.fuproc.2017.09.022.

106. Decker, M.; Schorn, F.; Samsun, R.C.; Peters, R.; Stolten, D. Off-Grid Power-to-Fuel Systems for a Market Launch Scenario – A Techno-Economic Assessment. *Applied Energy* 2019, *250*, 1099–1109, doi:10.1016/j.apenergy.2019.05.085.

107. Herz, G.; Reichelt, E.; Jahn, M. Techno-Economic Analysis of a Co-Electrolysis-Based Synthesis Process for the Production of Hydrocarbons. *Applied Energy* 2018, *215*, 309–320, doi:10.1016/j.apenergy.2018.02.007.

108. Green, D.W., Southard, M.Z. Perry's Chemical Engineers' Handbook; Eds.; Ninth edition, 85th anniversary edition.; McGraw Hill Education: New York, 2019. ISBN 978-0-07-183409-4.

109. DeSantis, D.; James, B.; Saur, G. H2A: Hydrogen Analysis Production Models - Future Central Hydrogen Production from PEM Electrolysis. 2019. Version 3.2018 2019.

110. Technical University of Denmark. Data Obtained from the "Global Wind Atlas 3.0, a Free, Web-Based Application Developed, Owned and Operated by the Technical University of Denmark (DTU). The Global Wind Atlas 3.0 Is Released in Partnership with the World Bank Group, Utilizing Data Provided by Vortex, Using Funding Provided by the Energy Sector Management Assistance Program (ESMAP). 2023. Available at: https://globalwindatlas.info. [Accessed: 23.10.2023].

111. European Commission. Photovoltaic Geographical Information System. 2023. Available at: https://re.jrc.ec.europa.eu/pvg_tools/en/. [Accessed: 23.10.2023].

112. Environment Agency Austria. Calculation of Greenhouse Gas Emissions of Different Energy Carriers. 2021. Available at: https://secure.umweltbundesamt.at/co2mon/co2mon.html. [Accessed: 19.10.2023].

113. European Environment Agency. Greenhouse Gas Emission Intensity of Electricity Generation in Europe. 2023. Available at: https://www.eea.europa.eu/ims/greenhouse-gas-emission-intensity-of-1. [Accessed: 19.10.2023].

114. Lauf, T.; Memmler, M.; Schneider, S. Emissionsbilanz Erneuerbarer Energieträger. German Environment Agency (UBA). 2019. Available at: https://www.umweltbundesamt.de/sites/default/files/medien/11850/publikationen/20231219_49_2023_cc_emissionsbilanz_erneuerbarer_energien_2022_bf.pdf. [Accessed: 4.3.2024].

115. Methanol Institute. Carbon Footprint of Methanol. 2022. Available at: https://www.methanol.org/wp-content/uploads/2022/01/CARBON-FOOTPRINT-OF-METHANOL-PAPER_1-31-22.pdf. [Accessed: 20.10.2023].

116. de Jong, M.; Bunse, M.; Hamelinck, C. Methanol Carbon Footprint and Certification. International Methanol Producers and Consumers Association IMPCA: Amsterdam, The Netherlands. 2022.

117. Herz, G.; Rix, C.; Jacobasch, E.; Müller, N.; Reichelt, E.; Jahn, M.; Michaelis, A. Economic Assessment of Power-to-Liquid Processes – Influence of Electrolysis Technology and Operating Conditions. *Applied Energy* 2021, *292*, 116655, doi:10.1016/j.apenergy.2021.116655.

118. Markowitsch, C.; Lehner, M.; Maly, M. Comparison and Techno-Economic Evaluation of Process Routes for Lower Olefin Production via Fischer–Tropsch and Methanol Synthesis. *International Journal of Greenhouse Gas Control* 2023, *129*, 103985, doi:10.1016/j.ijggc.2023.103985.

119. Hammerschmid, M.; Bartik, A.; Benedikt, F.; Veress, M.; Pratschner, S.; Müller, S.; Hofbauer, H. Economic and Ecological Impacts on the Integration of Biomass-Based SNG and FT Diesel in the Austrian Energy System. *Energies* 2023, *16*, 6097, doi:10.3390/en16166097.

120. Becker, W.L.; Braun, R.J.; Penev, M.; Melaina, M. Production of Fischer–Tropsch Liquid Fuels from High Temperature Solid Oxide Co-Electrolysis Units. *Energy* 2012, *47*, 99–115, doi:10.1016/j.energy.2012.08.047.

121. Markowitsch, C.; Lehner, M.; Maly, M. Evaluation of Process Structures and Reactor Technologies of an Integrated Power-to-Liquid Plant at a Cement Factory. *Journal of CO2 Utilization* 2023, *70*, 102449, doi:10.1016/j.jcou.2023.102449.

122. Marchese, M.; Giglio, E.; Santarelli, M.; Lanzini, A. Energy Performance of Power-to-Liquid Applications Integrating Biogas Upgrading, Reverse Water Gas Shift, Solid Oxide Electrolysis and Fischer-Tropsch Technologies. *Energy Conversion and Management: X* 2020, *6*, 100041, doi:10.1016/j.ecmx.2020.100041.

123. Marchese, M.; Buffo, G.; Santarelli, M.; Lanzini, A. CO2 from Direct Air Capture as Carbon Feedstock for Fischer-Tropsch Chemicals and Fuels: Energy and Economic Analysis. *Journal of CO2 Utilization* 2021, *46*, 101487, doi:10.1016/j.jcou.2021.101487.

124. Kratky, K. Power-and-Biogas-to-Liquid and Power-and-Gas-to-Liquid. CAPHENIA. 7th Central European Biomass Conference. Graz, Austria, 2023.

125. ChemAnalyst. Methanol Price Trend and Forecast. 2022. Available at: https://www.chemanalyst.com/Pricing-data/methanol-1. [Accessed: 23.10.2023].

126. Markets Insider. OIL (BRENT). 2023. Available at: https://markets.businessinsider.com/commodities/oil-price/euro. [Accessed: 16.11.2023].

127. International Air Transport Association. Jet Fuel Price Monitor. 2023. Available at: https://www.iata.org/en/publications/economics/fuel-monitor/. [Accessed: 22.11.2023].

128. Global Oil and Gas Trading. Jet Fuel Price / ATF (Aviation Turbine Fuel) Price This Week. 2023. Available at: https://globaloilandgastrading.com/aviation-fuel-jetfuel-1. [Accessed: 22.11.2023].

129. FlightDeckFriend. The Price of Jet Fuel and Fueling an Aircraft. 2022. Available at: https://www.flightdeckfriend.com/ask-a-pilot/how-much-does-jet-fuel-cost/. [Accessed: 22.11.2023].

130. ChemAnalyst. Paraffin Wax Price Trend and Forecast. 2023. Available at: https://www.chemanalyst.com/Pricing-data/paraffin-wax-1205#:~:text=Therefore%2C%20the%20price%20of%20Paraffin,(USA)%20in%20December%202022. [Accessed: 14.11.2023].

131. Unnasch, S.; Wiesenberg, R.; Sanchez, S.T. Assessment of Direct and Indirect GHG Emissions Associated with Petroleum Fuels; Life Cycle Associates. 2009. Available at: https://d35t1syewk4d42.cloudfront.net/file/851/NFA_PImpacts_v35.pdf. [Accessed: 4.3.2024].

132. Probas. Process Details: Crude Oil Mix RO-2020. German Environment Agency. 2023. Available at: https://www.probas.umweltbundesamt.de/php/prozessdetails.php?id={DC4882B5-B2F3-423B-91DA-6F9ACE39B667}. [Accessed: 22.11.2023].

133. Probas. Process Details: Kerosene-2020. German Environment Agency. 2023. Available at: https://www.probas.umweltbundesamt.de/php/prozessdetails.php?id={6076C5C7-A37F-405F-ACC9-67A2158088C6}. [Accessed: 22.11.2023].

134. Probas. Process Details: Lubricating Oil-2020. German Environment Agency. 2023. Available at: https://www.probas.umweltbundesamt.de/php/prozessdetails.php?id={8C6B3AFA-8299-474D-9057-FA639B06CD35}. [Accessed: 22.11.2023].

135. Statista. European Union Emission Trading System (EU-ETS) Carbon Pricing from January 2022 to April 2023. 2023. Available at: https://www.statista.com/statistics/1322214/carbon-prices-european-union-emission-trading-scheme/. [Accessed: 23.10.2023].

136. Federal Ministry Republic of Austria – Finance. Initial Information on the 2022 National Emissions Certificates Trading Law (NEHG 2022). 2022. Available at: https://www.bmf.gv.at/en/topics/Climate-policy/initial_nehg_2022_en.html. [Accessed: 23.10.2023].

137. Government Offices of Sweden. Sweden's Carbon Tax. 2023. Available at: https://www.government.se/government-policy/swedens-carbon-tax/#:~:text=Swedish%20carbon%20tax%20rates&text=The%20carbon%20tax%20was%20introduced,of%20SEK%2010.87%20per%20EUR). [Accessed: 23.10.2023].

138. Brynolf, S.; Taljegard, M.; Grahn, M.; Hansson, J. Electrofuels for the Transport Sector: A Review of Production Costs. *Renewable and Sustainable Energy Reviews* 2018, *81*, 1887–1905, doi:10.1016/j.rser.2017.05.288.

139. Nyári, J.; Magdeldin, M.; Larmi, M.; Järvinen, M.; Santasalo-Aarnio, A. Techno-Economic Barriers of an Industrial-Scale Methanol CCU-Plant. *Journal of CO2 Utilization* 2020, *39*, 101166, doi:10.1016/j.jcou.2020.101166.

140. Otto, A. Chemische, verfahrenstechnische und ökonomische Bewertung von Kohlendioxid als Rohstoff in der chemischen Industrie. Forschungszentrum Jülich, Zentralbibliothek: Jülich, 2015. ISBN 978-3-95806-064-7.

141. Yousaf, M.; Mahmood, A.; Elkamel, A.; Rizwan, M.; Zaman, M. Techno-Economic Analysis of Integrated Hydrogen and Methanol Production Process by CO2 Hydrogenation. *International Journal of Greenhouse Gas Control* 2022, *115*, 103615, doi:10.1016/j.ijggc.2022.103615.

142. Peters, R.; Wegener, N.; Samsun, R.C.; Schorn, F.; Riese, J.; Grünewald, M.; Stolten, D. A Techno-Economic Assessment of Fischer–Tropsch Fuels Based on Syngas from Co-Electrolysis. *Processes* 2022, *10*, 699, doi:10.3390/pr10040699.

143. Herz, G.; Rix, C.; Jacobasch, E.; Müller, N.; Reichelt, E.; Jahn, M.; Michaelis, A. Economic Assessment of Power-to-Liquid Processes – Influence of Electrolysis Technology and Operating Conditions. *Applied Energy* 2021, *292*, 116655, doi:10.1016/j.apenergy.2021.116655.

144. Fasihi, M.; Bogdanov, D.; Breyer, C. Techno-Economic Assessment of Power-to-Liquids (PtL) Fuels Production and Global Trading Based on Hybrid PV-Wind Power Plants. *Energy Procedia* 2016, *99*, 243–268, doi:10.1016/j.egypro.2016.10.115.

145. Herz, G.; Reichelt, E.; Jahn, M. Techno-Economic Analysis of a Co-Electrolysis-Based Synthesis Process for the Production of Hydrocarbons. *Applied Energy* 2018, *215*, 309–320, doi:10.1016/j.apenergy.2018.02.007.

146. Zang, G.; Sun, P.; Elgowainy, A.A.; Bafana, A.; Wang, M. Performance and Cost Analysis of Liquid Fuel Production from H2 and CO2 Based on the Fischer-Tropsch Process. *Journal of CO2 Utilization* 2021, *46*, 101459, doi:10.1016/j.jcou.2021.101459.

147. Albrecht, F.G.; König, D.H.; Baucks, N.; Dietrich, R.-U. A Standardized Methodology for the Techno-Economic Evaluation of Alternative Fuels – A Case Study. *Fuel* 2017, *194*, 511–526, doi:10.1016/j.fuel.2016.12.003.

148. EMR. Europe Methanol Market Outlook. Expert Market Research. 2023. Available at: https://www.expertmarketresearch.com/reports/europe-methanol-market#:~:text=The%20Europe%20methanol%20market%20size,13.25%20million%20tons%20by%202032. [Accessed: 09.11.2023].

149. The Global Economy. Jet Fuel Consumption – Country Rankings. 2023. Available at: https://www.theglobaleconomy.com/rankings/jet_fuel_consumption/European-union/. [Accessed: 10.11.2023].

150. Eurostat. Heavy Fuel Oil - Production, Trade and Use. 2021. Available at: https://ec.europa.eu/eurostat/statistics-explained/index.php?title=Heavy_fuel_oil_-_production,_trade_and_use&stable=0&redirect=no#Use_of_fuel_oil_in_the_EU. [Accessed: 09.11.2023].

151. Millinger, M.; Reichenberg, L.; Hedenus, F.; Berndes, G.; Zeyen, E.; Brown, T. Are Biofuel Mandates Cost-Effective? - An Analysis of Transport Fuels and Biomass Usage to Achieve Emissions Targets in the European Energy System. *Applied Energy* 2022, *326*, 120016, doi:10.1016/j.apenergy.2022.120016.

List of Figures

List of Tables

Journal Articles

Journal Article I

energies

MDPI

Article

Power-to-Green Methanol via CO_2 Hydrogenation—A Concept Study including Oxyfuel Fluidized Bed Combustion of Biomass

Simon Pratschner [1,*], Pavel Skopec [2], Jan Hrdlicka [2] and Franz Winter [1]

[1] Institute of Chemical, Environmental and Bioscience Engineering, TU Wien, Getreidemarkt 9/166, 1060 Vienna, Austria; franz.winter@tuwien.ac.at
[2] Department of Energy Engineering, Faculty of Mechanical Engineering, Czech Technical University in Prague, Technicka 4, 166 07 Prague, Czech Republic; p.skopec@fs.cvut.cz (P.S.); jan.hrdlicka@fs.cvut.cz (J.H.)
* Correspondence: simon.pratschner@tuwien.ac.at

Abstract: A revolution of the global energy industry is without an alternative to solving the climate crisis. However, renewable energy sources typically show significant seasonal and daily fluctuations. This paper provides a system concept model of a decentralized power-to-green methanol plant consisting of a biomass heating plant with a thermal input of 20 $MW_{th.}$ (oxyfuel or air mode), a CO_2 processing unit (DeOxo reactor or MEA absorption), an alkaline electrolyzer, a methanol synthesis unit, an air separation unit and a wind park. Applying oxyfuel combustion has the potential to directly utilize O_2 generated by the electrolyzer, which was analyzed by varying critical model parameters. A major objective was to determine whether applying oxyfuel combustion has a positive impact on the plant's power-to-liquid (PtL) efficiency rate. For cases utilizing more than 70% of CO_2 generated by the combustion, the oxyfuel's O_2 demand is fully covered by the electrolyzer, making oxyfuel a viable option for large scale applications. Conventional air combustion is recommended for small wind parks and scenarios using surplus electricity. Maximum PtL efficiencies of $\eta_{PtL,Oxy}$ = 51.91% and $\eta_{PtL,Air}$ = 54.21% can be realized. Additionally, a case study for one year of operation has been conducted yielding an annual output of about 17,000 t/a methanol and 100 $GWh_{th.}$/a thermal energy for an input of 50,500 t/a woodchips and a wind park size of 36 MWp.

Keywords: green methanol; power-to-X; CCU; oxyfuel; renewables; alkaline electrolysis; biomass

Citation: Pratschner, S.; Skopec, P.; Hrdlicka, J.; Winter, F. Power-to-Green Methanol via CO_2 Hydrogenation—A Concept Study including Oxyfuel Fluidized Bed Combustion of Biomass. *Energies* **2021**, *14*, 4638. https://doi.org/10.3390/en14154638

Academic Editors: Attilio Converti and Prasad Kaparaju

Received: 11 June 2021
Accepted: 19 July 2021
Published: 30 July 2021

1. Introduction

The climate crisis poses a major threat to human civilization on a long-term basis. The global monthly average CO_2 concentration in the atmosphere reached a level of 415 ppm in December 2020, with average growth rates of 2–3 ppm per year in the previous five years [1,2]. Combustion processes for power generation account for about 42% of global anthropogenic CO_2 emissions, indicating the energy industry's key role for mitigating global warming [3]. In 2019, the European Commission launched its Green Deal program, including the goal to become the first climate-neutral continent by 2050, as well as decoupling economic growth and resource usage [4].

To reach these ambitious targets, intersectional concepts, based on renewable energy sources, for the provision of power and heat need to be empowered and improved. Carbon capture and storage (CCS) and carbon capture and utilization (CCU) pose promising technologies in fighting the climate crisis. However, CCS goes hand in hand with several difficulties (e.g., safety issues and substantial efforts for the transportation of captured CO_2). Additionally, CCS is illegal in numerous countries and therefore, a limited option for the mitigation of CO_2 emissions. A variety of promising CCU technologies (e.g., power-to-gas (PtG), power-to-liquid (PtL), power-to-fuels (PtF) and power-to-chemicals (PtC)) are on the verge of becoming economically feasible within this decade. Significant advantages are the on-site usage of CO_2 sources, as well as the development of new business cases to produce renewable fuels or chemicals. Crucial parameters defining the sustainability

of CCU technologies are the CO_2's origin as well as the product's (H_2, CH_4, methanol, Fischer-Tropsch products) scope of application. Possible CO_2 capture systems (i.e., direct air capture (DAC), post combustion, pre combustion, oxyfuel combustion or industrial processes) are listed and explained in detail in the IPCC special report on carbon dioxide capture and storage [5]. In general, sources with a high concentration of CO_2 are favored due to a smaller technological effort of CO_2 capture.

In May 2018, 128 PtG projects were in progress or have been finished in Europe. A list of conducted projects as well as an overview of possible PtG process routes can be found in [6]. Three PtG demo sites for CO_2 valorization to methane using different reactor technologies (i.e., a catalytic honeycomb reactor, a biological stirred bubble column reactor and a catalytic milli-structured reactor) are analyzed in [7]. Within the pan-European project MefCO_2, a PtL pilot plant with an annual output of 500 t/a methanol was realized. Captured CO_2 was valorized using a polymer electrolyte membrane electrolyzer powered with solar-generated electricity in Niederaußem, Germany [8]. Another successful example is the George Olah Plant, located in Iceland, a PtL plant at industrial scale, designed and constructed by the Icelandic company Carbon Recycling International (CRI). Over 4000 t/a methanol can be produced valorizing geothermal CO_2 with H_2 generated by an alkaline electrolyzer powered by Iceland's 100% renewable grid electricity [9]. After winning the Nobel Prize in 1994, George Olah's scientific focus shifted towards producing green fuels (e.g., methanol using captured CO_2 as feedstock), making him a pioneer in PtL processes before the term came into existence [10]. The German start-up company, INERATEC, announced the construction of a PtF plant at industrial scale at Frankfurt, Germany, until 2022. A total of 3500 t/a Fischer-Tropsch products will be produced using a maximum of 10,000 t/a biogenic CO_2 [11]. Research analyzing CO_2 hydrogenation to methanol at lab-scale can be found in [12] (applying an In_2O_3/ZrO_2 catalyst) and [13] (conventional $Cu/ZnO/Al_2O_3$ catalyst). Within the past years PtL technologies transitioned from a niche application at laboratory scale to a viable option for the process and energy industry regarding CCU technologies. Current projects aim at proofing the process' feasibility at pilot scale obtaining reasonable efficiency rates. Major challenges within the following years will be the provision of cost-effective renewable H_2 by electrolyzers surpassing a power input of several MW. Power-to-liquid processes have the potential to provide renewable eFuels as the intermediate power source until individual mobility is fully electrified. In the long run, eFuels could be applied as the power source for aviation and goods transport, requiring a high energy density.

Oxyfuel combustion was first proposed in 1982 to provide a CO_2-rich gas stream for enhanced oil recovery applications, and experienced a technological renaissance in the early 2000s when being rediscovered as a suitable option for CCU processes. Oxyfuel combustion tackles the issue of low CO_2 concentrations in flue gases obtained by conventional air combustion processes [14]. In oxyfuel combustion technologies, fuels are burned in a mixture of O_2 with a technical purity of at least 95 vol% and recirculated flue gas. The recirculation of flue gas is mandatory, as the missing volume stream of the air's N_2 needs to be replaced. Furthermore, the combustor's flame temperature can be controlled by adjusting the amount of recirculated flue gas. The main differences when comparing oxyfuel combustion with conventional air combustion are [14]:

- O_2 concentrations of about 30 vol% in the oxidant are required to obtain a comparable flame temperature;
- Volume flow streams of emitted flue gas are reduced by about 80% since no N_2 passes the combustor as inert gas;
- Different combustion regimes are observed due to deviating physical properties of CO_2 and N_2. For example, the density of flue gas generated by an oxyfuel combustion process is larger due to a higher molar mass of CO_2, concluding in a larger specific heat capacity as well.

The "Callide" oxyfuel project, successfully completed in 2015, can be considered a showcase regarding oxyfuel combustion at an industrial scale. A power plant located in the

state of Queensland, Australia, with a thermal input of 24–29 $MW_{th.}$ (coal) was combined with a CCS project located in Victoria, Australia. Detailed scientifical results can be found in the project's final report [15]. Another oxyfuel project launched by Vattenfall in 2006 at Schwarze Pumpe, Germany, aimed at retrofitting an existing coal power plant with a thermal input of 30 $MW_{th.}$ for CCS applications. However, Vattenfall cancelled the project in 2014 due to economic difficulties without publishing a final report. A detailed study on oxyfuel combustion of biomass in a 20 kW_{th} fluidized bed combustor can be found in [16], analyzing effects of combustion environments (oxyfuel combustion vs. conventional air combustion) on fuel combustion, temperature profiles and CO and NO_x emissions.

As stated previously, power-to-X technologies will play a significant role in fighting the climate crisis due to their potential to chemically store excess power generated by renewable energy carriers as H_2, CH_4, methanol or Fischer-Tropsch products. Renewable power sources (i.e., wind or solar) undergo daily and seasonal fluctuations leading to difficulties regarding the storage of surplus electricity. Generated energy carriers could also be integrated in grid-stabilizing systems, tackling another major disadvantage of renewable power sources.

Furthermore, hydrogenating CO_2 comes with several process advantages compared to conventional methanol production by syngas [9,17]:

- Fewer impurities can be found in the crude methanol;
- The chemical reaction of CO_2 and H_2 is less complex and less exothermal compared to the synthesis based on CO and H_2;
- Boiling water reactors (BWRs) including a recirculation of unconverted gases can easily be applied instead of adiabatic reactors in series since less reaction heat needs to be transferred out of the catalyst bed, resulting in a larger economic feasibility of the process;
- Milder process conditions are required;
- The methanol selectivity of CO_2 hydrogenation is larger compared to conventional methanol synthesis processes based on syngas as the reactor input.

The design and simulation, using Aspen Plus, of a plant producing methanol via CO_2 hydrogenation can be found in [18]. CO_2 generated by a thermal power plant using coal as fuel was hydrogenated with H_2 produced by water electrolysis. The authors declared that O_2, generated by the electrolyzer, had to be sold as a by-product and highlighted the possible potential of using it as feedstock for oxyfuel combustion processes without calculating detailed scenarios. A feasibility analysis of a plant producing renewable methanol by chemically storing wind power can be found in [19]. The production costs of H_2, being the most significant model parameter, as well as the selling price of methanol were varied. Consequently, selling or using O_2 generated by water splitting could be a major factor in improving the facility's economic feasibility.

This article aims at finding and conceptualizing different process routes for a decentralized power-to-green methanol plant, with a thermal input of 20 $MW_{th.}$, using woodchips as fuel (Figure 1). As a result, the proposed concept has the potential to achieve a negative CO_2 balance. A foundation for future research projects should be provided with the goal to increase the concept's level of details. Furthermore, proposed process routes will be evaluated by comparing obtained power-to-liquid efficiency rates to values stated in reviewed literature. In comparison with previous studies, this paper includes the application of oxyfuel combustion in combination with methanol production (CO_2 hydrogenation) by directly applying O_2 (by-product of water splitting) to the oxyfuel combustor. Furthermore, a direct comparison of oxyfuel and air process routes in combination with CCU, regarding the efficiency rates of power-to-green methanol facilities, should answer the question whether oxyfuel process routes are a viable option for future PtL plants.

Figure 1. Power-to-green methanol plant.

A specific hypothesis of this work is whether the replacement of conventional air by oxyfuel combustion enhances the performance of power-to-methanol plants using post combustion CO_2 capture. The preferable combustion technology as well as the synergy between oxyfuel combustion and water electrolysis (generating O_2 as byproduct) was determined for different assumed scenarios.

2. Materials and Methods

The main aspect of this work was to model several subprocesses (oxyfuel combustion in combination with a DeOxo reactor, air combustion including CO_2 capture by absorption, methanol synthesis, alkaline electrolyzer). Combining them resulted in models of different process routes. Microsoft Visio (2016) was applied for process visualization (i.e., creating process flow charts). A list of auxiliary equipment for all subprocesses can be found in the Appendix A (Table A9).

2.1. Oxyfuel Combustion in a Bubbling Fluidized Bed Combustor (BFBC)

As described previously, oxyfuel combustion is defined as combustion reaction in a mixture of O_2 with a technical purity of at least 95 vol% and recirculated flue gas. A standard combustion calculation was conducted.

Fuel-N and fuel-O were assumed to be released as N_2 and O_2, respectively. Gases were assumed to behave like ideal gases. Complete combustion was assumed for subsequent combustion calculations. A similar approach can be found in [20] for comparison.

Subsequent mass balances are based on assumed properties of woodchips stated in Table 1 (ultimate analysis) and Table 2 (proximate analysis). These parameters serve as a benchmark but can easily be adjusted to different scenarios or alternating fuels (e.g., bark or municipal waste). The fuel's lower heating value (LHV) in MJ/kg was calculated with the equation after Boie. Small letters refer to the different mass participations of the fuel's elemental components in kg/kg fuel.

$$LHV = 34.8 \cdot c + 93.9 \cdot h + 6.3 \cdot n + 10.5 \cdot s - 10.8 \cdot o - 2.5 \cdot w \text{ [MJ/kg]}. \quad (1)$$

Table 1. Assumed ultimate analysis of woodchips.

Ultimate Analysis—Woodchips (Dry and Ash Free) [wt%]					
C	**H**	**N**	**S**	**O**	**SUM**
50	6	0.4	0.05	43.55	100

Table 2. Assumed proximate analysis of woodchips.

Proximate Analysis—Woodchips [wt%]			
Water Content W	**Ash Content A**	**Volatiles**	**Fixed Carbon**
30	2	80	20

The combustion reaction's specific O_2 demand per kg of combusted species, stated in the Appendix A (Table A1), was calculated with previously stated assumptions.

O_2 is either provided by an air separation unit (ASU) or the alkaline electrolyzer. Excess of O_2 in the oxidant α was defined as the ratio of actual volume flow stream of O_2 related to the volume flow stream of O_2 required for a stoichiometric combustion, as described in [20].

$$\alpha = \frac{\dot{V}_{Ox.,O_2,Real}}{\dot{V}_{O_2,Stoichiometric}}. \quad (2)$$

Since the recirculation of flue gas is mandatory for controlling the combustion temperature, O_2 provided by the recycled flue gas needs to be considered as well. The excess of O_2 in the fluidization medium, defined as sum of O_2 provided by an ASU or alkaline electrolyzer plus recirculated flue gas, was defined by parameter β, being comparable to the air ratio λ for conventional air combustion calculations.

$$\alpha = \frac{\dot{V}_{FM,O_2,Real}}{\dot{V}_{O_2,Stoichiometric}} = \frac{\dot{V}_{Ox.,O_2,Real} + \dot{V}_{FGR,O_2,Real}}{\dot{V}_{O_2,Stoichiometric}}. \quad (3)$$

A definition of the recirculation ratio r, the ratio of volume flow rate of recirculated flue gas related to the volume flow rate of generated flue gas, can be found in [21].

$$r = \frac{\dot{V}_{FGR}}{\dot{V}_{FG}}. \quad (4)$$

Condenser modeling was done with the Antoine Equation (5) and water loading X of flue gas for specific temperatures (6). The assumed parameters A, B and C for water are listed in the Appendix A (Table A6). Parameters of water at the triple point ($p_{Tr.}$ = 611.657 Pa) are stated in [22].

$$\ln\left(\frac{p_S}{p_{Tr.}}\right) = A + \frac{B}{\vartheta + C}. \quad (5)$$

$$X = \frac{0.622 \cdot p_S}{p - p_S}. \quad (6)$$

Assumed parameters regarding the BFBC's design, based on benchmarks given in [23] for a thermal input of 20 $MW_{th.}$, are listed in the Appendix A (Table A7). BFBC is the best available technology for combusting fuels with high contents of volatiles (e.g., biomass) for small-scale decentralized applications [24].

To ensure the fluidization of bed material (e.g., silica sand and woodchips), a fluidization velocity u_f of 1–2.5 m/s is recommended [25]. Mixing inside the reactor is increased significantly with increasing u_f, leading to an improved combustion reaction regime. As a result, segregation of bed material is prevented and the bed's heat transfer is improved [26].

The amount of utilized CO_2 is a function of H_2 provided by the alkaline electrolyzer, since H_2 is required for CO_2 hydrogenation inside the methanol reactor. In real applications, the generation of H_2 will vary due to fluctuating power levels provided by a wind park. The share of utilized CO_2 was defined by the allocation coefficient γ, describing the ratio of flue gas being transferred to downstream process steps and the total amount of flue gas

generated. In case no H_2 is generated by the electrolyzer, the total amount of generated flue gas is released into the atmosphere ($\gamma = 0$).

$$\gamma = \frac{\dot{V}_{FG\ to\ MeOH\ synthesis}}{\dot{V}_{FG,\ total}}. \quad (7)$$

2.2. Conventional Air Combustion in a BFBC

Comparing different process routes of a decentralized power-to-green methanol plant, processing CO_2 generated by the combustion of woodchips, was the main goal of this work. Therefore, modeling a scenario using conventional air combustion technology based on assumptions listed in Section 2.1 was mandatory. The following differences were included:

- Ambient air is used as fluidization medium instead of a mixture of O_2 and recirculated flue gas;
- Parameter β was replaced by λ (conventional air ratio);

Physical properties of air can be found in [22]. Components like H_2O, CO_2 and noble gases other than Argon were neglected.

2.3. Flue Gas Cleaning

A simplified flue gas cleaning model was introduced in the plant's model. Desulfurization is realized by injecting $Ca(OH)_2$ (i.e., slaked lime) into the gas stream prior to a baghouse filter unit, ensuring fly ash removal. SO_2 and $Ca(OH)_2$ react to $CaSO_3$, subsequently collected by the baghouse filter, and water.

$$SO_2 + Ca(OH)_2 \rightarrow CaSO_3 + H_2O. \quad (8)$$

The required mass flow rate of $Ca(OH)_2$ for desulfurization was calculated stoichiometrically based on Equation (8) including an assumed excess of 50% $Ca(OH)_2$. A desulfurization efficiency of 95% was assumed [27].

Removing NO_x from the flue gas stream is achieved by using a SCR-DeNO_x unit. NH_4OH (i.e., ammonia water), with a concentration of 19–29 wt%, is inserted prior to a ceramic honeycomb catalyst at temperatures in the range of 453–703 K, resulting in the reduction of NO_x to N_2 and water [28].

$$4NO + 4NH_3 + O_2 \rightarrow 4N_2 + 6H_2O. \quad (9)$$

The flue gas' NO_x concentration was based on experimental data listed in [25]. Wooden pellets with a fuel-N content of 0.3 wt% (dry and ash free) were burned in a BFBC under lab conditions. NO_x emissions are converted to the fuel-N content of the assumed woodchips stated in Section 2.1. The injected amount of NH_4OH was assumed to be 50% larger than stoichiometrically required for the conversion of NO_x according to Equation (9).

2.4. CO_2 Processing

Before entering the methanol synthesis process, generated CO_2 needs to be concentrated and processed. The applied technology depends on the upstream combustion technology (oxyfuel vs. air combustion). Flue gas produced by oxyfuel combustion processes is rich in CO_2 after removing H_2O in a condenser. Therefore, mainly excess O_2 needs to be removed (inert N_2 does not pose a problem in the downstream methanol synthesis process). When using conventional air combustion, CO_2 needs to be captured and concentrated (e.g., realized by a monoethanolamine (MEA) absorption process). Both configurations require a catalyst protection unit, for example, a fixed bed reactor using ZnO or CuO as adsorbent to remove catalyst poisons (e.g., H_2S and SO_2) from the flue gas stream.

2.4.1. DeOxo Reactor

Removing excess O_2 is necessary when using oxyfuel combustion technologies, since β will always exceed a value of 1. The following assumptions were made regarding the modeling of a DeOxo reactor:

- Gases behave like ideal gases;
- The amount of required H_2 was calculated stoichiometrically;
- H_2O and N_2 were considered inert gases and therefore, have no influence on the reactor's performance;
- Reactor pressure p_{DeOxo} = 10 bar;
- Heat required for the regeneration of activated alumina was not taken into account;
- Reactor temperature T_{DeOxo} = 323 K.

Equation (10) describes the reactor's underlying chemical reaction. The catalyst bed must be cooled since the reaction is strongly exothermic. H_2O is formed as product and needs to be separated by two adsorbent beds loaded with activated alumina. As noted previously, a catalyst guard unit must be installed in front of the DeOxo reactor.

$$H_2 + \frac{1}{2}O_2 \rightarrow H_2O \qquad \Delta H_r^0 = -285.8\frac{kJ}{mol}. \tag{10}$$

2.4.2. CO_2 Capture—MEA Absorption

CO_2 capture based on absorption processes using aqueous MEA solutions obtain the highest technology readiness level (TRL) regarding carbon capture technologies [29] and are solely applicable at an industrial scale [30]. Detailed information regarding process parameters and reactor design can be found in [31]. Alternatively, CO_2 capture processes can be realized using adsorption processes in fluidized bed reactors. Experimental data and data obtained from simulations can be found in [32–37].

The modeled CO_2 capture system was required for process routes using conventional air combustion with flue gas CO_2 concentrations below 20 vol%, including an absorber, a regenerator, conveyor units cycling the MEA solution and a heat exchanger improving the process' heat integration. Main model input parameters were the amount of utilized flue gas as well as the flue gas' composition. The first output stream, a purified CO_2 stream, is transported to a downstream methanol synthesis unit. Off-gas, with a low concentration of CO_2 leaving the regenerator, is added to non-utilized flue gas and emitted to the atmosphere. The following parameters have been assumed:

- CO_2 capture efficiency $\eta_{Capture}$ = 0.9;
- Energy demand $Q'_{CO_2,MEA}$= 3.8 MJ/kg CO_2 captured;
- Absorber temperature $T_{Abs.}$ = 308 K;
- Regenerator temperature $T_{Des.}$ = 393 K;
- Pressure $p_{Abs.} = p_{Des.} = p_{Atm.}$;
- CO_2 stream purity = y_{CO_2} = 99 vol%.

Additionally, subsequent assumptions have been made:

- Gases behave like ideal gases;
- Stripping gas required for the desorption was not considered;
- Examined species: CO_2, H_2O, O_2, N_2, SO_2, Ar;
- Non-CO_2 gases had the same probability of getting dragged into the CO_2-rich stream unintentionally.

2.5. Methanol Synthesis

The methanol synthesis is the facility's core operation unit. Model input parameters were process streams given by the CO_2 processing unit (DeOxo reactor or CO_2 capture), as well as H_2 generated by the alkaline electrolyzer. Methanol reaching a purity of 99.85 wt% (dry basis), as stated by the IMPCA [38], is obtained at the distillation column's head. Water, a byproduct of CO_2 hydrogenation, is obtained at the column's bottom and recirculated to

the electrolyzer surpassing a water treatment unit. Significant parameters of the methanol synthesis model were:

- CO_2 conversion rate ψ = 98.11% [39];
- H_2:CO_2 ratio $\omega > 3$.

Detailed information regarding the design and modeling of methanol synthesis units valorizing CO_2 can be found in [3,8,9,17,40,41].

Methanol is synthesized in a single multi-tubular fixed-bed BWR with closed-loop configuration. The evaporation of boiling water ensures an isothermal operation by transferring reaction heat. Catalyst bed cooling is mandatory, since agglomeration of catalyst particles (a conventional $Cu/ZnO/Al_2O_3$ catalyst is applied for methanol synthesis) occurs as soon as a critical temperature level inside the reactor is exceeded [40]. The reactor's input streams are CO_2, H_2 as well as unconverted gases (a mixture of CO_2, CO and H_2). The output stream consists of methanol, water and unconverted gases being conveyed to a downstream flash drum. The main chemical reactions occurring are the following:

$$CO_2 + 3H_2 \leftrightarrow CH_3OH + H_2O \qquad \Delta H_r^{298K,50bar} = -40.9 \frac{kJ}{mol}. \tag{11}$$

$$CO_2 + H_2 \leftrightarrow CO + H_2O \qquad \Delta H_r^{298K,50bar} = 42.0 \frac{kJ}{mol}. \tag{12}$$

Low temperature and high pressure levels favor the conversion of CO_2 following the principle of Le Chatelier. Regarding the temperature inside the reactor, a trade-off between thermodynamics (favored by low temperatures) and kinetics (favored by high temperatures) needs to be found. Furthermore, a critical temperature level must not be exceeded to avoid catalyst deactivation. Preventing the occurrence of the reverse water–gas shift reaction (12) is another key aspect for reactor design, since CO_2 and H_2 are reactants for the main reaction (11). A minimum H_2:CO_2 ratio of 3 must be ensured inside the reactor to prevent the formation of elemental C due to the Boudouard reaction [40]. The reactor was chosen to operate at a temperature of T_{MeOH} = 513 K and a pressure of p_{MeOH} = 40 bar.

Separating crude methanol from non-condensable gases is realized by a flash drum following the BWR. Product gas leaving the reactor is cooled to a temperature of T_{FD} = 323 K by depressurization over a relief valve. Condensed H_2O and methanol are pumped to a downstream distillation column, whereas non converted gases are recycled back to the reactor inlet including a compression step to p_{MeOH} = 40 bar. The mass flow rate of recirculated gases was calculated with a mass balance over the methanol reactor at steady state (13). The mass flow rate of excess H_2 was calculated by subtracting the required stoichiometric volume flow rate of H_2 from the real volume flow rate of H_2 going into the reactor (14), whereas the mass flow rate of unconverted CO_2 was defined by the CO_2 conversion rate ψ (15). Conversions regarding mass, volume and material balances were conducted with parameters listed in the Appendix A (Table A4).

$$\dot{m}_{Unc.} = \dot{m}_{CO_2,Unc.} + \dot{m}_{H_2,Excess}. \tag{13}$$

$$\dot{V}_{H_2,Excess} = \dot{V}_{H_2,MeOH} - 3 \cdot \dot{V}_{CO_2,MeOH}. \tag{14}$$

$$\dot{n}_{CO_2,Unc.} = (1 - \psi) \cdot \dot{n}_{CO_2}. \tag{15}$$

Product separation is realized with a conventional distillation column including the following assumptions:

- T_{Feed} = 353 K;
- T_{Head} = 337 K;
- T_{Bottom} = 373 K;
- Mass fraction of methanol in the feed m'_{Feed} = 64 wt% (50 mol% methanol);
- Mass fraction of methanol in the head m'_{Head} = 99.85 wt% [38].

2.6. Alkaline Electrolyzer

The required mass flow rate of H_2 depends on the amount of utilized CO_2 defined by the allocation coefficient γ, the DeOxo reactor's H_2 demand for process routes including oxyfuel combustion, as well as the chosen H_2:CO_2 ratio ω. The electrolyzer's power and water demands were defined by the mass flow rate of valorized CO_2. In addition to H_2, O_2 is generated by water splitting, which can either be used as oxidant for process routes, including oxyfuel combustion, or be sold as by-product.

The underlying chemical reactions of water splitting for alkaline electrolysis cells, as well as further information regarding electrolytes, can be found in [42].

Conventional alkaline electrolyzers operate at pressure levels ranging from 1 to 30 bar and at temperatures below 353 K to prevent material degradation [43].

The following assumptions were made:

- $p_{Electrolyzer}$ = 32 bar;
- $T_{Electrolyzer}$ = 353 K;
- Specific power demand of 4.45 kWh/Nm^3 H_2;
- Specific water demand of 0.804 kg/Nm^3 H_2.

2.7. Energy Balance Model

2.7.1. Global Efficiency and Power-to-Liquid Efficiency

The plant's global efficiency rate $\eta_{Tot.}$ includes chemical energy stored in produced methanol $\dot{U}_{MeOH}$ and heat provided to adjacent villages via a district heating network $\dot{Q}_{DH}$ (Outputs), as well as chemical energy stored in woodchips $\dot{U}_{Woodchips}$, the electrolyzer's electricity demand $P_{Electrolyzer}$ and the ASU power input P_{ASU} (Inputs) (16). Chemical energy stored in woodchips and methanol was calculated with Equation (17).

$$\eta_{Tot.} = \frac{\dot{U}_{MeOH} + \dot{Q}_{DH}}{\dot{U}_{Woodchips} + P_{Electrolyzer} + P_{ASU}}. \quad (16)$$

$$\dot{U}_{Fuel/Product} = \dot{m}_{Fuel/Product} \cdot LHV_{Fuel/Product} \quad (17)$$

The plant's power-to-liquid efficiency is defined by Equation (18) [44].

$$PtL - efficiency = \frac{Fuel\ output}{Electricity\ input}. \quad (18)$$

2.7.2. Combined Heat and Power (CHP) Process

Since the plant needs to be able to cover its on-site demand, even if no wind is available, adding a steam turbine for power generation is mandatory. Generated electricity surpassing the plant's on-site demand is used to power the alkaline electrolyzer. CHP output parameters undergo seasonal variations. In winter months the focus is to provide as much heat as possible for nearby villages, whereas the power output will be maximized in summer. The following maximum efficiencies, related to the thermal input into the BFBC, were assumed:

- Maximum electric efficiency $\eta_{CHP,el.,max.}$ = 25%;
- Maximum thermal efficiency $\eta_{CHP,th.,max.}$ = 65%.

2.7.3. Wind Park

Wind power should be prioritized over solar power due to the lower specific CO_2-equivalent per kg H_2 generated [40]. Manufacturers of commercial wind turbines generally list their products' performance as rated power, and add graphs displaying the turbine's annual energy production as the function of the average wind speed at hub height. Calculating real annual average power outputs of wind turbines can be done for annual average

wind velocities of certain regions. A hyperlink to the Austrian Windatlas can be found in [45], indicating annual average wind velocities at a height of 100 m above ground level.

The following assumptions, regarding a wind park adjacent to the designed power-to-green methanol plant, were made:

- Annual average wind velocity u_{Wind} = 7.5 m/s;
- 12 wind turbines with a total rated power of $P_{Wind\ park}$ = 36 MWp;
- Annual average power level of $P_{Wind\ park}$ = 17.14 MW at u_{Wind} = 7.5 m/s (47.6% of the rated power).

2.7.4. Fluidization of Fuel and Bed Material

To ensure the fluidization of fuel and bed material, a blower is required for overcoming the pressure difference caused by the bed itself, the distributor plate, a baghouse filter, a SCR-DeNO$_x$ unit and a condenser, as indicated in Equation (19). The pressure drop due to the fluidization of fuel and bed material was calculated with Equation (20). Typical properties of silica sand as bed material are listed in the Appendix A (Table A8).

$$\Delta p_{Blower} = \Delta p_{Bed} + \Delta p_{Dis.} + \Delta p_{Bag.} + \Delta p_{SCR} + \Delta p_{Con.} \quad (19)$$

$$\Delta p_{Bed} = (1 - \varepsilon) \cdot (\rho_P - \rho_g) \cdot g \cdot h_{Bed}. \quad (20)$$

The following assumptions were made:

- 80% of Δp_{BFBC} were caused by fuel and bed;
- 20% of Δp_{BFBC} were caused by the distributor plate;
- Pressure drop caused by the baghouse filter $\Delta p_{Bag.}$ = 2000 Pa;
- Pressure drop caused by the SCR-DeNO$_x$ unit Δp_{SCR} = 500 Pa;
- Pressure drop caused by the condenser $\Delta p_{Con.}$ = 5000 Pa;
- Blower efficiency η_{Blower} = 0.9.

Consequently, the required power could be calculated using Equation (21). A power reserve was added to ensure smooth operation for real applications.

$$P_{Blower} = \frac{\dot{V} \cdot \Delta p_{Blower}}{\eta_{Blower}} + P_{Reserve}. \quad (21)$$

2.7.5. Conveyor Units

A screw conveyor, fans and pumps were added to the model to estimate the plant's on-site demand. Compared to major energy consuming units (i.e., compressors, alkaline electrolyzer and ASU), the power demand of conveyor units was almost negligible. Estimations, using conventional models to calculate parameters like the pipe friction factor ξ, the Reynolds number Re and the pressure drop per length unit Δp, were added. The screw conveyor's power demand was set constant at a value of 0.7 kW for the assumed input of woodchips, based on an online tool calculating the power demand of bulk handling systems [46].

2.7.6. Compressors

Compressors are needed to realize required pressure levels inside the DeOxo (p_{DeOxo} = 10 bar) and methanol synthesis reactor (p_{MeOH} = 40 bar). The following assumptions were made:

- Gases behave like ideal gases;
- Isothermal change of states;
- Compressor efficiency $\eta_{Compr.}$ = 0.9;
- The stream of unconverted, recirculated gases consists of 33.33 vol% of H_2, CO and CO_2, respectively.

The specific technical work for compressing gas streams was calculated by Equation (22). Consequently, the required power could be calculated by Equation (23). Values regarding specific gas constants of relevant species R_i can be found in the Appendix A (Table A5).

$$w_t = R_i \cdot T \cdot \ln\left(\frac{p_2}{p_1}\right). \quad (22)$$

$$P_{Compr.} = \frac{\dot{m}_i \cdot w_t}{\eta_{Compr.}}. \quad (23)$$

2.7.7. Air Separation Unit

For the implementation of process routes involving oxyfuel combustion, the addition of an ASU is mandatory, since plant operation must be independent from daily and seasonal wind fluctuations. If u_{Wind} falls below a threshold of 3–4 m/s, no power is generated by the wind park and hence no O_2 is generated by the electrolyzer. As a result, the ASU should be connected to the local power grid to avoid plant downtime. For simplification purposes, only N_2, O_2 and Ar output streams were considered. Additionally, a specific energy consumption of 0.45 kWh/Nm^3 O_2 was assumed. Finding the required volume flow stream of O_2 provided by the ASU was done with Equation (24).

$$\dot{V}_{ASU,O_2} = \dot{V}_{Ox.,O_2} - \dot{V}_{Electrolyzer,O_2}. \quad (24)$$

3. Results and Discussion

After modeling subprocesses and linking them together, several operating points were defined by varying critical model parameters (mainly the current wind velocity u_{wind} and, consequently, the possible share of utilized CO_2 γ). Mass, material, volume and energy balances were evaluated for defined operating points. Values assumed for the CHP process refer to an operation during winter months, aiming to maximize the output of heat transferred to a district heating network ($\dot{Q}_{CHP}$ = 13 $MW_{th.}$, P_{CHP} = 3 MW). In this work the total amount of electricity generated by an adjacent wind park (rated power of $P_{Wind\ park}$ = 36 MWp) and power generated by the CHP process was used for H_2 production. Using only surplus electricity, not required by supplied villages, might pose a promising alternative process configuration. However, this case was not considered in this paper.

3.1. Oxyfuel Combustion

Parameters regarding oxyfuel combustion (α, β, r, $T_{Con.}$) are constant for all operating points due to a constant thermal input of 20 $MW_{th.}$. Figure 2 shows a detailed flow chart of the oxyfuel combustion model including mass and volume balances. A total input of 6133 kg/h woodchips (thermal load of 20 $MW_{th.}$) with properties assumed in Section 2.1 and 6187 kg/h O_2 is required. A recirculation ratio of r = 4 ensures a fluidization velocity of u_f = 1–2 m/s (21,664 Nm^3/h of fluidization medium). Since biomass requires a relatively high amount of O_2 in the fluidization medium to avoid incomplete combustion, a value of α = 1.08 was chosen (β = 1.4). The volume flow rate of generated flue gas is $\dot{V}_{FG}$ = 4333 Nm^3/h, obtaining a CO_2 concentration of 89.8 vol% at a temperature of 288 K. Main impurities are excess O_2 (7.41 vol%), H_2O (2.48 vol%) and N_2 (0.31 vol%). A mass flow rate of 4066 kg/h condensed water is pumped to the alkaline electrolyzer after passing a water treatment unit. A total of 2.54 kg/h NH_4OH and 7.23 kg/h $Ca(OH)_2$ are required for the removal of NO_x and SO_x. A baghouse filter was added to the flowchart for dust removal without being analyzed in further detail.

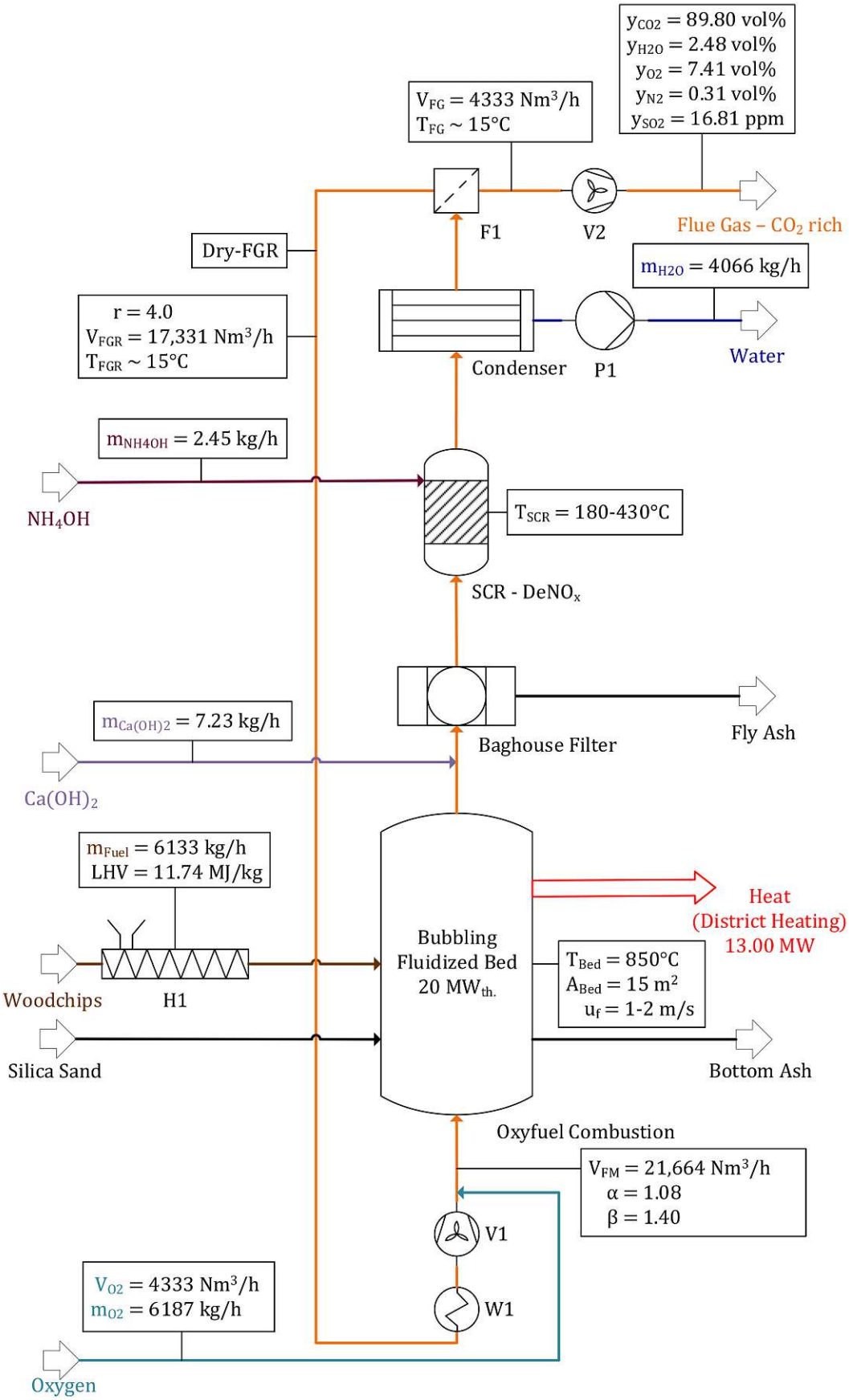

Figure 2. Oxyfuel combustion with dry flue gas recirculation (FGR).

3.2. Reference Operating Point—Oxyfuel Combustion

The "reference operating point" serves as a benchmark for process routes, including oxyfuel combustion, with all parameters set at average values. As aforementioned, the wind park consists of 12 windmills with a rated power of 3 MWp each. Parameter u_{Wind} was assumed to be 7.5 m/s at hub height corresponding to the Austrian Windatlas [45]. A total of 1637.4 kg/h methanol is produced utilizing 30% (about 2300 kg/h) of generated CO_2 (γ = 0.3). Process indicators, including specific consumptions per kg methanol produced, can be found in Table 3. A total of 10.76 kWh of power is required per kg methanol produced. Key parameters for the reference operating point are listed in Table 4. To meet the BFBC's total O_2 demand of 6187 kg/h, 3437 kg/h O_2 (55.55%) needs to be provided by an ASU (in addition to 2713 kg/h O_2 (44.45%) provided by the electrolyzer), resulting in a power demand of P_{ASU} = 4.73 MW. The facility's input and output streams can be found in the Appendix A (Table A2). The on-site demand of 0.72 MW is calculated in Table A3, listed in the Appendix A. A global power balance is listed in Table 5, showing a power input into the electrolyzer of $P_{Electrolyzer}$ = 17.14 MW, as well as a power input into the ASU of P_{ASU} = 4.73 MW.

Table 3. Process indicators regarding the production of methanol—reference operating point.

Process Indicators	kg/h	kg/kg Fuel	$kWh_{el.}$ Consumed/kg	kg/kg H_2	kg/kg O_2	kg/kg CO_2
Methanol	1637.4	0.267	10.76	4.792	0.265	0.306

Table 4. Key parameters—reference operating point.

Parameter	Value [Unit]
Thermal input	20 $MW_{th.}$
Woodchips input	6133 kg/h
Water content	30 wt%
α	1.08
β	1.40
FGR	Dry
r	4.0
$T_{Con.}$	15 °C
γ	0.3
CO_2 conversion ψ	98.11%
$P_{Wind\ park}$	36 MWp
$P_{Electrolyzer}$	17.14 MW
u_{Wind}	7.5 m/s

Table 5. Global power balance.

Name	Power [MW]
Power generation (CHP)	3.0
On-site demand	−0.72
$P_{Electrolyzer}$	−17.14
P_{ASU}	−4.73

Results regarding the subprocesses are visualized in the figures below. The mass and material balance of the DeOxo model, using parameters stated in Table 4, are illustrated in Figure 3. For γ = 0.3, a total of $\dot{V}_{FG}$ = 1300 Nm^3/h with a CO_2 concentration of y_{CO_2} = 89.8 vol% needs to be processed by the DeOxo reactor. Excess O_2, with a material flow rate of $\dot{n}_{O_2}$= 4.3 kmol/h (7.41%), is separated catalytically with H_2 generated by the alkaline electrolyzer ($\dot{V}_{H_2}$ = 193 Nm^3/h). A total amount of 2292 kg/h CO_2 with a purity of 99.66 vol% is provided for the downstream methanol synthesis process step.

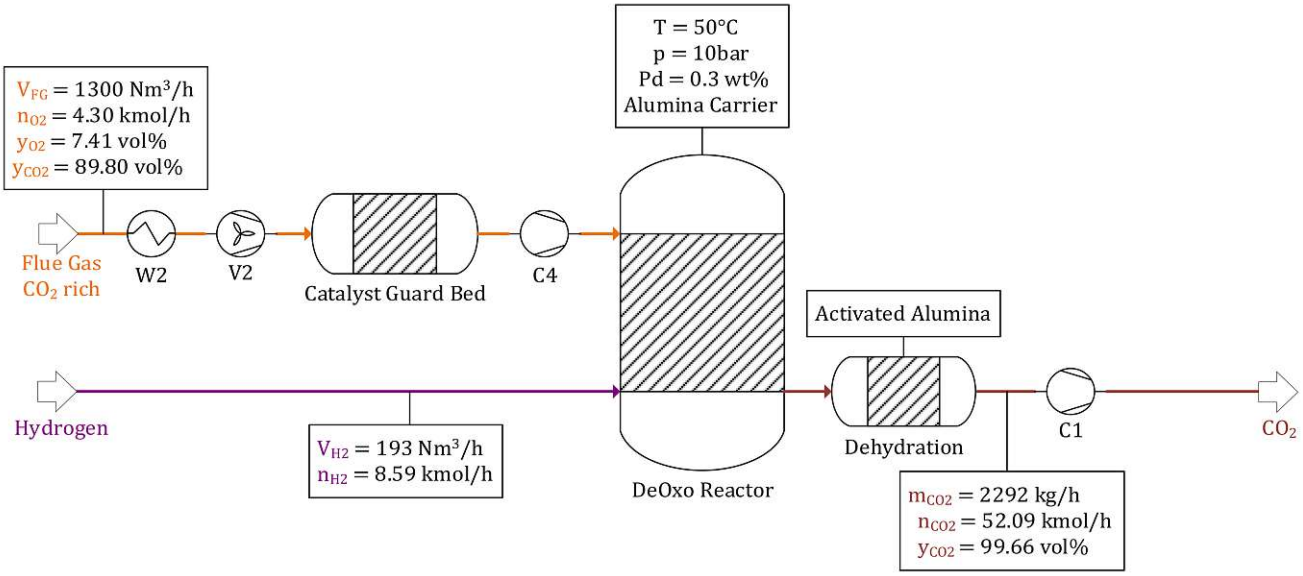

Figure 3. DeOxo reactor—reference operating point.

A material and mass balance of the methanol synthesis for the reference operating point is shown in Figure 4. A total of 52.09 kmol/h of CO_2, provided by the upstream DeOxo reactor, as well as recirculated unconverted gases are transferred into the reactor alongside 160.97 kmol/h H_2 (resulting in a H_2:CO_2 ratio of ω = 3.09). The gas mixture containing CO_2, CO, H_2 and small impurities of N_2 is compressed before passing the $Cu/ZnO/Al_2O_3$ catalyst bed inside the BWR's tubes, at a temperature of T_{MeOH} = 240 °C and a pressure of p_{MeOH} = 40 bar. The reaction products, methanol and H_2O, are then separated from non-condensable gases in a flash drum by depressurization to $p_{Atm.}$. Subsequently, crude methanol is separated into methanol (1637 kg/h) and H_2O (920 kg/h) in a multi-staged distillation column.

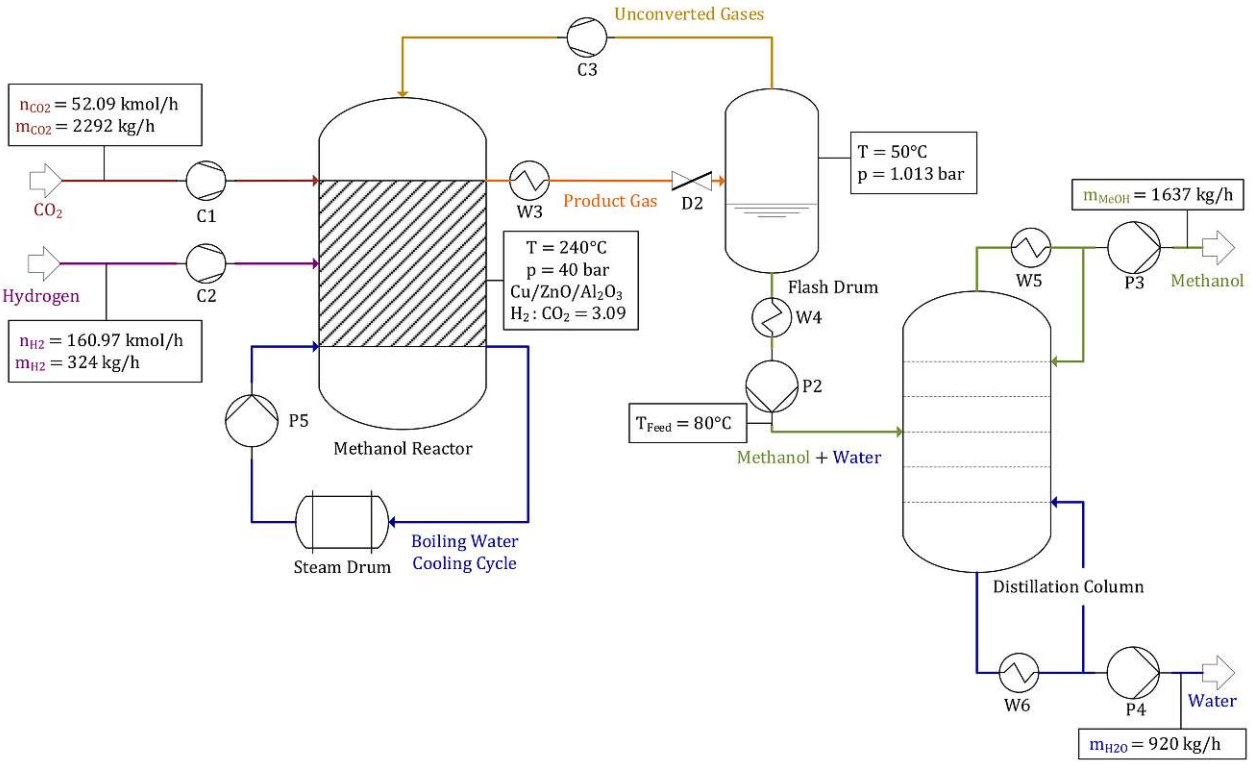

Figure 4. Methanol synthesis—reference operating point.

H_2 required for CO_2 purification in the DeOxo reactor and CO_2 hydrogenation is generated by an alkaline electrolyzer. A total of 3056 kg/h of H_2O and 17.14 MW power are required to produce $\dot{V}_{H_2}$ = 3800 Nm^3/h and $\dot{V}_{O_2}$ = 1900 Nm^3/h at process conditions of $T_{Electrolyzer}$ = 80 °C and $p_{Electrolyzer}$ = 32 bar. Figure 5 shows the alkaline electrolyzer's balance for the reference operating point.

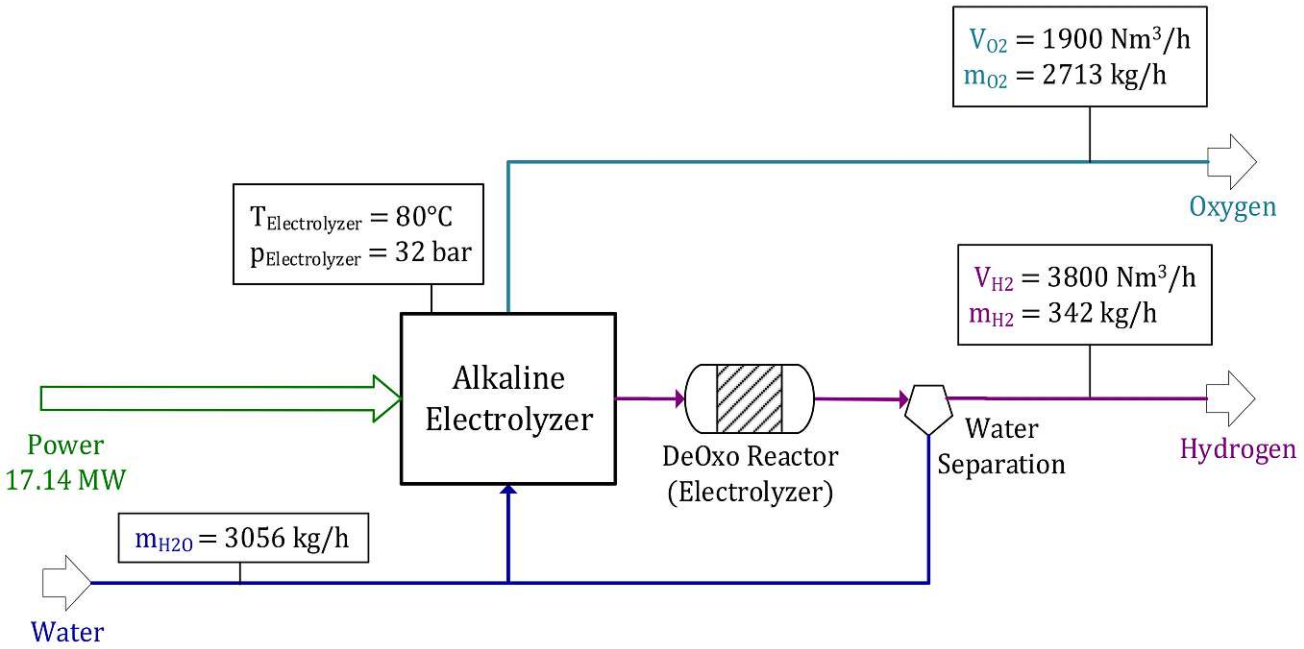

Figure 5. Alkaline electrolyzer—reference operating point.

3.3. Air Combustion and Methanol Synthesis—Operating Point "Air"

Determining whether oxyfuel combustion or conventional air combustion should be prioritized to maximize the facility's efficiency rates is a key aspect of this paper. The air combustion model is based on the oxyfuel model with some adaptions (i.e., using λ as the combustion parameter instead of α and applying a MEA absorption process for CO_2 processing). Tables 6 and 7 present process indicators as well as key parameters regarding the "Air" operating point. Compared to the reference operating point applying oxyfuel combustion, the specific power consumption of 9.829 $kWh_{el.}/kg$ methanol is significantly lower since no additional H_2 is required for flue gas processing. A global power balance is stated in Table 8. The plant's on-site demand is calculated similarly, as explained previously for the "reference operating point". The facility's on-site demand of 0.8 MW is slightly higher compared to the reference operating point's on-site demand of 0.72 MW, since more power is required for gas compression due to a higher CO_2 utilization rate of γ = 0.35. This configuration obtains a methanol output of about $\dot{m}_{MeOH}$ = 1719 kg/h.

Table 6. Process indicators regarding the production of methanol—operating point "Air".

Process Indicators	kg/h	kg/kg Fuel	$kWh_{el.}$ Consumed/kg	kg/kg H_2	kg/kg CO_2
Methanol	1719.23	0.280	9.829	5.032	0.328

Table 7. Key parameters—operating point "Air".

Parameter	Value [Unit]
Thermal input	20 $MW_{th.}$
Woodchips input	6133 kg/h
Water content	30 wt%
λ	1.2
$T_{Con.}$	15 °C
γ	0.35
$\eta_{Capture}$	0.9
Purity CO_2 stream	99 vol%
CO_2 conversion ψ	98.11%
$P_{Wind\ park}$	36 MWp
$P_{Electrolyzer}$	17.14 MW
u_{Wind}	7.5 m/s

Table 8. Global power balance—operating point "Air".

Name	Power [MW]
Power generation (CHP)	3.0
On-site demand	−0.80
$P_{Electrolyzer}$	−17.14

Mass and volume balances of the air combustion model including flue gas treatment units can be found in Figure 6. Since air is used as fluidization medium, the amount and composition of emitted flue gas differ significantly in comparison with oxyfuel combustion. A volume flow rate of $\dot{V}_{FG}$ = 27,175 Nm^3/h with a CO_2 concentration of only 14.33 vol% is either emitted to the atmosphere or processed in a downstream CO_2 capture unit. 22,968 Nm^3/h air are required to achieve an air ratio of λ = 1.2. A total of 4066 kg/h of condensed water is pumped to the electrolyzer surpassing a water treatment unit. The balance of MEA absorption cycle processing of 35% (γ = 0.35) of generated flue gas can be found in Figure 7, processing a volume flow rate of $\dot{V}_{FG}$ = 9511 Nm^3/h in the absorber at $T_{Abs.}$ = 308 K. CO_2 is absorbed by a cycling MEA solution ($\dot{m}_{MEA}$ = 53,136 kg/h) and subsequently released in the desorber at $T_{Des.}$ = 393 K, demanding 2.54 MW thermal power for regeneration. A mass flow rate of purified CO_2 $\dot{m}_{CO_2}$ = 2407 kg/h with a purity larger than 99 vol% is conveyed to the downstream methanol synthesis process step. Since small shares of CO_2 and other components are not absorbed, $\dot{V}_{FG,Lean}$ = 8137 Nm^3/h is emitted to the atmosphere with a CO_2 concentration of 2.54 vol%.

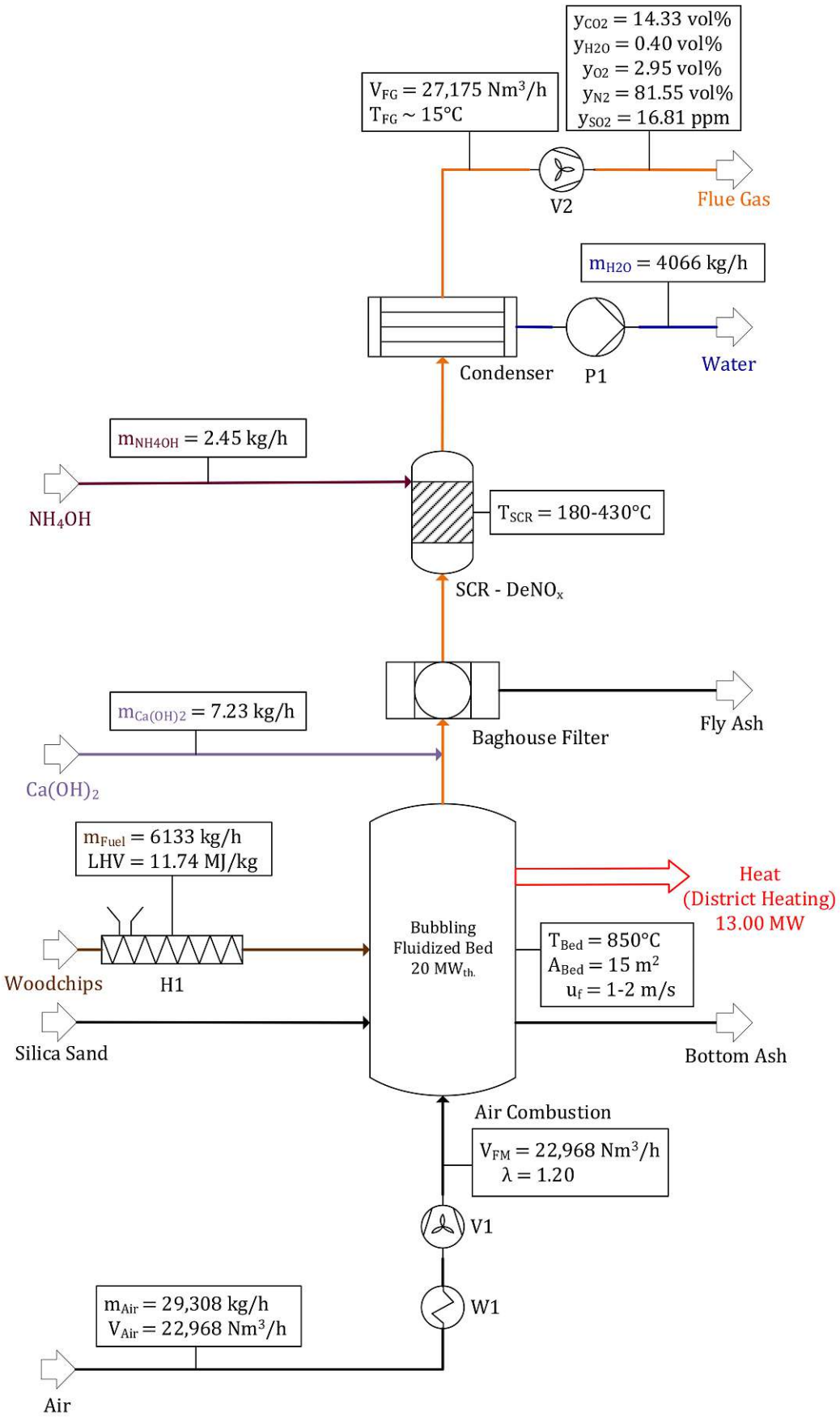

Figure 6. Air combustion of woodchips in a BFBC.

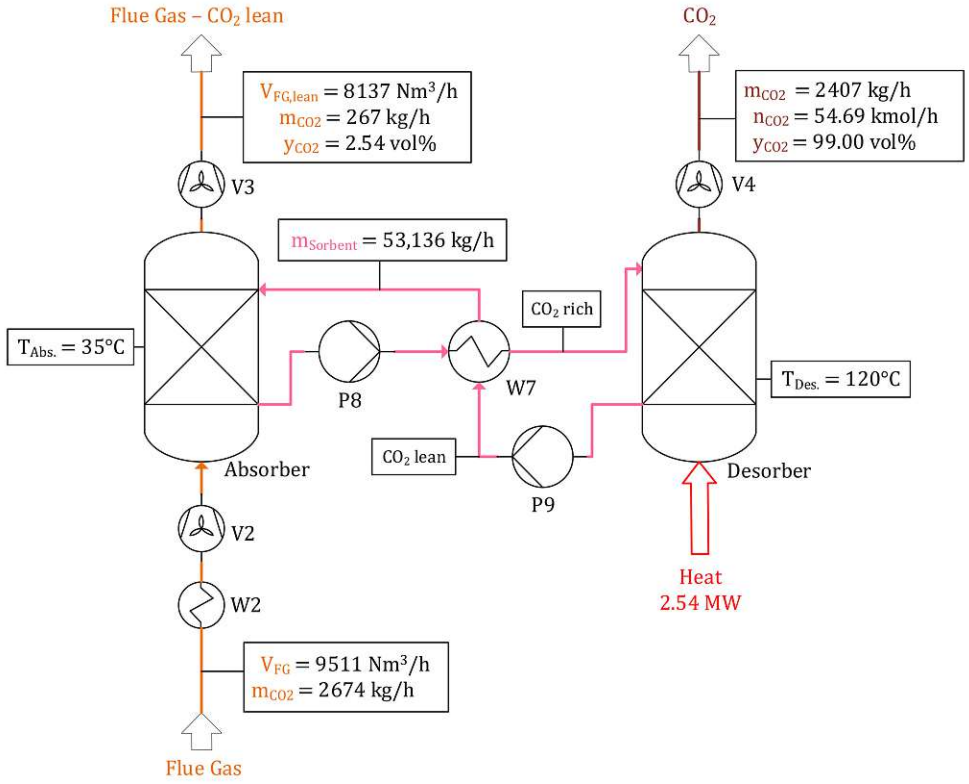

Figure 7. CO_2 capture by MEA absorption—operating point "Air".

After being purified, the CO_2 stream is valorized to methanol, as explained in Section 2.5. The reactor's input streams are $\dot{n}_{CO_2}$ = 54.69 kmol/h and $\dot{n}_{H_2}$ = 169.57 kmol/h, resulting in a H_2:CO_2 ratio of ω = 3.1. After being separated in a distillation column, a product stream of 1719 kg/h methanol and 966 kg/h H_2O are acquired. Figure 8 shows the methanol synthesis' balance.

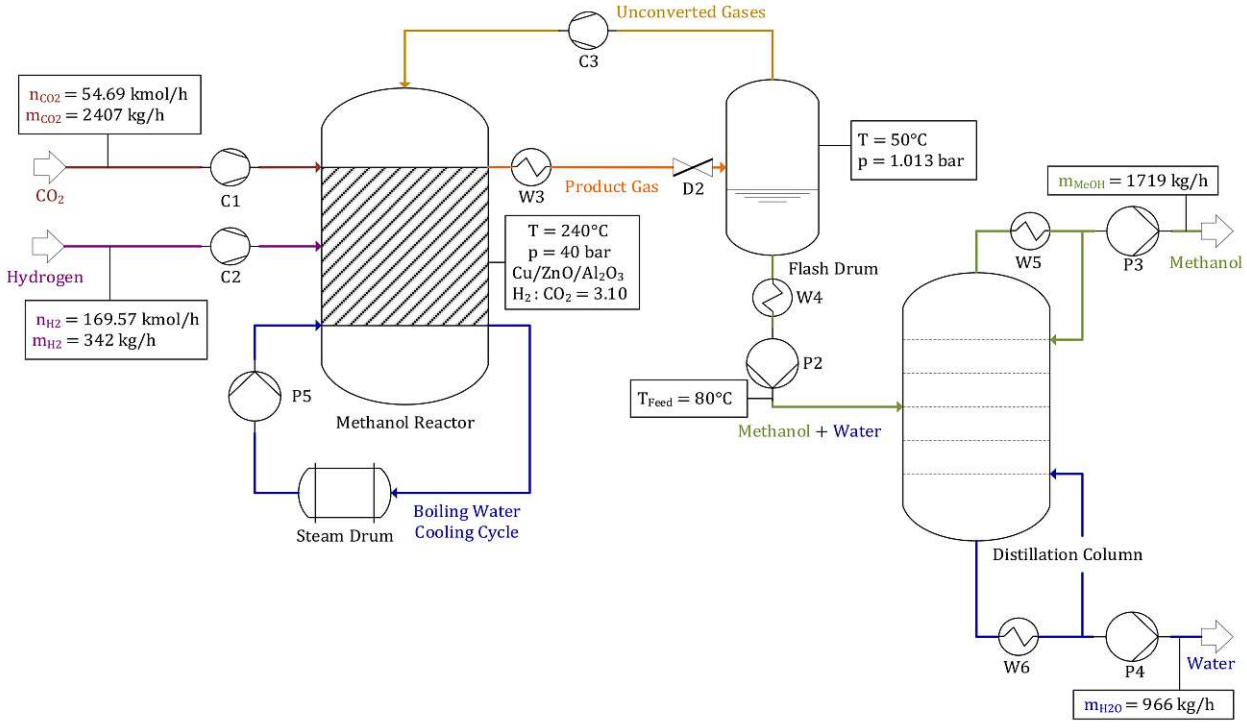

Figure 8. Methanol synthesis—operating point "Air".

Similar to the oxyfuel process route, H_2 is provided by an alkaline electrolyzer powered by a wind park. Input parameters ($\dot{m}_{H_2O}$ = 3056 kg/h and $P_{Electrolyzer}$ = 17.14 MW) and output parameters ($\dot{V}_{H_2}$ = 3800 Nm^3/h and $\dot{V}_{O_2}$ = 1900 Nm^3/h) are similar to the reference operating point described in Section 3.2.

3.4. Sensitivity Analysis

A sensitivity analysis was conducted to present how critical model parameters (e.g., α, γ, ω, u_{Wind}) affect the facility's performance.

3.4.1. O_2 Supply for Oxyfuel Process Routes

For process routes including oxyfuel combustion, a constant mass flow rate of $\dot{m}_{O_2}$ = 6187 kg/h must be provided to maintain the combustion reaction (α = 1.08, β = 1.4, $\dot{m}_{Woodchips}$ = 6133 kg/h, thermal heat load = 20 $MW_{th.}$,). The mass flow rate of O_2 into the combustor, as well as the flue gas' O_2 concentration, are a function of α. Higher O_2 concentrations lead to an increased H_2 demand of the DeOxo reactor and hence results in the plant's performance parameters' decrease. Figure 9 shows how $\dot{m}_{O_2}$ (blue line) and $y_{FG,\,O_2}$ (red line) are influenced by α. Small values of α conclude in a smaller power demand of ASU and CO_2 purification; however, they will possibly lead to incomplete combustion regimes.

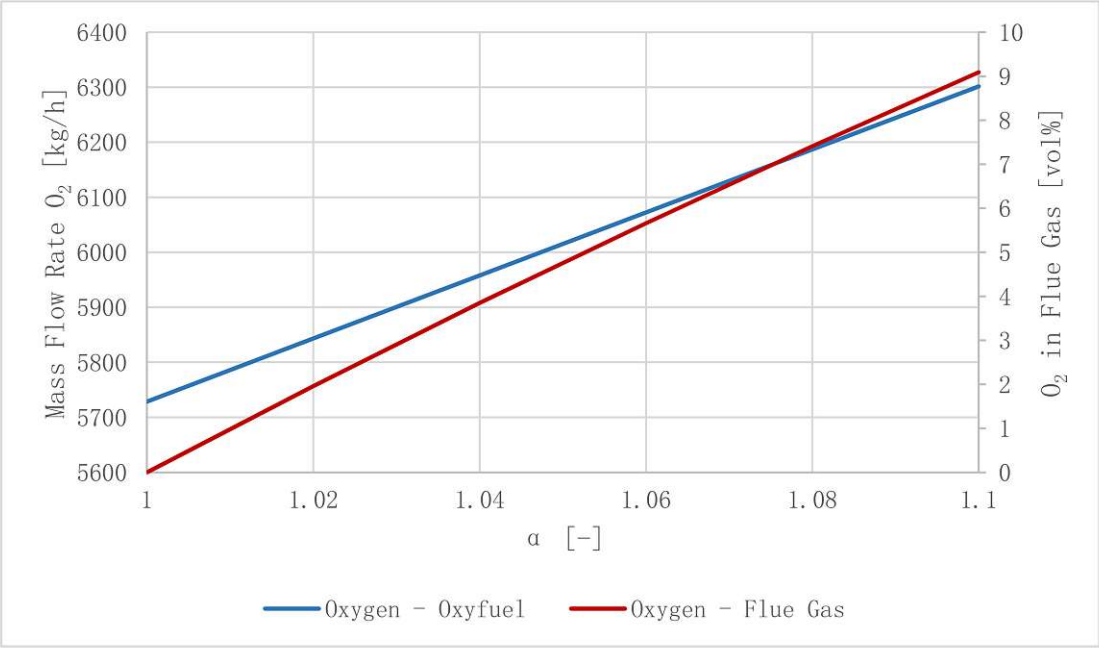

Figure 9. Influence of α on the oxyfuel combustion (α = 1.08, γ = 0.3, r = 4.0).

The provided volume flow rate of O_2 is a mixture of O_2 generated by an ASU and the electrolyzer as by-product of water splitting. Figure 10 displays the share of O_2 provided for the oxyfuel combustion by an ASU and the alkaline electrolyzer, with a power input of $P_{Electrolyzer}$ = 17.14 MW, for the reference operating point (γ = 0.3, see Section 3.2). An O_2 stream of 1925.84 Nm^3/h is provided by the electrolyzer (44.45%), 2406.96 Nm^3/h is provided by the ASU (55.55%) to meet the oxyfuel combustor's total demand of 4332.8 Nm^3/h as indicated by the green line. The "break-even point" of O_2 supply is reached at $P_{Electrolyzer}$ = 38.56 MW. Consequently, oxyfuel process routes do not require an additional ASU if γ > 0.7, hence operating points surpassing an allocation coefficient of 0.7 produce excess O_2 as by-product, making oxyfuel combustion a viable option for large-scale applications.

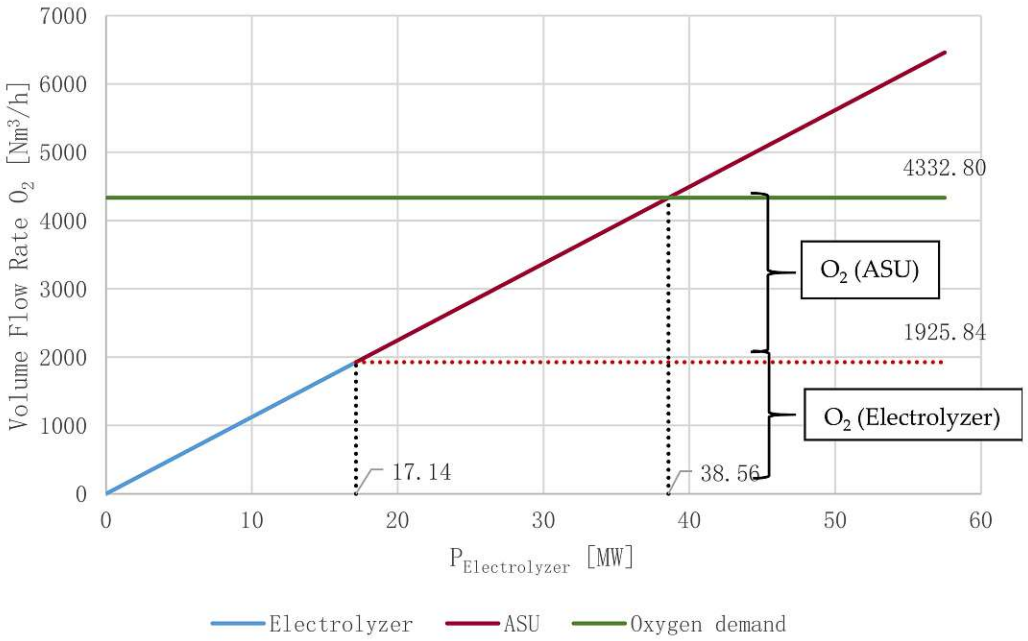

Figure 10. O_2 supply for the oxyfuel combustion—reference operating point.

3.4.2. Methanol Production and Analyzed Operating Points

H_2 production was identified as the facility's bottleneck defining the output of methanol. The amount of H_2 provided by the electrolyzer depends on the electrolyzer's size (=const.), the wind park's size (=const.) and the wind velocity (≠const.). Depending on these parameters, the allocation coefficient γ can reach values between 0 (no flue gas is processed to methanol) and 1 (the total amount of flue gas is processed to methanol). Besides operating points explained previously (reference operating point and operating point "Air"), additional operating points were analyzed by varying u_{Wind}, γ and $P_{Wind\ park}$, as displayed in Table 9. Operating point "Dead Calm" refers to a scenario with no power generated by the wind park due to u_{Wind} = 0 m/s, thus the electrolyzer is only powered with surplus electricity generated by the CHP process ($P_{Electrolyzer}$ = 2 MW). The maximum yield of methanol can be produced in combination with a wind park at a rated power of $P_{Wind\ park}$ = 123 MWp and u_{Wind} = 7.5 m/s, as indicated by operating point "Max.MeOH". Processing the whole amount of generated CO_2 (γ = 1.0) would require a power input into the electrolyzer of about 60 MW. Therefore, this scenario is not realistic regarding the size of currently used electrolyzer units. At u_{Wind} = 4 m/s, the lowest possible wind velocity for wind turbines to operate economically feasible, a yield of 545.8 kg/h of methanol can be produced (γ = 0.1, $P_{Wind\ park}$ = 36 MWp). A total of 3274.7 kg/h of methanol can be produced at wind velocities surpassing u_{Wind} = 12 m/s (γ = 0.6, $P_{Wind\ park}$ = 36 MWp).

Table 9. Analyzed operating points.

Operating Point	$P_{Wind\ park}$ [MWp]	u_{Wind} [m/s]	γ [-]	$\dot{m}_{MeOH}$ [kg/h]
Reference operating point	36	7.5	0.3	1637.4
Max. output of methanol "Max. MeOH"	123	7.5	1	5457.9
Low wind velocity "Min Wind"	36	4	0.1	545.8
Max. wind velocity "Max. Wind"	36	12	0.6	3274.7
Air combustion mode "Air"	36	7.5	0.35	1719.2
Biomass heating plant "Dead Calm"	36	0	0.04	196.5

The mass flow rate of produced methanol (green line), as well as the required power input of the electrolyzer (red line) as a function of allocation coefficient γ, can be found in Figure 11.

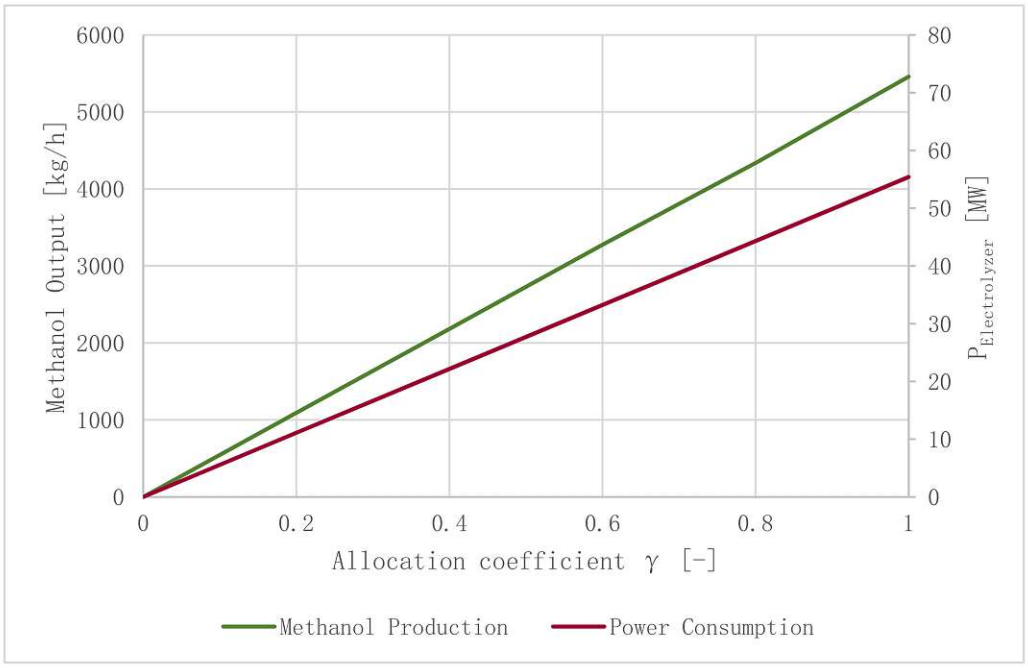

Figure 11. Methanol production and the electrolyzer's electricity demand as a function of γ (α = 1.08, ω = 3.2).

3.4.3. H_2 Demand

Producing renewable H_2 is the determining factor when regarding the conceptualized power-to-green methanol plant's power consumption. Stoichiometrically, a H_2:CO_2 ratio ω larger than 3 is mandatory. For real applications, ω is expected to be set at values ranging from 3 to 3.5. Increasing mass flow rates of H_2 for methanol production as a function of ω are displayed in Figure 12. The electrolyzer's required power input ranges from $P_{Electrolyzer}$ = 15.58 MW (ω = 3, $\dot{m}_{H_2}$ = 314.86 kg/h) to $P_{Electrolyzer}$ = 18.18 MW (ω = 3.5, $\dot{m}_{H_2}$ = 367.34 kg/h) for the reference operating point, as stated in Section 3.2 (γ = 0.3). The reader should keep in mind that these values only serve as benchmarks, since recirculated gases (H_2, CO, and CO), which are not discussed in this concept, will have a significant impact on the reactor's operating parameters for real application scenarios.

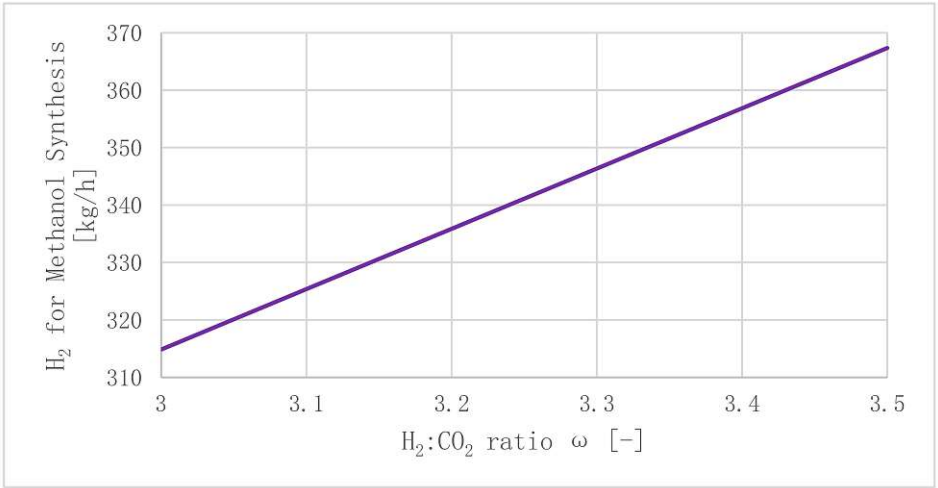

Figure 12. Methanol synthesis H_2 demand as a function of ω (γ = 0.3, $\dot{m}_{MeOH}$ = 1637.36 kg/h).

3.5. Global Efficiency and Power-to-Liquid Efficiency

Obtained efficiency rates for operating points presented in Section 3.4.2 are listed in Table 10. When analyzing process routes including oxyfuel combustion, $\eta_{Tot.,Oxy}$ increases with increasing γ, obtaining a maximum of $\eta_{Tot.,Oxy}$ = 57.04% (γ = 0.6) for the "Max. Wind" operating point. $\eta_{PtL,Oxy}$ increases with increasing γ, obtaining a maximum of $\eta_{PtL,Oxy}$ = 51.91% (γ = 1) for the operating point "Max MeOH". Increasing the wind park's size ($\gamma\uparrow$); therefore, leads to increased efficiency rates, $\eta_{Tot.,Oxy}$ and $\eta_{PtL,Oxy}$, for oxyfuel process routes. This can be explained by the fact that no additional O_2 needs to be provided by an ASU if $\gamma > 0.7$ ($P_{Electrolyzer} > 38.56$ MW), as mentioned in Section 3.4.1, resulting in a significantly decreasing global power consumption. Therefore, power-to-green methanol plants based on oxyfuel combustion routes obtain significantly higher efficiency rates at a large scale.

Table 10. Efficiency rates for analyzed operating points (As defined in Section 2.7.1).

Operating Point	$\eta_{Tot.}$ [%]	η_{PtL} [%]	γ [-]	$\dot{m}_{MeOH}$ [kg/h]
Low wind velocity "Min Wind"	47.28	20.97	0.1	545.8
Reference operating point	53.19	40.19	0.3	1637.4
Max. wind velocity "Max. Wind"	57.04	51.10	0.6	3274.7
Max. output of methanol "Max. MeOH"	56.09	51.91	1	5457.9
Air combustion mode "Air"	54.36	54.21	0.35	1719.2

Significant deviations can be found when comparing process routes, including oxyfuel combustion (reference operating point) to conventional air combustion ("Air"), obtaining comparable methanol product output streams ($\dot{m}_{Reference}$ = 1637.4 kg/h, $\dot{m}_{Air}$ = 1719.2 kg/h). The PtL efficiency of operating point "Air" $\eta_{PtL,Air}$ = 54.21% is substantially higher than the PtL efficiency of the reference operating point $\eta_{PtL,Reference}$ = 40.91%. Two reasons need to be highlighted: Firstly, the ASU's high-power consumption, providing 44.45% of the combustion's O_2 demand, has a negative impact on η_{PtL}. Secondly, H_2 needs to be provided for CO_2 processing in the DeOxo reactor, resulting in a significant penalty on η_{PtL}.

3.6. Case Study for One Year of Operation

The power-to-green methanol plant's expected annual input and output parameters are determined in this Section. Adjacent villages are supplied with heat generated by the CHP process via a district heating network. Electricity generated by the CHP process and the wind park is used for the generation of green H_2 needed to produce methanol. It was assumed that electricity is solely used to power the alkaline electrolyzer. Alternatively, surplus electricity generated by the wind park may be stored chemically by producing green methanol. The following assumptions were made:

- The CHP process output undergoes seasonal fluctuations obtaining a total efficiency of $\eta_{CHP,Tot.}$ = 80% with respect to a thermal input of 20 $MW_{th.}$;
- Electricity generated by the CHP process is used to power the alkaline electrolyzer;
- The plant's on-site power demand was set at 0.72 MW, referring to the reference operating point analyzed in Section 3.2;
- The plant is out of operation for three consecutive weeks in June for revision and maintenance work (8256 operating hours per year);
- $P_{Wind\ park}$ = 17.14 MW (annual average output—reference operating point);
- Seasonal fluctuations of the wind park's power generation in central Europe were based on Figure A1 in the Appendix A;
- Power consumption of 10.32 kWh/kg methanol produced;
- Power consumption of 4.415 kWh/year and household;
- Heat demand of 1.8 kW/household in winter (central Europe).

CHP operation parameters for one year of operation are listed in Table 11, including an annual heat output of 99,528 $MWh_{th.}$ and an annual power output of 26,622 MWh.

The power output will be maximized in summer since no heat needs to be transferred to a district heating network. The wind park's monthly power generation over the year is listed in Table 12. A total of 150,382 MWh of power was expected to be generated by the wind park per year. The wind index indicates the wind park's potential to generate power throughout the year for Central Europe, obtaining its maximum throughout winter months. Plant revision and maintenance was scheduled in June considering that the wind park's power output is expected to be lowest during summer.

Table 11. CHP process—annual output.

Season	Months	P_{CHP} [MW]	$\dot{Q}_{CHP}$ [MWth.]	Op. Time [h]	$P_{Tot.}$ [MWh]	$Q_{Tot.}$ [MWh$_{th.}$]
Winter	Dec, Jan, Feb	2.28	13	2160	4924	28,080
Spring	Mar, Apr, May	3.28	12	2208	7242	26,496
Summer	Jun, Jul, Aug	4.28	11	1704 [1]	7293	18,744
Autumn	Sep, Oct, Nov	3.28	12	2184	7163	26,208
SUM	-	-	-	8256	26,622	99,528

[1] No operation for three weeks due to revision and maintenance work.

Table 12. Wind park—annual output.

Month	Wind Index [-]	$P_{Wind\ park}$ [MW]	Op. Time [h]	$P_{Tot.}$ [MWh]
Jan	149	25.53	744	18,894
Feb	128	21.93	672	14,737
Mar	133	22.79	744	16,956
Apr	93	15.94	720	11,477
May	81	13.88	744	10,327
Jun	68	11.65	216 [1]	2516
Jul	77	13.19	744	9813
Aug	73	12.51	744	9307
Sep	90	15.42	720	11,102
Oct	107	18.34	744	13,645
Nov	126	21.59	720	15,545
Dec	126	21.59	744	16,063
SUM	-	-	8256	150,382

[1] No operation for three weeks due to revision and maintenance work.

Table 13 provides a summary, based on the reference operating point presented in Section 3.2, of the expected annual input and output streams of the designed power-to-green methanol plant. For an annual input of 50,632 t/a woodchips, a total of 17,161 t/a methanol, equivalent to 177.11 GWh/a of power, can be produced. Additionally, 99.53 GWh$_{th.}$/a heat is provided to adjacent settlements via a district heating network.

Table 13. Annual input and output—one year of operation.

Season	Months	Operating Time [h]	Fuel Input [t]	Methanol Output [t]	Power equ. [GWh]	Heat Output [GWh$_{th.}$]
Winter	Dec, Jan, Feb	2160	13,247	5302	54.72	28.08
Spring	Mar, Apr, May	2208	13,541	4457	46.00	26.50
Summer	Jun, Jul, Aug	1704 [1]	10,450	2803	28.93	18.74
Autumn	Sep, Oct, Nov	2184	13,394	4599	47.46	26.21
SUM	-	8256	50,632	17,161	177.11	99.53

[1] No operation for three weeks due to revision and maintenance work.

4. Conclusions

The main objective of this paper was to conceptualize and model a decentralized power-to-green methanol plant including oxyfuel combustion for CCU applications. A biomass heating plant, either operated as oxyfuel or conventional air combustor, including a CHP process with a thermal input of 20 $MW_{th.}$, provides adjacent villages with heat and functions as a CO_2 source for a downstream methanol synthesis unit. Using woodchips as fuel comes with several advantages (e.g., the potential to achieve a negative CO_2 balance, empowering local economies and being independent from imported fossil energy carriers). Processing the CO_2 stream is either realized by a DeOxo reactor (for oxyfuel process routes) or a MEA temperature swing absorption cycle (for conventional air combustion process routes). Required H_2 is produced by an alkaline electrolyzer powered with electricity generated by a nearby wind park. O_2 as by-product can either be used as oxidant for the oxyfuel combustion or be sold when applying process routes based on air combustion. Methanol is produced by valorizing CO_2 in a multi-tubular BWR including a closed gas loop configuration.

PtX technologies are on the verge of becoming key technologies within this decade, as they neutralize a major disadvantage of renewable energy carriers (i.e., the challenge of chemically storing surplus electricity due to seasonal and daily fluctuations). Furthermore, CO_2 is captured and valorized to fuels or feedstocks for the chemical industry.

A variety of operating points have been defined by alternating critical process parameters (i.e., u_{Wind}, the wind park's size and the allocation coefficient γ, as explained in Section 3.4.2). Input and output streams of defined operating points were analyzed. Figures A2 and A4, listed in the Appendix A, show a detailed as well as a simplified flow chart of the reference operating point's balance, a process route including oxyfuel combustion and a DeOxo reactor for CO_2 processing, with parameters set to values with the highest probability for real applications. A product output of 1637 kg/h methanol as well as 13 $MW_{th.}$ heat is realized for an input of 6133 kg/h woodchips, $P_{Electrolyzer}$ = 17.14 MW and P_{ASU} = 4.73 MW. A total amount of H_2 of 342 kg/h is required for the methanol synthesis unit (324 kg/h) and the DeOxo reactor (18 kg/h). Furthermore, 6187 kg/h of O_2 is required for the oxyfuel combustion. For a CO_2 utilization rate of γ = 0.3, 3474 kg/h O_2 (55.55%) must be provided by an ASU (P_{ASU} = 4.73 MW). In this case, only 2713 kg/h O_2 (44.45%) is provided by the electrolyzer at a power input of $P_{Electrolyzer}$ = 17.14 MW. If $P_{Electrolyzer}$ exceeds a value of 38.56 MW (γ = 0.7), no additional O_2 would be required by an ASU. Global flow charts of a comparable scenario using air combustion can be found in Figures A3 and A5 in the Appendix A. In this scenario, 35% of generated flue gas (9511 Nm^3/h with a CO_2 concentration of 14.33 vol%) can be converted to methanol. A yield of 1719 kg/h of methanol can be obtained with a fuel input of 6133 kg/h woodchips. Additionally, no ASU is required to save 4.73 MW of power. It is noted that condensed water is pumped to the electrolyzer, which is not indicated in the simplified flow charts.

This paper also focuses on answering the question whether process routes including oxyfuel combustion should be preferred over air combustion, since O_2 generated by the electrolyzer could be used as oxidant substituting an ASU. To evaluate this assumption, plant efficiency parameters were defined and analyzed. The plant's power-to-liquid efficiency increases significantly with an increasing share of utilized CO_2 (increasing γ) for oxyfuel combustion applications; nevertheless, it is constant for air combustion process routes ($\eta_{Tot.,Air}$ = 54.36%≠f(γ), $\eta_{PtL,Air}$ = 54.21%≠f(γ)). The maximum efficiency rates for oxyfuel combustion process routes were $\eta_{Tot.,Max.,Oxy}$ = 57.04% (γ = 0.6) and $\eta_{PtL,Max.,Oxy}$ = 51.91% (γ = 1.0), whereas the minimum efficiency rates are significantly lower at $\eta_{Tot.,Min.,Oxy}$ = 47.28% (γ = 0.1) and $\eta_{PtL,Min.,Oxy}$ = 20.97% (γ = 0.1). This aspect is linked to the ASU's high power consumption for operating points with low γ values. For plants utilizing less than 70% of the generated flue gas, air combustion process routes should be preferred, as they obtain a higher $\eta_{PtL,Air}$ = 54.21% (γ = 0.35) compared to $\eta_{PtL,Oxy,Reference}$ = 40.91 (γ = 0.3) for the reference operating point. However, oxyfuel applications have the potential to reach a higher $\eta_{Tot.}$ ($\eta_{Tot.,Max.}$ = 57.04%) in comparison to air

combustion modes, since no additional heat is required for regenerating the MEA solution for CO_2 processing.

The presented concept has the potential to work as a carbon sink if the methanol produced is utilized as feedstock in the chemical industry. Wooden biomass is used as fuel, while providing decentralized communities with heat generated by combusting local wood, hence empowering regional development. In case methanol is used as fuel, the proposed concept can be described as almost carbon neutral, as CO_2 bound by wood is subsequently emitted to the atmosphere. Additionally, a business case for small-to-medium sized villages situated in regions obtaining a high wind potential is generated. For applications using surplus electricity, a process route including conventional air combustion in combination with a CO_2 capture unit is highly recommended, since no additional ASU is required. This is also true for applications including small-scale wind parks. Oxyfuel combustion processes have a high potential in combination with water electrolysis, since generated O_2 can be directly used as oxidant. However, this configuration is only reasonable if $P_{Electrolyzer} > 38.56$ MW (for power plants with a thermal input of 20 $MW_{th.}$), the threshold when the combustor's O_2 demand can be fully covered with O_2 generated by the electrolyzer. Substituting O_2 with an ASU always comes with a significant penalty on η_{PtL} and should consequently be avoided. As a result, oxyfuel process configurations are only recommended for large-scale investments, including wind parks with a rated power of $P_{Wind\ park} > 100$ MWp and large annual average u_{Wind}.

In addition, a case study analyzing the facility's annual major input and output streams was conducted assuming process parameters of the reference operating point presented in Section 3.2. An annual output of 17,161 t/a methanol and 99.53 $GWh_{th.}$/a heat can be realized for an input of 50,632 t/a woodchips and 177.11 GWh/a power, generated by a local wind park and the CHP process.

Combining oxyfuel combustion with CCU technologies (e.g., the valorization of CO_2 to methanol) is a promising system configuration for future PtL plants which use large-scale electrolyzers. Scaling up water electrolysis plants is going to be one of the major challenges for engineers in this decade. The combination of solid oxide electrolysis units and CCU technologies has the potential to significantly improve the efficiency rates of PtL plants by thermal process integration. Heat generated by the combustor (oxyfuel or air) and the methanol synthesis unit can be transferred to the SOEC (solid oxide electrolysis cell) unit, which results in the decrease of the required power for water splitting.

Future research should include the following aspects:

- Basic and detail engineering for all unit operations as well as their interaction;
- Implementation of heat integration by, for example, conducting a pinch analysis;
- Finding new process routes (e.g., using photovoltaic modules as power source, using other CO_2 sources like direct air capture, pre combustion or industrial processes). Exchanging the methanol synthesis unit with a Fischer-Tropsch synthesis or methanation unit are possible options if other products are preferred by possible customers. Additionally, process routes including SOEC units have the potential to significantly improve the facility' efficiency rates;
- Evaluating the facility's potential for grid stabilization;
- Developing a technology impact analysis as well as an LCA.

Detailed and simplified global flow charts of process routes applying oxyfuel and air combustion can be found in the Appendix A.

Author Contributions: Conceptualization, S.P. and F.W.; methodology, S.P. and F.W.; visualization, S.P.; writing—original draft preparation, S.P.; review, S.P., F.W. and J.H.; writing—editing, S.P.; validation, P.S. and J.H.; supervision, F.W. All authors have read and agreed to the published version of the manuscript.

Funding: The authors would like to thank the TU Wien Bibliothek for financial support through its Open Access Funding Program, the TU Wien Doctoral College 'CO_2 Refinery', the Austrian Research Promotion Agency (FFG) and the Ministry BMK for the financial support of the project IEA-FBC (No. #876737).

Data Availability Statement: For further information regarding data presented in this paper, please contact the corresponding author. The findings of this paper are based on results obtained from the corresponding author's master thesis 'Power to Green Methanol—A Concept Study'.

Acknowledgments: Open Access Funding by TU Wien.

Conflicts of Interest: The authors declare no conflict of interest.

Abbreviations

ASU	Air separation unit
BFBC	Bubbling fluidized bed combustor
BWR	Boiling water reactor
CCS	Carbon capture and storage
CCU	Carbon capture and utilization
CHP	Combined heat and power
CRI	Carbon Recycling International
DAC	Direct air capture
DH	District heating
FD	Flash drum
FG	Flue gas
FGR	Flue gas recirculation
FM	Fluidization medium
IMPCA	International Methanol Consumers and Producers Association
IPCC	Intergovernmental Panel on Climate Change
LCA	Life cycle assessment
LHV	Lower heating value
MEA	Monoethanolamine
MeOH	Methanol
PtC	Power-to-chemicals
PtF	Power-to-fuels
PtG	Power-to-gas
PtL	Power-to-liquid
PtX	Power-to-X
SCR	Selective catalytic reduction
SOEC	Solid oxide electrolysis cell
TRL	Technology readiness level
Abs.	Absorber
Atm.	Atmospheric
Bag.	Baghouse filter
Compr.	Compressor
Con.	Condenser
Des.	Desorber
Dis.	Distributor plate
el.	Electric
f	Fluidization
g	Gas
i	Species i
max.	Maximum
Op.	Operating conditions
Ox.	Oxidant
s	Saturated
sv	Equivalent diameter

sv	Equivalent diameter
th.	Thermal
Tr.	Triple point
Unc.	Unconverted gases

Nomenclature

A	Area [m^2]
d	Diameter [m]
h	Height [m]
V	Volume [m^3]
T, θ	Temperature [K,°C]
p	Pressure [Pa,bar]
X	Water loading [kg/kg]
$\dot{V}$	Volume flow rate [m^3/s]
$\dot{m}$	Mass flow rate [kg/s]
$\dot{n}$	Material flow rate [kmol/s]
m'	Mass fraction [wt%]
y	Volume fraction [vol%]
$\dot{Q}$	Rate of heat flow [W]
Q'	Specific heat demand [MJ/kg]
$Q_{Tot.}$	Total heat demand [$GWh_{th.}$]
LHV	Lower heating value [MJ/kg]
P	Power [W]
$P_{Tot.}$	Total electricity demand [GWh]
$\dot{U}$	Flow rate of chemical energy [J/s]
w_t	Specific technical work [J/kg]
R	Universal gas constant [J/(mol·K)]
R_i	Specific gas constant of species i [J/(kg·K)]
ΔH_r	Reaction enthalpy [kJ/mol]
u	Velocity [m/s]
r	Recirculation ratio [-]
α	Excess of oxygen in the oxidant [-]
β	Excess of oxygen in the fluidization medium [-]
γ	Allocation coefficient [-]
ε	Porosity [-]
λ	Air ratio [-]
ρ	Density [kg/m^3]
μ	Dynamic viscosity [Pa·s]
η	Efficiency rate [%,-]
ψ	CO_2 conversion [%]
ω	H_2:CO_2 ratio [-]

Appendix A

Table A1. Specific O_2 demand of the combustion reaction per species i.

Species	O_2 Demand [Nm^3/kg of Species i]
C	1.8659
H	5.5608
O	−0.7003
S	0.6988

Table A2. Input and output—reference operating point.

	Parameter	Value [kg/h]	kg/kg Fuel	kg/kg MeOH
Input	$\dot{m}_{Fuel}$	6132.90	-	3.746
	$\dot{m}_{H_2}$	341.68	0.056	0.209
	MeOH synthesis (H_2)	324.36	0.053	0.198
	DeOxo reactor (H_2)	17.31	0.003	0.011
	$\dot{m}_{O_2}$ (Oxyfuel)	6186.95	1.009	3.779
	O_2 from Electrolyzer	2713.07	0.442	1.657
	O_2 from ASU	3473.83	0.556	2.122
	$\dot{m}_{Ca(OH)_2}$	7.226	0.001	0.004
	$\dot{m}_{NH_4OH}$	2.447	0.0004	0.001
	$\dot{m}_{Air}$	14,999	2.446	9.160
Output	$\dot{m}_{MeOH}$	1637.40	0.267	-
	$\dot{m}_{N_2}$	11,334.45	1.848	6.992
	$\dot{m}_{Ar}$	190.33	0.031	0.116
	$\dot{m}_{FG}$	5744.46	0.937	3.508
	$\dot{m}_{CO_2}$	5348.72	0.872	3.267
	$\dot{m}_{H_2O}$ (net value)	1929.95	0.315	1.179
CO_2	CO_2 generated	7461.03	1.246	4.667
	CO_2 utilized	2292.31	0.374	1.400
	CO_2 emitted	5348.72	0.872	3.267

Table A3. On-site demand—reference operating point.

	Process	Symbol	Type	Species	[kg/s]	[Nm^3/s]	Power [kW]
Oxyfuel	OXY.1	V1	Blower	FM	10.83	6.02	500
	OXY.2	V2	Fan	FG	0.68	0.42	0.75
	OXY.3	V3	Fan	FG	1.60	0.84	1.5
	OXY.4	P1	Pump	H_2O	1.13	-	0.4
	OXY.5	H1	Twin screw	Fuel	1.70	-	0.7
						SUM Oxyfuel	503.35
DeOxo	DeOxo.1	V2	Fan	FG		See OXY.2	
	DeOxo.2	C4	Compressor	FG	0.684	-	95.24
						SUM DeOxo	95.24
Methanol	MeOH.1	P2	Pump	MeOH + H_2O	0.71	-	0.4
	MeOH.2	P3	Pump	MeOH	0.46	-	0.4
	MeOH.3	P4	Pump	H_2O	0.26	-	0.4
	MeOH.4	P5	Pump	H_2O	0.26	-	0.4
	MeOH.5	C1	Compressor	CO_2	0.64	-	59.87
	MeOH.6	C2	Compressor	H_2	0.09	-	32.55
	MeOH.7	C3	Compressor	Rec. gases	0.019	-	27.94
						SUM Methanol	121.96
Electrolyzer	ELE.1	P1	Pump	H_2O		See OXY.4	
						SUM Electrolyzer	0
					Total on-site power demand		720.55

Table A4. Molar masses of relevant species.

Species	Molar Mass [kg/kmol]
C	12.01
H_2	2.015
O_2	32.00
S	32.07
N_2	28.01
H_2O	18.02
SO_2	64.07

Table A5. Specific and universal gas constants.

Species	Gas Constant [J/(mol·K)]
$R_{Univ.}$	8.314
CO_2	188.91
H_2	4126.05
CO	296.82
Rec. Gases (H_2, CO, CO_2)	1084.06

Table A6. Parameters for water—Antoine equation.

Parameter	Value [-]
A	17.2799
B	4102.99
C	237.431

Table A7. Assumed parameters of the BFBC.

Parameter	Value [Unit]
Bed surface area A_{Bed}	15 m^2
Bed volume V_{Bed}	15 m^3
Bed height h_{Bed}	1 m
Bed diameter d_{Bed}	4.37 m
Bed temperature T_{Bed}	850 °C

Table A8. Assumed properties of silica sand as bed material.

Parameter	Value [Unit]
ρ_P	2660 kg/m^3
ρ_{Bulk}	1490 kg/m^3
ε	0.44
d_P	0.7 mm
d_{SV}	0.61 mm

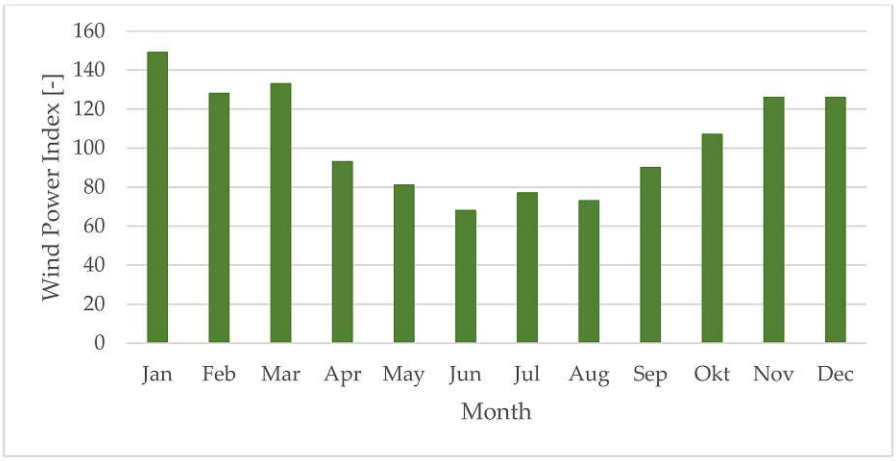

Figure A1. Seasonal fluctuation of wind power [47].

Table A9. Machine list.

Name	Machine
H1	Twin screw conveyor
V1	Blower
V2,V3	Fans
W1	Preheating heat exchanger
W2–7	Heat exchangers
C1–4	Multi-staged compressors
P1–8	Rotary pumps
D1,D2	Relief valves
F1,F2,F3,F4	Distribution valves

Global Process Flow Charts

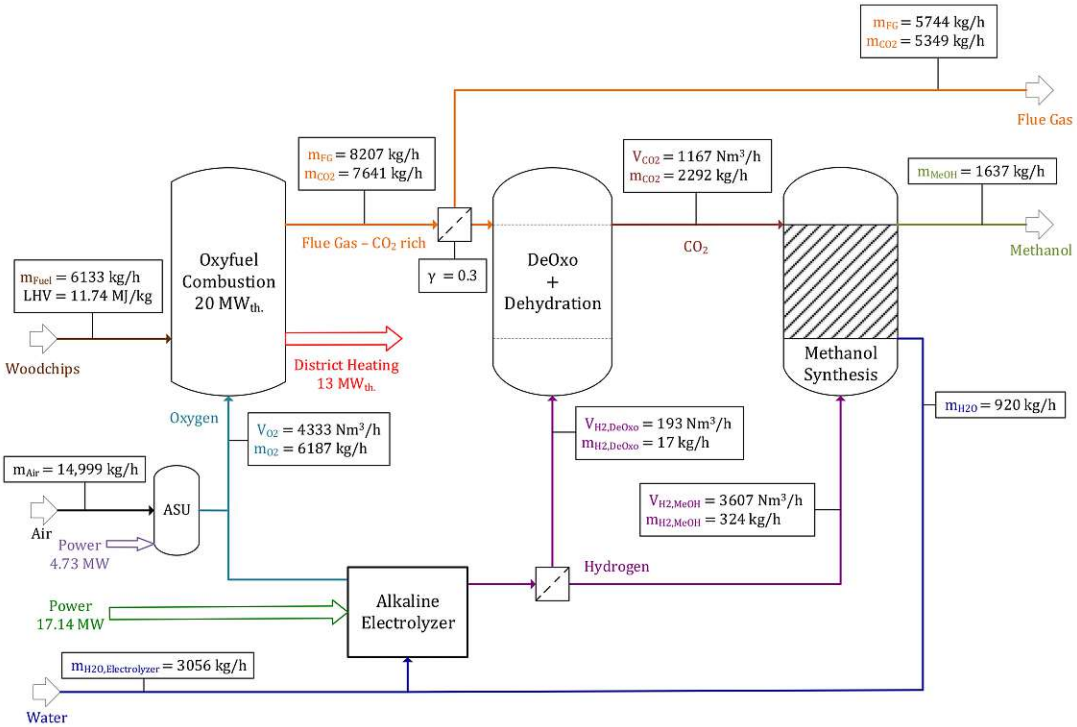

Figure A2. Reference operating point (Oxyfuel combustion)—simplified global flow chart.

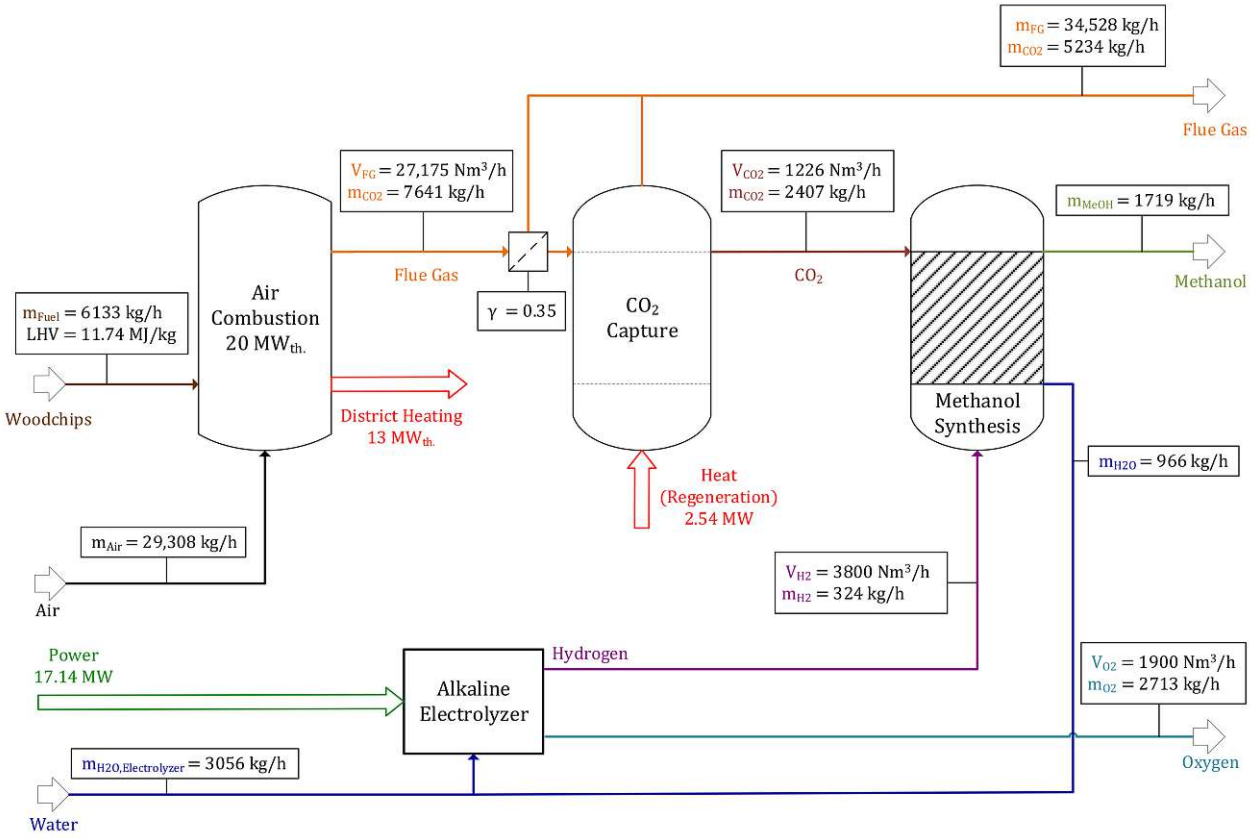

Figure A3. Operating point "Air" (air combustion)—simplified global flow chart.

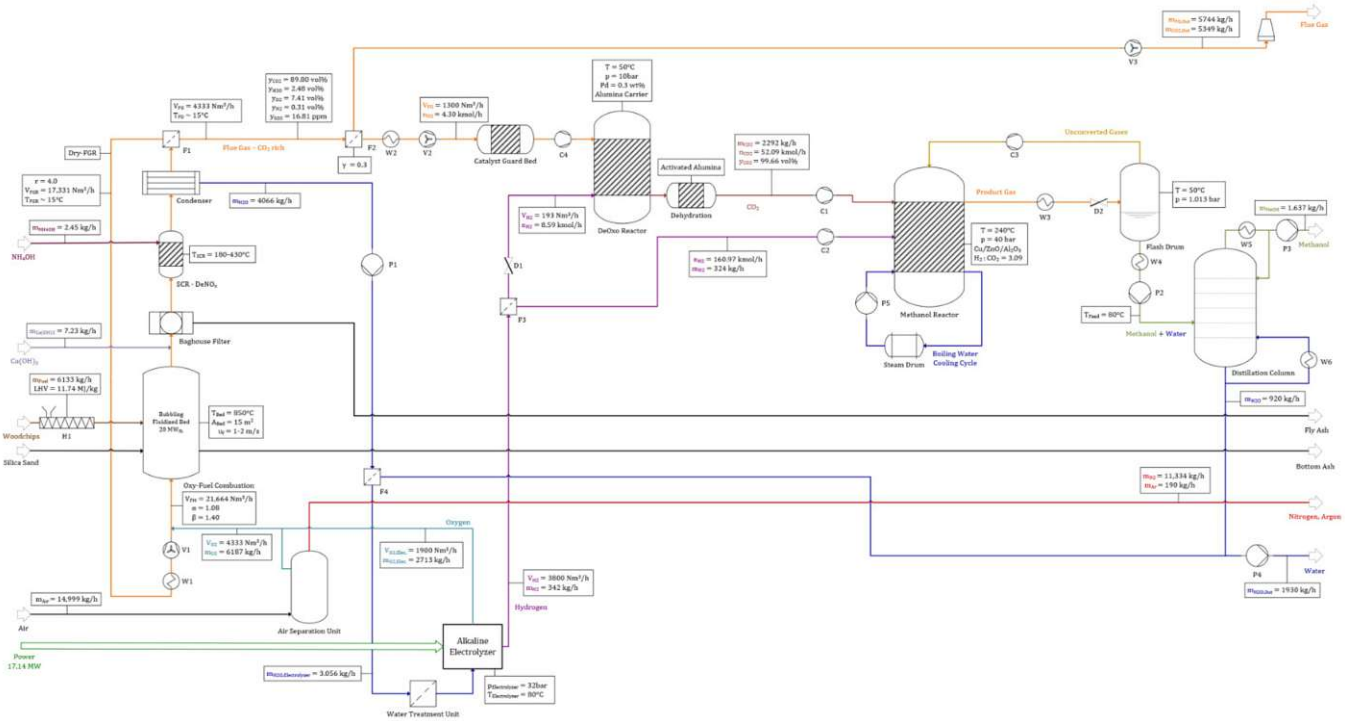

Figure A4. Reference operating point (oxyfuel combustion)—detailed global flow chart.

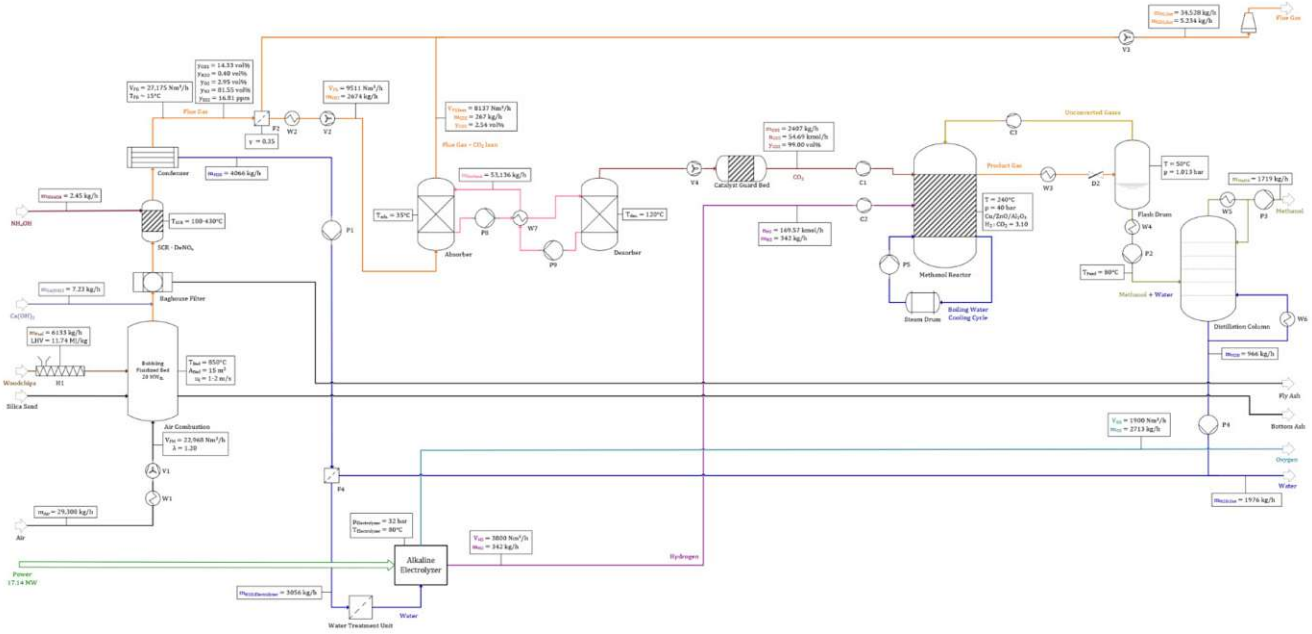

Figure A5. Operating point "Air" (air combustion)—detailed global flow chart.

References

1. Trends in Atmospheric Carbon Dioxide. Available online: https://www.esrl.noaa.gov/gmd/ccgg/trends/global.html (accessed on 6 April 2021).
2. Trends in Atmospheric Carbon Dioxide. Available online: https://www.esrl.noaa.gov/gmd/ccgg/trends/gl_gr.html (accessed on 6 April 2021).
3. Meunier, N.; Chauvy, R.; Mouhoubi, S.; Thomas, D.; de Weireld, G. Alternative Production of Methanol from Industrial CO_2. *Renew. Energy* **2020**, *146*, 1192–1203. [CrossRef]
4. A European Green Deal—Striving to be the First Climate-Neutral Continent. Available online: https://ec.europa.eu/info/strategy/priorities-2019-2024/european-green-deal_en (accessed on 6 April 2021).
5. Metz, B.; Intergovernmental Panel on Climate Change (Eds.) *IPCC Special Report on Carbon Dioxide Capture and Storage*; Cambridge University Press, for the Intergovernmental Panel on Climate Change: Cambridge, UK, 2005; ISBN 978-0-521-86643-9.
6. Wulf, C.; Linßen, J.; Zapp, P. Review of Power-to-Gas Projects in Europe. *Energy Procedia* **2018**, *155*, 367–378. [CrossRef]
7. Schlautmann, R.; Böhm, H.; Zauner, A.; Mörs, F.; Tichler, R.; Graf, F.; Kolb, T. Renewable Power-to-Gas: A Technical and Economic Evaluation of Three Demo Sites within the STORE&GO Project. *Chem. Ing. Tech.* **2021**, *93*, 568–579. [CrossRef]
8. Bowker, M. Methanol Synthesis from CO_2 Hydrogenation. *ChemCatChem* **2019**, *11*, 4238–4246. [CrossRef] [PubMed]
9. Marlin, D.S.; Sarron, E.; Sigurbjörnsson, Ó. Process Advantages of Direct CO_2 to Methanol Synthesis. *Front. Chem.* **2018**, *6*, 446. [CrossRef]
10. Mathew, T. George Andrew Olah (1927–2017). *Nature* **2017**, *544*, 162. [CrossRef]
11. Industrial Power-to-Liquid Pioneer Plant 2022 in Germany. Available online: https://ineratec.de/wp-content/uploads/2020/12/ineratec-pionieranlage-presseinformation.pdf (accessed on 2 April 2021).
12. Schühle, P.; Reichenberger, S.; Marzun, G.; Albert, J. Slurry Phase Hydrogenation of CO_2 to Methanol Using Supported In_2O_3 Catalysts as Promising Approach for Chemical Energy Storage. *Chem. Ing. Tech.* **2021**, *93*, 585–593. [CrossRef]
13. Bukhtiyarova, M.; Lunkenbein, T.; Kähler, K.; Schlögl, R. Methanol Synthesis from Industrial CO_2 Sources: A Contribution to Chemical Energy Conversion. *Catal. Lett.* **2017**, *147*, 416–427. [CrossRef]
14. Wall, T.; Liu, Y.; Spero, C.; Elliott, L.; Khare, S.; Rathnam, R.; Zeenathal, F.; Moghtaderi, B.; Buhre, B.; Sheng, C.; et al. An Overview on Oxyfuel Coal Combustion—State of the Art Research and Technology Development. *Chem. Eng. Res. Des.* **2009**, *87*, 1003–1016. [CrossRef]
15. Callide Oxyfuel Project—Final Results. Available online: https://www.globalccsinstitute.com/archive/hub/publications/202090/cop-finalresults-publicreport-march2018.pdf (accessed on 8 April 2021).
16. Sher, F.; Pans, M.A.; Sun, C.; Snape, C.; Liu, H. Oxy-Fuel Combustion Study of Biomass Fuels in a 20 KWth Fluidized Bed Combustor. *Fuel* **2018**, *215*, 778–786. [CrossRef]
17. Leonzio, G.; Zondervan, E.; Foscolo, P.U. Methanol Production by CO_2 Hydrogenation: Analysis and Simulation of Reactor Performance. *Int. J. Hydrog. Energy* **2019**, *44*, 7915–7933. [CrossRef]
18. Van-Dal, É.S.; Bouallou, C. Design and Simulation of a Methanol Production Plant from CO_2 Hydrogenation. *J. Clean. Prod.* **2013**, *57*, 38–45. [CrossRef]

19. Matzen, M.; Alhajji, M.; Demirel, Y. Chemical Storage of Wind Energy by Renewable Methanol Production: Feasibility Analysis Using a Multi-Criteria Decision Matrix. *Energy* **2015**, *93*, 343–353. [CrossRef]
20. Skopec, P.; Hrdlička, J. Specific Features of the Oxyfuel Combustion Conditions in a Bubbling Fluidized BED. *Acta Polytech.* **2016**, *56*, 312–318. [CrossRef]
21. Hrdlicka, J.; Skopec, P.; Opatril, J.; Dlouhy, T. Oxyfuel Combustion in a Bubbling Fluidized Bed Combustor. *Energy Procedia* **2016**, *86*, 116–123. [CrossRef]
22. VDI e. V. (Ed.) *VDI-Wärmeatlas*; Springer: Berlin/Heidelberg, Germany, 2013; ISBN 978-3-642-19980-6.
23. Vakkilainen, E.K. *Steam Generation from Biomass: Construction and Design of Large Boilers*; Butterworth-Heinemann: Oxford, UK, 2017; ISBN 978-0-12-804389-9.
24. Anthony, E.J.; Hack, H. Oxy-fired fluidized bed combustion: Technology, prospects and new developments. In *Fluidized Bed Technologies for Near-Zero Emission Combustion and Gasification*; Elsevier: Amsterdam, The Netherlands, 2013; pp. 867–894. ISBN 978-0-85709-541-1.
25. Vodička, M.; Hrdlička, J.; Skopec, P. Experimental Study of the NOX Reduction through the Staged Oxygen Supply in the Oxy-Fuel Combustion in a 30 KWth Bubbling Fluidized Bed. *Fuel* **2021**, *286*, 119343. [CrossRef]
26. Cluet, B.; Mauviel, G.; Rogaume, Y.; Authier, O.; Delebarre, A. Segregation of Wood Particles in a Bubbling Fluidized Bed. *Fuel Process. Technol.* **2015**, *133*, 80–88. [CrossRef]
27. Strauß, K. *Kraftwerkstechnik*; Springer: Berlin/Heidelberg, Germany, 2009; ISBN 978-3-642-01430-7.
28. The EPA Air Pollution Control Manual. Available online: https://www3.epa.gov/ttncatc1/dir1/cs4-2ch2.pdf (accessed on 9 April 2021).
29. Moioli, S.; Nagy, T.; Langé, S.; Pellegrini, L.A.; Mizsey, P. Simulation Model Evaluation of CO_2 Capture by Aqueous MEA Scrubbing for Heat Requirement Analyses. *Energy Procedia* **2017**, *114*, 1558–1566. [CrossRef]
30. Nouri, M.; Rahpaima, G.; Nejad, M.M.; Imani, M. Computational Simulation of CO_2 Capture Process in a Fluidized-Bed Reactor. *Comput. Chem. Eng.* **2018**, *108*, 1–10. [CrossRef]
31. Nakao, S.; Yogo, K.; Goto, K.; Kai, T.; Yamada, H. *Advanced CO_2 Capture Technologies: Absorption, Adsorption, and Membrane Separation Methods*; Springer Briefs in Energy; Springer International Publishing: Cham, Switzerland, 2019; ISBN 978-3-030-18857-3.
32. Pröll, T.; Schöny, G.; Sprachmann, G.; Hofbauer, H. Introduction and Evaluation of a Double Loop Staged Fluidized Bed System for Post-Combustion CO_2 Capture Using Solid Sorbents in a Continuous Temperature Swing Adsorption Process. *Chem. Eng. Sci.* **2016**, *141*, 166–174. [CrossRef]
33. Schöny, G.; Dietrich, F.; Fuchs, J.; Pröll, T.; Hofbauer, H. A Multi-Stage Fluidized Bed System for Continuous CO_2 Capture by Means of Temperature Swing Adsorption—First Results from Bench Scale Experiments. *Powder Technol.* **2017**, *316*, 519–527. [CrossRef]
34. Veneman, R.; Li, Z.S.; Hogendoorn, J.A.; Kersten, S.R.A.; Brilman, D.W.F. Continuous CO_2 Capture in a Circulating Fluidized Bed Using Supported Amine Sorbents. *Chem. Eng. J.* **2012**, *207–208*, 18–26. [CrossRef]
35. Cloete, S.; Giuffrida, A.; Romano, M.C.; Zaabout, A. The Swing Adsorption Reactor Cluster for Post-Combustion CO_2 Capture from Cement Plants. *J. Clean. Prod.* **2019**, *223*, 692–703. [CrossRef]
36. Das, D.; Behera, S.K.; Meikap, B.C. Removal of CO_2 in a Multistage Fluidized Bed Reactor by Amine Impregnated Activated Carbon: Optimization Using Response Surface Methodology. *Int. J. Coal Sci. Technol.* **2019**, *6*, 445–458. [CrossRef]
37. Kim, K.; Seo, H.; Kim, D.J.; Lee, C.; Min, D.Y.; Kim, H.M.; Park, Y.-K. Experimental Evaluation of CO_2 Capture with an Amine Impregnated Sorbent in Dual Circulating Fluidized Bed Process. *Int. J. Greenh. Gas. Control* **2020**, *101*, 103141. [CrossRef]
38. IMPCA Methanol Reference Specifications. Available online: http://www.methanol.org/wp-content/uploads/2016/07/IMPCA-Ref-Spec-08-December-2015.pdf (accessed on 12 April 2021).
39. Carbon Recycling International: Commercial Scale CO_2-to-methanol Plant in Norway. Available online: https://www.co2value.eu/wp-content/uploads/2019/09/2.-CRI.pdf (accessed on 12 April 2021).
40. Roode-Gutzmer, Q.I.; Kaiser, D.; Bertau, M. Renewable Methanol Synthesis. *ChemBioEng Rev.* **2019**, *6*, 209–236. [CrossRef]
41. Borisut, P.; Nuchitprasittichai, A. Methanol Production via CO_2 Hydrogenation: Sensitivity Analysis and Simulation—Based Optimization. *Front. Energy Res.* **2019**, *7*, 81. [CrossRef]
42. Coutanceau, C.; Baranton, S.; Audichon, T. Hydrogen Production from Water Electrolysis. In *Hydrogen Electrochemical Production*; Elsevier: Amsterdam, The Netherlands, 2018; pp. 17–62. ISBN 978-0-12-811250-2.
43. Brauns, J.; Turek, T. Alkaline Water Electrolysis Powered by Renewable Energy: A Review. *Processes* **2020**, *8*, 248. [CrossRef]
44. Power-to-Liquids Potentials and Perspectives for the Future Supply of Renewable Aviation Fuel. Available online: https://www.umweltbundesamt.de/en/publikationen/power-to-liquids-potentials-perspectives-for-the (accessed on 20 April 2021).
45. Austrian Windatlas. Available online: http://ispacevm11.researchstudio.at/index_v.html (accessed on 15 April 2021).
46. Jansen&Heuning Calculation Program. Available online: https://www.jh.nl/en/berekeningsprogramma/ (accessed on 16 April 2021).
47. Seasonal Variation in Wind Energy. Available online: http://ele.aut.ac.ir/~{}wind/en/tour/grid/season.htm (accessed on 22 April 2021).

Journal Article II

energies

MDPI

Article

Simulation of a Pilot Scale Power-to-Liquid Plant Producing Synthetic Fuel and Wax by Combining Fischer–Tropsch Synthesis and SOEC

Simon Pratschner *, Martin Hammerschmid, Florian J. Müller, Stefan Müller and Franz Winter

Institute of Chemical, Environmental and Bioscience Engineering, TU Wien, Getreidemarkt 9/166, 1060 Vienna, Austria; martin.hammerschmid@tuwien.ac.at (M.H.); florian.johann.mueller@tuwien.ac.at (F.J.M.); stefan.mueller@tuwien.ac.at (S.M.); franz.winter@tuwien.ac.at (F.W.)

* Correspondence: simon.pratschner@tuwien.ac.at

Abstract: Power-to-Liquid (PtL) plants can viably implement carbon capture and utilization technologies in Europe. In addition, local CO_2 sources can be valorized to substitute oil and gas imports. This work's aim was to determine the PtL efficiency obtained by combining a solid oxide electrolyzer (SOEC) and Fischer–Tropsch synthesis. In addition, a recommended plant configuration to produce synthetic fuel and wax at pilot scale is established. The presented process configurations with and without a tail gas reformer were modeled and analyzed using IPSEpro as simulation software. A maximum mass flow rate of naphtha, middle distillate and wax of 57.8 kg/h can be realized by using a SOEC unit operated in co-electrolysis mode, with a rated power of 1 $MW_{el.}$. A maximum PtL efficiency of 50.8% was found for the process configuration without a tail gas reformer. Implementing a tail gas reformer resulted in a maximum PtL efficiency of 62.7%. Hence, the reforming of tail gas is highly beneficial for the PtL plant's productivity and efficiency. Nevertheless, a process configuration based on the recirculation of tail gas without a reformer is recommended as a feasible solution to manage the transition from laboratory scale to industrial applications.

Keywords: Power-to-Liquid; carbon capture and utilization; synthetic fuel and wax; Fischer–Tropsch; SOEC; co-electrolysis of CO_2 and H_2O; tail gas reforming; pilot scale

Citation: Pratschner, S.; Hammerschmid, M.; Müller, F.J.; Müller, S.; Winter, F. Simulation of a Pilot Scale Power-to-Liquid Plant Producing Synthetic Fuel and Wax by Combining Fischer–Tropsch Synthesis and SOEC. *Energies* **2022**, *15*, 4134. https://doi.org/10.3390/en15114134

Academic Editor: Francesco Frusteri

Received: 4 May 2022
Accepted: 28 May 2022
Published: 4 June 2022

1. Introduction

Despite increased media interest in the consequences of the climate crisis, the global mean CO_2 level in the atmosphere is still rising by about 2.5 ppm per year and reached a value of 414 ppm in October 2021, an increase of 2.4 ppm compared to October 2020 [1,2]. In 2020, about 83% of the global primary energy demand was still derived from fossil sources [3]. An increase in the EU27 transportation sector's greenhouse gas (GHG) emissions of 33% compared to 1990 highlights the urgency of a sustainable reformation to reach the goal of being climate-neutral in 2050, whereas other sectors managed to reduce their GHG emissions by 32%. Transportation is responsible for about 29% of the EU27's total GHG emissions: 15% of the total GHG emissions are produced by passenger cars and vans, 5% by trucks and buses and 4% respectively by aviation and marine navigation [4,5]. A comprehensive overview of several technologies and scenarios to tackle the mobility sector's weak performance concerning GHG emissions can be found in [6].

Besides battery electric vehicles, plug-in hybrid technologies and biofuels, synthetic fuels pose an attractive transitional solution for individual mobility and have the potential to replace conventional fossil fuels in applications requiring high energy density—i.e., aviation, marine navigation and off-road vehicles, e.g., construction, agricultural or forestry vehicles—on a long-term basis [7]. In summary, the implementation of synthetic fuels includes the following advantages:

- High energy density;

- Applicability for existing technologies;
- Suitability for heavy-duty applications;
- Quick deployment, since no infrastructural adaptions are required.

An overview of current Power-to-X (PtX) projects throughout Europe was given by Wulf et al. in [8]. In June 2020, 220 PtX research and demonstration projects were realized, finished or planned in Europe. Some of the mentioned plants were not commissioned at release and have not been constructed as of April 2022. Germany, Spain and the UK have the highest shares of PtX plants in Europe. Power-to-Gas (PtG) plants obtained the highest share of 94%. Power-to-H_2 applications had a share of 67%, whereas Power-to-Methane plants had a share of 27%. The production of methanol and other technologies, i.e., the production of DME or Fischer–Tropsch products, accounted for 3%. Low-temperature electrolysis technologies, i.e., alkaline electrolyzers and proton exchange membrane electrolyzers (PEMEC), were by far the preferred technology for H_2 production, as shown by their share being larger than 90%, whereas high-temperature solid oxide electrolyzers (SOEC) were applied in less than 10% of the analyzed projects.

An overview concerning completed and ongoing Power-to-Liquid projects based on the synthesis of methanol or Fischer–Tropsch products is given in Table 1.

Finding a way to commercialize liquid fuels produced by lignocellulosic feedstocks or CO_2 streams in combination with renewable H_2 is one goal of [9] within the "Advancefuel" project, which is analyzing several conversion technologies to produce fuels such as methanol, DME, gasoline and diesel. An alternative route for the production of Fischer–Tropsch products based on syngas generated via biomass gasification, i.e., Biomass-to-Liquid, is presented in [10]. The upcycling of waste, e.g., municipal waste, sewage sludge or residues from the pulp and paper industry to renewable fuel and wax via dual-fluidized bed gasification and Fischer–Tropsch synthesis is planned to be realized within the "Waste2Value" project conducted in Vienna, Austria [11]. A concept for a PtL plant based on the synthesis of methanol in combination with a biomass heating plant and a conventional alkaline electrolyzer was analyzed in [12]. Besides the produced methanol, heat was transferred to a district heating network provided by a fluidized bed combustor operating in air or oxyfuel mode.

Table 1. Overview of completed and ongoing Power-to-Liquid projects.

Name	Location	CO_2 Source	Power Source	Electrolyzer	Synthesis	$m_{Products}$ [1]	Source
Haru Oni	Magellanes, CHL	DAC	Wind power	PEM	Methanol	- [2]	[13]
George Olah Plant	Svartsengi, IS	Geothermal	Geothermal	Alkaline	Methanol	4000 t/a	[14]
MefCO_2	Niederaussem, GER	Coal plant	Surplus el.	PEM	Methanol	365 t/a	[15]
Norsk e-fuel	Mosjøen, NOR	DAC	Wind power	SOEC	Fischer–Tropsch	12.5 t/a	[16]
- [2]	Werlte, GER	Biogas + DAC	Renewable	- [2]	Fischer–Tropsch	350 t/a	[17]
- [2]	Frankfurt, GER	Biogas plant	- [2]	- [2]	Fischer–Tropsch	3500 t/a	[18]

[1] According to the stated source. [2] Information not available.

Fischer–Tropsch synthesis has been researched and optimized for several decades, and hence is well established at an industrial scale. De Klerk provided an extensive overview of the process itself and industrial plants in [19]. Martinelli et al. gave a comprehensive examination of the Fischer–Tropsch process in combination with SOEC or biomass gasification as syngas production technologies [20]. Detailed information about the impacts of process conditions—temperature, pressure, space velocity, H_2:CO ratio, etc.—can be found in [21–26]. Refining Fischer–Tropsch syncrude to on-specification diesel fuel is far from trivial, since several technological aspects need to be synchronized with national diesel fuel standards to comply with required intervals for parameters, i.e., the cetane number, density and viscosity [27]. Lately, Fischer–Tropsch waxes have received increasing attention due to their low amounts of aromatic and sulfurous compounds, hence having high potential as feedstock for the cosmetic industry [28].

Choosing the appropriate reactor design for PtL plants at a pilot scale is crucial. Fluidized bed reactor systems, either stationary or circulating, are applied for high-temperature

Fischer–Tropsch (HTFT) synthesis processes [29] but are not considered in this work, since the system aims at maximizing the middle distillate and wax fractions. In general, three reactor types can be considered for low-temperature Fischer–Tropsch (LTFT) applications, i.e., slurry bubble column reactors (SBCR), fixed bed multitubular reactors (FBMR) and microstructured reactors. The advantages and disadvantages of SBCR and FBMR reactors can be found in [29–31]. Detailed information regarding existing reactors at an industrial scale is stated in [19]. The current status of microstructured reactors and an analysis concerning the effect of process parameters can be found in [32,33].

Previous work concerning the simulation of Power-to-Liquid plants via Fischer–Tropsch synthesis is summarized in Table 2. The syngas was either provided by a solid-oxide electrolyzer operating in co-electrolysis mode, a low-temperature electrolyzer in combination with a reverse water-gas shift (rWGS) reactor, or biomass gasification. The simulation of the Fischer–Tropsch synthesis was based on a Co-based catalyst with different approaches concerning the chemistry inside the reactor, i.e., the standard Anderson–Schulz–Flory (ASF) distribution, kinetic modeling and basic reaction stoichiometry. In general, the chosen values concerning the chain growth probability were around 0.9 to maximize the yield of long-chain hydrocarbons. Most of the authors assumed rather optimistic CO conversions of higher than 70%. The recirculation of tail gas (TG) to the inlet of the SOEC unit or rWGS reactor was considered in the majority of the listed works. Another option is to realize a short recycle configuration to the Fischer–Tropsch reactor's inlet.

Table 2. Overview of previous works on the simulation of Power-to-Liquid plants based on Fischer–Tropsch synthesis.

Syngas Production	Fischer–Tropsch Model	Catalyst	Chain Growth Probability α	CO Conversion	Tail Gas Recirculation	Source
SOEC/rWGS	Standard ASF + kinetic model	Co-based	- [1]	70% (per pass)	Inlet SOEC/ inlet rWGS	[34]
SOEC	Standard ASF	Co-based	0.94	87% (per pass)	Inlet SOEC	[35]
rWGS	Standard ASF	Co-based	- [1]	100% (plant)	Inlet rWGS/ inlet FT reactor	[36]
SOEC	Standard ASF + kinetic model	Co-based	0.90	80% (per pass)	No recirculation	[37]
SOEC	- [1]	Co-based	0.90	80% (per pass)	Inlet SOEC/ inlet FT reactor	[38]
rWGS	Reaction stoichiometry	Co-based	- [1]	- [1]	Inlet rWGS	[39]
Biomass gasification [2]	Standard ASF	Co-based	0.89–0.93	40% (per pass)	No recirculation	[40]

[1] Not specified. [2] Combining process simulation and experimental validation.

The main aim of this work was to answer the question of which Power-to-Liquid efficiencies can be realized by pilot scale plants combining an SOEC unit with Fischer–Tropsch synthesis. In addition, an ideal plant configuration for the production of synthetic liquid fuels and wax at a pilot scale is provided as a result of the presented work. In comparison to the comparable research stated in Table 2, the underlying work shifts the focus toward the Fischer–Tropsch process itself by applying the extended ASF distribution model and analyzing the recirculation of tail gas prior to the Fischer–Tropsch reactor instead of the SOEC. Furthermore, a process route including a tail gas reformer to convert short-chain hydrocarbons and CO_2 to syngas is analyzed.

2. Materials and Methods

The presented work is based on the results obtained by the process simulation of two design configurations for a PtL plant producing Fischer–Tropsch products. IPSEpro (version 8), stationary equation-orientated simulation software based on the numerical solving of equation systems via the Newton–Raphson method, was applied to develop the underlying model consisting of the following subprocesses:

- Co-electrolysis of CO_2 and H_2O with a subsequent syngas condenser;
- Using a blower to overcome the pressure drop caused by the syngas condenser;

- Three-staged syngas compression with intermediate cooling by ambient air;
- Fischer–Tropsch reaction;
- Product separation;
- Tail gas recirculation and tail gas reforming;
- Tail gas combustion.

An overview of a process configuration of a PtL plant at the pilot scale without a tail gas reformer is given in Figure 1. Syngas provided by the SOEC unit is transferred to the condenser by a blower to overcome its pressure drop. After water separation, the syngas is compressed to the Fischer–Tropsch reactor's pressure level via a three-stage compression step with intermediate cooling by ambient air. The SOEC's syngas and the recirculated tail gas are mixed before being transferred into the reactor. A hot water cooling cycle ensures the removal of the reaction heat. A share of the produced middle distillate and wax leave the reactor as a liquid. The rest of the Fischer–Tropsch products, water and unconverted gases are drained as gases and transferred to the subsequent product separation unit. Within this process configuration, the separation of wax, middle distillate, naphtha and water is realized by three heat exchangers based on water as a cooling agent. Subsequently, a share of the tail gas stream is recirculated in front of the Fischer–Tropsch reactor, whereas the remaining tail gas leaves the system as purge gas.

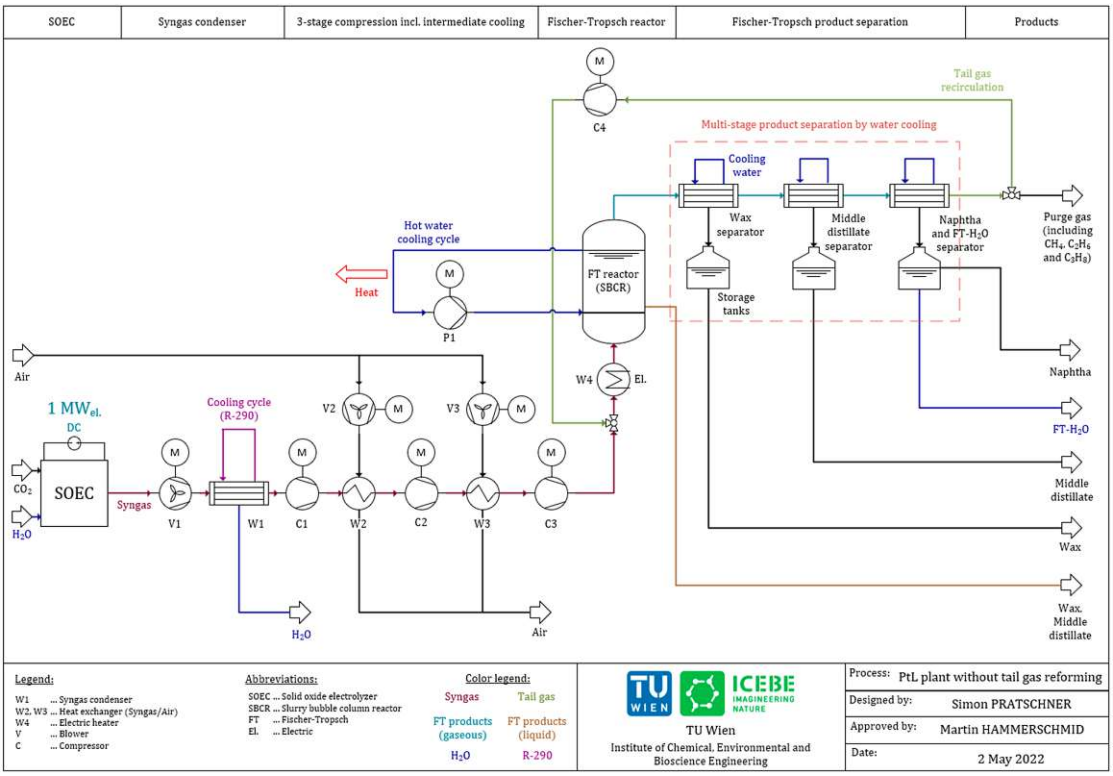

Figure 1. Scheme of the Power-to-Liquid plant without tail gas reforming.

The proposed process route that includes a tail gas reformer is displayed in Figure 2, showing the following differences from Figure 1:

- The recirculated tail gas is inserted in front of the syngas condenser;
- The product separation is realized by a multi-stage flash distillation;
- Purge gas is combusted to heat the recirculated tail gas;
- A tail gas reformer ensures the conversion of CO_2 and hydrocarbons inside the recirculated tail gas stream.

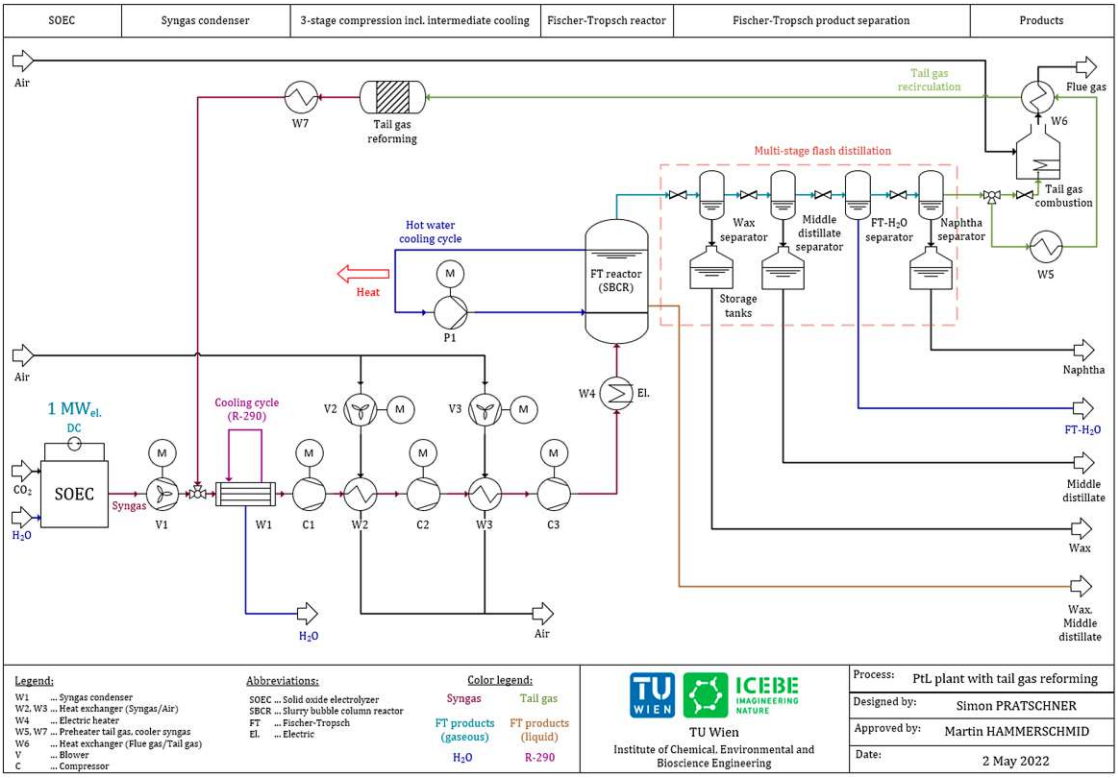

Figure 2. Scheme of the Power-to-Liquid plant with tail gas reforming.

The implementations of the presented flowcharts in IPSEpro are shown in Figure 3 for the process configuration without a tail gas reformer and in Figure 4 for the one including a tail gas reformer.

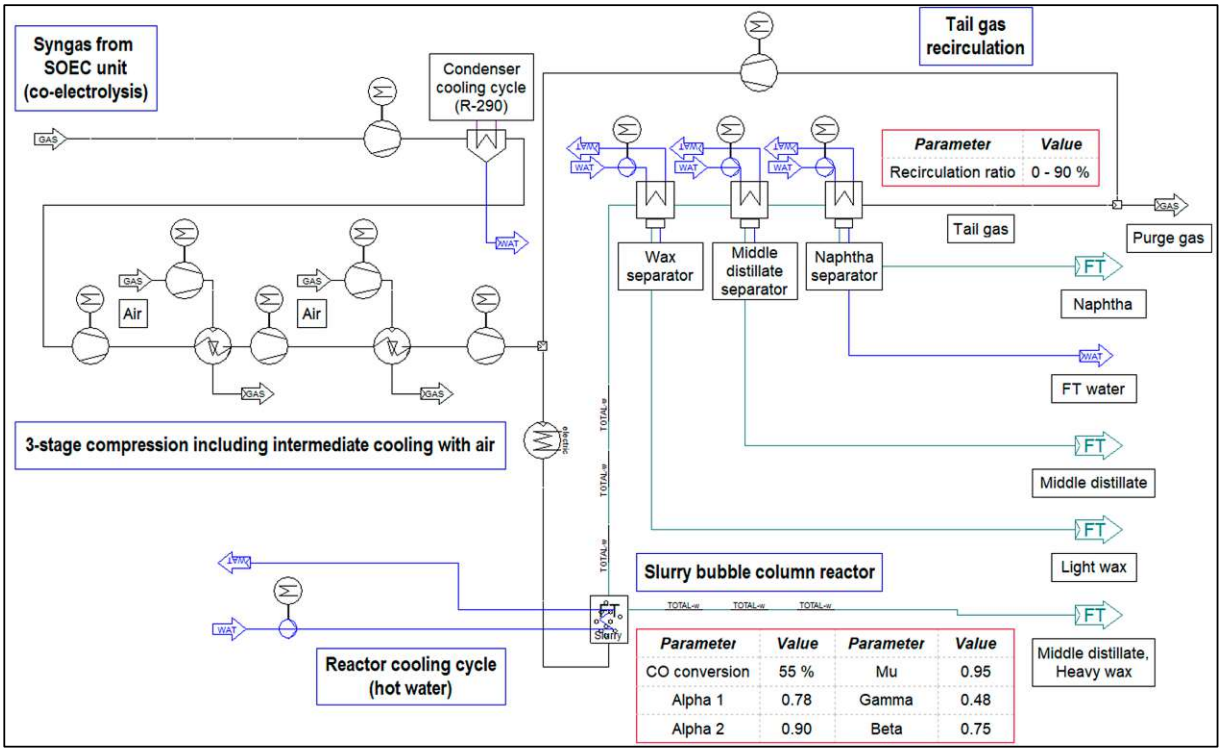

Figure 3. Implementation in IPSEpro—process configuration without tail gas reforming.

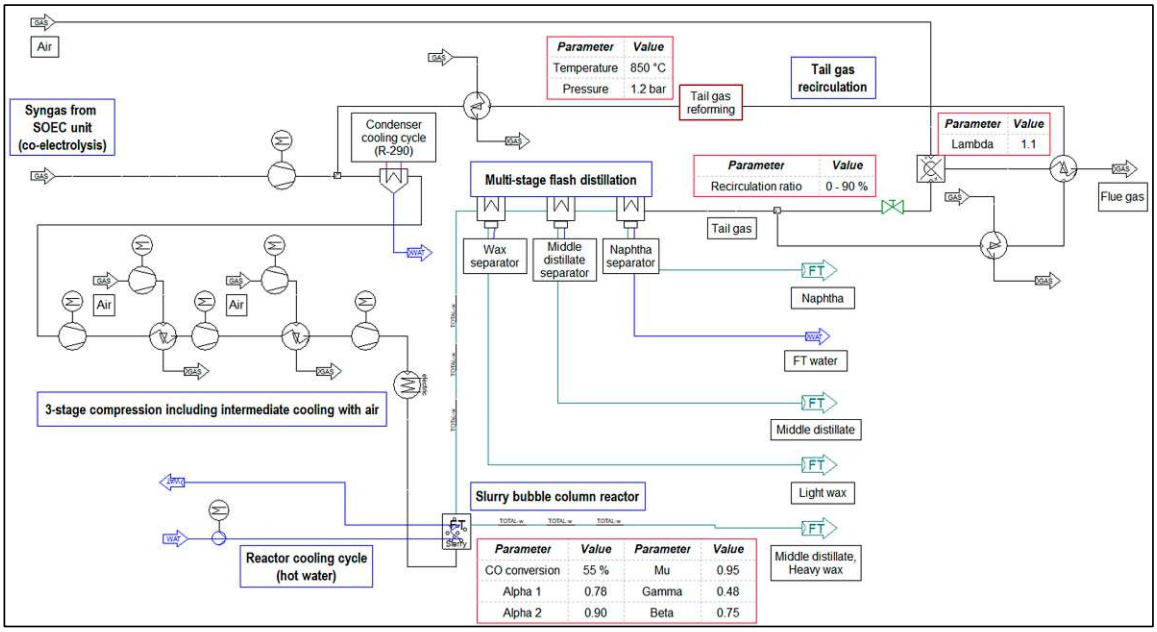

Figure 4. Implementation in IPSEpro—process configuration including tail gas reforming.

Table 3 provides a list of the parameters chosen for the process simulation. Detailed explanations of the subprocesses are given within the following subsections.

Table 3. Important parameters of the process simulation.

Parameter	Symbol	Value	Unit	Source
SOEC and syngas				
SOEC power input	P_{SOEC}	1	$MW_{el.}$	Chosen design
Syngas mass flow rate	m_{Syngas}	190	kg/h	Calculation [41]
Temperature syngas	T_{Syngas}	120	°C	Assumption
Volume share of CO	y_{CO}	27.9 [1]	vol%	[34]
Volume share of H_2	y_{H2}	55.8 [1]	vol%	[34]
Volume share of H_2O	y_{H2O}	5.5 [2]	vol%	[34]
Volume share of CO_2	y_{CO2}	10.5 [2]	vol%	[34]
Volume share of CH_4	y_{CH4}	0.3 [2]	vol%	[34]
Temperature condenser OUT	$T_{Con.}$	10	°C	Assumption
Syngas compression and intermediate cooling				
Pressure condenser OUT	$p_{Con.}$	1	bar	Assumption
Pressure C1	p_{C1}	3	bar	[42]
Pressure C2	p_{C2}	8	bar	[42]
Pressure C3	p_{C3}	21	bar	[42]
Temperature W2 and W3	$T_{W2,W3}$	50	°C	Assumption
Fischer–Tropsch synthesis				
Temperature FT reactor	T_{FT}	210	°C	[19]
Pressure FT reactor	p_{FT}	21	bar	[19]
CO conversion FT reactor	$X_{CO,Reactor}$	55	%	[43,44]
rWGS activity FT reactor	$X_{rWGS,Reactor}$	0	%	[19]
Chain growth probability	α_1	0.78	-	Based on [43]
Chain growth probability	α_2	0.90	-	Based on [43]
Factor to merge α_1 and α_2	μ	0.95	-	Based on [43]
Readsorption factor	γ	0.48	-	Based on [43]
Termination factor	β	0.75	-	Based on [43]
Tail gas recirculation and reforming				
Recirculation ratio	RR	0–90	%	Chosen design
Temperature reformer	$T_{Reformer}$	850	°C	Chosen design
Pressure reformer	$p_{Reformer}$	1.2	bar	Chosen design
Tail gas combustion				
Air ratio	λ	1.1	-	Assumption
Temperature flue gas	$T_{Flue\ gas}$	1100	°C	Assumption
Product fractions				
Methane	C_1		Number of carbon atoms	
Ethane and propane	C_2–C_3		Number of carbon atoms	
Naphtha	C_4–C_9		Number of carbon atoms	
Middle distillate	C_{10}–C_{19}		Number of carbon atoms	
Wax	C_{20+}		Number of carbon atoms	

[1] Varied to maintain H_2:CO_{FT} = 2. [2] constant.

2.1. SOEC (Co-Electrolysis) and Condenser

Thermodynamically, the required enthalpy for water splitting is provided by electrical and thermal energy, as can be seen in Equation (1). An increase in the thermal energy provided to the cell decreases the required input of electricity [45].

$$\Delta_r H = \Delta_r G + T \cdot \Delta_r S, \quad (1)$$

Due to this behavior, the application of high-temperature electrolysis technologies, i.e., SOEC, has the potential to significantly improve the efficiency of PtL plants when combined with strongly exothermal chemical synthesis processes [46]. Since conventional syngas consisting of CO and H_2 is required for Fischer–Tropsch processes applying a Co-based catalyst, we chose to have the electrolysis unit operate under co-electrolysis conditions, converting CO_2 and H_2O to CO and H_2, at atmospheric pressure and a temperature of 850 °C. Detailed information about state-of-the-art materials used for electrodes and the electrolyte in high-temperature electrolysis cells can be found in [47]. Equations (2)–(4) show the underlying chemical reactions of a high-temperature electrolyzer in co-electrolysis mode [34].

$$\text{Cathode: } H_2O + 2\,e^- \rightarrow H_2 + O^{2-}, \quad (2)$$

$$\text{Cathode: } CO_2 + 2\,e^- \rightarrow CO + O^{2-}, \quad (3)$$

$$\text{Anode: } O^{2-} \rightarrow 0.5\,O_2 + 2\,e^-, \quad (4)$$

According to literature, an assumed mass flow rate of 190 kg/h of syngas is provided by the SOEC unit, operating at T_{SOEC} = 850 °C and p_{SOEC} = 1 bar, consuming 1 $MW_{el.}$ of electric power. The amount of H_2 inside the syngas stream and the required amount of H_2 for the formation of CO via the rWGS reaction correspond to an energy demand of 3.37 kWh/Nm^3 H_2 according to [41], for the syngas' base case composition listed in Table 3 [34], and an efficiency of 80%. The volume fractions of CO and H_2 can be varied by adapting the share of H_2O at the SOEC unit's inlet to adjust the required H_2:CO ratio for process routes that include the recirculation of tail gas [34]. The data listed in Table 3 imply a reactant utilization rate of around 80% [38].

A blower after the SOEC unit ensures overcoming the pressure difference of 0.2 bar caused by the condenser, applying C_3H_8, i.e., R-290, as a cooling medium.

2.2. Syngas Compression with Intermediate Cooling

Syngas leaves the SOEC unit at atmospheric pressure, and hence needs to be compressed to the synthesis pressure of p_{FT} = 21 bar. In addition, the recirculated syngas needs to be re-pressurized after being separated via multi-stage flash distillation [48] for the process route that includes tail gas reforming. The compressors' efficiencies were assumed as $\eta_{Compr.,s} = \eta_{Compr.,m.} = 0.9$, whereas the electric motors' efficiencies were chosen as $\eta_{Motor,m.} = 0.99$ and $\eta_{Motor,el.} = 0.96$.

2.3. Fischer–Tropsch Synthesis

The applied Fischer–Tropsch model is based on an LTFT process in an SBCR using a Co-based catalyst, operating at a temperature of T_{FT} = 210 °C and a pressure of p_{FT} = 21 bar. At industrial scale, Fischer–Tropsch catalysts are either based on cobalt, obtaining higher activity, fewer by-products and longer lifetimes; or iron, which is cheaper and shows activity in the rWGS reaction. Important properties are the possible hydrogenating nature of the applied material, which will result in a higher share of non-saturated hydrocarbons, and the selectivity for by-products, which can be manipulated by the addition of alkali metals as promoters [20,30]. Additional information regarding the production of Fischer–Tropsch catalysts can be found in [49].

It is assumed that the formed Fischer–Tropsch products are solely paraffins, as shown in Equation (5).

$$n\,CO + (2n + 1)\,H_2 \rightarrow H(CH_2)_nH + n\,H_2O,\ \Delta_rH = -166.4\ kJ/mol \quad (5)$$

2.3.1. Extended ASF Distribution

The extended ASF (eASF) model, as proposed by Förtsch et al., was used to find the product spectrum of the synthesized hydrocarbons [50], since the standard ASF distribution does not consider three primary deviations from real applications:

- Underestimation of the formation of CH_4;
- Overestimation of the formation of C_2H_6;
- Deviation of the chain growth probability α for long-chain hydrocarbons, C_{13+}.

The following parameters and equations were introduced by Förtsch et al. to minimize the deviation from real applications:

- α_1: Chain growth probability for hydrocarbons ranging from C_1 to C_7;
- α_2: Chain growth probability for hydrocarbons with C_{13+};
- μ: Factor for merging α_1 and α_2;
- γ: Termination factor to depict the higher selectivity for CH_4;
- β: Readsorption factor to depict the lower selectivity for C_2H_6.

The molar fractions of CH_4, C_2H_6 and $C_{n>2}$ can be determined by Equations (6)–(8), respectively [50].

$$x_{CH_4} = (1-\mu)\cdot[1-\alpha_1\cdot(1-\gamma)] + \mu\cdot(1-\alpha_2), \quad (6)$$

$$x_{C_2H_6} = (1-\mu)\cdot(1-\alpha_1)\cdot\alpha_1\cdot\frac{1-\beta}{1-\beta\cdot(1-\alpha_1)}\cdot(1-\gamma) + \mu\cdot(1-\alpha_2)\cdot\alpha_2, \quad (7)$$

$$x_{C_nH_{2n+2}} = (1-\mu)\cdot(1-\alpha_1)\cdot\alpha_1^{(n-1)}\cdot\frac{1-\gamma}{1-\beta\cdot(1-\alpha_1)}\cdot\mu\cdot(1-\alpha_2)\cdot\alpha_2^{(n-1)}, \quad (8)$$

The Co-based catalyst's assumed eASF parameters, as listed in Table 3, were based on the findings of Guilera et al. [43].

2.3.2. Reactor Cooling

Since Fischer–Tropsch synthesis is a highly exothermic process (see Equation (5)), the reaction heat needs to be transferred out of the reactor to avoid hot spots which might result in alternating the product selectivity and catalyst deactivation due to sintering processes. Industrial reactors are preferably cooled by the evaporation of boiling water at a certain pressure level, i.e., boiling water reactors. However, this reactor type requires a rather sophisticated design which might not be feasible for pilot scale applications; thus, a cooling design circulating pressurized hot water was chosen for the modeled Fischer–Tropsch reactor.

2.3.3. Chemical Conversion

A CO conversion of $X_{CO,Reactor}$ = 55% was assumed for the Fischer–Tropsch reactor according to [43,44]. As stated previously, Co-based Fischer–Tropsch catalysts are not active for the rWGS reaction, and hence $X_{rWGS,Reactor}$ was set to 0%.

2.4. Products and Product Separation

2.4.1. Fischer–Tropsch Products

As stated in Section 2.3, besides water only alkanes are considered as Fischer–Tropsch products. Table 3 shows the chosen division of product fractions based on the molecule's number of carbon atoms.

2.4.2. Product Separation without Tail Gas Reforming

The separation of products without tail gas reforming is realized by a series of separators being cooled with pressurized water, as can be seen in Figure 1. To minimize the required power to repressurize the tail gas to p_{FT} = 21 bar, the pressure level after the product separation step should be as high as possible while separating H_2O and condensable hydrocarbons. Light waxes and the middle distillate fraction can be drained as liquids within a first separation step, whereas H_2O, naphtha, methane, ethane and propane remain gaseous.

2.4.3. Product Separation with Tail Gas Reforming

Since the reforming of tail gas is favored at low-pressure levels, as explained in Section 2.6, the separation of products can be realized by serial flash distillation, as depicted in Figure 2. Light waxes, the middle distillate, the naphtha fraction and H_2O, are gradually separated by depressurizing the gas mixture to a pressure level of $p_{Reformer}$ = 1.2 bar, including an excess of 0.2 bar to overcome downstream heat exchanger units.

2.5. Tail Gas Recirculation

The recirculation of tail gas is a profound method with which to increase the overall conversion of CO for chemical plants based on syngas as a precursor, going hand in hand with an increase in the synthesized products and hence the plant's PtL efficiency. The recirculation ratio RR is defined as the mass flow rate of recirculated tail gas divided by the total mass flow rate of tail gas (Equation (9)). To avoid the accumulation of CO_2 and CH_4 in the recirculated tail gas, a share of the stream needs to be drained from the system as purge gas. For the process configuration including tail gas reforming, the purge gas is combusted to heat the recirculated tail gas to the reformer's operating temperature of 850 °C.

$$RR = \frac{m_{\text{Tail gas,Rec.}}}{m_{\text{Tail gas,Total}}}, \quad (9)$$

2.5.1. Process Configuration without Tail Gas Reforming

Since the separation of products is realized under synthesis pressure, only one additional compressor is required to compensate for the separator's pressure drops, and the recirculated tail gas can be inserted before the Fischer–Tropsch reactor, as shown in Figure 1.

2.5.2. Process Configuration with Tail Gas Reforming

As illustrated in Figure 2, the purge gas is combusted to heat the recirculated tail gas to the reformer's temperature of $T_{Reformer}$ = 850 °C. Before the reformer, a water injector can be installed to add an extra degree of freedom to manipulate the chemical reactions inside the tail gas reformer. An additional heat exchanger after the reformer is required to cool the gas stream before it is inserted prior to the syngas condenser, removing non-converted water of the co-electrolysis process and excess water leaving the reformer. It is recommended to utilize the transferred heat for preheating and evaporating the SOEC's water input. A maximum value of $RR_{max.}$ = 0.9 was defined to ensure the heating of recirculated tail gas to the reformer's temperature level. In addition, the limitation of RR to 0.9 secures the comparability of process configurations with and without a tail gas reformer.

2.6. Tail Gas Reforming

The tail gas reformer was modeled as a Gibbs reactor with the "Equilib" model of FactSage version 8.1, reforming the tail gas in accordance with the chemical equilibrium at a temperature of $T_{Reformer}$ = 850 °C and a pressure of $p_{Reformer}$ = 1.2 bar. A sufficient residence time inside the reactor was assumed to ensure the realization of chemical equilib-

rium. The following chemical reactions were assumed to have the highest impact on the reformer's performance.

$$CO_2 + H_2 \leftrightarrow CO + H_2O, \Delta H_r = +41.2\ kJ/mol \quad (10)$$

The rWGS reaction (Equation (10)) has its chemical equilibrium at a temperature of around 800–850 °C, as sufficient conversion rates exist at temperatures surpassing 800 °C and are not affected by a change in pressure. The addition of H_2 favors the conversion of CO_2, whereas H_2O inside the feed stream mitigates the CO_2 conversion [51].

$$CH_4 + H_2O \leftrightarrow CO + 3\ H_2, \Delta H_r = +206.2\ kJ/mol \quad (11)$$

$$CH_4 + CO_2 \leftrightarrow 2\ CO + 2\ H_2, \Delta H_r = +247.0\ kJ/mol \quad (12)$$

$$C_2H_6 + 2\ H_2O \leftrightarrow 2\ CO + 5\ H_2, \Delta H_r = +356.8\ kJ/mol \quad (13)$$

$$C_3H_8 + 3\ H_2O \leftrightarrow 3\ CO + 7\ H_2, \Delta H_r = +512.2\ kJ/mol \quad (14)$$

Equations (11)–(14) show the underlying chemical reactions of the steam reforming of methane, ethane and propane. To boost the conversion of short-chain hydrocarbons, the addition of H_2O into the tail gas stream was considered but was not realized in the process simulation, since the H_2O demand of Equations (11)–(14) can be fully covered by the formed H_2O due to the rWGS reaction (Equation (10)). After the principle of Le Chatelier, the reforming of short-chain hydrocarbons by steam is enhanced with a high temperatures, low pressure and high share of water inside the stream [19].

$$CO + 3\ H_2 \leftrightarrow CH_4 + H_2O, \Delta H_r = -206.2\ kJ/mol \quad (15)$$

$$CO_2 + 4\ H_2 \leftrightarrow CH_4 + 2\ H_2O, \Delta H_r = -165.0\ kJ/mol \quad (16)$$

The methanation via CO (15) and CO_2 (16) hydrogenation should be avoided, since CH_4 is a product of the Fischer–Tropsch synthesis, and hence reduces the Fischer–Tropsch reactor's productivity. After Le Chatelier, the formation of CH_4 can be reduced by a low pressure level inside the reformer and the addition of steam at the reactor's inlet [52].

In summary, to maximize the conversion of CO_2 and short-chain hydrocarbons, the tail gas reformer should be operated at a high temperature and low pressure. The addition of H_2 would favor the conversion of CO_2 according to the rWGS reaction (Equation (10)). However, this would conclude in high shares of short-chain hydrocarbons after the reformer (Equations (15) and (16)), and was hence not included. A high share of steam inside the tail gas stream lowers the conversion of CO_2 but is essential to reform hydrocarbons according to Equations (11), (13) and (14).

2.7. Power-to-Liquid Efficiency and Plant Efficiency

The Power-to-Liquid efficiency η_{PtL} is defined as the chemical energy stored in products divided by the system's total electric power input. Two different efficiency rates were defined to be able to directly compare process routes with and without tail gas reforming: Firstly, the PtL efficiency excluding methane, ethane and propane (17); and secondly, the plant efficiency including methane, ethane and propane (18).

$$\eta_{PtL} = \frac{\sum_j m_j \cdot LHV_j}{P_{el.,Total}},\ j = [\text{naphtha, middle distillate, wax}] \quad (17)$$

$$\eta_{Plant} = \frac{\sum_k m_k \cdot LHV_k}{P_{el.,Total}},\ k = [CH_4, C_2H_6, C_3H_8, \text{naphtha, middle distillate, wax}] \quad (18)$$

2.8. Utilization of Purge Gas

To avoid the accumulation of CO_2 and short-chain hydrocarbons, i.e., methane, ethane and propane, a share of the tail gas needs to be drained from the system as purge gas.

Either this gas stream can be used for downstream synthesis processes, or the stream's chemical energy can be utilized to evaporate H_2O or heat the recirculated tail gas when using a tail gas reformer.

3. Results

3.1. Recommended Design Parameters for a Pilot Scale Power-to-Liquid Plant

The recommended design parameters for the provided configurations of a Power-to-Liquid plant with and without a tail gas reformer, as illustrated in Figures 1 and 2, are presented within this section. The shown mass flow rates, volume flow rates, temperature levels, pressure levels and stream compositions are based on the parameters listed in Table 3 and a recirculation ratio of tail gas of RR = 90%. Figure 5 shows the obtained design parameters for the process configuration without a tail gas reformer.

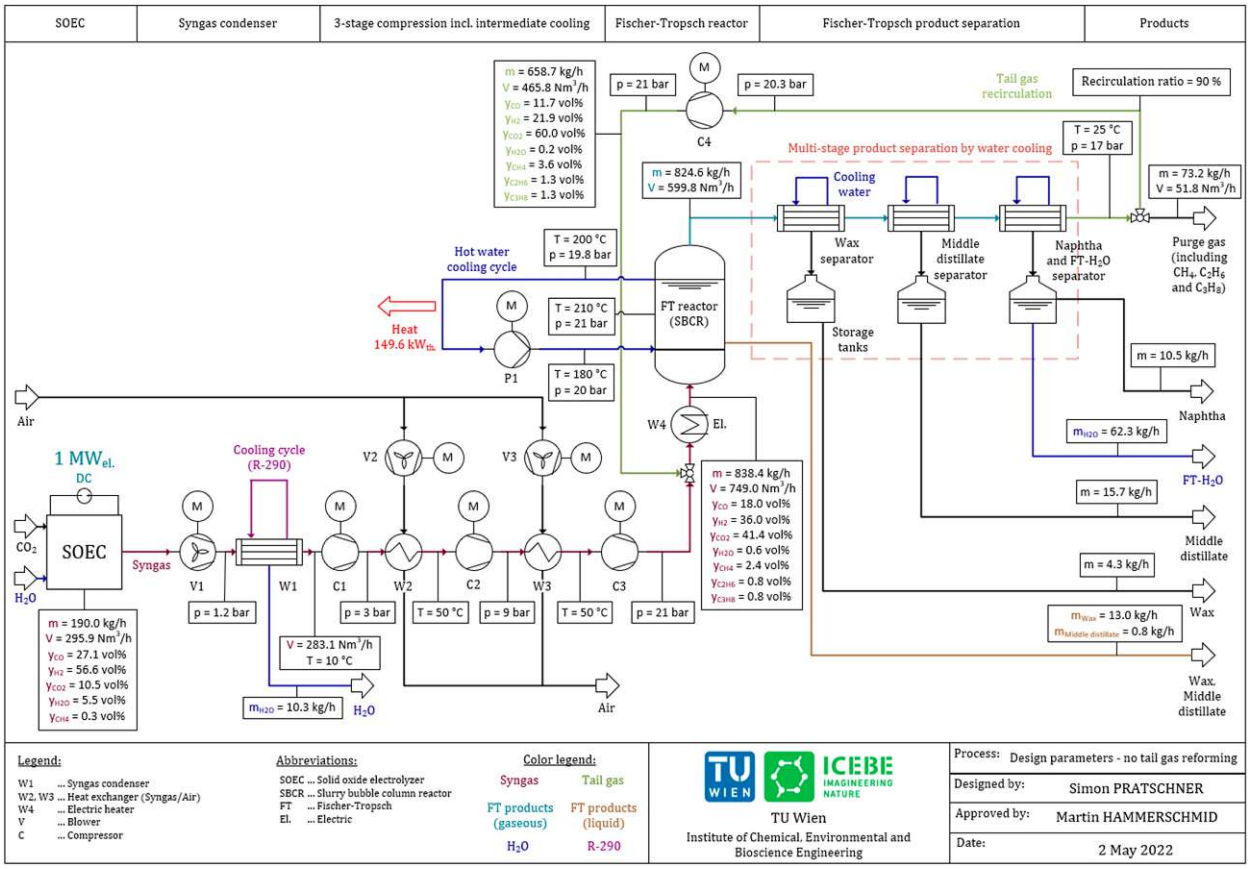

Figure 5. Design parameters of the plant configuration without tail gas reforming.

Figure 6 shows the recommended design parameters of a pilot scale Power-to-Liquid plant for the process configuration including a tail gas reformer based on the parameters listed in Table 3 and a recirculation ratio of RR = 90%.

The plant's parameters, e.g., Power-to-Liquid efficiency, Fischer–Tropsch products and CO conversion, are analyzed within the following sections.

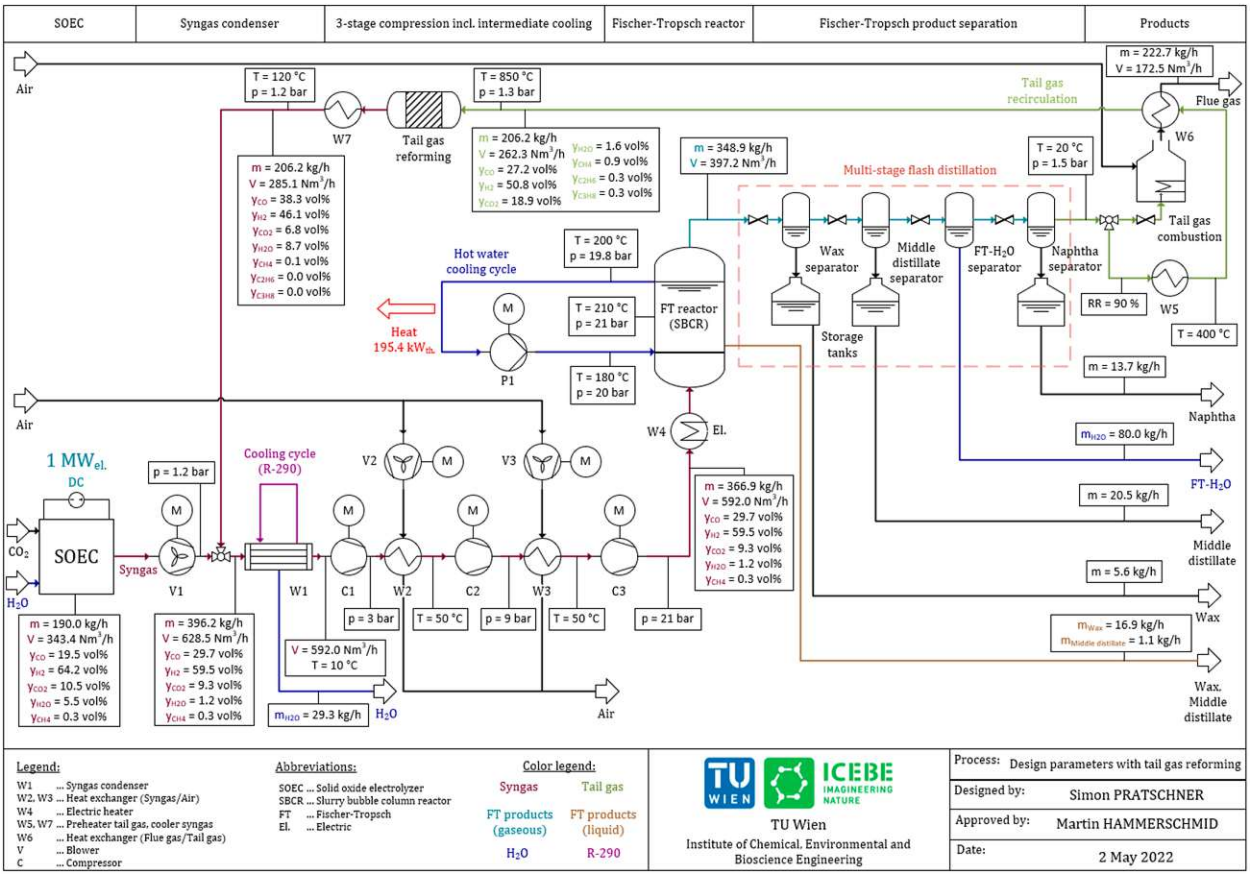

Figure 6. Design parameters of the plant configuration including tail gas reforming.

3.2. Fischer–Tropsch Synthesis—Products and Reaction Heat

The mass flow rates and distributions of the produced hydrocarbons, the produced Fischer–Tropsch water and the reaction heat are analyzed in this section. According to Table 3, the product fractions are divided into methane, ethane, propane, naphtha, middle distillate and wax. Table 4 summarizes the findings concerning the mass flow rates of Fischer–Tropsch products and the released reaction heat for process configurations with or without a tail gas reformer. The once-through configuration can be seen as a basic scenario with no recirculation of tail gas. As expected, high values of the recirculation ratio led to a significant rise in the obtained product streams. Without a tail gas reformer, a maximum mass flow rate of 47.8 kg/h could be realized. The integration of a tail gas reformer resulted in a maximum achievable product stream of 57.8 kg/h. However, this came at the price of combusting the purge gas, making it unavailable for potential downstream applications.

Table 4. Fischer–Tropsch products and reaction heat for various process configurations.

	Process Configuration (Recirculation Ratio of Tail Gas)		
Fischer–Tropsch Products [kg/h]	**Once-Through (RR = 0%)**	**No Reformer (RR = 90%)**	**With Reformer (RR = 90%)**
CH_4	1.1 [1]	1.3 [1]	- [2]
Ethane and propane	1.3 [1]	2.2 [1]	- [2]
Naphtha	6.3	10.5	13.7
Middle distillate	10.0	16.5	21.5
Wax	10.4	17.3	22.6
Σ Fischer–Tropsch products	29.1	47.8	57.8
Fischer–Tropsch H_2O	36.5	62.3	80.0
Reaction heat [$kW_{th.}$]	90.3	149.6	195.4

[1] Entrained inside the purge gas stream. [2] Purge gas is combusted to heat the tail gas before the reformer.

Figure 7 depicts the rise in hydrocarbons obtained with an increase in the recirculation ratio. In general, the mass flow rates of products rise exponentially with an increase in RR but show a significantly higher slope when including a tail gas reformer. As mentioned before, the purge gas needs to be combusted to heat the recirculated tail gas before the reformer. Hence, no methane, ethane or propane can be obtained when applying a tail gas reformer.

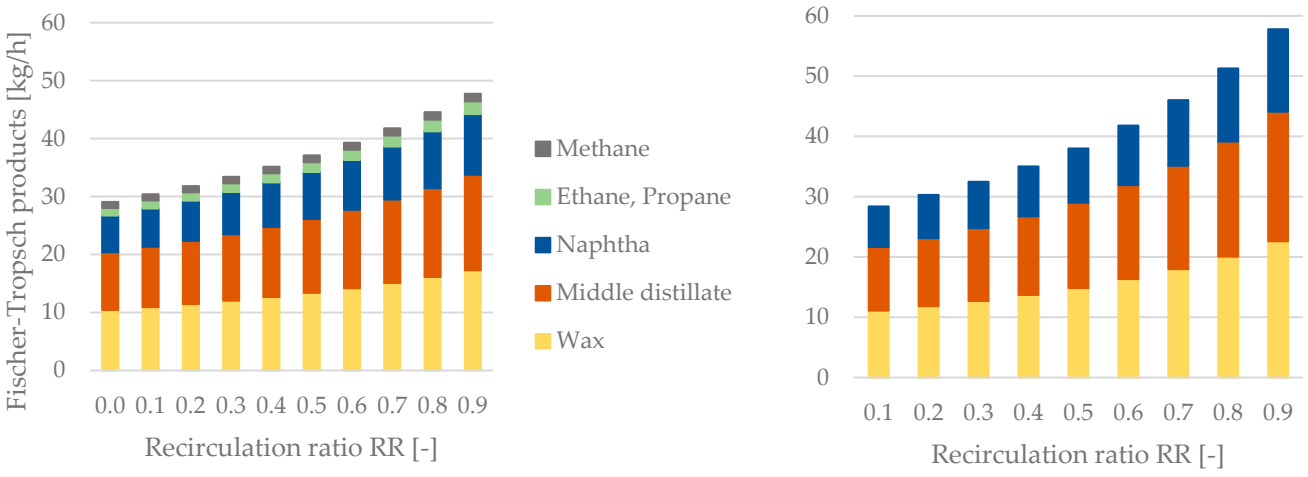

(**a**) without a tail gas reformer (**b**) with a tail gas reformer

Figure 7. Fischer-Tropsch products as a function of the recirculation ratio RR—(**a**) process configuration without a tail gas reformer, (**b**) process configuration with a tail gas reformer.

3.3. H_2:CO Ratio of the SOEC (Co-Electrolysis) Unit

As explained in Section 2.1, the SOEC unit controls the reactor's H_2:CO ratio at $H_2:CO_{FT} = 2$ by adjusting its H_2:CO ratio. For process routes excluding tail gas reforming, $H_2:CO_{SOEC}$ does only change from 2.00 (RR = 0.0) to 2.09 (RR = 0.9), whereas $H_2:CO_{SOEC}$ increases to a value of 3.30 (RR = 0.9) when implementing the reforming of tail gas. A graphical display for $H_2:CO_{SOEC}$ as a function of RR is plotted in Figure 8.

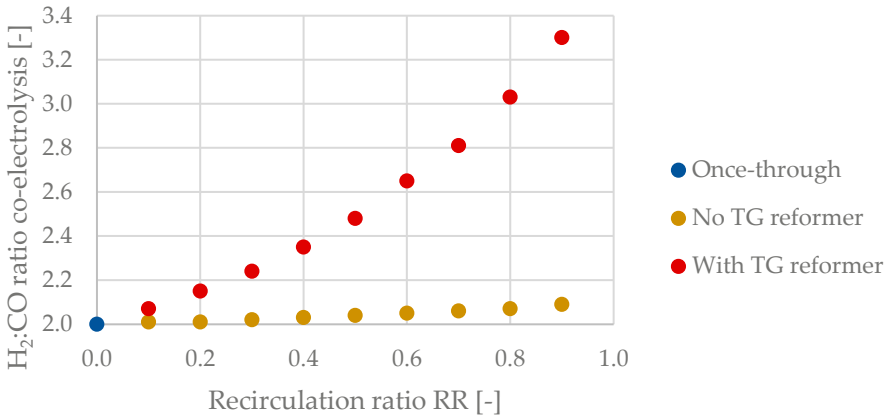

Figure 8. H_2:CO ratio of the SOEC (co-electrolysis) unit with and without a tail gas reformer.

3.4. Tail Gas

Analyzing the mass flow and volume flow rates, along with the composition of the recirculated tail gas stream, is critical to answering the posed questions and will be elaborated in detail in this section.

3.4.1. Mass Flow and Volume Flow Rates of recirculated Tail Gas

Figure 9 highlights the significant difference in the recirculated tail gas streams when comparing process configurations with and without tail gas reforming. The difference between the mass flow rates is negligible for RR < 0.5. However, the amounts of recirculated tail gas diverge rapidly as the recirculation ratio surpasses a value of 0.5. A maximum difference of 452.5 kg/h can be seen for a recirculation ratio of 0.9. This rapid growth for configuration B can be explained by the accumulation of CO_2 inside the tail gas stream, as elaborated in Section 3.4.2. The differences appear to be less critical when analyzing the volume flow rates of recirculated tail gas with diverging values for recirculation ratios of 0.7 and higher.

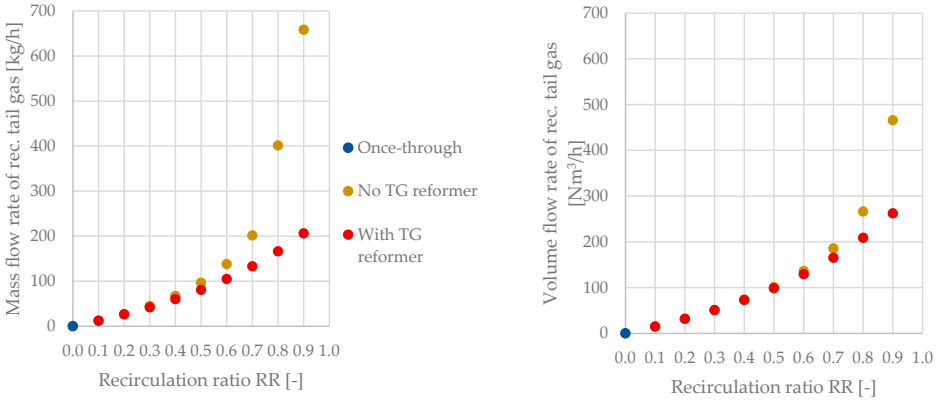

(**a**) (**b**)

Figure 9. Recirculated tail gas as a function of the recirculation ratio RR and the process configuration—(**a**) mass flow rate, (**b**) volume flow rate.

3.4.2. Composition of Tail Gas and Tail Gas Reforming

The tail gas leaving the product separation step consists of the following compounds:

- Non-reacted reactants, i.e., CO and H_2;
- Inert gases, i.e., CO_2;
- Non-condensed products, i.e., CH_4, ethane, propane and Fischer–Tropsch H_2O.

The tail gas compositions for the respective process configuration and recirculation ratio are stated in Table 5. Implementing a tail gas reformer reduces the shares of CO_2, CH_4, ethane and propane inside the tail gas stream significantly. A disadvantage is the increased percentage of water due to the reverse water–gas shift reaction.

Table 5. Tail gas composition for process configurations with and without a tail gas reformer.

			Process Configuration (Recirculation Ratio of Tail Gas)			
Parameter	**Symbol**	**Unit**	**Once-Through (RR = 0%)**	**No Reformer (RR = 90%)**	**Reformer IN (RR = 90%)**	**Reformer OUT (RR = 90%)**
CO	y_{CO}	vol%	26.0	11.7	27.2	38.4
H_2	y_{H2}	vol%	48.7	21.9	50.8	45.2
CO_2	y_{CO2}	vol%	21.7	60.1	18.9	7.2
H_2O	y_{H2O}	vol%	2.0	0.2	1.6	9.1
CH_4	y_{CH4}	vol%	1.0	3.6	0.9	0.1
Ethane	y_{C2H6}	vol%	0.3	1.3	0.3	0.0
Propane	y_{C3H8}	vol%	0.3	1.2	0.3	0.0

The tail gas composition of the process route without a reformer as a function of the recirculation ratio is plotted in Figure 10. A significant rise in the share of CO_2 can be seen after surpassing a recirculation ratio of 0.6. Non-condensable products, i.e., CH_4, ethane and propane, also accumulate in the tail gas stream but are less crucial than CO_2. The maximum share of y_{CO2} = 60.1 vol% inside the system can be seen at RR = 0.9.

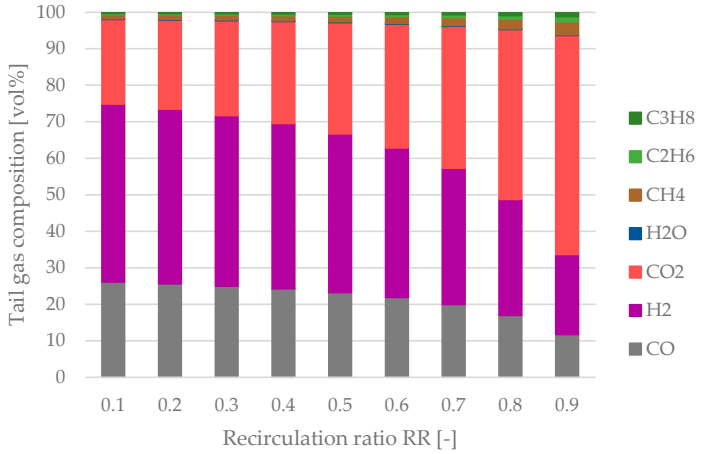

Figure 10. Tail gas composition as a function of the recirculation ratio RR for the process configuration without a tail gas reformer.

The tail gas composition at the reformer's inlet and outlet is plotted in Figure 11. A relative constant regime before and after the reactor can be noted. The share of CO at the reformer's inlet remains almost constant, whereas the share of H_2 increases slightly with a rise in the recirculation ratio. Small shares of gaseous hydrocarbons can be seen at the reactor's inlet, which are almost entirely converted to H_2 and CO inside the reformer. A significant increase concerning the share of H_2O after the reformer occurs. Hence, the insertion of additional steam before the tail gas reformer is not beneficial. A sufficient amount of H_2O is formed by the rWGS reaction inside the reformer (Equation (10)) to cover the H_2O demand for the reforming of gaseous hydrocarbons.

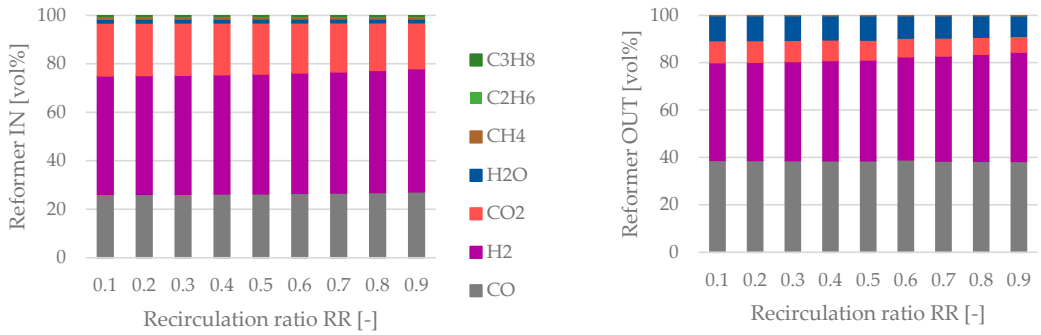

(**a**) (**b**)

Figure 11. Tail gas reforming—(**a**) tail gas composition at the reformer's inlet, (**b**) tail gas composition at the reformer's outlet as a function of the recirculation ratio.

3.5. Purge Gas

The combustion of purge gas is not necessary for process configurations without a tail gas reformer. Hence, the mass flow rate of purge gas and the stream's chemical energy are important factors for designing potential downstream processes.

Figure 12 shows the mass flow rate of purge gas being drained from the system (Figure 12a) and the purge gas stream's chemical energy (Figure 12b) as a function of the recirculation ratio RR. The mass flow rate of purge gas ranges from 116.6 to 73.2 kg/h. The stream's chemical energy decreases disproportionately from 365.3 to 102.1 kW due to the stream's increasing share of CO_2 for an increase in the amount of recirculated tail gas.

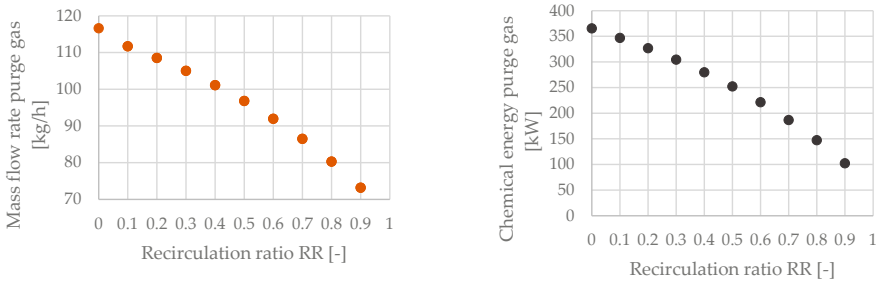

(**a**) [1] (**b**) [1]

Figure 12. Purge gas stream for the configuration without a tail gas reformer—(**a**) mass flow rate as a function of the recirculation ratio, (**b**) chemical energy as a function of the recirculation ratio. [1] No purge gas stream occurs for the process route that includes a tail gas reformer.

3.6. Power Demand of Auxiliary Equipment

The PtL plant's auxiliary power demand includes all devices except the SOEC unit, i.e., compressors, blowers, the syngas condenser and pumps. Since the SOEC's power input was set as constant, 1 $MW_{el.}$, the electricity demand of auxiliary devices defines the plant's PtL efficiency, in combination with the product's chemical energy. The following process steps require electricity:

- Syngas compression;
- Syngas condensing;
- Syngas intermediate cooling;
- Tail gas recirculation;
- Pumping for the reactor cooling cycle and the separation of products.

Figure 13 shows a comparison of the auxiliary equipment's power demand between plant configurations without (Figure 13a) and with (Figure 13b) a tail gas reformer. The syngas compression accounts for the highest share, whereas the power demand of pumps is negligible. If no tail gas reformer is integrated, the recirculation ratio has almost no effect on the power demand. An exponential increase can be seen when analyzing the process configuration including a tail gas reformer. Reasons for this behavior are the recirculation of tail gas to the condenser's inlet and the depressurization via a multi-stage flash distillation to increase the conversion of CO_2 and hydrocarbons inside the reformer.

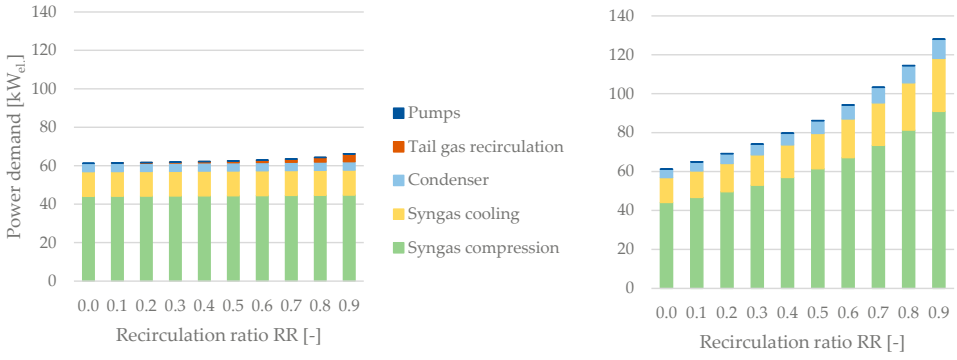

(**a**) (**b**)

Figure 13. Power demand of auxiliary equipment excluding the SOEC unit as a function of the recirculation ratio—(**a**) without a tail gas reformer, (**b**) with a tail gas reformer.

3.7. Power-to-Liquid Efficiency and Plant Efficiency

As described in Section 2.7, the PtL efficiency η_{PtL} is defined as the rate of the products' chemical energy generation, excluding CH_4 and LPG and the total electricity input into the system (Equation (17)). To enhance comparability between process configurations with

and without a tail gas reformer, an additional indicator, the plant efficiency η_{Plant}, has been introduced (Equation (18)).

Table 6 sums up the Power-to-Liquid efficiency and plant efficiency of the analyzed process configurations. A significant increase in η_{PtL} can be realized by raising the recirculation ratio RR with a maximum value of 62.7% when implementing a tail gas reformer.

Table 6. Power-to-Liquid efficiency and plant efficiency for the chosen process configurations.

			Process Configuration (Recirculation Ratio of Tail Gas)		
Parameter	**Symbol**	**Unit**	**Once-Through (RR = 0%)**	**No Reformer (RR = 90%)**	**With Reformer (RR = 90%)**
Power-to-Liquid efficiency [1]	η_{PtL}	%	30.8	50.8	62.7
Plant efficiency [2]	η_{Plant}	%	33.8	55.2	62.7
Total power demand	P_{Total}	$kW_{el.}$	1061.3	1066.3	1128.1

[1] Excluding CH_4, ethane and propane inside the purge gas stream. [2] Including CH_4, ethane and propane inside the purge gas stream.

The exponential development of η_{PtL} and η_{Plant} as a function of the recirculation ratio is plotted in Figure 14.

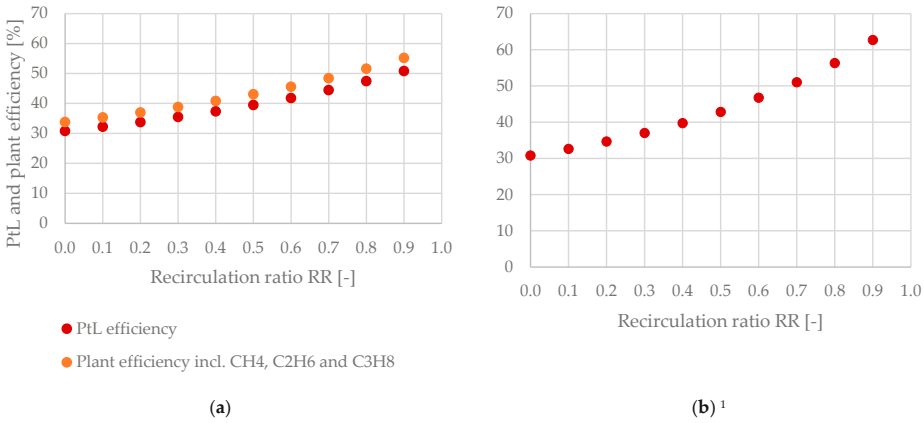

(**a**) (**b**) [1]

Figure 14. Power-to-Liquid efficiency and plant efficiency as a function of the recirculation ratio—(**a**) without tail gas reforming, (**b**) with tail gas reforming. [1] η_{PtL} and η_{Plant} are equal due to the combustion of the purge gas stream.

3.8. CO Conversion of the Power-to-Liquid Plant

The growth of $X_{CO,Plant}$ is exponential for the process configuration without a reformer and linear when implementing a tail gas reformer, as depicted in Figure 15. This behavior can be explained by the significant change of the tail gas composition without a reformer, whereas the composition of tail gas is almost constant at the reformer's outlet, as stated in Section 3.4.2. The maximum values obtained were 92.4% with no tail gas reformer and 96.5% when implementing a reformer.

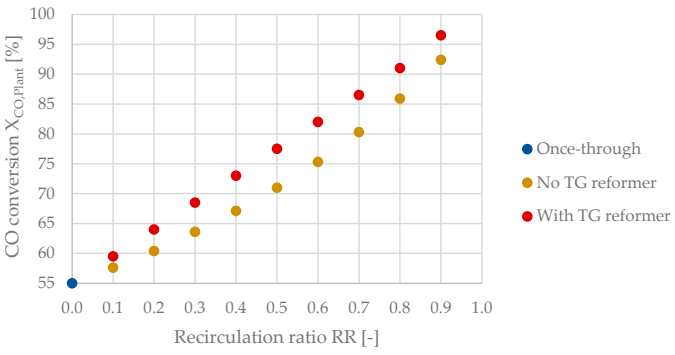

Figure 15. CO conversion at a system level as a function of the recirculation ratio.

4. Discussion

The underlying work highlights the importance of tail gas recirculation to achieve feasible Power-to-Liquid efficiencies. A maximum value of 62.7% could be realized by adding a tail gas reformer to the recirculation line compared to only 30.8% via a once-through configuration. A significant accumulation of CO_2 inside the system of up to 60.1vol% was observed without a tail gas reforming step, limiting the performance of process configurations without a tail gas reformer to a maximum Power-to-Liquid efficiency of 50.8%. A possible option to solve this problem is to increase the SOEC's CO_2 conversion. In addition, the application of a Fe-based Fischer–Tropsch catalyst might be a viable option due to its activity in the rWGS reaction.

Becker et al. determined a system efficiency of 51% for a plant including the subsequent processing of the Fischer–Tropsch syncrude to gasoline and diesel [37]. Cinti et al. included the recirculation of tail gas to the SOEC (operating in co-electrolysis mode) unit's inlet in combination with a Fischer–Tropsch reactor, and obtained a PtL efficiency of 57% [35]. Maximum PtL efficiencies of 54.2% (air mode) and 51.9% (oxyfuel mode) were obtained for a PtL plant valorizing biogenic CO_2 derived from the combustion of woodchips to methanol by [12]. PtL efficiencies of up to 63% are possible for systems including a high-temperature electrolyzer valorizing CO_2 originating from a highly concentrated source, e.g., a biogas upgrading plant, according to [46]. Hence, this work's maximum Power-to-Liquid efficiency of 62.7% seems reasonable, since the CO_2 capture unit's power demand was not considered.

Table 7 sums up the advantages and disadvantages of process configurations with and without a tail gas reformer. The plant's key performance indicators, i.e., the Power-to-Liquid efficiency and the mass flow rates of produced hydrocarbons, benefit significantly from implementing a tail gas reformer. However, to keep the system's complexity at a feasible level for the swift deployment of pilot scale PtL plants, a configuration without an additional tail gas reformer is a viable option.

Table 7. Performances and feasibility of pilot scale plants producing synthetic fuels and wax with and without implementing a tail gas reformer.

	Process Configuration	
Parameter	**Without Tail Gas Reformer**	**With Tail Gas Reformer**
PtL efficiency η_{PtL}	–	+
Fischer–Tropsch products	–	+
Technical expenditure	+	– [1]
Costs	+	– [1]
Deployment speed	+	–
Utilization of purge gas	+	– [2]

[1] Additional reactor and catalyst are required for tail gas reforming. [2] Purge gas is combusted to heat the tail gas before the reformer.

PtL plants at pilot scale can potentially be combined with decentralized wind turbines or solar power plants to avoid rising electricity prices, making renewable fuels and wax economically competitive to products derived from increasingly expensive fossil resources.

This work aimed to shift the focus towards the Fischer–Tropsch synthesis by applying the extended ASF distribution and internal tail gas recirculation to the Fischer–Tropsch reactor's inlet. Hence, we added value to previous studies, which mainly used the standard ASF distribution and rather idealized assumptions concerning the Fischer–Tropsch synthesis. In addition, two process configurations, i.e., with and without a tail gas reformer, were analyzed to provide a recommendation concerning the ideal plant configuration for the quick deployment of Power-to-Liquid plants at a pilot scale.

5. Conclusions

The presented work was conducted to answer the question of which Power-to-Liquid efficiencies can be realized by pilot scale plants combining a SOEC unit with Fischer–

Tropsch synthesis. In addition, a recommended plant configuration for the production of synthetic fuels and wax at a pilot scale was provided.

Table 8 sums up this work's central findings by comparing the key performance indicators obtained by the respective process configuration.

Table 8. Obtained key performance indicators of the Power-to-Liquid plant for the respective process configurations with and without a tail gas reformer.

			Process Configuration (Recirculation Ratio of Tail Gas)		
Parameter	**Symbol**	**Unit**	**Once-Through (RR = 0%)**	**No Reformer (RR = 90%)**	**With Reformer (RR = 90%)**
Power-to-Liquid efficiency	η_{PtL}	%	30.8	50.8	62.7
Fischer–Tropsch products [1]	m_{FT}	kg/h	26.7	44.3	57.8
CO conversion of the plant	$X_{CO,Plant}$	%	55.0	92.4	96.5
Required H_2:CO ratio (SOEC)	H_2:CO_{SOEC}	-	2.00	2.09	3.30
Total power demand [2]	$P_{el.}$	$kW_{el.}$	1061.3	1066.3	1128.1
Purge gas chemical energy	$U_{Purge\ gas}$	kW	365.3	102.1	- [3]

[1] Excluding CH_4, ethane and propane inside the purge gas stream. [2] Power demand of the SOEC is 1000 $kW_{el.}$. [3] Purge gas is combusted to heat the tail gas before the reformer.

A more sophisticated model concerning the SOEC should be developed and applied for future research to evaluate the presented results. Furthermore, the synergy between the SOEC unit and the Fischer–Tropsch reactor needs to be analyzed from an engineering perspective for various modes of operation. Designing the tail gas reforming process in detail has significant potential to improve the concept's feasibility at an industrial scale. Another possibility for improvement is the validation and extension of the presented Fischer–Tropsch model by conducting laboratory-scale experiments including several catalysts based on cobalt or iron. Process heat integration is a crucial way to secure the presented concept's feasibility but was not within this work's scope. Hence, future research should focus on implementing state-of-the-art heat integration methods, e.g., pinch analysis and multi-criteria analysis. In addition, a cost estimate of the respective process routes needs to be conducted to persuade possible investors to fund Power-to-Liquid plants producing synthetic fuel and wax. Conducting a techno-economic assessment is essential to transfer PtL plants to the next level, and thus should be prioritized in future research projects.

Author Contributions: Conceptualization, S.P., S.M. and F.W.; methodology, S.P. and M.H.; software, S.P. and M.H.; validation, S.P., M.H. and F.J.M.; investigation, S.P.; resources, M.H. and S.M.; data curation, S.P. and M.H.; writing—original draft preparation, S.P.; writing—review and editing, S.P., F.W.; visualization, S.P., M.H. and F.J.M.; supervision, S.M. and F.W.; project administration, S.M.; All authors have read and agreed to the published version of the manuscript.

Funding: The underlying work has received funding from the Mobility of the Future program—a research, technology and innovation funding program of the Federal Ministry of Climate Action, Environment, Energy, Mobility, Innovation and Technology, Republic of Austria. The Austrian Research Promotion Agency (FFG) has been authorized for the program management of the project "IFE—Innovation Flüssige Energie" (project #884340). In addition, the authors would like to thank TU Wien Bibliothek for covering the APC through its Open Access Funding Program.

Data Availability Statement: For further information regarding data presented in this article, please contact the corresponding author.

Acknowledgments: The authors would like to acknowledge the "IFE—Innovation Flüssige Energie" consortia, the doctoral college CO_2Refinery at TU Wien and the open access funding by TU Wien.

Conflicts of Interest: The authors declare no conflict of interest.

Abbreviations

ASF	Anderson–Schulz–Flory distribution
C	Compressor
CCU	Carbon capture and utilization
DAC	Direct air capture
DME	Dimethyl ether
eASF	Extended Anderson-Schulz-Flory distribution
FBMR	Fixed bed multitubular reactor
FT	Fischer–Tropsch
GHG	Greenhouse gas
HTFT	High-temperature Fischer–Tropsch synthesis
LTFT	Low-temperature Fischer–Tropsch synthesis
PEMEC	Proton exchange membrane electrolysis cell
rWGS	Reverse water-gas shift
SBCR	Slurry bubble column reactor
SOEC	Solid oxide electrolysis cell
Syngas	Synthesis gas provided by the SOEC unit
TG	Tail gas
PtX	Power-to-X
PtG	Power-to-Gas
PtL	Power-to-Liquid
V	Blower
W	Heat exchanger

Nomenclature

LHV	Lower heating value [MJ/kg]
m	Mass flow rate [kg/h]
P	Power [$kW_{el.}$]
p	Pressure [bar]
RR	Recirculation ratio [-,%]
T	Temperature [K,°C]
U	Chemical energy [kW]
X_{CO}	CO conversion [%]
x	Molar fraction [-]
y	Volume fraction [vol%]
α_1	Dominant chain growth probability for C_1 to C_7 (eASF) [-]
α_2	Dominant chain growth probability for C_{13+} (eASF) [-]
β	Readsorption factor—selectivity for C_2H_6 (eASF) [-]
γ	Termination factor—selectivity for CH_4 (eASF) [-]
η	Efficiency [%]
λ	Air ratio [-]
μ	Factor to merge α_1 and α_2 (eASF) [-]
$\Delta_r G$	Gibbs free energy of a chemical reaction [kJ/mol]
$\Delta_r H$	Reaction enthalpy [kJ/mol]
$\Delta_r S$	Reaction entropy [kJ/(mol·K)]
m.	Mechanical
el.	Electric
th.	Thermal
max.	Maximum
s	Isentropic
Compr.	Compressor/compression
Con.	Condenser
Rec.	Recirculation/recirculated

References

1. Trends in Atmospheric Carbon Dioxide—Annual Mean Global Carbon Dioxide Growth Rates. Available online: https://gml.noaa.gov/ccgg/trends/gl_gr.html (accessed on 7 January 2022).
2. Trends in Atmospheric Carbon Dioxide—Global Monthly Mean CO2. Available online: https://gml.noaa.gov/ccgg/trends/global.html (accessed on 7 January 2022).
3. BP p.l.c. Statistical Review of World Energy—70th Edition. 2021. Available online: https://www.bp.com/content/dam/bp/business-sites/en/global/corporate/pdfs/energy-economics/statistical-review/bp-stats-review-2021-full-report.pdf (accessed on 7 January 2022).
4. Buysse, C.; Miller, J. Transport Could Burn up the EU's Entire Carbon Budget. Available online: https://theicct.org/blog/staff/eu-carbon-budget-apr2021 (accessed on 7 January 2022).
5. Josh A European Green Deal. Striving to Be the First Climate-Neutral Continent. Available online: https://ec.europa.eu/info/strategy/priorities-2019-2024/european-green-deal_en (accessed on 7 January 2022).
6. Austrian Automobile, Motorcycle and Touring Club. Expertenbericht Mobilität und Klimaschutz 2030. Available online: https://www.oeamtc.at/club/oeamtc-expertenbericht-mobilitaet-klimaschutz-2030-25873728#:~{}:text=%22Alles%20in%20allem%20werden%20die,betont%20%C3%96AMTC%2DDirektor%20Oliver%20Schmerold (accessed on 17 March 2022).
7. E-FUEL—The Renewable Fuel. Available online: https://www.sunfire.de/en/e-fuel (accessed on 7 January 2022).
8. Wulf, C.; Zapp, P.; Schreiber, A. Review of Power-to-X Demonstration Projects in Europe. *Front. Energy Res.* **2020**, *8*, 191. [CrossRef]
9. Karka, P.; Johnsson, F.; Papadokonstantakis, S. Perspectives for Greening European Fossil-Fuel Infrastructures Through Use of Biomass: The Case of Liquid Biofuels Based on Lignocellulosic Resources. *Front. Energy Res.* **2021**, *9*, 636782. [CrossRef]
10. Mailaram, S.; Kumar, P.; Kunamalla, A.; Saklecha, P.; Maity, S.K. Biomass, Biorefinery, and Biofuels. In *Sustainable Fuel Technologies Handbook*; Elsevier: Amsterdam, The Netherlands, 2021; pp. 51–87. ISBN 978-0-12-822989-7.
11. Green Fuel from Residual Waste. Available online: https://smartcity.wien.gv.at/en/waste2value/ (accessed on 24 May 2022).
12. Pratschner, S.; Skopec, P.; Hrdlicka, J.; Winter, F. Power-to-Green Methanol via CO_2 Hydrogenation—A Concept Study Including Oxyfuel Fluidized Bed Combustion of Biomass. *Energies* **2021**, *14*, 4638. [CrossRef]
13. Siemens Energy. Haru Oni: A New Age of Discovery. Available online: https://www.siemens-energy.com/global/en/news/magazine/2021/haru-oni.html (accessed on 7 January 2022).
14. Marlin, D.S.; Sarron, E.; Sigurbjörnsson, Ó. Process Advantages of Direct CO_2 to Methanol Synthesis. *Front. Chem.* **2018**, 6. [CrossRef]
15. Bowker, M. Methanol Synthesis from CO_2 Hydrogenation. *ChemCatChem* **2019**, *11*, 4238–4246. [CrossRef] [PubMed]
16. Norsk E-Fuel. Supplying Your Renewable Fuel. Unlimited. On the Road to Climate Neutral Transportation. Available online: https://www.norsk-e-fuel.com/en/ (accessed on 7 January 2022).
17. Fisch, I. Sustainable E-Fuels for Aviation. Available online: https://ineratec.de/en/e-fuels-for-aviation/ (accessed on 7 January 2022).
18. Industrial Power-to-Liquid Pioneer Plant in Germany 2022. INERATEC. Available online: https://ineratec.de/en/power-to-liquid-pioneer-plant-2022/ (accessed on 17 March 2022).
19. de Klerk, A. *Fischer-Tropsch Refining*, 1st ed.; Wiley-VCH: Weinheim, Germany, 2011; ISBN 978-3-527-63560-3.
20. Martinelli, M.; Gnanamani, M.K.; LeViness, S.; Jacobs, G.; Shafer, W.D. An Overview of Fischer-Tropsch Synthesis: XtL Processes, Catalysts and Reactors. *Appl. Catal. A Gen.* **2020**, *608*, 117740. [CrossRef]
21. Badoga, S.; Gnanamani, M.K.; Martinelli, M.; Sparks, D.E.; Ma, W. Effect of Start-up Solvent on the Performance of Co Catalyst for Fischer-Tropsch Synthesis in Stirred-Tank Reactor. *Fuel* **2020**, *272*, 117707. [CrossRef]
22. Visconti, C.G.; Lietti, L.; Tronconi, E.; Rossini, S. Kinetics of Low-Temperature Fischer-Tropsch Synthesis on Cobalt Catalysts: Are Both Slurry Autoclave and Tubular Packed-Bed Reactors Adequate to Collect Relevant Data at Lab-Scale? *Can. J. Chem. Eng.* **2016**, *94*, 685–695. [CrossRef]
23. Todic, B.; Nowicki, L.; Nikacevic, N.; Bukur, D.B. Fischer–Tropsch Synthesis Product Selectivity over an Industrial Iron-Based Catalyst: Effect of Process Conditions. *Catal. Today* **2016**, *261*, 28–39. [CrossRef]
24. Peña, D.; Griboval-Constant, A.; Lecocq, V.; Diehl, F.; Khodakov, A.Y. Influence of Operating Conditions in a Continuously Stirred Tank Reactor on the Formation of Carbon Species on Alumina Supported Cobalt Fischer–Tropsch Catalysts. *Catal. Today* **2013**, *215*, 43–51. [CrossRef]
25. Chambrey, S.; Fongarland, P.; Karaca, H.; Piché, S.; Griboval-Constant, A.; Schweich, D.; Luck, F.; Savin, S.; Khodakov, A.Y. Fischer–Tropsch Synthesis in Milli-Fixed Bed Reactor: Comparison with Centimetric Fixed Bed and Slurry Stirred Tank Reactors. *Catal. Today* **2011**, *171*, 201–206. [CrossRef]
26. de Klerk, A. Can Fischer−Tropsch Syncrude Be Refined to On-Specification Diesel Fuel? *Energy Fuels* **2009**, *23*, 4593–4604. [CrossRef]
27. Gruber, H.; Groß, P.; Rauch, R.; Reichhold, A.; Zweiler, R.; Aichernig, C.; Müller, S.; Ataimisch, N.; Hofbauer, H. Fischer-Tropsch Products from Biomass-Derived Syngas and Renewable Hydrogen. *Biomass Conv. Bioref.* **2021**, *11*, 2281–2292. [CrossRef]
28. Bekker, M.; Louw, N.R.; Jansen Van Rensburg, V.J.; Potgieter, J. The Benefits of Fischer-Tropsch Waxes in Synthetic Petroleum Jelly. *Int. J. Cosmet. Sci.* **2013**, *35*, 99–104. [CrossRef]
29. Guettel, R.; Kunz, U.; Turek, T. Reactors for Fischer-Tropsch Synthesis. *Chem. Eng. Technol.* **2008**, *31*, 746–754. [CrossRef]

30. Maitlis, P.M.; de Klerk, A. (Eds.) *Greener Fischer-Tropsch Processes for Fuels and Feedstocks*; Wiley-VCH: Weinheim, Germany, 2013; ISBN 978-3-527-32945-8.
31. Makhura, E.; Rakereng, J.; Rapoo, O.; Danha, G. Effect of the Operation Parameters on the Fischer Tropsch Synthesis Process Using Different Reactors. *Procedia Manuf.* **2019**, *35*, 349–355. [CrossRef]
32. Pfeifer, P.; Schmidt, S.; Betzner, F.; Kollmann, M.; Loewert, M.; Böltken, T.; Piermartini, P. Scale-up of Microstructured Fischer–Tropsch Reactors—Status and Perspectives. *Curr. Opin. Chem. Eng.* **2022**, *36*, 100776. [CrossRef]
33. Yang, J.; Boullosa, E.; Myrstad, R.; Venik, H.; Pfeifer, P.; Holmen, A. Fischer-Tropsch Synthesis on Co-Based Catalysts in a Microchannel Reactor—Effect of Temperature and Pressure on Selectivity and Stability. In *Fischer-Tropsch Synthesis, Catalysts and Catalysis*; CRC Press: Boca Raton, FL, USA, 2016; Chapter 12; pp. 223–251. ISBN 978-1-4665-5529-7.
34. Marchese, M.; Giglio, E.; Santarelli, M.; Lanzini, A. Energy Performance of Power-to-Liquid Applications Integrating Biogas Upgrading, Reverse Water Gas Shift, Solid Oxide Electrolysis and Fischer-Tropsch Technologies. *Energy Convers. Manag. X* **2020**, *6*, 100041. [CrossRef]
35. Cinti, G.; Baldinelli, A.; Di Michele, A.; Desideri, U. Integration of Solid Oxide Electrolyzer and Fischer-Tropsch: A Sustainable Pathway for Synthetic Fuel. *Appl. Energy* **2016**, *162*, 308–320. [CrossRef]
36. König, D.H.; Freiberg, M.; Dietrich, R.-U.; Wörner, A. Techno-Economic Study of the Storage of Fluctuating Renewable Energy in Liquid Hydrocarbons. *Fuel* **2015**, *159*, 289–297. [CrossRef]
37. Becker, W.L.; Braun, R.J.; Penev, M.; Melaina, M. Production of Fischer–Tropsch Liquid Fuels from High Temperature Solid Oxide Co-Electrolysis Units. *Energy* **2012**, *47*, 99–115. [CrossRef]
38. Herz, G.; Reichelt, E.; Jahn, M. Techno-Economic Analysis of a Co-Electrolysis-Based Synthesis Process for the Production of Hydrocarbons. *Appl. Energy* **2018**, *215*, 309–320. [CrossRef]
39. Gao, R.; Zhang, C.; Jun, K.-W.; Kim, S.K.; Park, H.-G.; Zhao, T.; Wang, L.; Wan, H.; Guan, G. Green Liquid Fuel and Synthetic Natural Gas Production via CO_2 Hydrogenation Combined with Reverse Water-Gas-Shift and Co-based Fischer-Tropsch Synthesis. *J. CO2 Util.* **2021**, *51*, 101619. [CrossRef]
40. Müller, S.; Groß, P.; Rauch, R.; Zweiler, R.; Aichernig, C.; Fuchs, M.; Hofbauer, H. Production of Diesel from Biomass and Wind Power—Energy Storage by the Use of the Fischer-Tropsch Process. *Biomass Conv. Bioref.* **2018**, *8*, 275–282. [CrossRef]
41. HELMETH—High Temperature Electrolysis Cell (SOEC). Available online: http://www.helmeth.eu/index.php/technologies/high-temperature-electrolysis-cell-soec (accessed on 22 February 2022).
42. Avallone, E.A.; Baumeister, T.; Sadegh, A.M. *Marks' Standard Handbook for Mechanical Engineers*; McGraw-Hill: New York, NY, USA, 2007; Chapter 14; ISBN 978-1-60119-653-8.
43. Guilera, J.; Díaz-López, J.A.; Berenguer, A.; Biset-Peiró, M.; Andreu, T. Fischer-Tropsch Synthesis: Towards a Highly-Selective Catalyst by Lanthanide Promotion under Relevant CO_2 Syngas Mixtures. *Appl. Catal. A Gen.* **2022**, *629*, 118423. [CrossRef]
44. Sauciuc, A.; Abosteif, Z.; Weber, G.; Potetz, A.; Rauch, R.; Hofbauer, H.; Schaub, G.; Dumitrescu, L. Influence of Operating Conditions on the Performance of Biomass-Based Fischer–Tropsch Synthesis. *Biomass Conv. Bioref.* **2012**, *2*, 253–263. [CrossRef]
45. Coutanceau, C.; Baranton, S.; Audichon, T. Hydrogen Production from Water Electrolysis. In *Hydrogen Electrochemical Production*; Elsevier: Amsterdam, The Netherlands, 2018; pp. 17–62. ISBN 978-0-12-811250-2.
46. Schmidt, P.; Weindorf, W. *Power-to-Liquids: Potential and Perspectives for the Future Supply of Renewable Aviation Fuel 2016*; German Environment Agency: Dessau-Roßlau, Germany, 2016; ISSN 2363-829X. Available online: https://www.umweltbundesamt.de/sites/default/files/medien/377/publikationen/161005_uba_hintergrund_ptl_barrierrefrei.pdf (accessed on 17 March 2022).
47. Hauch, A.; Brodersen, K.; Chen, M.; Mogensen, M.B. Ni/YSZ Electrodes Structures Optimized for Increased Electrolysis Performance and Durability. *Solid State Ion.* **2016**, *293*, 27–36. [CrossRef]
48. Sattler, K. *Thermische Trennverfahren: Grundlagen, Auslegung, Apparate*; Wiley-VCH: Weinheim, Germany, 2007; Chapter 2; pp. 116–117. ISBN 978-3-527-30243-7.
49. Zhai, P.; Sun, G.; Zhu, Q.; Ma, D. Fischer-Tropsch Synthesis Nanostructured Catalysts: Understanding Structural Characteristics and Catalytic Reaction. *Nanotechnol. Rev.* **2013**, *2*, 547–576. [CrossRef]
50. Förtsch, D.; Pabst, K.; Groß-Hardt, E. The Product Distribution in Fischer–Tropsch Synthesis: An Extension of the ASF Model to Describe Common Deviations. *Chem. Eng. Sci.* **2015**, *138*, 333–346. [CrossRef]
51. Sengupta, S.; Jha, A.; Shende, P.; Maskara, R.; Das, A.K. Catalytic Performance of Co and Ni Doped Fe-Based Catalysts for the Hydrogenation of CO_2 to CO via Reverse Water-Gas Shift Reaction. *J. Environ. Chem. Eng.* **2019**, *7*, 102911. [CrossRef]
52. de Miranda, P.E.V. (Ed.) *Science and Engineering of Hydrogen-Based Energy Technologies: Hydrogen Production and Practical Applications in Energy Generation*; Academic Press Is an Imprint of Elsevier: London, UK; San Diego, CA, USA, 2019; ISBN 978-0-12-814251-6.

Journal Article III

Journal of CO2 Utilization 72 (2023) 102508

Contents lists available at ScienceDirect

Journal of CO2 Utilization

journal homepage: www.elsevier.com/locate/jcou

Evaluation of CO_2 sources for Power-to-Liquid plants producing Fischer-Tropsch products

Simon Pratschner [*,1], Martin Hammerschmid [2], Stefan Müller [3], Franz Winter [4]

Technische Universität Wien, Faculty of Technical Chemistry, Institute of Chemical, Environmental and Bioscience Engineering, Getreidemarkt 9/166, 1060 Vienna, Austria

ARTICLE INFO

Keywords:
Power-to-Liquid
Carbon capture and utilization
Solid-oxide electrolysis
Fischer-Tropsch synthesis
Process simulation
CO_2 sources

ABSTRACT

In addition to the climate crisis's looming dangers, Europe was recently affected by profoundly volatile energy markets, entailing soaring inflation and political uncertainty. Power-to-Liquid processes have the potential to curb global warming by valorizing CO_2 to produce synthetic fuels and platform chemicals while simultaneously substituting fossil energy imports. The impact of the CO_2 source, i.e., cement production, biogas upgrading and solid biomass combustion, on Power-to-Liquid plants was evaluated by implementing the designed configuration, including CO_2 capture, solid-oxide electrolyzer, Fischer-Tropsch synthesis and steam reforming, in IPSEpro, a stationary equation-based process simulation tool. Maximum Power-to-Liquid efficiency of 63.8% and maximum carbon efficiency of 88.6% were obtained by exploiting CO_2 emitted by a biogas upgrading unit. Solid-oxide electrolyzers ranging from 23 $MW_{el.}$ (biogas) to 504 $MW_{el.}$ (cement) are required to process CO_2 streams from 4.5 to 100 t/h. In addition, the mass and energy balances of the three considered configurations were determined and embedded in a process flow diagram. The presented study aims to facilitate future decisions concerning carbon capture and utilization policy by assessing the CO_2 source's influence on Power-to-Liquid plants' key performance indicators. Furthermore, the underlying work supports a sustainable realization of Power-to-Liquid plants by offering a framework for exploiting CO_2 sources.

1. Introduction

The climate crisis poses a major threat to global peace and prosperity in the upcoming decades. A global mean level of 414.6 ppm CO_2 was reported by the National Oceanic and Atmospheric Administration in September 2022, an increase of 2.6 ppm compared to September 2021 [49]. Responsible for this worrying increase are global CO_2 emissions of around 36 Gt per year, of which 2.4 Gt are directly emitted by the European Union's 27 member states [31]. The transport sector can be seen as the EU27's weak spot, which in contrast to all other sectors, still rises annually [8]. The respective CO_2 emissions can be allocated to road transportation (20.5%), marine navigation (4.0%) and aviation (3.8%) [18]. To combat this unsatisfactory development, the European Parliament has recently backed the European Commission's proposal of banning CO_2 emissions caused by private transport as of 2035. However, the opaque wording still leaves scope for interpretation and thus, sustainable synthetic fuels are still in the race to compete with individual electric mobility. In addition, hard-to-abate sectors, i.e., aviation, marine navigation and heavy-duty applications, still rely on high energy density fuels. Due to the vehicles' high mass, substituting conventional fuels with electricity or H_2 remains disadvantageous. Millinger et al. provide a comprehensive overview of the EU's transport sector and its projected development until 2050 [47]. The total transport fuel demand

Abbreviations: ASF, Anderson-Schulz-Flory distribution; BECCU, bioenergy with carbon capture and utilization; CCU, carbon capture and utilization; CHP, combined heat and power; DC, direct current; eASF, extended Anderson-Schulz-Flory distribution; El, electric; EU, European Union; FT, Fischer-Tropsch; KPI, key performance indicator; M, electric motor; MEA, monoethanolamine; No., stream number; P, pump; PtL, Power-to-Liquid; PtX, Power-to-X; Ref., Reformer; rWGS, reverse water-gas shift; SBCR, slurry bubble column reactor; SOEC, solid-oxide electrolysis cell; SOEL, solid-oxide electrolyzer; Sol., solution; SR, steam reformer; TG, tail gas; V, blower, compressor; W, heat exchanger.

* Corresponding author.
E-mail address: simon.pratschner@tuwien.ac.at (S. Pratschner).
[1] 0000-0001-6167-586X
[2] 0000-0002-1155-926X
[3] 0000-0001-8878-429X
[4] 0000-0001-9854-3836

https://doi.org/10.1016/j.jcou.2023.102508
Received 3 March 2023; Received in revised form 23 May 2023; Accepted 23 May 2023

Nomenclature

Parameters

$E_{Chem.}$	chemical energy MW_{ch}
H_2:CO	H_2 to CO ratio
m	mass flow rate kg/s, t/h
M	molar mass kg/kmol
n	molar flow rate kmol/h
P	power MW_{el}
p	pressure Pa, bar
RR	recirculation ratio %
RU	reactant utilization -, %
T	temperature °C, K
w	mass fraction wt%
X	conversion -, %
y	volume fraction vol%
ΔG_r	free Gibbs energy kJ/mol
ΔH_r	reaction enthalpy kJ/mol
ΔS_r	reaction entropy kJ/(mol•K)
η_{Carbon}	carbon efficiency %
η_{PtL}	Power-to-Liquid efficiency %
ρ	density kg/m^3

Table 1
Ongoing and planned Power-to-Liquid projects in Europe.

Company/ Project	Site	Year	Technology	Output	Source
Ineratec	Hamburg, GER	2022	FT	350 t/a	[35]
Ineratec	Frankfurt, GER	2024	FT	2500 t/a	[24]
ICO2CHEM	Frankfurt, GER	Ongoing	FT	-	[30]
Norsk e-fuel	Mosjøen, NOR	2024	FT	12.5 ML/a	[51]
Norsk e-fuel	Mosjøen, NOR	2026	FT	25 ML/a	[51]
Norsk e-fuel	Mosjøen, NOR	2029	FT	100 ML/a	[51]
Nordic Electrofuel	Porsgrunn, NOR	2025	FT	10 ML/a	[50]
Nordic Electrofuel	Porsgrunn, NOR	-	FT	200 ML/a	[50]
C2PAT	Mannersdorf, AUT	Ongoing	FT	2500 t/a[1])	[44]
Carbon2Chem	Duisburg, GER	Ongoing	Methanol, NH_3	-	[70]
Lipor	Porto, POR	tba	-	-	[40]

1) Calculation based on a stated CO_2 input of 10,000 t/a.

was 4851 TWh in 2018 and is anticipated to rise constantly within the following decades. The increase of aviation passenger kilometers is predicted to increase by 50% until 2040 and 100% until 2060. The demand for maritime fuel will increase by 50% until 2050.

Power-to-Gas (PtG) applications, i.e., H_2 and methane, have dominated Power-to-X (PtX) projects in Europe in the past years with a share of around 90% [75]. However, the pressing demand for sustainable solutions for the maritime and aviation industry has sparked an increased interest in Power-to-Liquid (PtL) plants, producing either methanol or fuels derived from Fischer-Tropsch (FT) products. An excerpt of ongoing PtL projects is given by Pratschner et al. [57]. Recently announced PtL projects are listed in Table 1. In addition, Ineratec has declared an upcoming cooperation with Japanese and Asian-pacific partners to establish industrial PtL plants in East and South East Asia [34].

The utilized CO_2 source is a critical factor when assessing the sustainability of PtL processes. The following properties need to be considered to maximize the PtL plant's potential to curb the climate crisis:

- Origin of CO_2, i.e., biogenic, inorganic or fossil CO_2.
- The concentration of CO_2, e.g., point sources vs. direct air capture.
- Amount of CO_2, i.e., the mass flow rate of point sources.

The concentration of CO_2 sources can vary from 400 ppm (direct air capture) to up to 98 vol% (biogas upgrading plant). Thermodynamically, the required energy, i.e., heat and electricity, to capture and separate CO_2 from air, industrial streams or power plants mainly depends on the CO_2 source's concentration. CO_2 capture technologies must be designed specifically to the gas stream's conditions, e.g., concentration, temperature and pressure. Vaz et al. provide an extensive overview of state-of-the-art CO_2 capture technologies [71]. Combined heat and power (CHP) plants emit an off-gas with a share of about 10–15 vol% CO_2. Likewise, the mass flow rates of typical CO_2 sources underlie vast differences ranging from around 120 t per day for a decentralized biomass heating plant and 103,000 t per day for Europe's largest coal plant in Belchatów, Poland [48].

Capturing CO_2 entails a high demand for thermal energy. Identifying and exploiting industrial waste heat streams thus have the potential to facilitate Power-to-Liquid plants. Bianchi et al. estimate the feasible potential of waste heat in the EU at 279 TWh/a. High-temperature waste heat streams surpassing temperatures of 300 °C hold a share of 55% of the stated potential [4]. Energy-intensive processes, e.g., steam generation and CO_2 desorption, could be supplied by enforcing sector coupling. An extensive review of conventional waste heat recovery technologies is provided by Jouhara et al. [36].

A cement plant, a biogas upgrading plant and a biomass CHP plant were elected as CO_2 sources within the presented study. Cement and clinker production has been studied in detail in numerous studies [29,5,74,10]. The cement industry is a major emitter of CO_2, responsible for 7% [33] of the global and 3% of the EU's CO_2 emissions [14]. Biogas upgrading plants provide a highly concentrated biogenic CO_2 stream and, thus, are predestined to serve as CO_2 sources for PtL applications. Operators of biogas upgrading plants must comply with local feed-in standards. Therefore, separating CO_2 from the main product CH_4 is a legal requirement. Downstream PtL plants are a viable solution to upgrade the by-product CO_2 to higher-grade products. As calculated by Millinger et al. [47], the biogas potential in Europe lies between 3.2% and 9.0% of the EU27's primary energy demand [17]. State-of-the-art biogas plants are a promising solution to increase the share of sustainable fuels and thus have received increased interest in recent studies [15,19,55,65,9]. Using solid biomass as an energy source underlies a controversial discussion in the EU27. According to the projections by Millinger et al., 2.5–14.9% of the EU27's primary energy demand can be covered by the combustion of solid biomass within the upcoming decades [16,47].

This study's main objective is to determine the CO_2 source's influence on the performance of PtL plants. In addition, a recommendation on which CO_2 sources should be prioritized to maximize PtL plants' potential to curb the environmental crisis will be given. The following research questions are posed to achieve the stated goals:

1. Which CO_2 sources should be prioritized for carbon capture and utilization applications based on Power-to-Liquid processes combining solid-oxide electrolysis and Fischer-Tropsch synthesis?
2. Which effect does the CO_2 source have on the key performance indicators of Power-to-Liquid plants?

Table 2
Chosen CO_2 sources for the presented case studies of Power-to-Liquid plants.

Sources for CO_2 feed streams			[7,6]	[15]	[56]
Parameter	Symbol	Unit	Cement plant[1)]	Biogas upgrading[2)]	CHP[3)]
Mass flow of CO_2	$\dot{m}_{CO_2}$	kg/h	100,000	4600	7700
Volume share CO_2	y_{CO_2}	vol %	19.0	98.0	14.3
Volume share N_2	y_{N_2}	vol %	61.0	-	82.3
Volume share H_2O	y_{H_2O}	vol %	10.0	0.3	0.4
Volume share CH_4	y_{CH_4}	vol %	-	1.7	-
Volume share O_2	y_{O_2}	vol %	10.0	-	3.0

1) Annual cement production of 1.2 million tons
2) Annual production of 30.5 million Nm^3 CH_4 (corresponds to 38 MW)
3) Thermal power input of 20 $MW_{th.}$. The flue gas is cooled to a temperature of 15 °C.

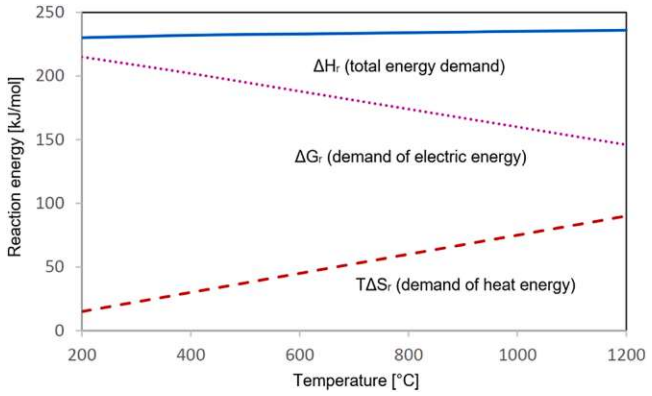

Fig. 1. Allocation of high-temperature electrolyzers' energy demand as a function of the temperature.
Reprinted with permission from [2] . Copyright 2020 Elsevier.

2. Methodology

The underlying study is founded on the obtained mass and energy balances of a Power-to-Liquid plant by applying IPSEpro 8.0, a stationary equation-based process simulation tool. The presented plant configuration is based on previous modeling work concerning the Fischer-Tropsch synthesis [57]. In addition, the following subprocesses were modeled and added to the existing process simulation flowchart:

- CO_2 capture by a monoethanolamine (MEA) absorption process.
- Solid-oxide electrolyzer (SOEL) operating in co-electrolysis mode.
- Steam reformer for tail gas reforming.

The subprocess modeling is elaborated on in further detail. Furthermore, the PtL plant's chosen key performance indicators (KPI) are defined to facilitate the comparison between the three analyzed CO_2 sources, i.e., a cement plant, a biogas upgrading plant and a CHP plant burning wood chips.

2.1. CO_2 sources

Three different CO_2 sources were taken as a foundation for the simulated PtL plant:

1. Norcem Brevik cement plant in Porsgrunn, Norway [7].
2. Biogas upgrading plant in Montello, Italy [15].
3. Decentralized CHP plant burning wood chips [56].

Table 2 displays the CO_2 sources' features.

2.2. Key performance indicators

The following KPIs were defined to facilitate the comparability between the presented scenarios.

2.2.1. Carbon efficiency η_{Carbon}

The carbon efficiency is defined as the ratio of carbon atoms being transformed into Fischer-Tropsch products, i.e., naphtha, middle distillate and wax, and calculated according to Eq. 1. Carbon atoms are inserted into the PtL plant as CO_2 or CH_4 molecules within the feed gas stream and emitted as CO_2 after the purge gas combustion.

$$\eta_{Carbon} = \frac{\dot{n}_{Carbon,in} - \dot{n}_{Carbon,out}}{\dot{n}_{Carbon,in}} \quad (1)$$

2.2.2. Power-to-Liquid efficiency η_{PtL}

The Power-to-Liquid efficiency η_{PtL} is defined as the ratio of chemically stored energy in the Fischer-Tropsch products and the PtL plant's total electricity demand, i.e., to power the SOEL unit, the syngas compressor, pumps and other auxiliary equipment.

$$\eta_{PtL} = \frac{E_{Chem.,FT\ products}}{P_{in,\ Total}} \quad (2)$$

2.2.3. Conversion of carbon monoxide X_{CO} and recirculation ratio of tail gas RR

The conversion of carbon monoxide is distinguished between the Fischer-Tropsch reactor's per pass CO conversion $X_{CO,FT}$ and the CO conversion at system level $X_{CO,System}$, see Eq. 3. Besides the per pass conversion, the recirculation ratio of tail gas RR, see Eq. 4, is a decisive factor influencing the system's total CO conversion.

$$X_{CO} = \frac{\dot{n}_{CO,in} - \dot{n}_{CO,out}}{\dot{n}_{CO,in}} \quad (3)$$

$$RR = \frac{\dot{m}_{Recirculated\ tail\ gas}}{\dot{m}_{Total\ tail\ gas}} \bullet 100\% \quad (4)$$

2.2.4. Scale of the solid-oxide electrolyzer P_{SOEL}

The electrolyzer's scale in $MW_{el.}$ is a benchmark parameter for the respective Power-to-Liquid plant size. In addition, P_{SOEL} can be used to ensure comparability to other conventional, e.g., fossil refineries, and innovative processes, e.g., Biomass-to-Liquid.

2.3. Fischer-Tropsch synthesis

A detailed elaboration of the Fischer-Tropsch process modeling has been conducted in a previous study [57]. The underlying model is based on assumptions concerning a low-temperature Fischer-Tropsch process, operating at a temperature of $T_{FT} = 230$ °C and a pressure of $p_{FT} = 21$ bar, realized in a slurry bubble column reactor (SBCR). A per-pass CO conversion of $X_{CO,FT} = 55\%$ was assumed. The synthesized Fischer-Tropsch products are considered paraffinic only, as shown by Eq. 5.

$$n\ CO + (2n+1)\ H_2 \rightarrow H(CH_2)_nH + n\ H_2O, \qquad \Delta H_R = -166.4 kJ/mol \quad (5)$$

The extended Anderson-Schulz-Flory (eASF) distribution, as established by Förtsch et al., has been applied to compensate for the standard ASF distribution's weaknesses, i.e., underestimation of CH_4 forming, overestimation of C_2H_6 and a lack of differentiation between short- and long-chained hydrocarbons [20]. The applied parameters and

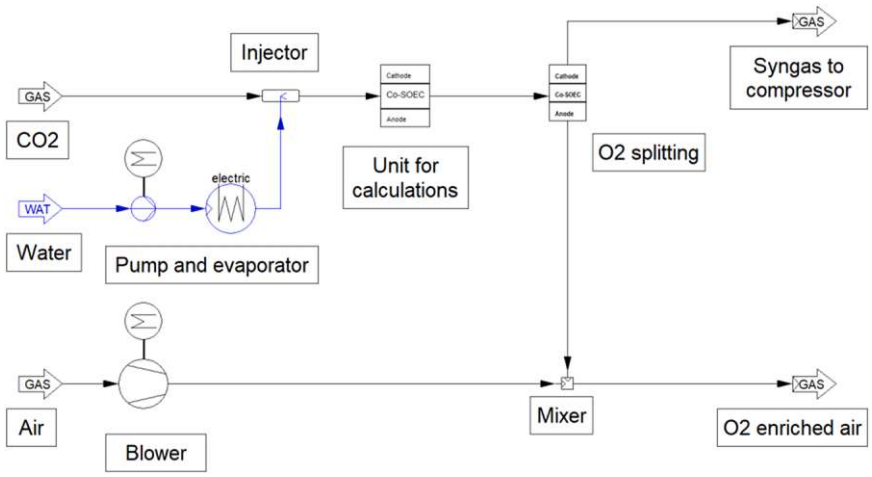

Fig. 2. Modeling of the solid-oxide electrolyzer in co-electrolysis mode.

assumptions concerning the eASF distribution are based on a previously conducted study [57].

A substantial technological effort is required to process Fischer-Tropsch syncrude into jet fuel, complying with international standards. Downstream processes such as hydrocracking, dehydrogenation, oligomerization and aromatization are necessary to adjust the hydrocarbon chain length and structure. A detailed elaboration of a Fischer-Tropsch syncrude refinery is given by Petersen et al., [54], suggesting a combined refinery efficiency of 86% with an additional H_2 demand of 0.016 kg H_2/kg fuel.

2.4. Solid-oxide electrolyzer in co-electrolysis mode

Solid-oxide electrolyzers exploit the decreasing demand for electric energy at increasing temperatures, concluding in a smaller power demand than low-temperature electrolysis technologies, i.e., alkaline water electrolysis and proton exchange membrane electrolysis. Fig. 1 displays the thermodynamic principle. The total energy required for water splitting (ΔH_r) is the sum of provided electric energy (ΔG_r) and heat energy ($T\Delta S_r$). Thus, the electrolyzer's power demand decreases with increasing temperatures.

State-of-the-art SOEL units operate at temperatures ranging from 800° to 900°C and at a pressure slightly above ambient pressure levels [62]. The world's first multi-megawatt high-temperature electrolyzer was installed in Rotterdam, the Netherlands, in April 2023, with a rated power of 2.6 $MW_{el.}$ [67]. Typical SOEL catalyst systems are based on dispersed nickel in an yttria-stabilized zirconia framework. Thus, a catalyst guard system is recommended to avoid catalyst poisoning [64]. In co-electrolysis mode, H_2O and CO_2 are converted to syngas. The chemical reactions occurring at the cathode under the provision of electrons are shown by Eq. 6 and 7.

$$H_2O\ (g) + 2\ e^- \rightarrow O^{2-} + H_2\ (g) \tag{6}$$

$$CO_2\ (g) + 2\ e^- \rightarrow O^{2-} + CO\ (g) \tag{7}$$

The generated oxygen ions are transferred to the anode via the solid electrolyte, where they are subsequently oxidized to gaseous O_2, as shown in Eq. 8.

$$2\ O^{2-} \rightarrow O_2\ (g) + 4\ e^- \tag{8}$$

Due to the increased operating temperatures of 800–900 °C, the rWGS reaction occurs, shown by Eq. 9.

$$CO_2 + H_2 \rightarrow CO + H_2O, \quad \Delta H_r = 41.2 kJ/mol \tag{9}$$

Wang et al. stated that almost no direct splitting of CO_2 occurred within their experimental tests and that the rWGS reaction is the main driver for the conversion of CO_2 to CO [72]. Thus, Eq. 7 is neglected for the presented SOEL model. Additional H_2 needs to be provided by the electrolyzer to meet the rWGS reaction's demand.

According to Cinti et al., the cell operating conditions have only a minor influence on the H_2:CO ratio provided by the SOEL unit [11]. It is instead determined by the feed ratio of H_2O to CO_2. The H_2:CO ratio of the syngas leaving the electrolyzer can be set within the presented model. The feed mass flow rates of H_2O and CO_2 are automatically adjusted to meet the required specifications. The conversion of H_2O and CO_2 is defined by Eq. 10 and Eq. 11. In addition, the reactant utilization RU is defined as the total conversion of feed streams, as seen in Eq. 12.

$$X_{H_2O} = \frac{\dot{n}_{H_2O,in} - \dot{n}_{H_2O,out}}{\dot{n}_{H_2O,in}} \tag{10}$$

$$X_{CO_2} = \frac{\dot{n}_{CO_2,in} - \dot{n}_{CO_2,out}}{\dot{n}_{CO_2,in}} \tag{11}$$

$$\mathrm{RU} = \frac{(\dot{n}_{CO_2,in} + \dot{n}_{H_2O,in}) - (\dot{n}_{CO_2,out} + \dot{n}_{H_2O,out})}{(\dot{n}_{CO_2,in} + \dot{n}_{H_2O,in})} \tag{12}$$

The electrolyzer's power demand is determined by the volume flow rate of H_2 leaving the SOEL unit and the required H_2 for converting CO_2 to CO via the rWGS reaction. Schmidt et al. propose a specific power demand of 3.2 (at stack level) to 3.7 (at system level) $kWh_{el.}/Nm^3$ H_2 [62]. Other sources list values ranging from 3.2 to 3.6 $kWh_{el.}/Nm^3$ H_2 [21,59,68]. A specific power demand of 3.37 $kWh_{el.}/Nm^3$ H_2 was chosen within this study according to the HELMETH project's outcome [26].

A detailed overview of the SOEL modeling can be found in Fig. 2. Steam and CO_2 are mixed before entering the main unit, where all stoichiometric and energy calculations occur. A subsequent unit separates the generated O_2 from the syngas stream. The removal of O_2 molecules from the anodic layer must be ensured in real applications to avoid mass transfer limitations. Thus, the separated O_2 leaving the SOEL's anode, is mixed with ambient air at an air:O_2 ratio of 1. The generated syngas leaves the electrolyzer at the cathodic side and gets transferred to the subsequent syngas condenser and compressor.

Numerous studies have focused on state-of-the-art solid-oxide electrolyzers, including applied materials [27,37,42,62,72]. Modeling SOEL units has been a major objective of various research articles [2,12,11,42,45,72,76]. In addition, several experimental studies have been conducted to evaluate established models of solid-oxide electrolyzers [11,25,66,76].

2.5. CO_2 capture – MEA absorption

CO_2 capture by MEA absorption is a mature technology. An MEA

Table 3
List of considered heat sources and sinks.

Heat sources				Heat sinks			
Unit	Material	T_{in} [°C]	T_{out} [°C]	Unit	Material	T_{in} [°C]	T_{out} [°C]
TG	Flue gas	1100	50	CO_2 capture	MEA[2)]	120	120
FT	Steam[1)]	220	220	CO_2 capture	H_2O	20	120
W8	Tail gas	850	50	SOEL	H_2O	20	200
W1	Syngas	850	20	Reformer	H_2O	20	200
				SOEL $\Delta H_r^{3)}$	-	850	850
				Ref. $\Delta H_r^{3)}$	-	850	850
				W7	Tail gas	30	850
				SOEL	CO_2, H_2O	120	850

1) Boiling water reactor - evaporation of boiling water
2) Heat demand of CO_2 desorption
3) Reaction enthalpy of occurring chemical reactions.

solution circulates between an absorber column, usually operating at temperatures of around 35 °C [39], and a desorber column, operating at elevated temperatures of about 120 °C [73]. Heat must be applied to regenerate the loaded solution, concluding in a specific heat demand of 3.1–4.0 $GJ_{th.}/t\ CO_2$ [39,58,73]. Current state-of-the-art CO_2 capture units based on MEA absorption obtain capture efficiencies of up to 90% [5,29,58,73] with gas purities higher than 99.9 vol% [46].

According to Machida et al., the heat demand of CO_2 capture by an MEA solution can be allocated as follows [41]:

- 53% reaction heat to dissolve the bound CO_2.
- 16% sensible heat to heat the loaded solution.
- 31% latent heat to evaporate the steam for stripping.

The mass flow rate of steam should be between 50 and 77 wt% of the CO_2 mass flow rate to ensure a sufficient desorption process [41,58].

In this study, the pump's electric duty was calculated according to Eq. 14 for an assumed mass fraction of MEA of $w_{MEA} = 0.35$ kg MEA/kg solution and a CO_2 loading difference of 0.2 between the absorber and the desorber [38]. A typical density of a 40 wt% MEA solution is 1100 kg/m^3 [23]. A pressure drop of 0.3 bar was assumed for the MEA solution [52].

$$\dot{m}_{MEA} = \frac{\dot{m}_{CO_2}}{0.35 \frac{kg\ MEA}{kg\ Solution} \bullet 0.2 \bullet \frac{M_{CO_2}}{M_{MEA}}} \tag{13}$$

$$P_{Pump} = \frac{\dot{m}_{Solution}}{\rho_{Solution}} \bullet \Delta p_{MEA} \tag{14}$$

2.6. Steam reforming of recirculated tail gas

A steam reformer has been implemented to reform hydrocarbons within the recirculated tail gas stream. In addition, CO_2 is converted to CO via the rWGS reaction. A temperature level of $T_{Reformer} = 850$ °C was chosen to maximize hydrocarbon conversion into syngas and shift the rWGS reaction's thermodynamic equilibrium to the product side. From a thermodynamic perspective, the reformer's pressure level should be as low as possible. The following chemical reactions were implemented in the designed model.

$$CH_4 + H_2O \rightarrow CO + 3H_2,\ \Delta H_r = 206.1 kJ/mol \tag{15}$$

$$C_2H_6 + 2H_2O \rightarrow 2CO + 5H_2,\ \Delta H_r = 347.3 kJ/mol \tag{16}$$

$$C_3H_8 + 3H_2O \rightarrow 3CO + 7H_2,\ \Delta H_r = 497.7 kJ/mol \tag{17}$$

$$CO_2 + H_2 \rightarrow CO + H_2O,\ \Delta H_r = 41.2 kJ/mol \tag{18}$$

The conversion of hydrocarbons is based on a stoichiometric calculation according to Eq. 19. Based on the experimental investigations conducted by Schädel et al., the following conversions of hydrocarbons were assumed at a temperature of 850 °C and a pressure of 1 bar [61].

$$X_{C_xH_y} = \frac{\dot{n}_{C_xH_y,in} - \dot{n}_{C_xH_y,out}}{\dot{n}_{C_xH_y,in}} \tag{19}$$

- Conversion of methane $X_{CH4} = 90\%$.
- Conversion of ethane $X_{C2H6} = 95\%$.
- Conversion of propane $X_{C3H8} = 99\%$.

The steam to carbon ratio S/C is defined as the steam's molar flow rate divided by the carbon atoms' molar flow rate bound within the reformed hydrocarbons, see Eq. 20. S/C ratios between 2.2 and 4.0 are recommended [2,61]. A detailed explanation of the S/C ratio's effects on process performance is given by Adiya et al. [1].

$$S/C = \frac{\dot{n}_{H_2O}}{\dot{n}_{CH_4} + 2 \bullet \dot{n}_{C_2H_6} + 3 \bullet \dot{n}_{C_3H_8}} \tag{20}$$

The rWGS reaction's activity inside the steam reformer was modeled by implementing a settable conversion of CO_2, in accordance with Eq. 18. A unit displaying the rWGS chemical equilibrium at the chosen process conditions was implemented after the steam reformer. The CO_2 conversion was set corresponding to the chemical equilibrium.

Further information concerning steam reforming catalysts is provided by de Klerk, Lopez et al. and Schädel et al. [13,60,61].

2.7. Heat balancing

Table 3 displays the PtL plant's heat sources and sinks at their respective temperature levels. Heat balances for all analyzed process configurations have been created. A way to meet the plant's heat demand is to increase the mass flow rate of burned tail gas. However, doing so concludes in smaller shares of recirculated tail gas and, thus, declines in the PtL plant's KPIs, e.g., Power-to-Liquid efficiency and Fischer-Tropsch product streams.

The following assumptions have been made concerning the respective CO_2 sources:

1. Cement plant as CO_2 source:
   The cement plant's waste heat covers a third of the MEA absorption heat demand [29,5]. In addition, the heat demand for the provision of stripping steam is internally covered by the Fischer-Tropsch reaction heat. Thus, the remaining specific heat demand of the MEA absorption process is set at 1 GJ/t CO_2. A recirculation rate of RR = 85% can be realized while covering the PtL plant's heat demand.
2. Biogas upgrading plant as CO_2 source:
   No additional CO_2 capture unit is required for this setup. A recirculation ratio of RR = 90% can be realized.
3. CHP plant burning wood chips as CO_2 source:
   Two scenarios were defined for this plant configuration. Within the first scenario, it is assumed that the CHP plant covers the MEA absorption's heat demand, and thus, a recirculation ratio of RR = 90% is realized. Additional tail gas is combusted in the second scenario to meet the PtL plant's heat demand resulting in a recirculation ratio of only RR = 75%.

3. Results

The following chapter includes the designed flowcharts of the simulated Power-to-Liquid plant as well as the results of the three analyzed process configurations based on the following CO_2 sources.

1. Norcem Brevik cement plant in Porsgrunn, Norway [7].

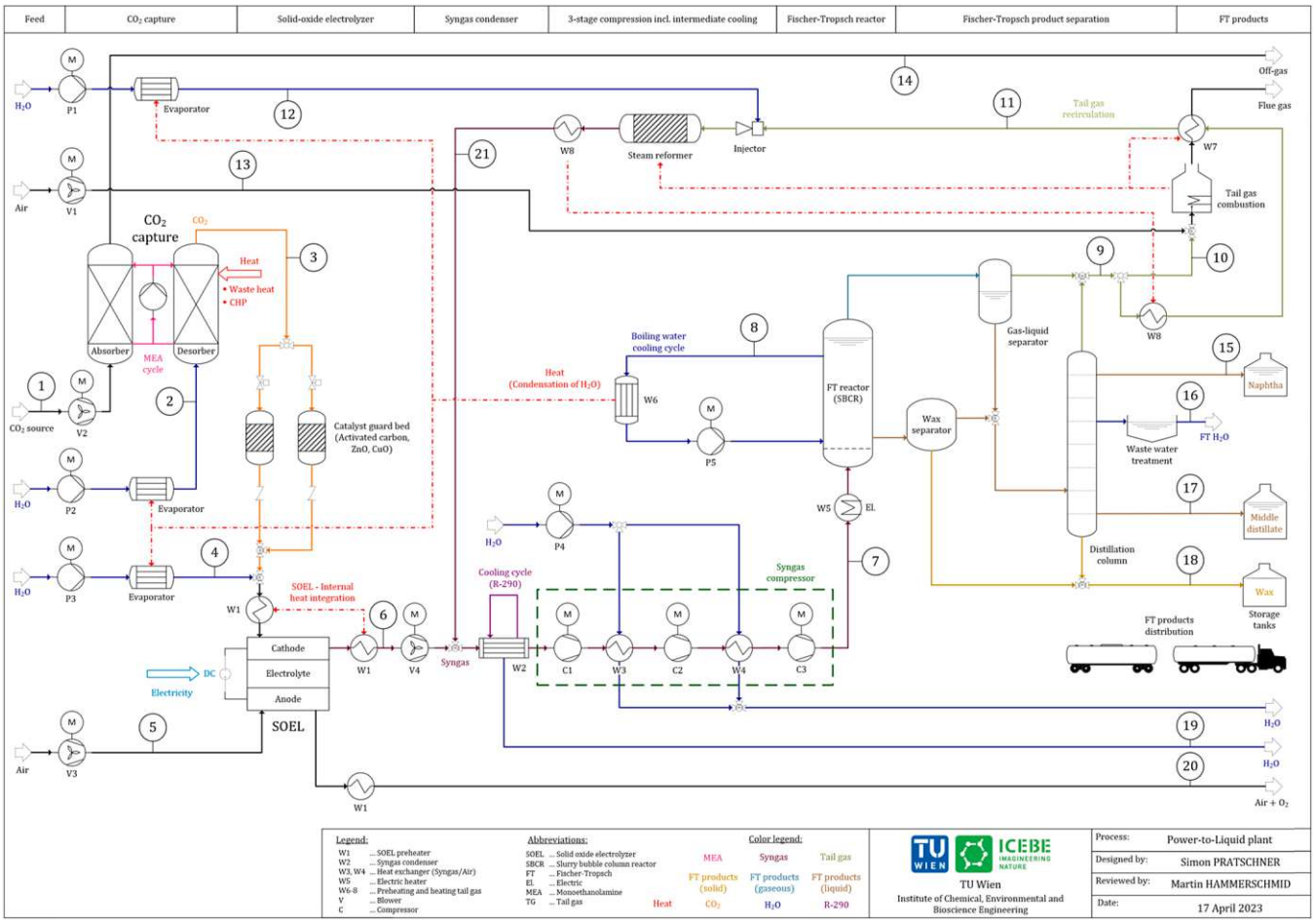

Fig. 3. Process flow diagram of a Power-to-Liquid plant based on high-temperature electrolysis and Fischer-Tropsch synthesis. The streams' mass flow rates for the respective CO_2 sources are listed in Table A.1 in the appendix.

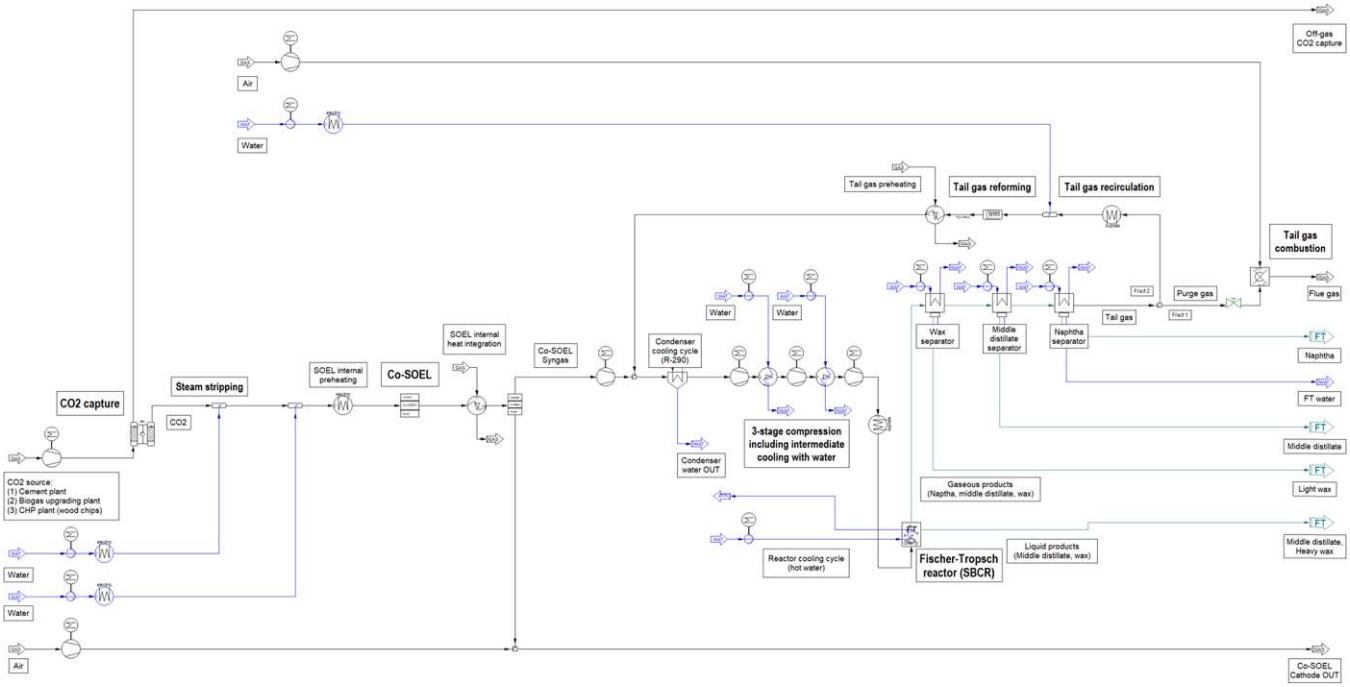

Fig. 4. Implementation of the designed Power-to-Liquid plant as process simulation flowchart in IPSEpro.

Table 4
Key performance indicators of scenario (1) - cement plant as a CO_2 source.

Key performance indicator	Symbol	Value	Unit
Carbon efficiency	η_{Carbon}	75.7	%
Power-to-Liquid efficiency	η_{PtL}	58.8	%
CO conversion	X_{CO}	93.3	%
Recirculation ratio	RR	85.0	%
SOEL scale	P_{SOEL}	504.0	$MW_{el.}$

Table 5
Input and output streams of scenario (1) - cement plant as a CO_2 source.

Input streams	Description	[t/h]	Output streams	Description	[t/h]
Flue gas	Cement plant	404.6	Naphtha	FT products	6.4
CO_2	Utilized CO_2	100.0	Middle distillate	FT products	10.1
H_2O_{MEA}	Stripping of CO_2	53.2	Wax	FT products	10.6
H_2O_{SOEL}	Additional feed	45.6	H_2O_{FT}	Waste water	37.3
$H_2O_{Reformer}$	Steam reformer	3.1	H_2O	Condenser	18.1
Ambient air	Anode purging	96.6	Flue gas	TG combustion	156.0
Ambient air	TG combustion	143.5	Off-gas_{MEA}	Desorber out	304.6
			O_2 enriched air	Anode out	203.4

Table 6
Power demand of scenario (1) - cement plant as a CO_2 source.

Process	Power demand [$MW_{el.}$]	Relative demand [%]
SOEL	504.0	89.1
Syngas compression	40.2	7.1
Syngas condenser	4.8	0.8
CO_2 capture	11.1	2.0
Auxiliaries	5.4	1.0
SUM	565.5	100.0

Table 7
Heat balance of scenario (1) - cement plant as a CO_2 source.

Heat sources			Heat sinks		
Unit	Material	Heat [$MW_{th.}$]	Unit	Material	Heat [$MW_{th.}$]
TG comb.	Flue gas	54.5	CO_2 capt.[1)]	MEA sol.	28.0
FT react.	Steam	91.8	CO_2 capt.	H_2O	38.8
W8	Tail gas	36.5	SOEL	H_2O feed	35.0
W1	Syngas	69.0	Reformer	H_2O feed	0.5
			SOEL ΔH_r	-	22.0
			Reformer ΔH_r	-	7.5
			W7	Tail gas	39.0
			SOEL	CO_2 and H_2O	66.0
SUM	-	251.8	SUM	-	236.8

1) 33% of the CO_2 capture unit's heat demand is covered by the cement plant's waste heat.

2. Biogas upgrading plant in Montello, Italy [15].
3. Decentralized CHP plant burning wood chips [56].

Based on the CO_2 sources mentioned above, the evaluated process routes will be assessed concerning their respective KPIs, as defined in chapter 2.2, and their mass and energy balances.

3.1. Process flow diagram and process simulation flowchart

Fig. 3 shows a process flow diagram of the designed Power-to-Liquid plant. The corresponding mass flow rates for the evaluated CO_2 sources are listed in table A.1 in the appendix. The processed gas stream provided by the respective CO_2 source is slightly pressurized to overcome the MEA absorption's pressure drop. After being cleaned by a catalyst guard bed, the pure CO_2 stream is mixed with steam and inserted into the SOEL unit. The generated syngas is then transferred to a condenser to avoid water condensation in the downstream syngas compressor. Subsequently, the syngas is pressurized and fed into the Fischer-Tropsch reactor. A heater at the reactor's inlet, W5, is required for plant start-up. However, this heater is inactive once steady-state operation has been reached. The streams, drained from the Fischer-Tropsch reactor, i.e., liquid and gaseous, are further processed and separated into the respective product fractions. Unconverted syngas and non-condensable hydrocarbons, i.e., methane, ethane and propane, are either recirculated and transferred to the tail gas reformer or the tail gas combustor. The recirculated tail gas share is heated and processed by a steam reformer before being mixed with the fresh syngas generated by the SOEL unit. The implementation of the designed process in IPSEpro is depicted in Fig. 4.

3.2. Cement plant as CO_2 source of the designed Power-to-Liquid plant

The first process configuration is based on a cement plant as a CO_2 source. Further details concerning the cement plant's off-gas properties are given in chapter 2.1.

3.2.1. Key performance indicators of scenario (1) – cement plant

The determined KPIs of a Power-to-Liquid plant utilizing CO_2 generated by a cement plant are listed in Table 4. With the presented concept, a carbon efficiency of 75.7% and a Power-to-Liquid efficiency of 58.8% are obtained. Varying the specific power demand of the SOEL unit from 3.2 to 3.7 kWh/Nm^3 H_2 results in a Power-to-Liquid efficiency ranging from 54.1% to 61.6%. A share of 15% of the generated tail gas must be combusted to meet the PtL plant's heat demand, concluding in a total CO conversion of 93.3%. The electrolyzer's scale is slightly above 500 $MW_{el.}$ power input to process a mass flow rate of 100 t/h CO_2.

3.2.2. Mass balance and gas compositions of scenario (1) – cement plant

Significant mass flow rates of this process route are listed in table A.1 in the appendix. The respective process stream numbers are defined in Fig. 3. A summary of all input and output streams is listed in Table 5. A mass flow rate of 100 t/h CO_2 is converted to 27.1 t/h Fischer-Tropsch products. A total water demand of 101.9 t/h is necessary to supply the CO_2 capture unit, the electrolyzer and the tail gas reformer. In addition, a mass flow rate of 240.1 t/h air is required to purge the electrolyzer's anodic layer of O_2 and to ensure a complete tail gas combustion. Relevant compositions of gas streams within the PtL plant are stated in table A.2 in the appendix. The H_2:CO ratio provided by the electrolyzer needs to be at 2.46 to ensure an H_2:CO ratio of 2.0 at the Fischer-Tropsch reactor's inlet.

3.2.3. Power and heat balances of scenario (1) – cement plant

The plant's power balance is listed in Table 6. The electrolyzer is the primary power consumer, being responsible for a relative share of almost 90%. Additionally, syngas compression accounts for around 7% of the plant's power demand. Additional power consumption for fluid conveying, caused by blowers and pumps, is almost negligible, with only 1%. The heat balance of process configuration (1) can be found in Table 7. Further details concerning the respective temperature levels are stated in Table 3, see chapter 2.7.

Table 8
Key performance indicators of scenario (2) - biogas upgrading plant as a CO_2 source.

Key performance indicator	Symbol	Value	Unit
Carbon efficiency	η_{Carbon}	88.6	%
Power-to-Liquid efficiency	η_{PtL}	63.8	%
CO conversion	X_{CO}	95.5	%
Recirculation ratio	RR	90.0	%
SOEL scale	P_{SOEL}	23.1	$MW_{el.}$

Table 9
Input and output streams of scenario (2) - biogas upgrading plant as a CO_2 source.

Input streams	Description	[t/h]	Output streams	Description	[t/h]
CO_2 rich off-gas	Biogas plant	4.6	Naphtha	FT products	0.3
CO_2	Utilized CO_2	4.5	Middle distillate	FT products	0.5
H_2O_{SOEL}	H_2O feed SOEL	4.5	Wax	FT products	0.5
$H_2O_{Reformer}$	Steam reformer	0.2	H_2O_{FT}	Waste water	1.8
Ambient air	Anode purging	4.4	H_2O	Condenser	0.9
Ambient air	TG combustion	4.8	Flue gas	TG combustion	5.2
			O_2 enriched air	Anode out	9.3

Table 10
Power demand of scenario (2) - biogas upgrading plant as a CO_2 source.

Process	Power demand [$MW_{el.}$]	Relative demand [%]
SOEL	23.1	90.9
Syngas compression	1.9	7.5
Syngas condenser	0.2	0.8
Auxiliaries	0.2	0.8
SUM	25.4	100.0

Table 11
Heat balance of scenario (2) - biogas upgrading plant as a CO_2 source.

Heat sources			Heat sinks		
Unit	Material	Heat [$MW_{th.}$]	Unit	Material	Heat [$MW_{th.}$]
TG comb.	Flue gas	1.8	SOEL	H_2O feed	3.3
FT react.	Steam	4.5	Reformer	H_2O feed	0.04
W8	Tail gas	1.9	SOEL ΔH_r	-	1.0
W1	Syngas	3.2	Reformer ΔH_r	-	0.5
			W7	Tail gas	2.1
			SOEL	CO_2 and H_2O	3.1
SUM	-	11.4	SUM	-	10.04

3.3. Biogas upgrading plant as CO_2 source of the designed Power-to-Liquid plant

The second scenario processes a CO_2-rich off-gas stream emitted by a biogas upgrading plant. The underlying assumptions regarding the CO_2 stream's properties are listed in chapter 2.1, see Table 2.

3.3.1. Key performance indicators of scenario (2) – biogas upgrading plant

The obtained KPIs of a PtL plant utilizing CO_2 of a biogas upgrading plant are listed in Table 8. Due to the CO_2 stream's high purity of 98 vol %, additional processing by an MEA absorption cycle is not required. Hence, a high tail gas recirculation ratio of 90% can be implemented, leading to a high carbon efficiency of 88.6% and an excellent Power-to-Liquid efficiency of 63.8%. A medium-scale electrolyzer with a power input of 23.1 $MW_{el.}$ is required to process the given mass flow rate of 4.5 t/h CO_2.

Table 12
Key performance indicators of scenarios (3.1) and (3.2) - utilization of CO_2 emitted by a biomass heating plant.

Key performance indicator	Scenario Symbol	(3.1)[1] Value	(3.2)[2]	Unit
Carbon efficiency	η_{Carbon}	80.0	68.4	%
Power-to-Liquid efficiency	η_{PtL}	60.9	54.7	%
CO conversion	X_{CO}	95.5	88.8	%
Recirculation ratio	RR	90.0	75.0	%
SOEL scale	P_{SOEL}	39.4	37.8	$MW_{el.}$

1) RR = 90% - the CO_2 capture unit's heat demand is covered by the CHP process
2) RR = 75% - the CO_2 capture unit's heat demand is covered by an increased share of combusted tail gas.

3.3.2. Mass balance and gas compositions of scenario (2) – biogas upgrading plant

Table 9 summarizes the input and output streams of a Power-to-Liquid plant valorizing the off-gas stream of a biogas upgrading plant. A more detailed mass balance is listed in table A.1 in the appendix. A stream of 4.5 t/h CO_2 is processed to 1.3 t/h Fischer-Tropsch products. Compared to process configurations (1) and (3), no additional purification of the feed stream by an MEA absorption unit is required. Due to this configuration's missing CO_2 stripping unit, the electrolyzer's whole H_2O demand must be injected after the catalyst guard bed. Detailed information regarding the gas composition of syngas, tail gas and the anode's purge gas stream is listed in table A.2 in the appendix.

3.3.3. Power and heat balances of scenario (2) – biogas upgrading plant

Converting CO_2 and H_2O to syngas accounts for almost 91% of the total power demand for a process configuration based on a biogas upgrading plant as a CO_2 source, as listed in Table 10. Similar to process route (1), the power demand of the syngas condenser and auxiliaries can be neglected. The syngas compressor consumes 7.5% of the Power-to-Liquid plant's electricity demand. The relatively small scale of biogas upgrading plants concludes in a medium-scale Power-to-Liquid plant with a total power consumption of 25.4 $MW_{el.}$. A detailed list of the heat sources and sinks is given in Table 11. Since no additional CO_2 capture unit is required, only 10% of the tail gas must be combusted to meet the PtL plant's heat demand.

3.4. CHP plant burning wood chips as CO_2 source of the designed Power-to-Liquid plant

The last of the three analyzed process routes is a bioenergy with carbon capture and utilization (BECCU) scenario based on CO_2 emitted by a CHP plant burning wood chips. Within the presented route, two scenarios have been analyzed:

1. In the first scenario, the remaining heat demand of the CO_2 capture unit is covered by the CHP process. Thus, the combustor's performance is decreased, and less heat can be utilized. A share of 90% of recirculated tail gas can be realized in scenario (3.1).
2. The CHP process's power and heat generation remain untouched in the second scenario. Hence, a larger share of tail gas must be combusted to ensure a sufficient heat supply for the CO_2 capture unit. Within scenario (3.2), only 75% of the tail gas can be recirculated.

Detailed information concerning the CHP process's assumptions and

Table 13
Input and output streams of scenarios (3.1) and (3.2) – utilization of CO_2 emitted by a biomass heating plant.

Input streams	Scenario Description	(3.1)[1] Mass flow rate [t/h]	(3.2)[2]	Output streams	Scenario Description	(3.1) Mass flow rate [t/h]	(3.2)
Flue gas	CHP plant	41.2	41.2	Naphtha	FT products	0.5	0.5
CO_2	Utilized CO_2	7.7	7.7	Middle dist.	FT products	0.8	0.7
H_2O_{MEA}	Stripping of CO_2	4.1	4.1	Wax	FT products	0.9	0.7
H_2O_{SOEL}	Additional feed	3.6	3.2	H_2O_{FT}	Waste water	3.0	2.6
$H_2O_{Reformer}$	Steam reformer	0.3	0.2	H_2O	Condenser	1.5	1.3
Ambient air	Anode purging	7.5	7.2	Flue gas	TG combustion	8.4	18.0
Ambient air	TG combustion	7.8	16.5	Off-gas_{MEA}	Desorber out	33.5	33.5
				O_2 enriched air	Anode out	15.9	15.3

1) RR = 90% - the CO_2 capture unit's heat demand is covered by the CHP process
2) RR = 75% - the CO_2 capture unit's heat demand is covered by an increased share of combusted tail gas.

Table 14
Power demand of scenarios (3.1) and (3.2) - utilization of CO_2 emitted by a biomass heating plant.

Scenario Process	(3.1)[1] Power demand [$MW_{el.}$]	(3.2)[2]	(3.1)[1] Relative demand [%]	(3.2)[2]
SOEL	39.4	37.8	88.7	89.4
Syngas compression	3.3	2.8	7.4	6.6
Syngas condenser	0.4	0.4	0.9	0.9
CO_2 capture	0.9	0.9	2.0	2.1
Auxiliaries	0.4	0.4	0.9	0.9
SUM	44.4	42.3	100	100

1) RR = 90% - the CO_2 capture unit's heat demand is covered by the CHP process
2) RR = 75% - the CO_2 capture unit's heat demand is covered by an increased share of combusted tail gas.

performance can be found in [56].

3.4.1. Key performance indicators – CHP plant combusting wood chips as CO_2 source (BECCU)

The KPIs of scenario (3) can be found in Table 12. Within scenario (3.1), the CO_2 capture unit's remaining heat demand is covered by the CHP process, and thus, 90% of the tail gas can be recirculated. Exploiting a fraction of the CHP process heat results in elevated KPIs of the subsequent PtL plant. A carbon efficiency of 80.0% and a PtL efficiency of 60.9% are realized. The electrolyzer's scale is 39.4 $MW_{el.}$, processing an input stream of 7.7 t/h CO_2. For scenario (3.2), the PtL plant's KPIs diminish, with a carbon efficiency of only 68.4% and a PtL efficiency of 54.7%. Additionally, the SOEL unit's scale is slightly reduced to a rated power of 37.8 $MW_{el.}$.

3.4.2. Mass balance and gas compositions – CHP plant combusting wood chips as CO_2 source

The input and output streams of scenario (3) are summarized in Table 13. A mass flow rate of 7.7 t/h CO_2 needs to be processed by the PtL plant. Mass flow rates of 7.5–8.0 t/h H_2O are required to produce a total mass flow rate of 1.9–2.2 t/h Fischer-Tropsch products. In addition, around 3.0 t/h of Fischer-Tropsch waste water needs to be treated. Detailed mass balances, including feed and product streams, are given in table A.1 in the appendix.

The differences in the respective gas compositions of scenario (3.1)

Table 15
Heat balance of scenarios (3.1) and (3.2) - utilization of CO_2 emitted by a biomass heating plant.

Heat sources Scenario Unit	Material	(3.1)[1, 2] Heat [$MW_{th.}$]	(3.2)[3]	Heat sinks Scenario Unit	Material	(3.1) Heat [$MW_{th.}$]	(3.2)
TG combustor	Flue gas	2.9	6.3	CO_2 capture	MEA solution	4.7	4.7
FT reactor	Steam	7.5	6.4	CO_2 capture	H_2O stripping	3.0	3.0
W8	Tail gas	3.1	2.2	SOEL	H_2O feed	2.6	2.4
W1	Syngas	5.4	5.2	Reformer	H_2O feed	0.04	0.04
				SOEL ΔH_r	-	1.7	1.7
				Reformer ΔH_r	-	0.7	0.5
				W7	Tail gas	3.4	2.4
				SOEL	CO_2 and H_2O	5.1	4.9
SUM	-	18.9	20.1	SUM	-	20.9	19.6

1) A share of 10% of tail gas is combusted.
2) The MEA absorption unit's heat demand is covered by the CHP process.
3) A share of 25% of tail gas is combusted.

Table 16
Power-to-Liquid efficiency – comparison to previous studies.

Source	[3]	[11]	[63]	[57]	[77]	[53]	[28]	[22]	[43]	This study
PtL efficiency [%] – lower limit	51.0	57.0	38.0[1]	50.8[3]	57.5	46.0	41.5[5]	53.6	44.0[6]	54.7
PtL efficiency [%] – upper limit			63.0[2]	62.7[4]		67.0	51.3[5]		53.9[7]	63.8

1) Direct air capture in combination with a low-temperature electrolyzer.
2) Biogas upgrading plant in combination with a high-temperature electrolyzer.
3) Without a tail gas reformer.
4) With an idealized tail gas reformer.
5) Proton exchange membrane electrolyzer vs. solid-oxide electrolyzer.
6) Proton exchange membrane electrolyzer in combination with an e-rWGS reactor.
7) High-temperature electrolysis.

Table 17
Key performance indicators of the Power-to-Liquid plant for the respective CO_2 sources.

	CO_2 source		Cement	Biogas upgrading	Solid biomass CHP	
Key performance indicator	Symbol	Unit	(1)	(2)	(3.1)[1)]	(3.2)[2)]
Carbon efficiency	η_{Carbon}	%	75.7	88.6	80.0	68.4
Power-to-Liquid efficiency	η_{PtL}	%	58.8	63.8	60.9	54.7
CO conversion	X_{CO}	%	93.3	95.5	95.5	88.8
Recirculation ratio	RR	%	85.0	90.0	90.0	75.0
Solid-oxide electrolyzer scale	P_{SOEL}	$MW_{el.}$	504.0	23.1	39.4	37.8
CO_2 input	m_{CO_2}	t/h	100.0	4.5	7.7	7.7
Fischer-Tropsch products	m_{FT}	t/h	27.1	1.3	2.2	1.9

1) 90% tail gas recirculation - the CO_2 capture unit's heat demand is covered by the CHP process.
2) 75% tail gas recirculation - the CO_2 capture unit's heat demand is covered by tail gas combustion.

Table A.1
Mass balances of the respective CO_2 sources – all streams in t/h.

		Cement	Biogas upgrading	Solid biomass CHP	
Stream [t/h]	Number	(1)	(2)[1)]	(3.1)[2)]	(3.2)[3)]
Flue gas feed	1	400.9	-	41.2	41.2
H_2O feed desorber	2	53.2	-	4.1	4.1
CO_2 feed SOEL	3	100.0	4.5	7.7	7.7
H_2O feed SOEL	4	45.6	4.5	3.6	3.2
Air feed SOEL	5	96.6	4.4	7.5	7.2
Syngas SOEL out	6	92.0	4.2	7.1	7.0
Syngas feed FT reactor	7	147.8	7.2	12.0	10.3
H_2O cooling cycle	8	171.9	8.4	14.0	11.9
Tail gas	9	83.4	4.1	6.8	5.8
Purge gas	10	12.5	0.4	0.7	1.4
Recirculated tail gas	11	70.8	3.7	6.1	4.4
H_2O feed reformer	12	3.1	0.2	0.3	0.2
Air feed combustor	13	143.5	4.4	7.8	16.5
Off-gas MEA out	14	300.9	-	33.5	33.5
Naphtha	15	6.4	0.3	0.5	0.5
Fischer-Tropsch H_2O	16	37.3	1.8	3.0	2.6
Middle distillate	17	10.1	0.5	0.8	0.7
Wax	18	10.6	0.5	0.9	0.7
H_2O condenser out	19	18.1	0.9	1.5	1.3
O_2 enriched air	20	203.4	9.3	15.9	15.3
Reformed tail gas	21	73.9	3.9	6.4	4.6

1) MEA CO_2 capture unit is not required.
2) 90% tail gas recirculation - the CO_2 capture unit's heat demand is covered by the CHP process.
3) 75% tail gas recirculation.

and scenario (3.2) are negligible. Thus, only the obtained gas compositions of scenario (3.1) are listed in table A.2 in the appendix. An H_2:CO ratio of 2.51 needs to be provided by the SOEL unit to balance the low H_2:CO ratio of 1.50 at the tail gas reformer's outlet.

3.4.3. Power and heat balance – CHP plant combusting wood chips as CO_2 source

The power demand of both scenarios utilizing CO_2 generated by the combustion of wood chips is listed in Table 14. Increasing the share of recirculated tail gas leads to a slight increase in the SOEL unit's power demand. In addition, more power must be provided to compress the increased syngas stream. Results concerning the MEA absorption unit's power demand remain constant since the same flue gas stream is processed.

The respective heat balances of scenarios (3.1) and (3.2) are listed in Table 15. Scenario (3.1)'s heat balance is negative since the CO_2 capture's heat demand is assumed to be covered by the CHP process.

4. Discussion

Cement plants are an abundant CO_2 source responsible for 3% of the EU27's and 7% of the global CO_2 emissions. Substantial advantages of cement plants are their immense availability, the significant mass flow rates of emitted CO_2 and the fact that about 30% of the CO_2 capture unit's heat demand can be covered by waste heat. Consequently, combining cement and PtL plants results in a satisfactory carbon efficiency of $\eta_{Carbon} = 75.7\%$ and a decent PtL efficiency of $\eta_{PtL} = 58.8\%$. However, cement plants emit a mixture of fossil and inorganic CO_2 and extremely large electrolyzers, around 500 $MW_{el.}$ rated power, are required to utilize the whole off-gas stream. Thus, exploiting cement plants as CO_2 sources is not ideal for current state-of-the-art electrolyzers but will become interesting as soon as electrolyzers reach scales above 100 $MW_{el.}$. A possible approach to tackle the fossil share of CO_2 emissions is the substitution of fossil fuels with biogenic methane. In addition, CO_2 emission mitigation and avoidance could be realized by applying green H_2 as fuel in the rotary kiln of cement plants.

Around 90 PtL plants of the presented concept would be necessary to process the total EU's cement industry CO_2 emissions of 0.072 Gt CO_2 per year. Exploiting the EU27's cement industry as a CO_2 source would lead to an annual output of 19.5 million tons of FT products. An estimated share of 3% of the EU's jet fuel demand could be covered by doing so, based on the annual jet fuel consumption determined by Surgenor [69] and a Fischer-Tropsch refinery efficiency of 86% [54]. At a global scale, about 680 million tons of FT products could be produced annually based on the cement industry's CO_2 emissions. To achieve this, approximately 3000 PtL plants would be required, as presented in chapter 3.2.

Utilizing biogas upgrading plants as a CO_2 source for PtL processes has several advantages. Biogas upgrading plants provide a highly concentrated CO_2 stream, making a downstream CO_2 capture unit unnecessary. As a result, the combination of biogas upgrading and PtL plants concludes in a superior PtL efficiency of $\eta_{PtL} = 63.8\%$ and carbon efficiency of $\eta_{Carbon} = 88.6\%$. In addition, valorizing biogenic CO_2 avails the global effort to curb the climate crisis. Biogas upgrading plants are usually located at decentralized sites and designed at a medium scale, thus ensuring a beneficial synergy with PtL plants. Electrolyzers at a scale of around 20 $MW_{el.}$ will be established within the upcoming years. Hence, developing a combined biogas upgrading and PtL plant, as presented in chapter 3.3, is feasible within the following decade.

The presented process route based on a biogas upgrading plant processes a mass flow rate of 4.5 t/h CO_2. About 4500 PtL plants at the suggested scale of $P_{SOEL} = 23$ $MW_{el.}$ are necessary to process the projected CO_2 emissions of biogas plants in Europe introduced by Millinger et al. [47]. As a result, around 47 million tons of FT products could be produced annually, corresponding to 7.3% of the EU's jet fuel demand, assuming a syncrude to jet fuel refinery efficiency of 86% [54].

Exploiting solid biomass CHP plants entails a detrimental controversy. Transferred heat is a key product of the biomass heating plant but is also required to separate the generated CO_2 from the flue gas stream. A possible solution for real applications could be to valorize only a part of the generated CO_2 stream during periods with an increased demand for heat and power by nearby settlements, e.g., in winter. In this case, optimized plant operation also needs to focus on economic circumstances, e.g., electricity and district heating prices, as well as potential revenue of Fischer-Tropsch products. Two scenarios have been analyzed within this work to evaluate this contradiction. Withdrawing heat from

Table A.2
Gas compositions of all scenarios in vol% - (1) cement plant, (2) biogas upgrading plant and (3) biomass heating plant..

[vol%] Stream (No.)	(1) Off-gas$_{MEA}$ (14)	(2)	(3)	(1) Syngas$_{SOEL}$ (6)	(2)	(3)	(1) Syngas$_{FT\ reactor}$ (7)	(2)	(3)	(1) Anode$_{SOEL}$ (20)	(2)	(3)	(1) Tail gas (9)	(2)	(3)	(1) Reformer$_{out}$ (21)	**(2)**	**(3)**
Ar	0.0	-	0.0	0.0	0.0	0.0	0.0	0.0	0.0	0.5			0.0	0.0	0.0	0.0	0.0	0.0
CH_4	0.0	-	0.0	0.0	0.5	0.0	0.02	0.4	0.02	0.0			0.5	1.2	0.5	0.05	0.1	0.05
C_2H_6	0.0	-	0.0	0.0	0.0	0.0	0.01	0.0	0.01	0.0			0.4	0.4	0.4	0.02	0.02	0.02
C_3H_8	0.0	-	0.0	0.0	0.0	0.0	0.0	0.0	0.0	0.0			0.3	0.3	0.3	0.0	0.0	0.0
CO	0.0	-	0.0	24.9	24.6	24.5	31.2	31.0	31.2	0.0			29.9	29.6	29.9	34.6	33.8	34.6
CO_2	2.3	-	1.6	4.4	4.3	4.4	5.17	5.2	5.17	0.0			11.0	11.0	11.0	5.3	5.4	5.3
H_2	0.0	-	0.0	61.1	61.1	61.5	62.4	62.2	62.4	0.0			56.0	55.6	56.0	52.0	52.08	52.0
H_2O	12.1	-	0.5	9.6	9.5	9.6	1.2	1.2	1.2	0.0			1.9	1.9	1.9	8.03	8.6	8.03
N_2	73.5	-	94.5	0.0	0.0	0.0	0.0	0.0	0.0	39.0			0.0	0.0	0.0	0.0	0.0	0.0
O_2	12.1	-	3.4	0.0	0.0	0.0	0.0	0.0	0.0	60.5			0.0	0.0	0.0	0.0	0.0	0.0

the CHP process, about 20% of the thermal input into the combustor, results in a PtL efficiency of $\eta_{PtL} = 60.9\%$ and carbon efficiency of $\eta_{Carbon} = 80.0\%$. In contrast, providing the required heat via an increased share of combusted tail gas results in an inferior PtL efficiency of $\eta_{PtL} = 54.7\%$ and carbon efficiency of $\eta_{Carbon} = 68.4\%$. BECCU has significant potential concerning the containment of global warming by substituting fossil commodities with alternative products based on biogenic CO_2. Furthermore, the implementation of electrolyzers at a scale of around 40 $MW_{el.}$ is a realistic scenario for this decade. However, it has to be stated that the EU's policy concerning the combustion of solid biomass is not yet decided and remains uncertain for intrigued investors.

An annual production capacity of 246 million tons of FT products could be realized by exploiting biomass heating plants in Europe, according to a scenario posed by Millinger et al. [47]. In doing so, 38% of the EU's jet fuel demand could be covered by implementing 14,000 PtL plants with a rated power of $P_{SOEL} = 39.4\ MW_{el.}$.

Within the presented study, PtL efficiencies of 54.7–63.8% were obtained by plant scales ranging from 20 to 500 $MW_{el.}$ power input into the electrolyzer. Table 16 offers a comparison to previously conducted studies with respect to the obtained PtL efficiencies. Valorizing CO_2 sources with even lower concentrations than the three analyzed scenarios, i.e., direct air capture, would decline the Power-to-Liquid efficiency to 52.8%, assuming a specific power demand of 2.3 $MJ_{el.}/kg\ CO_2$ [32]. In addition, a specific heat demand of 7.2 $MJ_{th.}/kg\ CO_2$ would be required. Thus, a feasible operation of Power-to-Liquid plants in combination with direct air capture cannot be realized under current conditions. To the best of the authors' knowledge, deriving the CO_2 source's influence on the carbon efficiency η_{Carbon} of PtL plants has not been performed by previous studies. The underlying work determined carbon efficiencies between 68.4% for a solid biomass CHP plant and 88.6% for a biogas upgrading plant.

In contrast to past studies, the performed work focuses on the CO_2 source itself by directly analyzing the key performance indicators of Power-to-Liquid plants as a function of the CO_2 source's properties. The Power-to-Liquid efficiency has been a significant indicator in previous studies. However, carbon efficiency itself has not gained the required attention. Furthermore, the underlying work improves preceding studies conducted by the authors by implementing detailed models of the solid-oxide electrolyzer, the steam reformer and the CO_2 capture unit.

5. Conclusions

The objective of this study was to answer the following research questions.

1. Which CO_2 sources should be prioritized for carbon capture and utilization applications based on Power-to-Liquid processes combining solid-oxide electrolysis and Fischer-Tropsch synthesis?
2. Which effect does the CO_2 source have on the key performance indicators of Power-to-Liquid plants?

To reach this goal, three different CO_2 sources, i.e., a cement plant, a biogas upgrading plant and a solid biomass combined heat and power plant, were analyzed concerning their influence on the performance of a Power-to-Liquid plant. Several subprocesses, i.e., CO_2 capture, solid-oxide electrolyzer, Fischer-Tropsch synthesis and steam reforming, were modeled and simulated using IPSEpro, a stationary equation-based process simulation tool. The respective key performance indicators, summarized in Table 17, as well as mass and energy balances, were determined for the assumed CO_2 sources. The results show that a maximum Power-to-Liquid efficiency of 63.8% can be achieved by exploiting biogas upgrading plants as a CO_2 source. Likewise, the maximum carbon efficiency of 88.6% is realized by the biogas upgrading process route. Capturing CO_2 from sources with a low concentration is energy-intensive [32,39]. Hence, CO_2 sources with either high concentrations or an abundance of waste heat should be prioritized to increase the Power-to-Liquid plant's share of recirculated tail gas. The detrimental effect of lacking waste heat source leads to a significant decrease in carbon, − 11.6%, and Power-to-Liquid efficiency, − 6.2%, as can be seen by comparing scenarios (3.1) and (3.2) in Table 17. This effect is caused by a decrease in the tail gas recirculation ratio required to increase the purge gas combustion's thermal load. Very large electrolyzers with a rated power of around 500 $MW_{el.}$ are required to utilize cement plant off-gas streams entirely, whereas medium-scale electrolysis units, approximately 20–40 $MW_{el.}$, can process CO_2 streams emitted by decentralized biogas and solid biomass heating plants. The mass flow rate of Fischer-Tropsch products ranges from 1.3 t/h (biogas upgrading plant) to 27.1 t/h (cement plant). The required water mass flow rate ranges from 4.7 t/h to 101.9 t/h, respectively.

Power-to-Liquid plants have the potential to curb the climate crisis by converting CO_2, water and electricity into Fischer-Tropsch products, which can subsequently be processed into synthetic fuels for the aviation, marine and heavy-duty industry. Especially plants valorizing biogenic CO_2 should be a linchpin of the EU's transition toward an ecologically and economically sustainable energy system. In addition, Power-to-Liquid plants ensure political and economic independence by exploiting local CO_2 sources instead of fossil imports. CO_2 sources are abundant and show significant differences concerning their properties. This study provides the necessary information to choose the most effective and efficient CO_2 sources concerning the plants' realizable carbon and Power-to-Liquid efficiency. Electricity is a scarce and precious resource. Hence, maximizing the Power-to-Liquid efficiency of Power-to-Liquid plants is inevitable for conscientious and sustainable electricity utilization. Additionally, the provided mass and energy balances facilitate the decision-making process of significant CO_2 emitters, e.g., companies and communities, whether their CO_2 sources should be exploited by a downstream Power-to-Liquid plant.

The underlying process simulation is solely based on static operating points, thus, leaving room for improvement by assessing the presented plant concept with a dynamic process simulation tool. In doing so, the electrolyzer's dynamic behavior, as well as uncertainties caused by intermittent renewable power sources, could be analyzed for an

extended period of plant operation. In addition, energy storage technologies, e.g., batteries or a syngas buffer tank, could be integrated and evaluated for different scenarios. Heat balances were determined within the presented plant concept. However, further elaboration, e.g., by designing a heat exchanger network, is necessary to achieve the determined efficiencies for real applications. Additionally, downstream processing of Fischer-Tropsch products is vital to ensure national standards and requirements concerning aviation and maritime navigation fuels.

Future projects founded on the presented study could implement a more sophisticated process simulation environment by designing dynamic models for the respective subprocesses. One possible question could be whether grid-powered or stand-alone solutions, directly powered by renewable energy sources, should be prioritized to ensure an economical and sustainable operation of Power-to-Liquid plants. Designing and optimizing a power supply system consisting of renewable power sources, e.g., wind and solar, combined with a grid connection, is required to boost technical practicability. In addition, an ecologic evaluation of the presented plant concept needs to be conducted to assess the environmental impact of the process and Fischer-Tropsch products. Furthermore, a techno-economic assessment, primarily focusing on the effects of an increase in the Power-to-Liquid plant scale, is required to evaluate the cost-competitiveness of synthetic fuels based on Fischer-Tropsch products with conventional fossil fuels.

Funding

The underlying work has received funding from the Mobility of the Future program – a research, technology and innovation funding program of the Federal Ministry of Climate Action, Environment, Energy, Mobility, Innovation and Technology, Republic of Austria. The Austrian Research Promotion Agency (FFG) has been authorized for the program management of the project “IFE – Innovation Flüssige Energie” (project #884340). In addition, the authors would like to thank TU Wien Bibliothek for covering article processing charges through its Open Access Funding program.

CRediT authorship contribution statement

Conceptualization: **Simon Pratschner, Martin Hammerschmid, Stefan Müller, Franz Winter:** Methodology: **Simon Pratschner, Martin Hammerschmid:** Software: **Simon Pratschner, Martin Hammerschmid, Stefan Müller:** Validation: **Simon Pratschner, Martin Hammerschmid:** Formal analysis: **Simon Pratschner:** Investigation: **Simon Pratschner:** Resources: **Stefan Müller, Franz Winter:** Data curation: **Martin Hammerschmid:** Writing – Original draft: **Simon Pratschner:** Writing – Review and editing: **Simon Pratschner, Martin Hammerschmid, Stefan Müller, Franz Winter:** Visualization: **Simon Pratschner:** Supervision: **Stefan Müller, Franz Winter:** Project administration: **Martin Hammerschmid, Stefan Müller, Franz Winter:** Funding acquisition: **Stefan Müller, Franz Winter**.

Declaration of Competing Interest

The authors declare that they have no known competing financial interests or personal relationships that could have appeared to influence the work reported in this paper.

Data availability

Data will be made available on request.

Acknowledgements

The authors would like to acknowledge the “IFE – Innovation Flüssige Energie” project consortium, the TU Wien doctoral college CO_2Refinery and the open access funding by TU Wien.

Appendix

.

References

[1] S.G. Adiya, Z.I. Dupont, V. Mahmud, T, Chemical equilibrium analysis of hydrogen production from shale gas using sorption enhanced chemical looping steam reforming, Fuel Process. Technol. 159 (2017) 128–144, https://doi.org/10.1016/j.fuproc.2017.01.026.

[2] S. Ali, K. Sørensen, M.P. Nielsen, Modeling a novel combined solid oxide electrolysis cell (SOEC) - biomass gasification renewable methanol production system, Renew. Energy 154 (2020) 1025–1034, https://doi.org/10.1016/j.renene.2019.12.108.

[3] W.L. Becker, R.J. Braun, M. Penev, M. Melaina, Production of Fischer–Tropsch liquid fuels from high temperature solid oxide co-electrolysis units, Energy 47 (2012) 99–115, https://doi.org/10.1016/j.energy.2012.08.047.

[4] G. Bianchi, G.P. Panayiotou, L. Aresti, S.A. Kalogirou, G.A. Florides, K. Tsamos, S. A. Tassou, P. Christodoulides, Estimating the waste heat recovery in the European Union Industry, Energ. Ecol. Environ. 4 (2019) 211–221, https://doi.org/10.1007/s40974-019-00132-7.

[5] L.-M. Bjerge, P. Brevik, CO_2 capture in the cement industry, norcem CO_2 capture project (Norway), Energy Procedia 63 (2014) 6455–6463, https://doi.org/10.1016/j.egypro.2014.11.680.

[6] A. Bosoaga, O. Masek, J.E. Oakey, CO_2 capture technologies for cement industry, Energy Procedia 1 (2009) 133–140, https://doi.org/10.1016/j.egypro.2009.01.020.

[7] Brevik C.C.S. 2022, Brevik CCS – World’s first CO2 capture facility at a cement plant. Available at: https://www.brevikccs.com/en. (Accessed: 22.12.2022).

[8] Buysse. C. and Miller. J. The International Council on Clean Transportation, 2021. Transport could burn up the EU’s entire Carbon Budget. Available at: https://theicct.org/transport-could-burn-up-the-eus-entire-carbon-budget/#:~:text=Yet%2C%20even%20under%20the%20most,than%20the%20entire%20EU%20economy’s. (Accessed: 27.12.2022).

[9] G. Caposciutti, A. Baccioli, L. Ferrari, U. Desideri, Biogas from anaerobic digestion: power generation or biomethane production? Energies 13 (2020) 743, https://doi.org/10.3390/en13030743.

[10] C. Carbone, D. Ferrario, A. Lanzini, S. Stendardo, A. Agostini, Evaluating the carbon footprint of cement plants integrated with the calcium looping CO_2 capture process, Front. Sustain 3 (2022), 809231, https://doi.org/10.3389/frsus.2022.809231.

[11] G. Cinti, G. Discepoli, G. Bidini, A. Lanzini, M. Santarelli, Co-electrolysis of water and CO $_2$ in a solid oxide electrolyzer (SOE) stack: Study of high-temperature co-electrolysis reactions in SOEC, Int. J. Energy Res. 40 (2016) 207–215, https://doi.org/10.1002/er.3450.

[12] Giovanni Cinti, A. Baldinelli, A. Di Michele, U. Desideri, Integration of solid oxide electrolyzer and Fischer-Tropsch: a sustainable pathway for synthetic fuel, Appl. Energy 162 (2016) 308–320, https://doi.org/10.1016/j.apenergy.2015.10.053.

[13] A. de Klerk, Fischer-Tropsch Refining, 1st. ed., Wiley-VCH,, Weinheim, Germany, 2011.

[14] Emele, L., Graichen, J., Mendelevitch, R., 2021, Decomposition analysis of CO2 emissions in the European cement sector. German Environment Agency, Berlin, Germany.

[15] E. Esposito, L. Dellamuzia, U. Moretti, A. Fuoco, L. Giorno, J.C. Jansen, Simultaneous production of biomethane and food grade CO $_2$ from biogas: an industrial case study, Energy Environ. Sci. 12 (2019) 281–289, https://doi.org/10.1039/C8EE02897D.

[16] European Environment Agency. 2022. Greenhouse gas emissions from transport in Europe. Available at: https://www.eea.europa.eu/ims/greenhouse-gas-emissions-from-transport. (Accessed: 21.12.2022).

[17] European Environment Agency. 2022a. Primary and final energy consumption in Europe. Available at: https://www.eea.europa.eu/ims/primary-and-final-energy-consumption#:~:text=The%2032.5%20%25%20target%20for%202030,the%20EU%2D27%20in%202030. (Accessed: 22.12.2022).

[18] European Parliament. 2022. Emissions from planes and ships: facts and figures. Available at: https://www.europarl.europa.eu/news/en/headlines/society/20191129STO67756/emissions-from-planes-and-ships-facts-and-figures-infographic. (Accessed: 21.12.2022).

[19] R. Feiz, M. Johansson, E. Lindkvist, J. Moestedt, S.N. Påledal, F. Ometto, The biogas yield, climate impact, energy balance, nutrient recovery, and resource cost of biogas production from household food waste—a comparison of multiple cases from Sweden, J. Clean. Prod. 378 (2022), 134536, https://doi.org/10.1016/j.jclepro.2022.134536.

[20] D. Förtsch, K. Pabst, E. Groß-Hardt, The product distribution in Fischer–Tropsch synthesis: an extension of the ASF model to describe common deviations, Chem. Eng. Sci. 138 (2015) 333–346, https://doi.org/10.1016/j.ces.2015.07.005.

[21] FuelCell Energy. 2023. Solid Oxide Electrolyzer specification sheet. Available at: https://go.fuelcellenergy.com/hubfs/solid-oxide-electrolyzer-spec-sheet.pdf. (Accessed: 14.4.2023).

[22] R. Gao, C. Zhang, K.-W. Jun, S.K. Kim, H.-G. Park, T. Zhao, L. Wang, H. Wan, G. Guan, Green liquid fuel and synthetic natural gas production via CO_2 hydrogenation combined with reverse water-gas-shift and Co-based Fischer-Tropsch synthesis, J. CO_2 Util. 51 (2021), 101619, https://doi.org/10.1016/j.jcou.2021.101619.

[23] J. Gaspar, A. Gladis, J.B. Jørgensen, K. Thomsen, N. von Solms, P.L. Fosbøl, Dynamic operation and simulation of post-combustion CO_2 capture, Energy Procedia 86 (2016) 205–214, https://doi.org/10.1016/j.egypro.2016.01.021.

[24] Handelsblatt.E-Fuels for Aviation and Marine Transportation: Federal Government funds Project in Frankfurt. Available at: https://www.handelsblatt.com/unternehmen/handel-konsumgueter/synthetische-treibstoffe-e-fuels-fuer-flugzeuge-und-schiffe-bund-foerdert-projekt-in-frankfurt/28835764.html. (Accessed: 21.12.2022).

[25] A. Hauch, K. Brodersen, M. Chen, M.B. Mogensen, Ni/YSZ electrodes structures optimized for increased electrolysis performance and durability, Solid State Ion. 293 (2016) 27–36, https://doi.org/10.1016/j.ssi.2016.06.003.

[26] HELMETH. 2018. High temperature electrolysis cell (SOEC). Available at: http://www.helmeth.eu/index.php/technologies/high-temperature-electrolysis-cell-soec. (Accessed: 23.02.2023).

[27] G. Herz, E. Reichelt, M. Jahn, Techno-economic analysis of a co-electrolysis-based synthesis process for the production of hydrocarbons, Appl. Energy 215 (2018) 309–320, https://doi.org/10.1016/j.apenergy.2018.02.007.

[28] G. Herz, C. Rix, E. Jacobasch, N. Müller, E. Reichelt, M. Jahn, A. Michaelis, Economic assessment of Power-to-Liquid processes – influence of electrolysis technology and operating conditions, Appl. Energy 292 (2021), 116655, https://doi.org/10.1016/j.apenergy.2021.116655.

[29] T. Hills, D. Leeson, N. Florin, P. Fennell, Carbon capture in the cement industry: technologies, progress, and retrofitting, Environ. Sci. Technol. 50 (2016) 368–377, https://doi.org/10.1021/acs.est.5b03508.

[30] ICO2CHEM. 2022. From industrial CO2 Streams to added value Fischer-Tropsch Chemicals. Available at: https://www.aspire2050.eu/ico2chem. (Accessed: 21.12.2022).

[31] IEA, 2021. Global Energy Review 2021. IEA - International Energy Agency, France. Available at: https://iea.blob.core.windows.net/assets/d0031107–401d-4a2f-a48b-9eed19457335/GlobalEnergyReview2021.pdf. (Accessed: 26.4.2023).

[32] IEA. 2022a. Direct Air Capture. Available at: https://www.iea.org/reports/direct-air-capture. (Accessed: 17.4.2023).

[33] IEA.2022. Cement, IEA, Paris. Available at: https://www.iea.org/reports/cement. (Accessed: 21.12.2022).

[34] Ineratec. 2022a. German e-fuel production technology to enter Japan and Asian-pacific market. Available at: https://ineratec.de/en/german-e-fuel-technology-to-enter-japan-asian-pacific-market/. (Accessed: 21.12.2022).

[35] Ineratec. 2022b. Start of Commissioning in Hamburg. Available at: https://ineratec.de/inbetriebnahmestart-in-hamburg/#:~:text=M%C3%A4rz%202022%20%E2%80%93%20In%20Hamburg%20beginnt,Chemikalien%20und%20e%2DFuels%20herstellen. (Accessed: 21.12.2022).

[36] H. Jouhara, N. Khordehgah, S. Almahmoud, B. Delpech, A. Chauhan, S.A. Tassou, Waste heat recovery technologies and applications, Therm. Sci. Eng. Prog. 6 (2018) 268–289, https://doi.org/10.1016/j.tsep.2018.04.017.

[37] Kecebas, A., Kayfeci, M., Bayat, M., 2019. Electrochemical hydrogen generation, in: Solar Hydrogen Production - Processes, Systems and Technologies.

[38] K. Kim, H. Seo, D.J. Kim, C. Lee, D.Y. Min, H.M. Kim, Y.-K. Park, Experimental evaluation of CO_2 capture with an amine impregnated sorbent in dual circulating fluidized bed process, Int. J. Greenh. Gas. Control 101 (2020), 103141, https://doi.org/10.1016/j.ijggc.2020.103141.

[39] K. Li, A. Cousins, H. Yu, P. Feron, M. Tade, W. Luo, J. Chen, Systematic study of aqueous monoethanolamine-based CO_2 capture process: model development and process improvement, Energy Sci. Eng. 4 (2016) 23–39, https://doi.org/10.1002/ese3.101.

[40] LIPOR. 2022. Cutting-edge Power-to-Liquid project transforms municipal waste-derived CO2 into sustainable aviation fuels (SAF). Available at: https://www.lipor.pt/en/press-releases/cutting-edge-power-to-liquid-project-transforms-municipal-waste-derived-co2-into-sustainable-aviation-fuels-saf/. (Accessed: 21.12.2022).

[41] H. Machida, R. Ando, T. Esaki, T. Yamaguchi, H. Horizoe, A. Kishimoto, K. Akiyama, M. Nishimura, Low temperature swing process for CO_2 absorption-desorption using phase separation CO_2 capture solvent, Int. J. Greenh. Gas. Control 75 (2018) 1–7, https://doi.org/10.1016/j.ijggc.2018.05.010.

[42] M. Marchese, E. Giglio, M. Santarelli, A. Lanzini, Energy performance of Power-to-Liquid applications integrating biogas upgrading, reverse water gas shift, solid oxide electrolysis and Fischer-Tropsch technologies, Energy Convers. Manag.: X 6 (2020), 100041, https://doi.org/10.1016/j.ecmx.2020.100041.

[43] C. Markowitsch, M. Lehner, M. Maly, Evaluation of process structures and reactor technologies of an integrated Power-to-Liquid plant at a cement factory, J. CO_2 Util. 70 (2023), 102449, https://doi.org/10.1016/j.jcou.2023.102449.

[44] Markowitsch, C., Lehner, M., Kitzweger, J., Haider, W., Ivanovici, S., Unfried, M., Maly, M., 2022. C2PAT - Carbon to Product Austria. Presented at the 17th Symposium Energieinnovation, Graz, Austria, p. 12.

[45] V. Menon, Q. Fu, V.M. Janardhanan, O. Deutschmann, A model-based understanding of solid-oxide electrolysis cells (SOECs) for syngas production by $H2O/CO_2$ co-electrolysis, J. Power Sources 274 (2015) 768–781, https://doi.org/10.1016/j.jpowsour.2014.09.158.

[46] Metz, B., Intergovernmental Panel on Climate Change (Eds.), 2005. IPCC special report on carbon dioxide capture and storage. Cambridge University Press, for the Intergovernmental Panel on Climate Change, Cambridge.

[47] M. Millinger, L. Reichenberg, F. Hedenus, G. Berndes, E. Zeyen, T. Brown, Are biofuel mandates cost-effective? – an analysis of transport fuels and biomass usage to achieve emissions targets in the European energy system, Appl. Energy 326 (2022), 120016, https://doi.org/10.1016/j.apenergy.2022.120016.

[48] R. Nassar, J.-P. Mastrogiacomo, W. Bateman-Hemphill, C. McCracken, C. G. MacDonald, T. Hill, C.W. O'Dell, M. Kiel, D. Crisp, Advances in quantifying power plant CO_2 emissions with OCO-2, Remote Sens. Environ. 264 (2021), 112579, https://doi.org/10.1016/j.rse.2021.112579.

[49] National Oceanic and Atmospheric Administration. 2022. Trends in Atmospheric Carbon Dioxide. Available at: https://gml.noaa.gov/ccgg/trends/global.html. (Accessed: 27.12.2022).

[50] Nordic Electrofuel. 2022. Plants and Projects. Available at: https://nordicelectrofuel.no/what-we-do/. (Accessed: 21.12.2022).

[51] Norsk e-fuel. 2022. Accelerating the Transition to renewable Aviation. Available at: https://www.norsk-e-fuel.com/. (Accessed: 21.12.2022).

[52] Park, K., Øi, L.E., 2017. Optimization of Gas Velocity and Pressure Drop in CO2 Absorption Column. Proceedings of the 58th SIMS. pp. 292–297. https://doi.org/10.3384/ecp17138292.

[53] R. Peters, N. Wegener, R.C. Samsun, F. Schorn, J. Riese, M. Grünewald, D. Stolten, A techno-economic assessment of Fischer–Tropsch fuels based on syngas from co-electrolysis, Processes 10 (2022) 699, https://doi.org/10.3390/pr10040699.

[54] A.M. Petersen, F. Chireshe, O. Okoro, J. Gorgens, J. Van Dyk, Evaluating refinery configurations for deriving sustainable aviation fuel from ethanol or syncrude, Fuel Process. Technol. 219 (2021), 106879, https://doi.org/10.1016/j.fuproc.2021.106879.

[55] R.C. Poudel, D. Khatiwada, P. Aryal, M. Sapkota, Large-scale biogas upgrading plants: future prospective and technical challenges, in: Emerging Technologies and Biological Systems for Biogas Upgrading, Elsevier, 2021, pp. 467–491, https://doi.org/10.1016/B978-0-12-822808-1.00017-9.

[56] S. Pratschner, P. Skopec, J. Hrdlicka, F. Winter, Power-to-green methanol via CO_2 hydrogenation—a concept study including oxyfuel fluidized bed combustion of biomass, Energies 14 (2021) 4638, https://doi.org/10.3390/en14154638.

[57] S. Pratschner, M. Hammerschmid, F.J. Müller, S. Müller, F. Winter, Simulation of a pilot scale Power-to-Liquid plant producing synthetic fuel and wax by combining Fischer–Tropsch synthesis and SOEC, Energies 15 (2022) 4134, https://doi.org/10.3390/en15114134.

[58] T. Pröll, G. Schöny, G. Sprachmann, H. Hofbauer, Introduction and evaluation of a double loop staged fluidized bed system for post-combustion CO 2 capture using solid sorbents in a continuous temperature swing adsorption process, Chem. Eng. Sci. 141 (2016) 166–174, https://doi.org/10.1016/j.ces.2015.11.005.

[59] Roy, S. and Ethakota, M., 2022. Solid oxide electrolysis cell (SOEC): Potential technology for low cost green H2. H2TECH. Available at: https://h2-tech.com/articles/2022/q4–2022/special-focus-future-of-hydrogen-energy/solid-oxide-electrolysis-cell-soec-potential-technology-for-low-cost-green-h-sub-2-sub/. (Accessed: 15.4.2023).

[60] J. Saavedra Lopez, V. Lebarbier Dagle, C.A. Deshmane, L. Kovarik, R.S. Wegeng, R. A. Dagle, Methane and ethane steam reforming over MgAl2O4-Supported Rh and Ir catalysts: catalytic implications for natural gas reforming application, Catalysts 9 (2019) 801, https://doi.org/10.3390/catal9100801.

[61] B.T. Schädel, M. Duisberg, O. Deutschmann, Steam reforming of methane, ethane, propane, butane, and natural gas over a rhodium-based catalyst, Catal. Today 142 (2009) 42–51, https://doi.org/10.1016/j.cattod.2009.01.008.

[62] O. Schmidt, A. Gambhir, I. Staffell, A. Hawkes, J. Nelson, S. Few, Future cost and performance of water electrolysis: an expert elicitation study, Int. J. Hydrog. Energy 42 (2017) 30470–30492, https://doi.org/10.1016/j.ijhydene.2017.10.045.

[63] Schmidt, P., Weindorf, W., 2016. Power-to-Liquids: Potential and Perspectives for the Future Supply of Renewable Aviation Fuel.

[64] B. Shri Prakash, S. Senthil Kumar, S.T. Aruna, Properties and development of Ni/YSZ as an anode material in solid oxide fuel cell: A review, Renew. Sustain. Energy Rev. 36 (2014) 149–179, https://doi.org/10.1016/j.rser.2014.04.043.

[65] J.S. Sravan, A. Tharak, S.V. Mohan, Status of biogas production and biogas upgrading: a global scenario, in: Emerging Technologies and Biological Systems for Biogas Upgrading, Elsevier, 2021, pp. 3–26, https://doi.org/10.1016/B978-0-12-822808-1.00002-7.

[66] C.M. Stoots, J.E. O'Brien, J.S. Herring, J.J. Hartvigsen, Syngas production via high-temperature coelectrolysis of steam and carbon dioxide, J. Fuel Cell Sci. Technol. 6 (2009), 011014, https://doi.org/10.1115/1.2971061.

[67] Sunfire. 2023. Renewable hydrogen project "Multiplhy": World's largest high-temperature electrolyzer from Sunfire successfully installed. Available at: https://www.sunfire.de/en/news/detail/renewable-hydrogen-project-multiplhy-worlds-largest-high-temperature-electrolyzer-from-sunfire-successfully-installed. (Accessed: 18.4.2023).

[68] Sunfire. 2023a. SUNFIRE-HYLINK SOEC. Available at: https://www.sunfire.de/files/sunfire/images/content/Sunfire.de%20(neu)/Sunfire-Factsheet-HyLink-SOEC-20210303.pdf. (Accessed: 18.4.2023).

[69] Surgenor, C., 2021. SAF could make up 5.5% of 2030 EU jet fuel demand with targeted support, estimates ICCT feedstock study. Available at: https://www.greenairnews.com/?p=749. (Accessed: 2.1.2023).

[70] Thyssenkrupp. 2022. The Carbon2Chem Project. Available at: https://www.thyssenkrupp.com/en/newsroom/content-page-162.html. (Accessed: 21.12.2022).

[71] S. Vaz, A.P. Rodrigues de Souza, B.E. Lobo Baeta, Technologies for carbon dioxide capture: a review applied to energy sectors, Clean. Eng. Technol. 8 (2022), 100456, https://doi.org/10.1016/j.clet.2022.100456.

[72] Yao Wang, T. Liu, L. Lei, F. Chen, High temperature solid oxide $H2O/CO_2$ co-electrolysis for syngas production, Fuel Process. Technol. 161 (2017) 248–258, https://doi.org/10.1016/j.fuproc.2016.08.009.

[73] Yuan Wang, L. Zhao, A. Otto, M. Robinius, D. Stolten, A review of post-combustion CO_2 capture technologies from coal-fired power plants, Energy Procedia 114 (2017) 650–665, https://doi.org/10.1016/j.egypro.2017.03.1209.

[74] E. Worrell, L. Price, N. Martin, C. Hendriks, L.O. Meida, Carbon dioxide emissions from the global cement industry, Annu. Rev. Energy Environ. 26 (2001) 303–329, https://doi.org/10.1146/annurev.energy.26.1.303.

[75] C. Wulf, P. Zapp, A. Schreiber, Review of Power-to-X demonstration projects in Europe, Front. Energy Res. 8 (2020) 191, https://doi.org/10.3389/fenrg.2020.00191.

[76] H. Xu, B. Chen, J. Irvine, M. Ni, Modeling of CH4-assisted SOEC for H2O/CO_2 co-electrolysis, Int. J. Hydrog. Energy 41 (2016) 21839–21849, https://doi.org/10.1016/j.ijhydene.2016.10.026.

[77] G. Zang, P. Sun, A.A. Elgowainy, A. Bafana, M. Wang, Performance and cost analysis of liquid fuel production from H2 and CO_2 based on the Fischer-Tropsch process, J. CO_2 Util. 46 (2021), 101459, https://doi.org/10.1016/j.jcou.2021.101459.

Journal Article IV

Journal of CO2 Utilization 75 (2023) 102563

Contents lists available at ScienceDirect

Journal of CO2 Utilization

journal homepage: www.elsevier.com/locate/jcou

Techno-economic assessment of a power-to-green methanol plant

Simon Pratschner [a,*,1], Frank Radosits [b,2], Amela Ajanovic [b,3], Franz Winter [a,4]

[a] Technische Universität Wien, Faculty of Technical Chemistry, Institute of Chemical, Environmental and Bioscience Engineering, Getreidemarkt 9/166, 1060 Vienna, Austria

[b] Technische Universität Wien, Faculty of Electrical Engineering and Information Technology, Institute of Energy Systems and Electrical Drives, Gußhausstraße 25-29, 1040 Vienna, Austria

ARTICLE INFO

Keywords:
Green methanol
Techno-economic assessment
Power-to-Liquid
Hybrid renewable power plant
Carbon capture and utilization

ABSTRACT

Power-to-Liquid plants are a potential linchpin of future energy systems. Economic evaluations are crucial to assess their competitiveness with conventional fossil-based and other innovative processes. A techno-economic assessment of a previously presented plant concept producing green methanol was performed, evaluating different scenarios based on the net present value and annuity method. A hybrid plant was designed to realize an availability comparable to industrial plants. Green methanol prices of 717–1107 €$_{2022}$/t are required to realize amortization periods between 5 and 25 years. Net production costs of 785 €$_{2022}$/t were obtained for the base scenario, a surcharge of 44% compared to German methanol prices in 2022. CO_2 prices of 220–310 €$_{2022}$/t are necessary to become cost-competitive with fossil-based methanol. A sensitivity analysis underscored the grid electricity price's negligible influence on the plant's economic performance due to the implemented hybrid power plant. Green methanol has the potential to decrease the chemical industry's carbon footprint while simultaneously substituting fossil imports with local CO_2 sources. The presented study provides a concept tackling Power-to-Liquid plants' major drawbacks by concurrently maximizing annual operating hours and economic performance due to the utilization of renewable electricity. Consequently, stable long-term scenarios for interested investors were established.

1. Introduction

Global mean temperatures will rise significantly without concrete action, increasing the probability of extreme weather conditions and drought periods. Global CO_2 emissions of over 36 Gt/a were reported by the International Energy Agency in 2020 [9]. According to the summary for policymakers within the latest IPCC synthesis report, maintaining annual CO_2 emissions at the 2019 level from 2020 to 2030 would almost exhaust the 1.5 °C limit carbon budget and deplete more than a third of the 2 °C goal's carbon budget [56]. In addition, due to multiple crises soaring natural gas and electricity prices in 2022 shook the European Union's energy markets and several industries entailing inflation rates of around 9% [49].

Power-to-Liquid (PtL) technologies can potentially mitigate global warming and the energy crisis' ramifications by valorizing CO_2, water and electricity to chemical feedstocks or liquid energy carriers, e.g., methanol. However, the following conditions need to be fulfilled when producing green methanol according to Roode-Gutzmer et al. [26]:

- The carbon source must be a waste product.
- Utilized hydrogen must not be derived from fossil sources.
- The required process energy must be provided by renewable energy sources.

Abbreviations: AEL, Alkaline Electrolyzer; AP, Amortization period; CAPEX, Capital expenditure; Capt., Capture; CEPCI, Chemical Engineering Plant Cost Index; CHP, Combined heat and power; Comm, Commissioning; DME, Dimethyl ether; ETS, EU Emissions Trading System; Equip, Equipment; FLH, Full load hours; IMPCA, International Methanol Producers and Consumers Association; LCDH, Levelized cost of district heating; LCOE, Levelized cost of electricity; Main, Maintenance; MEA, Monoethanolamine; MeOH, Methanol; Mil, Million; MTBE, Methyl tert-butyl ether; OPEX, Operational expenditure; PtL, Power-to-Liquid; PV, Photovoltaic; PVGIS, Photovoltaic Geographical Information System; USD, US dollar.

* Corresponding author.
E-mail address: simon.pratschner@tuwien.ac.at (S. Pratschner).
[1] ORCiDs: 0000-0001-6167-586X
[2] ORCiDs: 0000-0002-4961-4455
[3] ORCiDs: 0000-0001-6840-806X
[4] ORCiDs: 0000-0001-9854-3836

https://doi.org/10.1016/j.jcou.2023.102563
Received 4 July 2023; Received in revised form 3 August 2023; Accepted 8 August 2023
Available online 15 August 2023

Nomenclature

Parameters

C	Costs €$_{2022}$.
CRF	Capital recovery factor -.
d	Scaling exponent -.
FCI	Fixed capital investment €$_{2022}$.
i	Discount rate -, %.
I_0	Initial investment €$_{2022}$.
m	Mass flow rate kg/s, t/h.
NPC	Net production costs €$_{2022}$.
NPV	Net present value €$_{2022}$.
n, t	Investment period a.
P	Price €$_{2022}$.
Plant availability	h/a.
η	Fuel efficiency %.

A legal framework regarding the definition of green H_2 is currently being established by a European consortium cofounded by the European Union. According to this initiative, hydrogen produced by water electrolysis can be classified as green if a minimum emission reduction of 75% compared with hydrogen production via steam reforming can be guaranteed [32]. However, no official legal standards have yet been established concerning the requirements of renewable methanol. A possible solution for PtL plants powered with grid electricity is to establish direct purchase contracts with operators of renewable power plants, e.g., wind parks or photovoltaic (PV) farms.

Power-to-Green methanol plants potentially profit from low production costs of renewable electricity compared with 2022 grid electricity prices while ensuring an ecological operation due to the utilization of low-emission electricity.

Substituting fossil-based methanol with green methanol has the potential to cut CO_2 emissions by up to 95% [63]. The most significant factor is the electricity source's CO_2 footprint, e.g., 0.004 kg CO_2/kWh$_{el.}$ for wind power [75] and 0.067 kg CO_2/kWh$_{el.}$ for photovoltaic power [16]. Additional factors are the CO_2 footprints of the used biomass, operating materials and applied equipment.

A list of commissioned and planned methanol plants utilizing CO_2 as a feedstock is given in Table 1.

Conventional methanol production is still solely based on fossil feedstocks, i.e., natural gas and coal. Over 90 methanol plants operate worldwide with a combined annual production capacity of 110 million metric tons. The global daily methanol consumption amounts to 200,000 metric tons, making the methanol sector an industry obtaining around $55 billion annual turnover [62]. The main fields of application are the utilization as a precursor in the chemical industry, e.g., formaldehyde and acetic acid, as well as fuel applications, e.g., direct combustion or methyl tert-butyl ether (MTBE) production [26]. General information concerning state-of-the art reactor and plant design is given by Petersen et al., Dietrich et al. [1,7] and Haldor Topsoe [54]. Lange provided a comprehensive review of technology improvements' historical background [15]. Cu-based catalysts are applied for the methanol synthesis based on CO and CO_2 hydrogenation. Detailed information concerning the catalyst system is given by Ruland et al. [27]. A purity of over 99.85 wt% is required to adhere to standards introduced by the International Methanol Producers and Consumers Association (IMPCA) [55]. State-of-the-art methanol plants include a two-staged distillation process to realize the required degree of purity [36].

An extensive review analyzing technical and economic details of renewable methanol production was conducted by Roode-Gutzmer et al. Around 90% of the European methanol industry, mainly based on the steam reforming of natural gas, is located in Germany. Producing methanol in Europe is more expensive compared with other regions, e.g., the USA, Ukraine, Russia and China, due to increased feedstock prices [26]. A technical comparison between conventional and green methanol production based on CO_2 was provided by Bowker. Increased shares of CO_2 in the syngas result in a decreased per-pass conversion in the methanol reactor. Furthermore, more water is produced due to the occurrence of the reverse water-gas shift reaction in addition to the water produced via the direct CO_2 hydrogenation to methanol [3]. Milder process conditions are required for processes utilizing CO_2 instead of CO as a precursor. In addition, a higher methanol selectivity can be realized, resulting in fewer impurities inside the crude methanol [19]. Thermodynamic and kinetic studies of Power-to-Green methanol processes were conducted by Leonzio et al., stating a maximum CO_2 conversion of 69% at 473 K and 55 bar including the recirculation of unconverted gases [17].

Brynolf et al. provided an extensive review of the production costs of electrofuels, i.e., methanol, Fischer-Tropsch fuels and dimethyl ether (DME). No significant difference could be found between methanol and DME production. However, producing Fischer-Tropsch products entails an increase in net production costs due to the increased product separation expenditure [4]. A comprehensive elaboration of techno-economic evaluations of processes based on CO_2 as a feedstock is given by Otto [23]. Net production costs of 1.16–1.56 €$_{2022}$/kg methanol were obtained in a techno-economic assessment of off-grid Power-to-Fuel systems conducted by Decker et al. [5]. Schemme analyzed and assessed different production routes processing CO_2 into fuels [28]. Economic evaluations of carbon capture and utilization processes producing methanol conducted by Nyari et al. and Yousaf et al. resulted in methanol net production costs of 1.61–1.91 €$_{2022}$/kg methanol and 0.66–0.95 €$_{2022}$/kg methanol respectively [22,35].

The presented work aims to economically evaluate a previously introduced concept study of a Power-to-Green methanol plant [25]. The established plant concept is coupled with a newly established hybrid power plant combining wind power, photovoltaic power, a combined heat and power process (CHP) with a connection to the local electricity grid. This concept aims at substantially increasing the plant's availability to industrial standards which has been a major drawback of Power-to-Liquid plants based on renewable power sources so far. In addition, previous techno-economic assessments of green methanol plants are founded on pre-crisis economic assumptions. The underlying study has the potential to provide an alternative to plants based on fossil

Table 1
Commissioned and planned methanol plants utilizing CO_2 as feedstock.

Company/Project	Site	Year	Output	Status	Source
George Olah plant	Svartsengi, ISL	2011	4000 t/a	Commissioned	[19]
MefCO_2	Niederaußem, GER	2019	500 t/a	Commissioned	[3]
Haru Oni	Punta Arenas, CHI	2022	350 t/a	Commissioned	[67]
Shunli CO_2-to-Methanol	Henan, CHN	2022	110,000 t/a	Commissioned	[41]
M2SAF	-	Ongoing	Demo plant	Design phase	[65]
E-CO_2Met	Leuna, GER	Ongoing	Pilot plant	Design phase	[51]
Finnjord e-Methanol	Finnjord, NOR	Ongoing	100,000 t/a	Design phase	[40]
Sailboat CO_2-to-Green Methanol	Jiangsu, CHN	2023	100,000 t/a	Comm. in 2023	[42]
CiP	Aalborg, DEN	2027	130,000 t/a	Comm. in 2027	[66]

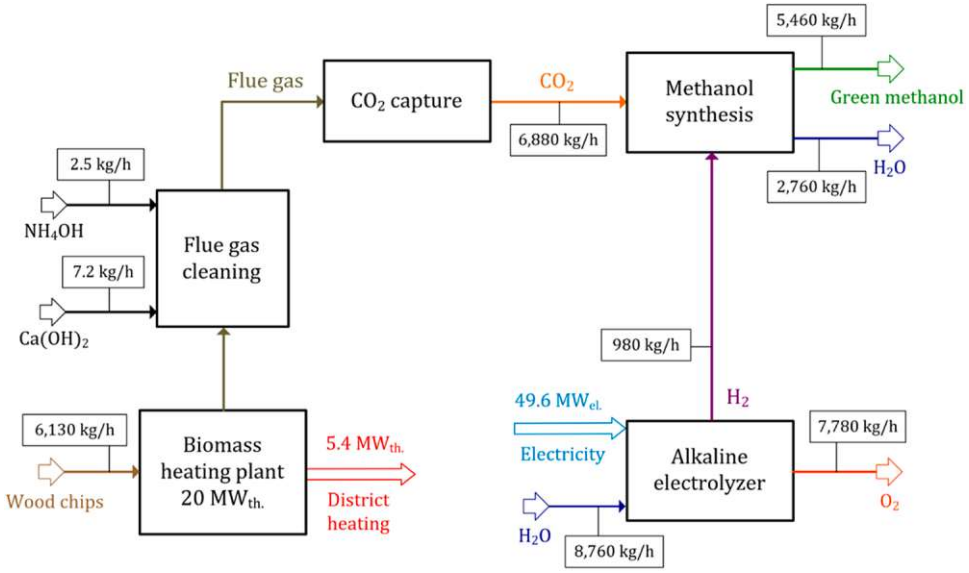

Fig. 1. Overview of the Power-to-Green methanol plant based on Pratschner et al. [25].

Table 2
Overview of the Power-to-Green methanol plant's subprocesses and scale.

Subprocess	Parameter	Value
Biomass heat. plant	Thermal load	20 $MW_{th.}$
CO_2 capture	CO_2 mass flow rate	6880 kg/h
MeoH synthesis	Methanol mass flow rate	5458 kg/h (30.2 MW_{MeOH})
Alk. electrolyzer	Rated power	49.6 $MW_{el.}$

feedstocks. A techno-economic assessment has been conducted based on previous findings concerning the plant's mass and energy balances to answer the following research questions:

1. What is the required surcharge for green methanol to make investments in Power-to-Green methanol plants a competitive alternative to conventional fossil-based processes?
2. Which CO_2 price is necessary to shift future investments from fossil-based processes toward the realization of green methanol plants?

2. Methodology

The underlying study is based on a previous study [25] focusing on the design and evaluation of a Power-to-Green methanol plant. An overview of the plant concept with a total electricity consumption of 52 $MW_{el.}$, including significant mass flow rates and energy streams, is displayed in Fig. 1. The CO_2 capture unit's heat demand is covered by the biomass heating plant. The Power-to-Green methanol plant consists of the following subprocesses:

- A biomass heating plant using wood chips as fuel.
- Post-combustion CO_2 capture realized by an monoethanolamine (MEA) absorption unit.
- Methanol synthesis via direct hydrogenation of CO_2.
- Alkaline water electrolysis.

Over 6 tons of wood chips per hour are combusted in a bubbling fluidized bed to supply a decentralized biomass heating plant based on a heating duty of 20 $MW_{th.}$. Calcium hydroxide and ammonium hydroxide are inserted to the flue gas cleaning unit to remove sulfur and nitrogen oxides. Subsequently, the flue gas stream is conveyed to the MEA absorption-based CO_2 capture unit. MEA absorption has been industrially established for several decades and is provided by multiple suppliers at the required scale and thus can be deployed faster compared to other CO_2 capture technologies. In the next process step, the CO_2 stream exiting the desorber is purified in a catalyst guard bed to prevent catalyst deactivation, pressurized and mixed with H_2 provided by the electrolyzer. An alkaline electrolyzer was chosen for the presented study due to its lower specific H_2 production costs, higher annual operating hours and market availability [73] compared with a proton exchange membrane electrolyzer. A hybrid power plant is implemented into the presented plant concept to guarantee a steady supply with electricity, as required for a feasible operation of alkaline electrolyzers. The CO_2/H_2 mixture is subsequently mixed with recirculated, unconverted gases and converted to methanol and water in a state-of-the-art fixed-bed boiling water reactor.

In addition, the energy supply system has been elaborated by designing a hybrid renewable power plant consisting of a wind park, a PV farm and the biomass heating plant's internal combined heat and power process. The goal was to realize a plant availability of 8000 h per year while maximizing the exploitation of renewable energy sources. Table 2 summarizes the subprocesses' respective design scales.

2.1. Economic modeling and assessment

Choosing realistic parameters is a keystone when conducting a techno-economic assessment. The discount rate is an essential parameter to evaluate an investment and future cash flows. In addition, it compares an investment's risk with alternative investment choices [45]. A discount rate of 8% has been chosen as a basis for subsequent dynamic economic models [20]. An investment period of 25 years was assumed with a plant availability of 8000 h/a, adhering with modern standards of industrial chemical plants according to Walas et al. [33]. Comparable studies assumed annual operating hours between 7000 and 8000 [5,21].

2.1.1. Net present value and net production costs of green methanol

Determining an investment's net present value (NPV) is a viable method for comparing the economic performance of the Power-to-Green methanol plant with comparable investment opportunities. The NPV is defined as the sum of the present value of obtained cash flows within the defined investment period t including the initial fixed capital investment (FCI), as shown in Eq. 1 [30]. Thus, considering the time value of money by discounting future cash flows based on the chosen discount rate i. The amortization period AP of an investment, in years, is defined as the required time after which the annual cash flows' sum equals the initial

Table 3
Fixed capital investment of the respective subprocesses.

Subprocess	Scaling exponent	Source	50 $MW_{el.}$ AEL[1)]	100 $MW_{el.}$ AEL[2)]
Biomass CHP	0.70	[12]	31.7 mil. €[3)]	51.5 mil. €
CO_2 capture	0.65	[18]	29.1 mil. €	45.6 mil. €
MeOH synthesis	0.80	[28]	18.3 mil. €	31.8 mil. €
Alk. electrolyzer	0.90	[34]	33.9 mil. €	63.3 mil. €
Grid connection	1.00	[60]	5.6 mil. €	11.2 mil. €
SUM	-	-	118.6 mil. €	203.4 mil. €

1) Corresponds with 30.2 MW_{MeOH}. Detailed information is provided in the appendix 2) Corresponds with 60.4 MW_{MeOH}. 3) All values in $€_{2022}$.

fixed capital investment FCI, as shown in Eq. 2.

$$NPV = FCI + \sum_{n=1}^{t} \frac{Cash\ flow_n}{(1+i)^n} \tag{1}$$

$$0 = FCI + \sum_{n=1}^{AP} \frac{Cash\ flow_n}{(1+i)^n} \tag{2}$$

The net production costs (NPC) of green methanol are based on the annual operational expenditure (OPEX), the revenue of by-products, i.e., district heating and oxygen, and the capital cost determined by the annuity method, dependent on the discount rate i and the investment period n, see Eqs. 3 and 4.

$$NPC = \frac{Annuity + OPEX - Revenue}{Annual\ methanol\ production} \tag{3}$$

$$Annuity = FCI \cdot \frac{(1+i)^n \cdot i}{(1+i)^n - 1} \tag{4}$$

2.1.2. Equipment and plant cost escalation, scale and conversion

Cost escalation for equipment was considered based on the chemical engineering plant cost index (CEPCI) provided by the Chemical Engineering magazine. An overview of major categories and their weighting is given in [2]. Cost data found in literature and reports were converted to 2022 levels by applying Eq. 5.

$$Costs_{2022} = Costs_{Base\ year} \cdot \left(\frac{CEPCI_{2022}}{CEPCI_{Base\ year}}\right) \tag{5}$$

In addition, a location factor of 1.11 has been applied to convert U.S. Gulf Coast price levels to German price levels [30]. The average exchange rate of 1.05 USD/€ in 2022 [69] has been assumed for converting cost data only available in USD.

Scaling cost data from literature $Scale_{Base}$, e.g., available in mass flow rates, reactor volume or power input, to the designed plant capacity $Scale_{Design}$ is realized with Eq. 6. Detailed information concerning the scaling exponent d for specific equipment or whole industries is elaborated on in various studies [14,24,29–31]. The assumed scaling exponents in this study are listed in Table 3.

$$Costs_{Design} = Costs_{Base} \cdot \left(\frac{Scale_{Design}}{Scale_{Base}}\right)^d \tag{6}$$

2.1.3. Fixed capital investment

A factorial method was chosen to determine the total required fixed capital investment FCI based on derived equipment costs [24,29,30], as shown in Eq. 7. Various cost items, e.g., engineering, process controlling and pipe installation, are considered by applying a factor to the equipment costs. Seider et al. propose a Lang factor of 5.04 for fluid processing plants under current economic circumstances [29].

$$FCI = 5.04 \cdot \sum Costs_{Equipment} \tag{7}$$

2.1.4. Operational expenditure, revenue and annual cash flow

The required OPEX are divided into fixed OPEX, e.g., labor, maintenance, insurance and taxes, and variable OPEX, e.g., feeds, electricity and consumables. Two different approaches proposed by Towler and Sinnot [30], as well as Neuling and Kaltschmitt, [21], were applied to assess the presented Power-to-Green methanol plant's fixed OPEX. The variable OPEX were calculated based on the mass and energy balances of the previously conducted concept study [25]. Variable cost items include the feed stream of wood chips into the biomass heating plant, electricity, fresh MEA for the CO_2 capture unit, flue gas cleaning consumables, deionized water and waste water treatment. Non-recurrent expenditures occur every three years due to the required replacement of the $Cu/ZnO/Al_2O_3$ catalyst loading inside the methanol synthesis reactor [21] and every ten years to replace the electrolyzer's stack, resulting in costs of 14% of the electrolyzer's fixed capital investment [5,6].

Revenue is generated by selling the main product, green methanol, as well as the by-products oxygen and district heating. The current prices of conventional fossil-based methanol can be found on the Methanol Institute's website and various market analysis databases [40,61]. A value of 545 $€_{2022}$/t methanol (German market) was chosen as a comparative value. The generated turnover by district heating is based on an internal calculation to find the levelized cost of district heating (LCDH) for the underlying biomass heating plant, as given in Eq. 8. The capital recovery factor (CRF), see Eq. 9, was multiplied by the biomass heating plant's fixed capital investment FCI to obtain the required annual interest payment. Fixed C_{Fixed} and miscellaneous OPEX $C_{Misc.}$, e.g., land renting and insurance, were subsequently added to the required annual payment rate and divided by the plant's full load hours (FLH). A reduced heat supply to the district heating network was assumed for the summer months. In accordance with the underlying study, a fuel efficiency of 90% was chosen. The produced electricity is transferred to the alkaline electrolyzer and, thus, is not considered. Additionally, the price of wood chips P_{WC} and other variable costs $C_{Var.}$ were counted in, resulting in LCDH of 0.076 €/$kWh_{th.}$. A selling price of 0.09 €/$kWh_{th.}$ was chosen to ensure a sufficient turnover while leaving a considerable margin of safety compared with district heating market prices in Austria, which accounted for around 0.12 €/$kWh_{th.}$ in 2022 [39]. Oxygen was assumed to be sold for 81.3 $€_{2022}$/t O_2 [35].

$$LCDH = \frac{CRF \cdot FCI + C_{Fixed} + C_{Misc.}}{FLH} + \frac{P_{WC}}{LHV \cdot \eta} + C_{Var.} \tag{8}$$

$$CRF = \frac{(1+\mathrm{i})^n \cdot i}{(1+\mathrm{i})^n - 1} \tag{9}$$

The yearly cash flow was determined by subtracting fixed and variable OPEX from the annual revenue generated by the sale of methanol, oxygen and district heating.

$$Cash\ flow_n = Revenue_n - \mathrm{OPEX}_{Fixed,n} - \mathrm{OPEX}_{Variable,n} \tag{10}$$

2.2. Energy system modeling

Designing Power-to-Liquid plants is a balancing act between maximizing the plant's availability to realize a short investment payback period and maximizing the supply power's share of renewable electricity. Renewable power sources, e.g., wind and PV, underlie daily and seasonal intermittency, thus, decreasing the operating hours of Power-

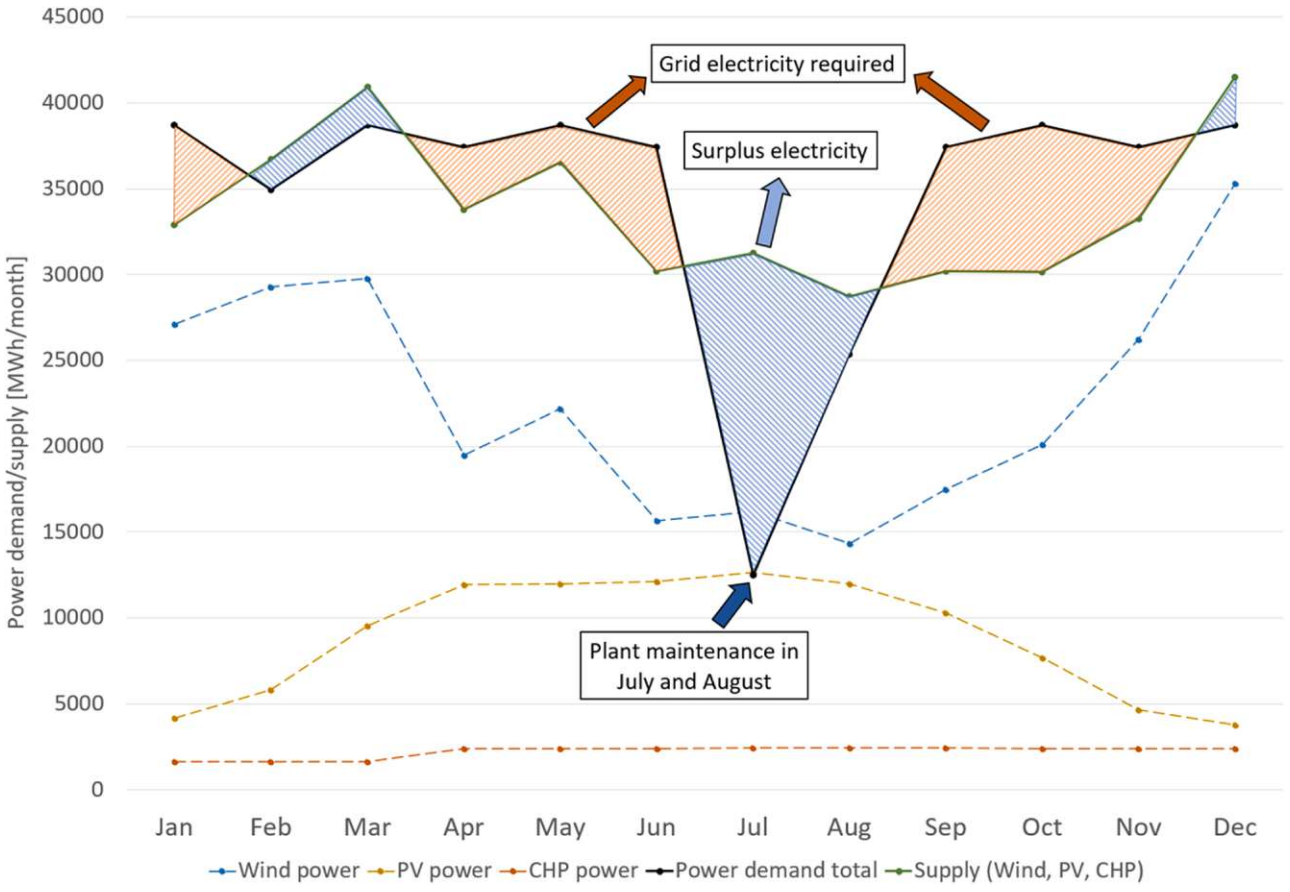

Fig. 2. Power demand curve of the Power-to-Green methanol and power supply curve of the hybrid renewable power plant.

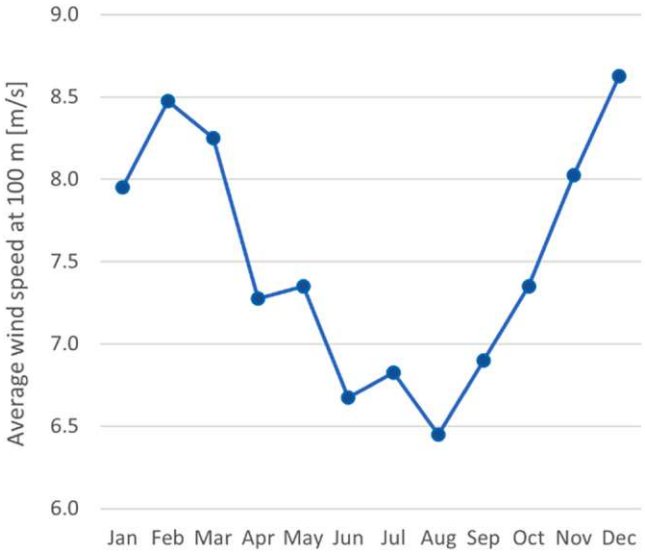

Fig. 3. Average wind speed in Neusiedl am See, Austria [74].

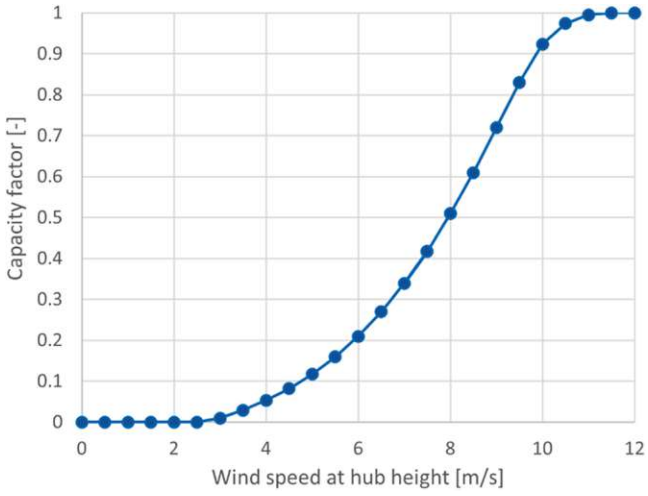

Fig. 4. Capacity factor of a windmill as a function of the wind speed at hub height.

to-Liquid plants to values below 3000 h/a. One objective of the presented study was to design a renewable hybrid power plant, combining wind, solar and the CHP process's power output, as an electricity source for the PtL plant to maximize the share of utilized renewable electricity and simultaneously realize a plant availability of 8000 h/a. Fig. 2 shows the PtL plant's demand curve and the hybrid plant's power supply curve. Detailed monthly power balances are provided in table A.4 in the appendix. The converse seasonal behavior of wind power, obtaining a maximum yield in winter, and solar power, obtaining a maximum yield in summer, results in a dampened power supply curve. However, a complete harmonization of the two curves is not possible. Hence, covering the difference with grid electricity is necessary for a continuous plant operation. In addition, green surplus electricity is fed into the local electricity grid when the hybrid power plant's supply exceeds the Power-to-Green methanol plant's demand. A maximum of surplus electricity is obtained in July and August due to plant maintenance.

Power input of 52 $MW_{el.}$ is required for H_2 provision and utilities, e.

Table 4
Annual fixed OPEX based on two methods [21,30] for the base scenario based on an electrolyzer with a rated power of 50 $MW_{el.}$.

	[30]			[21]		
Fixed OPEX[1)]	Factor	Base	OPEX	Factor	Base	OPEX
Labor	-	-	2.37 mil. €[2)]	0.005	FCI_{Total}	0.59 mil. €
Main. CHP	0.05	FCI_{CHP}	0.95 mil. €	0.015	FCI_{CHP}	0.48 mil. €
Main. CO_2 capt.	0.03	FCI_{CO2}	0.87 mil. €	0.015	FCI_{CO2}	0.44 mil. €
Main. MeOH	0.03	FCI_{MeOH}	0.55 mil. €	0.015	FCI_{MeOH}	0.27 mil. €
Main. electr.	0.03	FCI_{AEL}	1.02 mil. €	0.03	FCI_{AEL}	1.02 mil. €
Main. grid	0.03	FCI_{Grid}	0.17 mil. €	0.015	FCI_{Grid}	0.08 mil. €
Land renting	0.01	FCI_{Total}	1.19 mil. €	-	-	-
Property taxes	0.01	FCI_{Total}	1.19 mil. €	-	-	-
Insurance	0.01	FCI_{Total}	1.19 mil. €	0.01	FCI_{Total}	1.19 mil. €
Administration	-	-	-	0.005	FCI_{Total}	0.60 mil. €
Unforeseen expenses	-	-	-	0.01	FCI_{Total}	1.19 mil. €
Additional costs	-	-	-	0.0075	FCI_{Total}	0.89 mil. €
SUM	-	-	9.50 mil. €	-	-	6.75 mil. €
Stack replacement[3)]	0.14	FCI_{AEL}	4.75 mil. €	0.14	FCI_{AEL}	4.75 mil. €

1) All values in $€_{2022}$/a. 2) Includes five shift positions, supervision, management and labor overhead costs. 3) Stack replacement is required every ten years.

g., syngas compression and gas blowers. The hybrid plant's respective rated power levels were defined at 71.4 MWp for the wind park and 80 MWp for the photovoltaic farm to adapt and dampen the supply curve's yearly variation. The system's main objective is the production of green methanol. Hence, to avoid distorting the plant's economic performance due to increasingly large feed-in ratios, a cap was defined at a maximum surplus electricity share of 10% of the Power-to-Green methanol plant's annual power demand. A detailed elaboration of the hybrid plant's specifications is given in the following chapters.

2.2.1. Wind farm

The wind farm's design is based on data from the Global Wind Atlas 3.0 provided by the Technical University of Denmark (DTU) [74]. An average wind velocity at a hub height of 100 m of 7.5 m/s is obtained for the chosen region Neusiedl am See, Austria (Latitude: 47.947°, Longitude: 16.907°). The wind speed's seasonal variation at the selected location is depicted in Fig. 3. The E-138 EP3 E2 model with a rated power of 4.2 MWp by the largest German windmill provider Enercon was chosen for the underlying study. Detailed information concerning the turbine's specifications and power yield can be found on the company's website [47]. Subsequently, the wind farm's monthly power yield is calculated by determining the wind mills' capacity factor at the average wind speed for the respective months, see Fig. 4.

2.2.2. Photovoltaic farm

The photovoltaic farm's monthly power yield is obtained from the Photovoltaic Geographical Information System (PVGIS version 5.2) online tool provided by the European Commission [48]. Similar to chapter 2.3.1, Neusiedl am See, Austria (Latitude: 47.947°, Longitude: 16.907°) was chosen as the PV farm's location. Optimizing the PV panels' orientation resulted in an ideal slope of 38 and an azimuth of − 1°. Monthly power yields are based on standard crystalline silicon PV technology and the PVGIS-SARAH2 database with an assumed system loss of 5%.

2.2.3. Levelized cost of electricity, grid electricity price and feed-in rate

The electricity costs for the Power-to-Green methanol concept were calculated based on the capital recovery factor, see Eq. 9, and the levelized cost of electricity (LCOE) method, as stated in Eq. 11. According to the Global Wind Atlas, 2900 full load hours can be realized at the chosen location. A value of 1100 full load hours was assumed concerning the photovoltaic farm. Investment costs of technology pathway scenarios until 2050 were used to calculate the LCOE [8]. The capital recovery factor CRF multiplied by the investment costs I_0 of 1267 €/kW for wind and 700 €/kW for utility-scale PV gives the annual payment to the loan provider. In addition, the fixed OPEX C_{Fixed}, miscellaneous OPEX $C_{Misc.}$ and the variable OPEX $C_{Var.}$ must be considered. The chosen depreciation periods of the PV system and wind park were 25 years with interest rates of 3.5% and 4%, respectively. The European Commission provided yearly cost increases with plant age of the fixed operating costs [8]. On the contrary, learning effects for maintenance were also considered for this publication, leading to a 4% cost increase with plant age. The variable costs $C_{Var.}$ are low as no fuel input is required. The calculated LCOE for wind and solar electricity where then used as input for the electrolyzer's economic calculation and accounted in the variable OPEX. The biomass CHP's cost of electricity were not calculated separately because its CAPEX, OPEX, biomass input, etc. are considered within the total costs of methanol.

Average 2022 grid electricity prices were taken from Statistics Austria [71] to obtain the costs for the electricity purchase. A grid electricity price of 0.1753 $€_{2022}/kWh_{el.}$, including grid fees and value-added tax, was chosen for the underlying study. It is currently custom at Burgenland Energie and other energy suppliers to pay the market price as a feed-in tariff. Therefore, the feed-in tariff in this work was also set as the same amount as the grid electricity price.

$$LCOE = \frac{CRF \cdot I_0 + C_{Fixed} + C_{Misc.}}{FLH} + C_{Var.} \quad (11)$$

3. Results

The following chapter presents various economic scenarios to evaluate the economic feasibility of the proposed Power-to-Green methanol concept. These scenarios include base cases, amortization calculations, CO_2 tax examinations and the calculation of net production costs. Calculating the required fixed capital investment, operational expenditure and potential revenue provides the base of the conducted techno-economic assessment.

3.1. Foundation of the techno-economic assessment

3.1.1. Fixed capital investment

The presented Power-to-Green methanol plant concept consists of four main subprocesses, i.e., biomass heating plant, MEA CO_2 capture, methanol synthesis and an alkaline electrolyzer. An additional investment must be undertaken to connect the plant to the electricity grid. Table 3 summarizes the required fixed capital investments of the respective subprocesses at an electrolyzer scale of 50 $MW_{el.}$ and 100 $MW_{el.}$. Total initial investments of 118.6 mil. $€_{2022}$ and 203.4 mil. $€_{2022}$ are required for plant scales of 30.2 and 60.4 MW_{MeOH}.

3.1.2. Fixed OPEX, variable OPEX and revenue for the base scenario

Annual values concerning fixed OPEX, variable OPEX and revenue are required to determine the Power-to-Green methanol plant's yearly

Table 5
Annual variable OPEX and revenue for the base scenario at a rated electrolyzer power of 50 $MW_{el.}$.

Consumable	Price	Unit	Base year	Source	$Price_{2022}$	Annual demand	Costs[1)]
Sum electricity[2)]	-	€/$kWh_{el.}$	-	-	-	416 $GWh_{el.}$	19.95 mil. €
Wood chips	115	€/t (dry)	2022	[37]	115	32,000 t	3.68 mil. €
Demineralized H_2O	0.12	€/m^3	2020	[35]	0.16	70,060 t	11,506 €
MEA	-	€/t	-	[10,18,57]	1761	183.4 t	334,258 €
$Ca(OH)_2$	485	€/t	2022	[44]	485	57.8 t	28,052 €
NH_4OH	-	€/t	-	[43,58]	182.2	19.6 t	3528 €
Waste water	-	€/m^3	-	[21,24,30]	1.52	24,536 m^3	37,283 €
CuO catalyst[3)]	31.2	€/kg	2018	[21]	42.2	13.2 t/load	558,171 €
SUM	-	-	-	-	-	-	24.23 mil. €
Product	Price	Unit	Base year	Source	$Price_{2022}$	Annual production	Revenue[1)]
Methanol	545[4)]	€/t	2022	[46]	545	43,663 t	23.80 mil. €
Oxygen	54	€/t	2016	[35]	81.3	68,832 t	5.60 mil. €
District heating	0.09	€/$kWh_{th.}$	2022	See chapter 2.2.4	0.09	43.05 $GWh_{th.}$	3.87 mil. €
SUM	-	-	-	-	-	-	33.27 mil. €

1) All values in $€_{2022}$/a. 2) See chapter 2.2.3 or table A4 in the appendix for detailed information. 3) Catalyst replacement every three years. 4) Methanol price – Germany, September 2022.

Table 6
Net present value of the Power-to-Green methanol plant after 25 years, selling at the current methanol market price of 545 $€_{2022}$/t (i = 0.08, t = 25 a, plant availability = 8000 h/a).

	50 $MW_{el.}$ electrolyzer[1)]	100 $MW_{el.}$ electrolyzer[1)]
Initial investment	118.6 mil. $€_{2022}$	203.4 mil. $€_{2022}$
Net present value	103.6 mil. $€_{2022}$	146.9 mil. $€_{2022}$

1) Corresponds with 30.2 MW_{MeOH} / 60.4 MW_{MeOH}.

cash flow. A summary of the annual fixed operational expenditure for methods introduced by Towler and Sinnot [30], as well as Neuling and Kaltschmitt [21], is given in Table 4. A substantial difference can be seen regarding labor costs. Towler and Sinnot provide a decision tree differentiating between plants processing fluids or solids, batch or continuous operation and stand-alone plants versus large sites [30], whereas Neuling and Kaltschmitt determine a plant's labor cost based on a fixed share of the total capital investment [21]. The average of the two analyzed methods is used in subsequent chapters.

Table 5 summarizes the annual variable OPEX and the plant's achieved annual turnover for the base scenario with a rated electrolyzer power of 50 $MW_{el.}$. Detailed information concerning the plant's power supply system is elaborated on in chapter 2.2. Prices of consumables and product revenue have been adapted to $€_{2022}$ levels by applying the CEPCI index, as explained in chapter 2.1.2.

The obtained LCOE of renewable electricity are 4.1 ct./kWh for onshore wind and 6.4 ct./kWh for PV. Those values lie within the range of the determined LCOE for Germany, as presented in a report published by the Fraunhofer ISE [13]. The range in the mentioned report results from different full load hours for these technologies depending on the location. The calculated value for wind lies on the lower end of the obtained intervals as the full load hours of this case study in Burgenland are relatively high, whereas the value for PV is on the upper end.

3.2. Economic assessment based on the market price of fossil methanol

The Power-to-Green methanol plant's initial scale is based on a 50 $MW_{el.}$ alkaline electrolyzer. Table 6 lists the required initial fixed capital investment and the net present value after 25 years of plant operation. No break-even point can be realized by selling green methanol at the current market price of 545 $€_{2022}$/t. Scaling up the plant to 100 $MW_{el.}$ does not significantly improve the plant's economic performance since alkaline electrolyzers do not substantially profit on a scale-up. Analyzing scenarios with electrolyzers exceeding a rated power of 100 $MW_{el.}$ is unrealistic as of today and, thus, is not considered in this study. In addition, the variable OPEX have a significantly larger impact

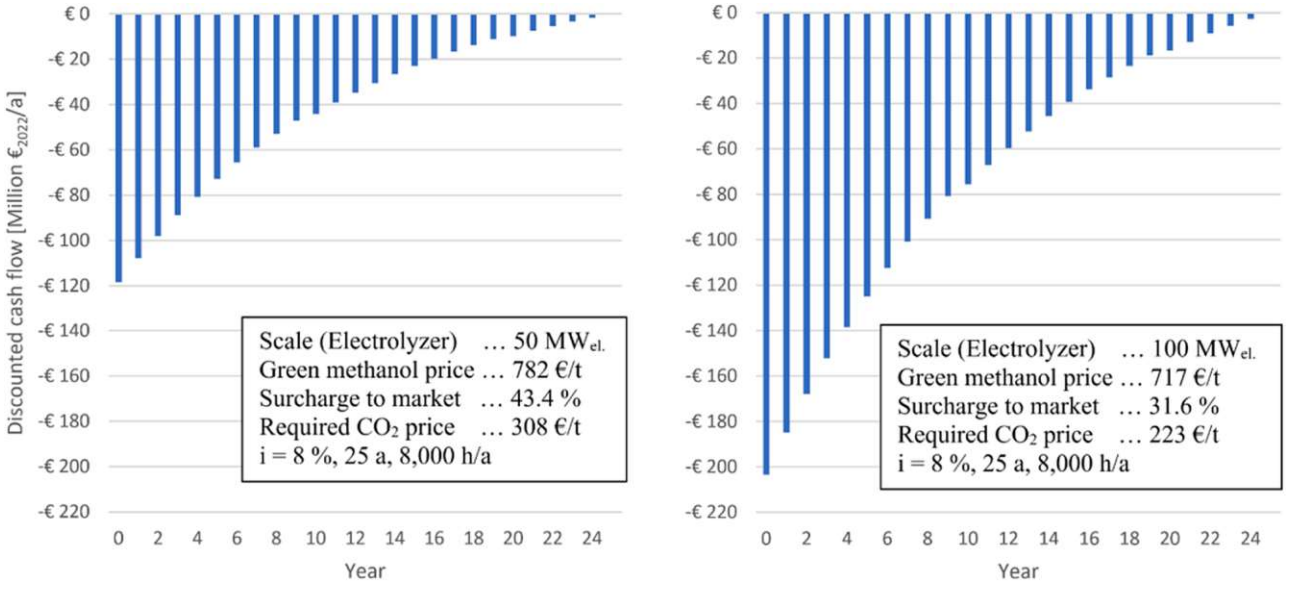

Fig. 5. Net present value of a Power-to-Green methanol plant for a non-profit scenario.

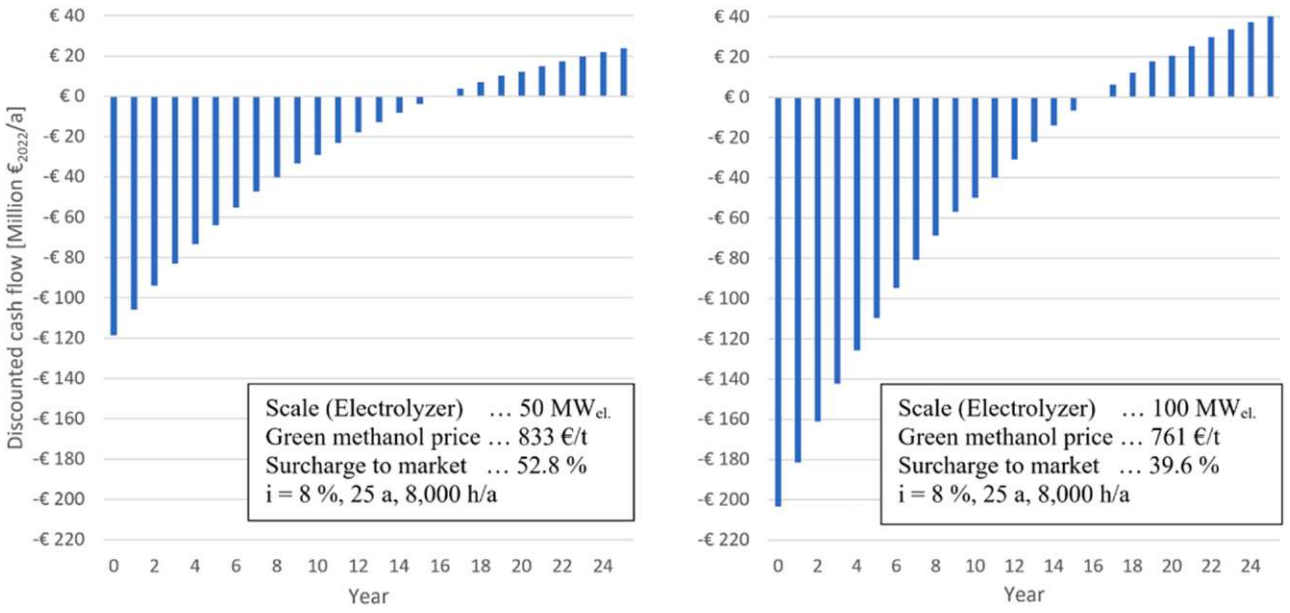

Fig. 6. Net present value of a Power-to-Green methanol plant with a desired amortization period of 15 years.

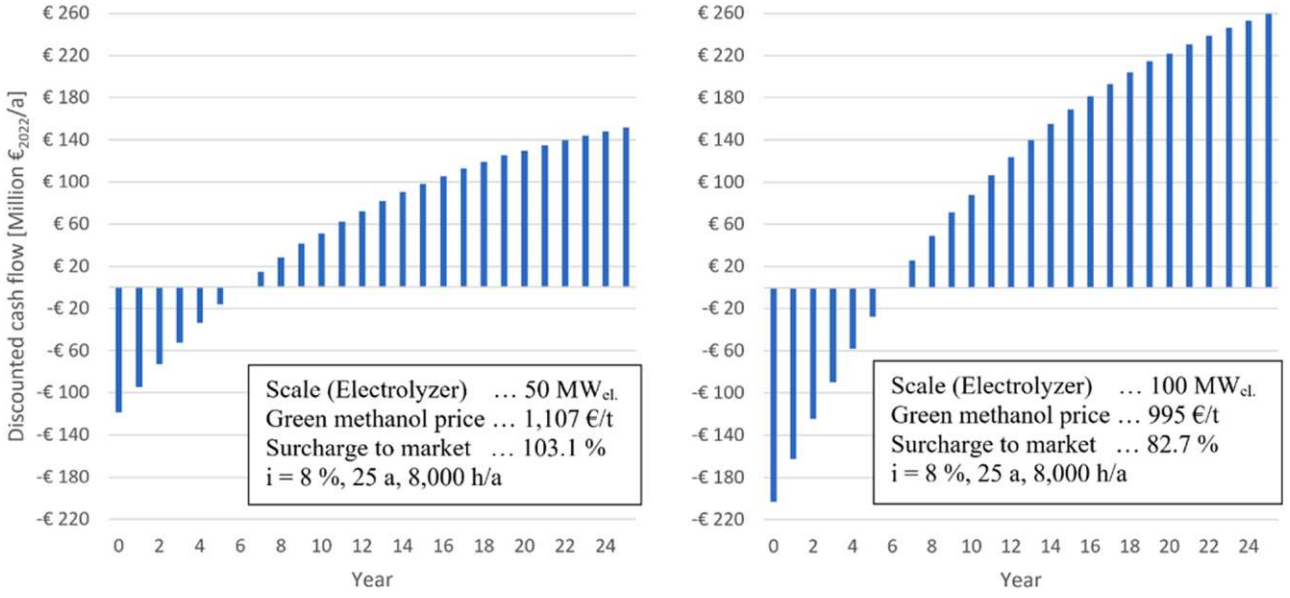

Fig. 7. Net present value of a Power-to-Green methanol plant with a desired amortization period of five years.

on the produced methanol's specific costs compared to the fixed capital investment's annuity. Business cases aiming at making Power-to-Green methanol plants an economically viable alternative to fossil methanol must either determine the required price level of green methanol to make the plant a worthwhile investment or focus on the required CO_2 price to make green methanol cost-competitive.

3.3. Required market price of green methanol

Determining the required market price of green methanol to create a potential business case is a crucial goal of the presented study. Within this chapter, different investment scenarios are elaborated by determining the required green methanol price for varying amortization periods of 5, 15 and 25 years. In addition to the desired amortization period, two plant scales, i.e., 50 $MW_{el.}$ and 100 $MW_{el.}$ were analyzed. All scenarios are based on a discount rate of 8%, an investment period of 25 a and a plant availability of 8000 h/a.

Fig. 5 displays two investment scenarios based on a non-profit investment. Green methanol prices of 782 $€_{2022}$/t and 717 $€_{2022}$/t, respectively, are required to reach a net present value of 0 € after an investment period of 25 years. These values correspond to surcharges of 43.4% and 31.6% compared to fossil-based methanol prices. A different approach is to derive the necessary CO_2 price in order to be cost-competitive with fossil-based methanol, resulting in required CO_2 prices ranging from around 220–310 $€_{2022}$/t CO_2.

A surcharge of 52.8% compared with the 2022 German market price is required for the selling price of green methanol for an electrolyzer scale of 50 $MW_{el.}$ for a desired amortization period of 15 years, as shown in Fig. 6. By scaling up to 100 $MW_{el.}$ electrolyzer power input, the necessary surcharge is decreased to slightly below 40%, corresponding to a green methanol price of 761 €/t.

Two scenarios based on a desired amortization period of five years

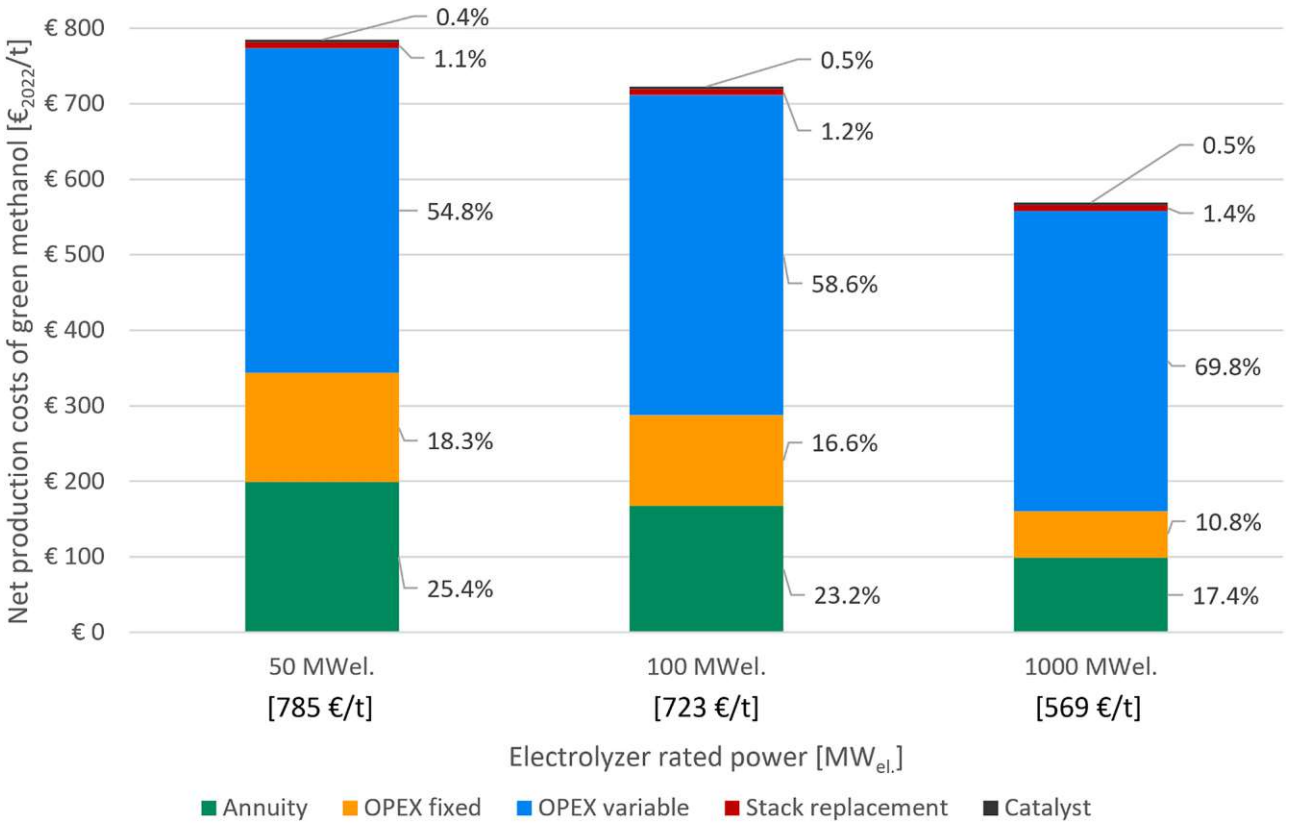

Fig. 8. Net production costs of green methanol, including cost allocation, for different plant scales based on the electrolyzer's rated power.

Table 7
Net production costs of green methanol and surcharge compared with 2022 methanol market prices.

Plant scale[1)]	NPC [€2022/t]	NPC [€2022/kWhMeOH]	Surcharge[2)]
50 MWel.	785.4	0.123	144.1%
100 MWel.	722.9	0.113	132.6%
1000 MWel.	569.0	0.089	104.4%

1) Rated power of the electrolysis unit. 2) Compared with the 2022 methanol market price in Germany of 545 €/t [43].

are displayed in Fig. 7. A surcharge of over 100%, corresponding to a green methanol selling price of 1107 €2022/t, compared with fossil methanol market prices, is required to realize a worthwhile investment amortizing after only five years of operation. Green methanol revenues of 995 €2022/t are needed to amortize a Power-to-Green methanol plant at an electrolyzer scale of 100 MWel..

3.4. Net production costs of green methanol

Calculating the net production costs of green methanol is essential to assess the cost-competitiveness compared with conventional fossil-based methanol. The net production costs are the sum of the annuity, i.e., annual capital expenditure (CAPEX), fixed OPEX, e.g., labor and maintenance, and variable OPEX, e.g., electricity and consumables. Fig. 8 displays the NPC of green methanol for three different plant scales, i.e., 50, 100 and 1000 MWel. electrolyzer rated power. NPC range from 785 €/t for a 50 MWel. plant to 569 €/t when implementing a 1000 MWel. electrolyzer. Thus, scaling up has the potential to decrease the NPC of green methanol by up to 30%. However, electrolyzers at a scale of 1 GWel. are highly unrealistic and probably won't be a viable future scenario for decentralized Power-to-Green methanol plants based on biomass and renewable electricity. In addition, scaling up PtL plants does not have the same effect as conventional fossil-based processes due to their substantial dependency on renewable electricity. The share of annuity and fixed OPEX can be curbed to a share below 30%. Nonetheless, variable OPEX, especially electricity, do not benefit from a scale-up, limiting the economies of scale benign effect on NPC.

An overview of the determined NPC of green methanol in €2022 per ton and kWhMeOH is given in Table 7. In addition, relative comparisons with the current methanol market price in Germany are assessed for green methanol by calculating the required surcharge. A surcharge of 44% has to be paid for green methanol produced by the presented base scenario at an electrolyzer scale of 50 MWel.. This value can be decreased to 4.5% by a scale-up to 1000 MWel. rated power input into the electrolyzer.

3.5. Sensitivity analysis

The influence of critical economic parameters, i.e., availability, discount rate, grid electricity price and oxygen revenue, on the net production costs of green methanol was analyzed within a sensitivity analysis. Fig. 9 highlights the substantial influence of the Power-to-Green methanol plant's availability on the plant's economic feasibility. Decreasing the annual operating hours to 2000 from 8000 h/a leads to an almost threefold increase in production costs, underpinning the need for a consistent power supply in the electrolyzer. The grid electricity price's impact on the net production costs is negligible due to the implementation of a power supply system, as introduced in chapter 2.2. An increase in the grid electricity price to 0.4 €/kWh from 0.2 €/kWh results in an increase in net production costs of only 3%. Applying a hybrid power plant consisting of wind and photovoltaic power in combination with a grid electricity connection facilitates a plant availability of 8000 h/a while curbing the influence of volatile energy markets on the Power-to-Green methanol plant's economic performance. Selling O_2, a by-product of the alkaline electrolyzer, can

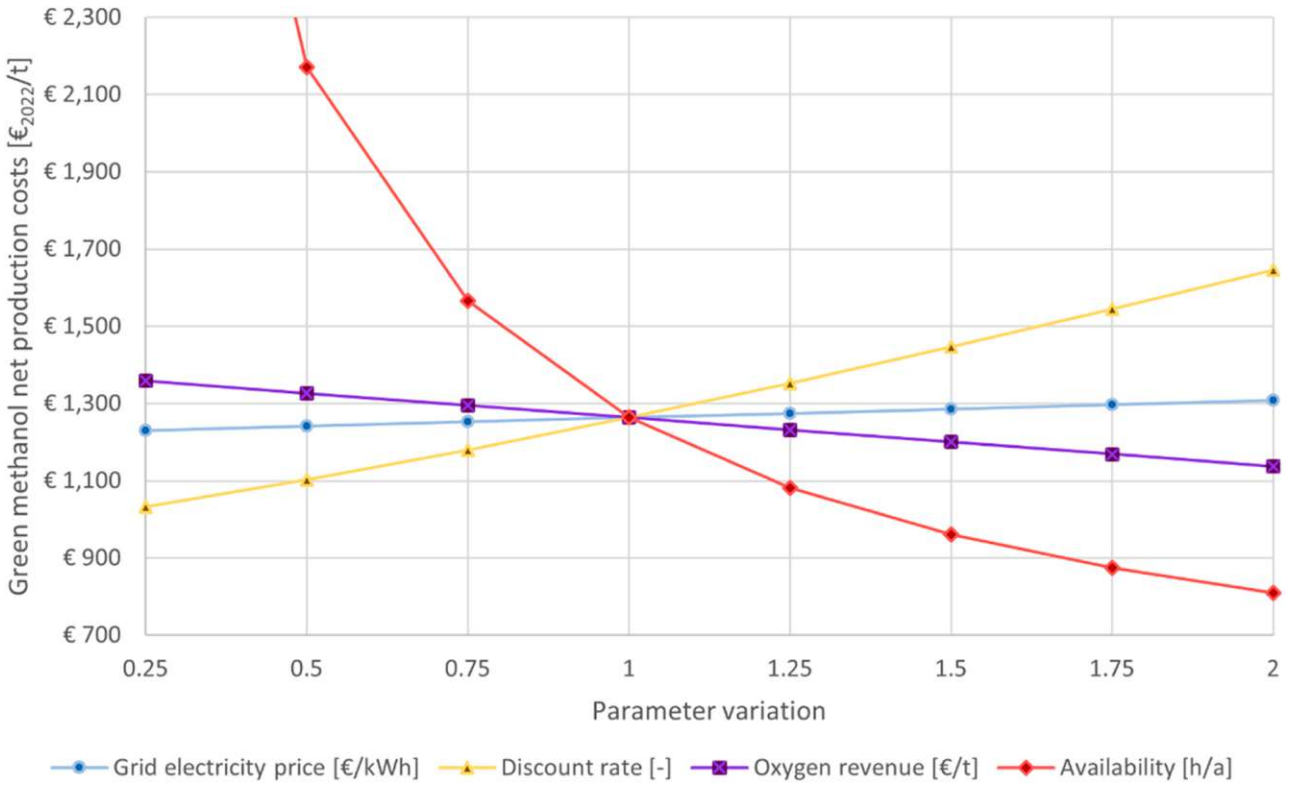

Fig. 9. Sensitivity analysis of green methanol production. Base values: Grid electricity price = 0.2 €$_{2022}$/kWh$_{el.}$; Discount rate = 0.08; Oxygen revenue = 80 €$_{2022}$/t; Availability = 4000 h/a.

Table 8
Net production costs of methanol based on CO_2 hydrogenation – comparison to previous studies.

Net production costs of methanol[1)]	[4]	[22]	[5]	[23]	[28]	[35]	This study
NPC – lower limit [€$_{2022}$/t]	1685	958[2)]	1159	1612	1421[4)]	665[3)]	569
NPC – upper limit [€$_{2022}$/t]			1562	1905		950[3)]	785

1) All values converted to 2022 levels (CEPCI = 816.0). 2) Plant scale exceeds the presented one by a factor of 50. 3) Study based on a high-temperature electrolyzer. Plant scale factor of 11.5 compared to the presented study. 4) Plant scale factor of 1.5 compared to the presented study.

Table 9
Required green methanol prices for various amortization periods.

Green MeOH price[1)]	Amortization period		
Electrolyzer scale	5 years	15 years	25 years
50 MW$_{el.}$[3)]	1107 €/t (+103%[2)])	833 €/t (+53%)	782 €/t (+43%)
100 MW$_{el.}$	995 €/t (+83%)	761 €/t (+40%)	717 €/t (+32%)

1) All values in €$_{2022}$/t, discount rate = 8%, plant availability = 8000 h/a. 2) Surcharge compared to German methanol market price in 2022 [43]. 3) Corresponds with 30.2 and 60.4 MW$_{MeOH}$.

further boost the plant's performance by decreasing the net production costs by up to 10%. In addition, the discount rate significantly influences the economic assessment. A variation of the discount rate from 2% to 16% results in a 60% increase in green methanol net production costs.

Table 10
Total and relative shares of green methanol net production costs.

Electrolyzer scale	NPC [€$_{2022}$/t]	CAPEX [%]	Variable OPEX [%]	Fixed OPEX [%]
50 MW$_{el.}$[1)]	785	25.4	56.3	18.3
100 MW$_{el.}$	723	23.2	60.3	16.6
1000 MW$_{el.}$	569	17.4	71.7	10.8

1) Corresponds with 30.2 MW$_{MeOH}$.

Table A1
Fixed capital investment of biomass heating plants.

Location	Thermal load [MW$_{th.}$]	FCI$_{Base\ year}$	Year	FCI$^{1}_{2022}$)	Source
Nykoping, SWE	97.5	45 mil. €	1994	35.3 mil. €	[12]
Cuijk, NLD	160	50 mil. €	1999	23.1 mil. €	[12]
Baden, AUT	28	20 mil. €	2006	25.8 mil. €	[59]
Siezenheim, AUT	19	41 mil. €	2022	40.3 mil. €	[68]
Heiligenkreuz, AUT	43	43.5 mil. €	2007	39.5 mil. €	[38]
St. Veit a. d. Glan, AUT	45	35 mil. €	2007	31 mil. €	[72]
Timelkam, AUT	50	35 mil. €	2006	30 mil. €	[64]
Chosen value	20	-	2022	31.7 mil. €	

1) Converted to a thermal load of 20 MW$_{th.}$.

4. Discussion

In general, Power-to-Liquid plants have two critical weaknesses. Firstly, off-grid concepts solely based on adjacent wind or solar power

Table A2
Fixed capital investment of CO_2 capture units based on MEA absorption.

Source	Capacity [t/h CO_2]	$FCI_{Base\ year}$	Year	$FCI_{2022}^{1),2)}$
[18]	207.5	27.1 mil. €	2012	20.8 mil. €
[11]	124.0	26.6 mil. €	2013	29.5 mil. €
[10]	112.5	31.8 mil. €	2008	37.0 mil. €
Chosen value	6.9	-	2022	29.1 mil. €

1) Converted to a mass flow rate of 6.9 t/h CO_2. 2) Lang factor = 5.04.

Table A3
Fixed capital investment of methanol synthesis plants based on CO_2 valorization.

Source	Capacity [MW_{MeOH}]	$C_{Equip.,\ base\ year}$	Year	$FCI_{2022}^{1)}$
[5]		350 €/kW	2019	14.2 mil. €
[28]	299.6	60 mil. €	2017	13.8 mil. €
[28]		390 €/kW	2017	16.9 mil. €
[4]		500 €/kW	2015	22.1 mil. €
[24]	41.5	15 mil. €	2000	24.4 mil. €
Chosen value	30.17	-	2022	18.3 mil. €

1) Converted to a methanol stream of 30.2 MW_{MeOH}.

farms are limited to plant availabilities below 3000 h/a, depending on the power source and site location, due to the intermittent behavior of renewable power sources. Inferior net production costs are a direct result of this issue. Secondly, PtL plants powered by grid electricity are prone to the economic uncertainties of volatile electricity markets. Within the presented study, a hybrid power supply solution combining wind, PV and grid electricity was established and optimized. A wind park with a rated power of 71.4 MWp and a photovoltaic farm obtaining a rated power of 80 MWp in combination with a combined heat and power process and grid electricity supply ensure a plant availability of 8000 operating hours per year while simultaneously curbing the grid electricity price's influence on the PtL plant's economic performance.

Fixed capital investments of 118.6 mil. $€_{2022}$ (50 $MW_{el.}$ electrolyzer plant scale) and 203.4 mil. $€_{2022}$ (100 $MW_{el.}$ electrolyzer plant scale) are required to realize the presented Power-to-Green methanol plant concept. The variable OPEX account for over 70% of the total OPEX of around 32–35 mil. $€_{2022}$/a. Electricity is the main cost driver, with annual expenses of almost 20 mil. $€_{2022}$/a for the base scenario producing 30.2 MW methanol. Based on 2022 market prices, a yearly turnover of 33 mil. $€_{2022}$ can be generated by producing methanol, 71% of total revenue, oxygen, 17% and district heating, 12%.

Selling green methanol at 2022 fossil methanol market prices does not result in a worthwhile investment scenario. Green methanol produced by the presented plant concept must be sold at 782 $€_{2022}$/t, a surcharge of 43.4% compared to the methanol market price, to realize a non-profit investment scenario, i.e., an amortization period of 25 years. A CO_2 price of 308 €/t is required to be cost-competitive with conventional fossil methanol based on natural gas as a feedstock [52], [20]. This value can be decreased to 233 €/t CO_2 by doubling the Power-to-Green methanol plant scale. Prices per ton of CO_2 ranged from 80 to 100 €/t in 2023 within the EU emissions trading system (ETS) [70]. Non-ETS sectors will be taxed with 55 €/t CO_2 in Austria in 2025 [50]. Sweden is a trailblazer concerning CO_2 taxes with a current rate of 122 €/t CO_2 [53]. Hence, policymakers must focus on substantially increasing CO_2 prices to tackle the dominance of conventional, fossil-based processes and incentivize Power-to-Liquid processes. Amortization periods of 15 and 5 years can be realized with green methanol prices of 833 and 1107$€_{2022}$/t, resulting in necessary surcharges of 52.8% and 103.1% compared with 2022 market levels in Germany, respectively.

Table 8 contextualizes the obtained results with previous studies. All net production costs were converted to the 2022 CEPCI level to facilitate a direct comparison. Implementing the presented Power-to-Liquid plant concept has the potential to reduce the net production costs of green methanol significantly. A large share of cheap renewable electricity in combination with a plant availability similar to industrial plants results in comparatively low net production costs. In addition, CAPEX and OPEX of electrolyzers were subject to dynamic improvements within the past years, hence, additionally boosting the presented concept's results in comparison to studies conducted before 2020. Scaling up Power-to-Liquid plants results in lower specific fixed capital investment and, consequently a decrease in net production costs but reaches its limits when exceeding a rated electrolyzer power of around 100 $MW_{el.}$. Variable OPEX, especially electricity costs, do not benefit from a scale-up and become the cost-driving factor. Thus, even scaling up by a factor of 50, a plant scale analyzed by Nyári et al. [22], does not conclude in a cost-competitive advantage.

The beneficial effect of scaling up Power-to-Liquid plants is limited, thus, underpinning the recommendation of implementing medium-scale plant concepts in combination with decentralized, biogenic CO_2 sources, e.g., biomass heating plants or biogas upgrading plants. In addition, concepts based on hybrid power plants, as presented in this study, have the potential to decouple the economic performance of Power-to-Liquid applications from volatile electricity markets.

A direct renewable electricity purchase contract is required to ensure the production of green methanol. The presented PtL plant's electricity balance is provided in table A4. A total of almost 30 $GWh_{el.}$ green electricity is fed into the local grid per year. The annual net grid electricity demand is below 10 $GWh_{el.}$, corresponding with only 2.37% of the PtL plant's annual electricity consumption.

However, the determined total fixed capital investment underlies uncertainties. Detailed P&ID flowcharts and specific equipment cost data should be the focus of future research efforts to improve this study's accuracy. In addition, the energy supply model's resolution should be increased by gathering and implementing data concerning daily yields of wind and photovoltaic farms throughout the seasons. The grid electricity demand could be further reduced by implementing innovative power storage technologies, transferring surplus electricity generated by the hybrid power plant to days obtaining lower wind velocities and

Table A4
Monthly power balance of the hybrid power plant.

Month	Operating hours [h/month]	Total power demand [$MWh_{el.}$]	Wind [$MWh_{el.}$]	PV farm [$MWh_{el.}$]	CHP [$MWh_{el.}$]	Grid electricity demand or feed [$MWh_{el.}$]
January	744	38,688	27,100	4176	1641	5771
February	672	34,944	29,261	5792	1641	-1750
March	744	38,688	29,748	9544	1641	-2245
April	720	37,440	19,461	11,912	2414	3653
May	744	38,688	22,172	11,968	2414	2134
June	720	37,440	15,676	12,096	2414	7254
July	240	12,480	16,198	12,640	2431	-18,789
August	488	25,376	14,351	11,960	2431	-3366
September	720	37,440	17,464	10,280	2431	7265
October	744	38,688	20,109	7656	2388	8535
November	720	37,440	26,226	4648	2388	4178
December	744	38,688	35,314	3784	2388	-2798
SUM	8000	416,000	273,080	106,456	26,622	9842

fewer sunshine hours.

The presented work adds value to previous studies by introducing a concept coupling hybrid renewable power plants with Power-to-Liquid plants based on post energy crisis economic parameters. In addition, the underlying plant concept has the potential to operate carbon-negative by valorizing biogenic CO_2 to green methanol.

5. Conclusions

The underlying study's objective was to assess the presented Power-to-Green methanol plant's economic competitiveness by answering the following research questions.

1. What is the required surcharge for green methanol to make investments in Power-to-Green methanol plants a competitive alternative to conventional fossil-based processes?
2. Which CO_2 price is necessary to shift future investments from fossil-based processes toward the realization of green methanol plants?

A hybrid power plant comprising wind power (71.4 MWp), solar power (80 MWp), a combined heat and power process (thermal load of 20 $MW_{th.}$) and a grid electricity connection has been established in the presented work. The proposed combination of a hybrid power plant and a Power-to-Green methanol plant has the potential to compensate Power-to-Liquid plants' two main disadvantages.

1. Off-grid plant concepts realize insufficient plant availabilities due to renewable power sources' intermittent nature.
2. Power-to-Liquid plants powered with grid electricity are highly dependent on grid electricity market prices, hence, impeding long-term investment prospects.

In addition, the presented concept has the potential to establish worthwhile investment scenarios if wholesale traders or direct consumers of methanol are willing to pay a 30–100% surcharge compared to conventional methanol market prices. Green methanol cannot compete with fossil-based methanol market prices. The required surcharges are summarized in Table 9.

CO_2 prices between 220 and 310 €/t CO_2 are necessary to make non-profit scenarios, based on amortization periods of 25 years, of green methanol production cost-competitive with conventional fossil-based methanol. The net production costs of green methanol and the cost categories' respective shares are stated in Table 10. Net production costs of green methanol can be reduced to a certain extent by plant scale-up, however, realizing electrolyzers larger than 100 $MW_{el.}$ rated power is unrealistic at this stage. Net production costs of 785 $€_{2022}$/t can be realized for the base scenario based on an electrolyzer with a rated power of 50 $MW_{el.}$. Variable OPEX, especially electricity and wood chips, account for over 50% of the observed costs for green methanol production. The annuitized fixed capital investment accounts for around 25% of net production costs, whereas fixed OPEX account for approximately 18%.

A sensitivity analysis underpinned the plant availability's crucial role for Power-to-Liquid processes. Implementing an adjacent hybrid power plant in combination with a connection to the local electricity grid enables annual operating hours of 8000, hence, significantly boosting the Power-to-Green methanol's economic performance. In addition, the grid electricity price's influence on green methanol net production costs could successfully be curbed by implementing a hybrid power plant with the ability to feed in surplus power generated by the adjacent wind and solar farm. Thus, potential electricity cost increases will not have a significant impact on the green methanol NPC obtained in this study. Furthermore, coupling Power-to-Liquid plants with oxygen-consuming processes is a keystone to improve their economic performance further.

The presented techno-economic assessment still has a relatively considerable uncertainty concerning the plant's fixed capital investment. Future research projects should focus on creating detailed P&ID flowcharts to facilitate factorial method economic evaluations based on the respective equipment's costs. Additionally, an increased resolution concerning the wind and photovoltaic farms' volatility, i.e., daily wind and solar power yields for the respective plant location, would be needed to enhance the energy supply model's accuracy further. CAPEX and OPEX of electrolyzers and renewable power sources are projected to decrease significantly within the upcoming years. Thus, various scenarios of a roadmap to 2050 might be of interest to research efforts based on the presented economic evaluation. Reductions in the costs of renewable electricity are expected within the following years. Thus, further cost reductions of green methanol are realistic since the electricity costs account for a substantial share of the plant's OPEX. Economic and ecological evaluations must go hand in hand to establish holistic, sustainable industrial concepts. Hence, conducting a life-cycle assessment of the underlying plant concept must be a linchpin of future research endeavors.

Funding

The authors would like to thank TU Wien Bibliothek for covering article processing charges through its Open Access Funding Program.

CRediT authorship contribution statement

Simon Pratschner: Conceptualization, Methodology, Software, Validation, Formal analysis, Investigation, Data curation, Visualization, Writing – original draft, Writing – review & editing. **Frank Radosits:** Conceptualization, Methodology, Software, Validation, Investigation, Writing – original draft, Writing – review & editing. **Amela Ajanovic:** Validation, Resources, Supervision, Project administration, Writing – review & editing. **Franz Winter:** Validation, Resources, Writing – review & editing, Supervision, Project administration, Funding acquisition.

Declaration of Competing Interest

The authors declare that they have no known competing financial interests or personal relationships that could have appeared to influence the work reported in this paper.

Data Availability

Data will be made available on request. Please contact the corresponding author for further information concerning the presented data.

Acknowledgements

The authors would like to acknowledge the TU Wien doctoral college CO_2 Refinery and the open access funding by TU Wien.

Appendix

Tables A1, A2, A3 and A4.

References

[1] K. Aasberg-Petersen, C. Nielsen Stub, I. Dybkjaer, J. Perregaard, Large scale methanol production from natural gas, Haldor Topsoe (2022).
[2] Access Intelligence LLC, Chemical Engineering, April 2023. Volume 130 (4) (2023).
[3] M. Bowker, Methanol synthesis from CO_2 hydrogenation, ChemCatChem 11 (2019) 4238–4246.
[4] S. Brynolf, M. Taljegard, M. Grahn, J. Hansson, Electrofuels for the transport sector: a review of production costs, Renew. Sustain. Energy Rev. 81 (2018) 1887–1905.

[5] M. Decker, F. Schorn, R.C. Samsun, R. Peters, D. Stolten, Off-grid power-to-fuel systems for a market launch scenario – a techno-economic assessment, Appl. Energy 250 (2019) 1099–1109.
[6] D. DeSantis, B. James, G. Saur, H2A: Hydrog. Anal. Prod. Models - Future Cent. Hydrog. Prod. PEM Electro (2019) Version 3 (2018) 2019.
[7] V. Dieterich, A. Buttler, A. Hanel, H. Spliethoff, S. Fendt, Power-to-liquid via synthesis of methanol, DME or Fischer–Tropsch-fuels: a review, Energy Environ. Sci. 13 (2020) 3207–3252.
[8] European Commission. Directorate General for Energy., E3 Modelling., Ecofys., Tractebel., Technology pathways in decarbonisation scenarios., Publications Office, LU, 2020.
[9] IEA, Global Energy Review 2021, IEA - International Energy Agency, France, 2021.
[10] IEA Greenhouse Gas R&D Programme (IEA GHG), CO2 Capture in the Cement Industry, 2008.
[11] IEAGHG, Deployment of CCS in the Cement Industry, 2013.
[12] J. Koornneef, M. Junginger, A. Faaij, Development of fluidized bed combustion—an overview of trends, performance and cost, Prog. Energy Combust. Sci. 33 (2007) 19–55.
[13] C. Kost, S. Shivenes, V. Jülch, H.-T. Nguyen, T. Schlegl, Stromgestehungskosten erneuerbare energien, Fraunhofer ISE (2018).
[14] D.O. Kunysz, Kostenschätzung im chemischen anlagenbau: cost estimation basics, springer Fachmedien Wiesbaden, Wiesbaden (2020).
[15] J.-P. Lange, Methanol synthesis: a short review of technology improvements, Catal. Today 64 (2001) 3–8.
[16] T. Lauf, M. Memmler, S. Schneider, Emissionsbilanz erneuerbarer Energieträger, Ger. Environ. Agency (UBA) (2019).
[17] G. Leonzio, E. Zondervan, P.U. Foscolo, Methanol production by CO_2 hydrogenation: analysis and simulation of reactor performance, Int. J. Hydrog. Energy 44 (2019) 7915–7933.
[18] X. Liang, J. Li, Assessing the value of retrofitting cement plants for carbon capture: a case study of a cement plant in Guangdong, China, Energy Convers. Manag. 64 (2012) 454–465.
[19] D.S. Marlin, E. Sarron, Ó. Sigurbjörnsson, Process advantages of direct CO_2 to methanol synthesis, Front. Chem. 6 (2018).
[20] N. Meunier, R. Chauvy, S. Mouhoubi, D. Thomas, G. De, Weireld, Alternative production of methanol from industrial CO_2, Renew. Energy 146 (2020) 1192–1203.
[21] U. Neuling, M. Kaltschmitt, Techno-economic and environmental analysis of aviation biofuels, Fuel Process. Technol. 171 (2018) 54–69.
[22] J. Nyári, M. Magdeldin, M. Larmi, M. Järvinen, A. Santasalo-Aarnio, Techno-economic barriers of an industrial-scale methanol CCU-plant, J. CO_2 Util. 39 (2020), 101166.
[23] A. Otto, Chemische, verfahrenstechnische und ökonomische Bewertung von Kohlendioxid als Rohstoff in der chemischen Industrie, Forschungszentrum Jülich, Zentralbibliothek, Jülich, 2015.
[24] M.S. Peters, K.D. Timmerhaus, R.E. West. Plant Design and Economics for Chemical Engineers, fifth ed.,, McGraw-Hill, New York, 2003.
[25] S. Pratschner, P. Skopec, J. Hrdlicka, F. Winter, Power-to-green methanol via CO_2 hydrogenation—a concept study including oxyfuel fluidized bed combustion of biomass, Energies 14 (2021) 4638.
[26] Q.I. Roode-Gutzmer, D. Kaiser, M. Bertau, Renewable methanol synthesis, ChemBioEng Rev. 6 (2019) 209–236.
[27] H. Ruland, H. Song, D. Laudenschleger, S. Stürmer, S. Schmidt, J. He, K. Kähler, M. Muhler, R. Schlögl, CO $_2$ Hydrogenation with Cu/ZnO/Al $_2$ O $_3$: a benchmark study, ChemCatChem 12 (2020) 3216–3222.
[28] S. Schemme, Techno-economic Assessment of Processes for the Production of Fuels from H2 and CO2, Rheinisch-Westfälische Technische Hochschule Aachen, Institut für Energie- und Klimaforschung, 2020.
[29] W.D. Seider, D.R. Lewin, J.D. Seader, S. Widagdo, R. Gani, K.M. Ng, Product and process design principles: synthesis. analysis, and evaluation, Fourth edition.,, John Wiley & Sons Inc,, New York, 2017.
[30] G.P. Towler, R.K. Sinnott, Chemical engineering design: principles, practice and economics of plant and process design, Third edition, Butterworth-Heinemann, Oxford [England]; Cambridge, MA, 2022.
[31] R. Turton (Ed.), Analysis, Synthesis, and Design of Chemical Processes, fourth ed., Prentice Hall, Upper Saddle River, NJ, 2012.
[32] A. Velazquez Abad, P.E. Dodds, Green hydrogen characterisation initiatives: Definitions, standards, guarantees of origin, and challenges, Energy Policy 138 (2020), 111300.
[33] S.M. Walas, Chemical process equipment: selection and design, Third edition, BH, Butterworth-Heinemann, an imprint of Elsevier, Amsterdam, 2012.
[34] J. Yates, R. Daiyan, R. Patterson, R. Egan, R. Amal, A. Ho-Baille, N.L. Chang, Techno-economic analysis of hydrogen electrolysis from off-grid stand-alone photovoltaics incorporating uncertainty analysis, Cell Rep. Phys. Sci. 1 (2020), 100209.
[35] M. Yousaf, A. Mahmood, A. Elkamel, M. Rizwan, M. Zaman, Techno-economic analysis of integrated hydrogen and methanol production process by CO_2 hydrogenation, Int. J. Greenh. Gas. Control 115 (2022), 103615.
[36] J. Zhang, S. Liang, X. Feng, A novel multi-effect methanol distillation process, Chem. Eng. Process.: Process.Intensif. 49 (2010) 1031–1037.

Online References

[37] Austrian Chamber of Agriculture. 2023. Lower Austria wood market week 09/2023. Available at: ⟨https://www.lko.at/holz+2400++1298002⟩. (Accessed: 10.3.2023).
[38] Austrian Court of Auditors. 2014. Bericht des Rechnungshofes. Available at: ⟨https://www.rechnungshof.gv.at/rh/home/home/BEGAS_Energie_AG.pdf⟩. (Accessed: 22.5.2023).
[39] Burgenland Energie. 2023. Feed-in rate for renewable electricity Burgenland. Available at: ⟨https://assets.burgenlandenergie.at/preisblatt_einspeisetarif_oekostrom_marktpreis_01012022_472ae29bb6.pdf?updated_at=2022-05-18T14:08:12.204Z⟩. (Accessed: 27 Mar 2023).
[40] Carbon Recycling International. 2022. The Finnjord e-Methanol Project: Commercial Scale e-Methanol Production in Norway. Available at: ⟨https://www.carbonrecycling.is/projects#finnfjord-emethanol⟩. (Accessed: 28 April 2023).
[41] Carbon Recycling International. 2022a. The Shunli CO2-to-Methanol Plant: Commercial Scale Production in China. Available at: ⟨https://www.carbonrecycling.is/projects#projects-shunli⟩. (Accessed: 28 April 2023).
[42] Carbon Recycling International. 2022b. The Sailboat CO2 to Green Methanol Project: Chemical Products from recycled CO2. Available at: ⟨https://www.carbonrecycling.is/projects#projects-sailboat⟩. (Accessed: 28 April 2023).
[43] ChemAnalyst. 2022 Methanol Price Trend and Forecast. Available at: ⟨https://www.chemanalyst.com/Pricing-data/methanol-1⟩. (Accessed: 10 Mar 2023).
[44] CHEMANALYST. 2023. Calcium Hydroxide Price Trend and Forecast. Available at: ⟨https://www.chemanalyst.com/Pricing-data/calcium-hydroxide-1204⟩ (Accessed: 10 Mar 2023).
[45] Corporate Finance Institute. 2023. Discount Rate. Available at: ⟨https://corporatefinanceinstitute.com/resources/valuation/discount-rate/⟩. (Accessed: 22 May 2023).
[46] ECHEMI. 2019. Ammonium hydroxide China Domestic Price. Available at: ⟨https://www.echemi.com/productsInformation/temppid160628001318-ammonia-water.html⟩. (Accessed: 10 Mar 2023).
[47] Enercon. 2023. ENERCON E-138 EP3 E2 / 4.2 MW Specifications. Available at: ⟨https://www.enercon.de/en/products/ep-3/e-138-ep3/⟩. (Accessed: 21 Mar 2023).
[48] European Commission. 2023. Photovoltaic Geographical Information System. Available at: https://re.jrc.ec.europa.eu/pvg_tools/en/. (Accessed: 5 May 2023).
[49] Eurostat. 2023. Annual inflation more than tripled in the EU in 2022. Available at: ⟨https://ec.europa.eu/eurostat/web/products-eurostat-news/w/DDN-20230309-2#:~:text=In%202022%2C%20EU%20annual%20inflation,2013%2D2022%20was%202.1%25⟩. (Accessed: 7 Jul 2023).
[50] Federal Ministry Republic of Austria – Finance. 2022. Initial information on the 2022 national emissions certificates trading law (NEHG 2022). Available at: ⟨https://www.bmf.gv.at/en/topics/Climate-policy/initial_nehg_2022_en.html⟩. (Accessed: 10 Mar 2023).
[51] Fraunhofer C.B.P. 2023. E-CO2Met-Electricity and CO2 to Methanol. Available at: ⟨https://www.cbp.fraunhofer.de/en/reference-projects/e-co2met.html⟩. (Accessed: 28.4.2023).
[52] German Environment Agency. 2023. Process Details: Chem-OrgMethanol-DE-2020. Available at: https://www.probas.umweltbundesamt.de/php/prozessdetails.php?id={E7B2AF34-BEF2–4352-B256–4F817731D830}. (Accessed: 10 May 2023).
[53] Government Offices of Sweden. 2023. Sweden's Carbon Tax. Available at: ⟨https://www.government.se/government-policy/swedens-carbon-tax/swedens-carbon-tax/#:~:text=Swedish%20carbon%20tax%20rates&text=The%20carbon%20tax%20was%20introduced,of%20SEK%2010.87%20per%20EUR)⟩. (Accessed: 10 May 2023).
[54] Haldor Topsoe. 2023. SYNCOR METHANOL. Available at: ⟨https://www.topsoe.com/our-resources/knowledge/our-products/process-licensing/syncor-methanoltm⟩. (Accessed: 5 May 2023).
[55] IMPCA. 2015. IMPCA Methanol Reference Specifications. Available at: http://www.methanol.org/wp-content/uploads/2016/07/IMPCA-Ref-Spec-08-December-2015.pdf. (Accessed: 5 May 2023).
[56] Intergovernmental Panel on Climate Change. 2023. Synthesis Report of the IPCC Sixth Assessment Report (AR6). Available at: ⟨https://www.ipcc.ch/report/ar6/syr/downloads/report/IPCC_AR6_SYR_SPM.pdf⟩. (Accessed: 5 May 2023).
[57] Intratec. 2022. Monoethanolamine prices. Available at: ⟨https://www.intratec.us/chemical-markets/monoethanolamine-price⟩. (Accessed: 10 Feb 2023).
[58] Intratec. 2023. Ammonium Hydroxide Prices – France. Available at: ⟨https://www.intratec.us/chemical-markets/ammonium-hydroxide-price⟩. (Accessed: 10 Mar 2023.
[59] Koch, G., 2022. Baden: District heating network (NÖ). Klima- und Energiemodellregionen. Available at: ⟨https://www.klimaundenergiemodellregionen.at/ausgewaehlte-projekte/best-practice-projekte/showbpp/39⟩. (Accessed: 22 May 2023).
[60] Legal Information System of the Republic of Austria. 2022. Bundesrecht konsolidiert: Elektrizitätswirtschafts- und organisationsgesetz 2010 § 54, Fassung vom 16.03.2022. Available at: ⟨https://www.ris.bka.gv.at/NormDokument.wxe?Abfrage=Bundesnormen&Gesetzesnummer=20007045&FassungVom=2022–03-16&Artikel=&Paragraf=54&Anlage=&Uebergangsrecht=⟩. (Accessed: 22 May 2023).
[61] Methanol Institute. 2023. Methanol price. Methanol Price and Supply/Demand. 2023. ⟨https://www.methanol.org/methanol-price-supply-demand/⟩. (Accessed: 10 Mar 2023).
[62] Methanol Institute. 2023a. The Methanol Industry. Available at: ⟨https://www.methanol.org/the-methanol-industry/⟩. (Accessed: 28 Apr 2023).
[63] Methanol Institute. 2023b. Renewable Methanol. Available at: ⟨https://www.methanol.org/renewable/⟩. (Accessed: 31Jul 2023).

[64] Nöstler, M., 2005. Biomasse-Vertrag abgeschlossen. Holzkurier. Available at: ⟨https://www.holzkurier.com/energie/2005/04/biomasse-vertragabgeschlossen.html⟩. (Accessed: 22 May 2023).
[65] OMV. 2022. Consortium formed for developing new process technology to produce Sustainable Aviation Fuel. Available at: ⟨https://www.omv.com/en/news/221116-consortium-formed-for-developing-new-process-technology-to-produce-sustainable-aviation-fuel⟩. (Accessed: 28 Apr 2023).
[66] Sate of Green. 2021. Power-to-X plant in Aalborg will produce green methanol from local waste-based CO2. Available at: ⟨https://stateofgreen.com/en/news/power-to-x-plant-in-aalborg-will-produce-green-methanol-from-local-waste-based-co2/⟩. (Accessed: 22 May 2023).
[67] Siemens Energy. 2022. Haru Oni: A New Age of Discovery. Available at: ⟨https://www.siemens-energy.com/global/en/news/magazine/2021/haru-oni.html⟩. (Accessed: 28 May 2023).
[68] Sprenger, S., 2022. Siezenheim heizt Salzburg ein – neues Biomasseheizkraftwerk um 41 Mill. Euro geht in Bau. Salzburger Nachrichten. Available at: ⟨https://www.sn.at/salzburg/wirtschaft/siezenheim-heizt-salzburg-ein-neues-biomassekraftwerk-um-41-mill-euro-geht-in-bau-116842738⟩. (Accessed: 22 May 2023).
[69] Statista. 2023. Yearly development of the exchange rate between € and USD from 1999 to 2022. Available at: ⟨https://de.statista.com/statistik/daten/studie/200194/umfrage/wechselkurs-des-euro-gegenueber-dem-us-dollar-seit-2001/#:~:text=Wechselkurs%20Euro%2FUS%2DDollar%20bis%202022%20(Jahresdurchschnittswerte)&text=Im%20Jahr%202022%20erhielt%20man,%2C47%20US%2DDollar%20wert⟩. (Accessed: 4 May 2023).
[70] Statista. 2023a. European Union Emission Trading System (EU-ETS) carbon pricing from January 2022 to April 2023. Available at: ⟨https://www.statista.com/statistics/1322214/carbon-prices-european-union-emission-trading-scheme/⟩. (Accessed: 10 May 2023).
[71] Statistik Austria. 2023. Energy prices, taxes. Available at: ⟨https://www.statistik.at/en/statistics/energy-and-environment/energy/energy-prices-taxes⟩. (Accessed: 22 May 2023).
[72] Strobl, G., 2017. Spanplattenhersteller Fundermax zieht sich mit Biomasse Schiefer ein. Der Standard. Available at: ⟨https://www.derstandard.at/story/2000064746498/spanplattenhersteller-fundermax-tritt-sich-mit-biomasse-schiefer-ein⟩. (Accessed: 22 May 2023).
[73] Sunfire. 2023. Sunfire-HyLink Alkaline Factsheet. Available at: ⟨https://www.sunfire.de/files/sunfire/images/content/Sunfire.de%20(neu)/Sunfire-Factsheet-HyLink-Alkaline.pdf⟩. (Accessed: 4 May 2023).
[74] Technical University of Denmark. 2023. Data obtained from the "Global Wind Atlas 3.0, a free, web-based application developed, owned and operated by the Technical University of Denmark (DTU). The Global Wind Atlas 3.0 is released in partnership with the World Bank Group, utilizing data provided by Vortex, using funding provided by the Energy Sector Management Assistance Program (ESMAP). Available at: https://globalwindatlas.info" (Accessed: 21 Mar 2023).
[75] Vestas Wind Systems A/S. 2023. 4 MW Platform Brochure. Available at: ⟨https://nozebra.ipapercms.dk/Vestas/Communication/4mw-platform-brochure/?page=1⟩. (Accessed: 31 Jul 2023).

Journal Article V

Chemical Engineering Journal 481 (2024) 148413

Contents lists available at ScienceDirect

Chemical Engineering Journal

journal homepage: www.elsevier.com/locate/cej

Off-grid vs. grid-based: Techno-economic assessment of a power-to-liquid plant combining solid-oxide electrolysis and Fischer-Tropsch synthesis

Simon Pratschner [*,1], Martin Hammerschmid [2], Stefan Müller [3], Franz Winter [4]

Technische Universität Wien, Faculty of Technical Chemistry, Institute of Chemical, Environmental and Bioscience Engineering, Getreidemarkt 9/166, 1060 Vienna, Austria

ARTICLE INFO

Keywords:
Techno-economic assessment
Power-to-Liquid
Fischer-Tropsch
Solid-oxide electrolysis
Off-grid vs. grid-powered
Carbon capture and utilization

ABSTRACT

The economic performance of Power-to-Liquid processes depends substantially on the power source's features, i.e., electricity costs and full load hours. Off-grid solutions can ensure cheap, green electricity without being exposed to fluctuating electricity markets. A techno-economic assessment of a Power-to-Liquid plant combining solid-oxide electrolysis and Fischer-Tropsch synthesis has been conducted. Off-grid and grid-based scenarios of three process configurations at plant scales from 1 to 1000 $MW_{el.}$ rated electrolyzer power were evaluated. Net production costs of Fischer-Tropsch products ranging from 2.42 to 4.56 $€_{2022}$/kg were obtained for the grid-based scenarios. In contrast, values of 1.28 to 2.40 $€_{2022}$/kg were determined for the evaluated off-grid scenarios. Scaling up the plant showed a weakened decrease in net production costs after surpassing a threshold of 100 $MW_{el.}$ due to substantial relative electricity costs of up to 88 %. Thus, future Power-to-Liquid projects should be designed at a scale of 100 $MW_{el.}$ rated electrolyzer power. In addition, an availability exceeding 4000 h/a is recommended for off-grid plants, e.g., by implementing hybrid renewable power plants as well as electricity and syngas storage technologies.

1. Introduction

Combining CO_2 utilization with a business case is increasingly vital for economic and political institutions. The Danish Government published a national Power-to-X (PtX) strategy plan in 2021, including companies such as Vestas, Haldor Topsoe and Vattenfall as well as aviation and maritime companies [70]. A national hydrogen and PtX strategy has been initiated by the German Federal Ministry for Economic Cooperation and Development in 2023 [71]. The year 2022 and its effect on the electricity market [72] have disclosed the main weakness of Power-to-Liquid (PtL) processes: their substantial dependency on electricity costs. Innovative plant concepts are required to guarantee a steady supply of green and cheap electricity. Hence, the underlying study focuses on the economic performance of PtL plants based on grid-connected and off-grid systems.

The European Council is currently elaborating on two proposals to gradually increase the share of sustainable fuels in the aviation and maritime industry, i.e., ReFuelEU aviation and FuelEU maritime. According to ReFuelEU aviation, EU airport suppliers must provide sustainable aviation fuel shares of 2 % (2025), 6 % (2030), 20 % (2035), 34 % (2040), 42 % (2045) and 70 % by 2050. FuelEU maritime demands a greenhouse gas intensity reduction of vessels of 2 % (2025), 6 % (2030), 14.5 % (2035), 31 % (2040), 60 % (2045) and 80 % (2050) compared with the average in 2020 [73].

Wulf et al. provided an extensive review of Power-to-X, combining Power-to-Liquid and Power-to-Gas, projects in Europe, analyzing the plants' locations, scales and applied technologies. About a third of the listed projects process hydrogen into methane, methanol or Fischer-Tropsch (FT) products. Solid-oxide electrolyzers (SOEL) have only been a niche application in the years before 2020 [1]. The Norwegian company norsk e-fuel plans to commission three FT-based plants with a combined production capacity of 80,000 t/a synthetic aviation fuel until 2029 [2]. PtL projects producing methanol exceeding a capacity of 100,000 t/a are planned to be commissioned within the next five years [3]. The locations and scales of global Fischer-Tropsch plants, including

* Corresponding author.
E-mail address: simon.pratschner@tuwien.ac.at (S. Pratschner).
[1] 0000-0001-6167-586X.
[2] 0000-0002-1155-926X.
[3] 0000-0001-8878-429X.
[4] 0000-0001-9854-3836.

https://doi.org/10.1016/j.cej.2023.148413

Available online 2 January 2024

Nomenclature

Parameters:

ΔH_r	Reaction enthalpy, kJ/mol
C	Costs, €$_{2022}$
d	Scaling exponent, –
FCI	Fixed capital investment, €$_{2022}$
i	Discount rate, -, %
n	Plant lifetime, a
$\dot{n}$	Material flow rate, mol/s
NPC	Net production costs, €$_{2022}$/kg
P	Electrical power, W
Plant availability	–, h/a
X	Conversion, –, %

Abbreviations:

AEL	Alkaline electrolyzer
ASF	Anderson-Schulz-Flory
BtL	Biomass-to-Liquid
CAPEX	Capital expenditure
CEPCI	Chemical Engineering Plant Cost Index
eASF	Extended Anderson-Schulz-Flory
Equ.	Equipment
FT	Fischer-Tropsch
IRENA	International Renewable Energy Agency
LCOE	Levelized cost of electricity
MEA	Monoethanolamine
Mil.	Million
OPEX	Operational expenditure
PEMEL	Proton exchange membrane electrolyzer
PtL	Power-to-Liquid
rWGS	Reverse water-gas shift
SOEL	Solid-oxide electrolyzer
SR	Steam reforming
TRL	Technology readiness level
USGC	U.S. Gulf Coast

Biomass-to-Liquid (BtL) projects, were summarized by Advanced Energy Technologies [74].

Solid-oxide electrolyzers have the lowest Technology Readiness Level (TRL) compared with other water electrolysis technologies, i.e., alkaline (AEL) and proton exchange membrane (PEMEL) electrolysis [4,5]. Nonetheless, the technology has the potential to be a central building block of future energy systems due to its lower specific electricity consumption [75]. The largest high-temperature electrolyzer, with a rated power of 2.6 $MW_{el.}$, has recently been installed at the Rotterdam harbor [76]. The Danish company Topsoe has laid the foundation for the world's first industrial-scale SOEL factory with an annual production capacity of 500 $MW_{el.}$ at Herning, Denmark [77]. Current data concerning the required fixed capital investment of SOEL units is still uncertain due to low production capacities [6–9]. The technical background regarding cell design, operating conditions and materials has been elaborated in previous studies [4,5,9–11]. In addition, numerous studies have focused on experimental studies to validate and improve established kinetic models [12–16]. Water electrolysis is highly sensitive to impurities affecting its performance, H_2 quality and stack lifetime. The understanding of the impact of impurities and associated degradation mechanisms is currently limited. Becker at al. recommend using ultra-pure water with a total organic carbon content below 50 µg/L [17].

Fischer-Tropsch processes have been industrially well-established for several decades [18]. State-of-the-art reactor concepts include fixed-bed multitubular, slurry bubble column and microchannel reactors [19,20] applying cobalt or iron-based catalysts [20,21]. Complex product mixtures, i.e., alkanes, alkenes, alcohols, aldehydes and carboxylic acids with chain lengths ranging from one to more than 40 carbon atoms as well as water, are produced via the Fischer-Tropsch synthesis. Thus, intricate product separation and upgrading concepts, e.g., hydrocracking, hydrotreating oligomerization, alkylation and adding fuel additives, are required [18,22,23]. A detailed composition of Fischer-Tropsch product water, typically showing oxygenate contents between 1 and 2 wt%, was provided by Rahman et al. [24]. It is an acidic solution comprising various oxygenates, e.g., alcohols, carboxylic acids, aldehydes and ketones, treated as waste water by existing industrial facilities [25].

Several methods at different levels of detail have been established to determine the required fixed capital investment (FCI) of chemical plants. Towler and Sinnott provide an overview of the AACE international cost estimate classes ranging from order of magnitude estimates, with almost no design information, to check estimates based on a completed plant design [26]. Towler and Sinnott, as well as Seider et al., provide additional details concerning factorial methods, i.e., Lang factor, location factor and material factor, and suggest cost curves for general plant equipment [26,27]. A detailed potential allocation of the Lang factor is given by Peters and Timmerhaus [28].

Determining a chemical plant's fixed operational expenditure (OPEX) can be based on factors as a function of the required capital expenditure (CAPEX) [6,9,29]. In contrast, Towler and Sinnot provide a method founded on the production rate [26]. Acquiring appropriate cost and price data can become a challenging task. Possible data sources are internal company forecasts, trade journals, consultants, online suppliers or reference books [26].

A previous techno-economic assessment by Herz et al. determined net production costs (NPC) of Fischer-Tropsch products ranging from 3.56 to 8.08 €$_{2022}$/kg, in combination with SOEL, and 4.60 to 7.62 €$_{2022}$/kg, in combination with PEMEL. Cost reductions to 2.60 (SOEL) and 3.36 €/kg (SOEL) were figured out for a 2050 scenario [30]. Peters et al. obtained NPC of 1.45 to 2.85 €$_{2022}$/kg for a PtL plant based on SOEL and FT synthesis [31]. An assessment, including reverse water–gas shift (rWGS) and FT synthesis, conducted by Zang et al., resulted in NPC of 2.73 to 2.98 €$_{2022}$/kg [32]. NPC of 8.4 to 10.6 €$_{2022}$/kg were found by Markowitsch et al. by combining either rWGS or SOEL technology with Fischer-Tropsch synthesis [33]. Decker et al. assessed the economic performance of off-grid PtL plants, including a salt cavern as hydrogen intermediate storage, resulting in NPC of FT products of 3.20 to 5.01 €$_{2022}$/kg [6]. Neuling and Kaltschmitt evaluated a comparable process producing FT products via a Biomass-to-Liquid (BtL) route. NPC of 1.49 to 4.04 €$_{2022}$/kg were found within their evaluation of alternative aviation fuels [29]. An overview of comparable studies is given in

Table 1
Overview of comparable techno-economic assessments.

Technology	NPC [€$_{2022}$/kg]	FCI [mil. €$_{2022}$]	Scale MW_{FT}	Source
SOEL + FT [1)]	3.56–8.08	–	34.0	[30]
SOEL + FT [2)]	2.60–3.36	203.5	34.0	[30]
PEMEL + FT	4.60–7.62	429.6	29.9	[30]
SOEL + FT	1.45–2.85	949.9	392.7	[31]
PEMEL + FT	2.73–2.98	436.7 [3)]	349.4	[32]
PEMEL/SOEL + FT	8.40–10.6	46.4–60.4	4.6	[33]
PEMEL + FT	3.20–5.01	–	27.4	[6]
BtL	1.49–4.04	2798.6	1317.0	[29]

[1)] 2020 scenario.
[2)] 2050 scenario.
[3)] Excluding PEMEL. H_2 costs were accounted as variable OPEX.

Table 1. All values have been converted to 2022 levels based on the Chemical Engineering Plant Cost Index (CEPCI).

An essential factor of Fischer-Tropsch products is their CO_2 footprint compared with conventional fossil fuels, which mainly depends on the emission factor of the used electricity. Applying the EU's 2022 average grid electricity mix resulted in a greenhouse gas emission increase of 46 % compared with fossil fuels [34]. On the other hand, coupling PtL plants with renewable power sources led to a potential 95 % decrease in CO_2 emissions based on wind power and a 65 % decrease based on photovoltaic power [34]. Micheli et al. determined a CO_2 emission reduction potential between 52.6 % and 88.9 % for synthetic kerosene produced by a PtL plant combining direct air capture, high-temperature electrolysis and FT synthesis [35].

The majority of previously conducted techno-economic assessments of PtL processes are based on grid electricity [9,30,32,36] due to stable and cheap electricity prices in the European Union from 2008 to 2019 [72]. 2021 and 2022 caused a paradigm shift in the European electricity and energy markets, entailing soaring electricity prices for household and industrial consumers [72]. Thus, updated TEAs are essential to evaluate the performance of PtL processes for the 2022 European economic framework and to find alternative ways to avoid their substantial dependency on fluctuating grid electricity market prices. In addition, previous studies, e.g., by Spurgeon and Kumar [37], assume utilizing fossil power plants as a CO_2 source. Renewable power sources are vital to ensure the benign effect of PtL processes on the climate and to prevent the lock-in of fossil power generation.

The presented study adds value to preceding techno-economic assessments of Power-to-Liquid processes by simultaneously evaluating the effects of plant availability and electricity costs on the net production costs of Fischer-Tropsch products for grid-based and off-grid scenarios. Several renewable electricity sources, i.e., wind, solar, hydro and geothermal power, are applied and compared to the performance of grid-based process routes founded on 2022 economic parameters. In addition, the optimum scale of Power-to-Liquid plants from an economic vantage point is analyzed. Off-grid PtL plants profit from reduced electricity costs of renewable power sources, potentially balancing out their lower availability due to daily and seasonal fluctuations. Thus, off-grid PtL plants can potentially produce Fischer-Tropsch products at lower net production costs than grid-based options. This study's objective is to answer the following research question:

Should off-grid Power-to-Liquid plants powered with renewable electricity be prioritized over the supply with grid electricity?

2. Methodology

The presented techno-economic assessment is founded on a previously conducted study of a Power-to-Liquid plant by the authors [2]. The established plant concept comprises the following sub-processes:

- MEA-based CO_2 capture
- Solid-oxide electrolyzer operated in co-electrolysis mode
- Three-stage syngas compression
- Fischer-Tropsch synthesis
- Fischer-Tropsch product separation
- Tail gas recirculation and steam reforming of tail gas
- Purge gas combustion

2.1. Process modeling and process simulation

IPSEpro version 8.0, a stationary and equation-based process simulation tool, was applied to model the sub-processes and establish the designed plant configuration. The plant's main design parameter is the power input into the SOEL unit P_{SOEL}, ranging from 1 to 1000 $MW_{el.}$. Three process configurations were designed:

1. Short tail gas recirculation to the Fischer-Tropsch reactor's inlet without tail gas reforming
2. Short tail gas recirculation, including steam reforming of tail gas
3. Long tail gas recirculation to the SOEL unit's inlet

Figure 1 presents a simplified process flowchart including the mass balance of a grid electricity-based scenario at a scale of 100 $MW_{el.}$ rated electrolyzer power. The detailed IPSEpro process simulation flowchart can be found in a previous study conducted by the authors [2]. The CO_2 source's gas stream, e.g., raw biogas or off-gases emitted by the cement or steel industry, is transferred to the CO_2 capture unit's absorber column. Captured CO_2 is released in the desorber column, passes a catalyst guard bed based on activated carbon, ZnO and CuO and is further conveyed to the SOEL unit's inlet. The CO_2 stream is mixed with steam and converted to syngas consisting of CO, H_2 and unconverted components. As a next step, excess steam is condensed out of the syngas, which is subsequently pressurized by a three-stage compressor to the required synthesis pressure of 21 bar. The syngas and recirculated tail gas are converted into gaseous and liquid Fischer-Tropsch products, which are separated into naphtha, middle distillate, wax and FT water. A tail gas share of 85 % is recirculated to the syngas condenser's inlet, process configurations 1 and 2, or the SOEL's inlet, process configuration 3. The remaining share is purged from the system and combusted to supply the evaporators, the CO_2 capture unit and the tail gas reformer with the required heat.

2.1.1. Solid-oxide electrolyzer in co-electrolysis mode

The SOEL unit, operating at 850 °C and atmospheric pressure, is realized by a stoichiometric model based on the conversion of CO_2, X_{CO2} = 85 %, and water, X_{H2O} = 90 %, see equations (1) and (2). As stated by Wang et al., the rWGS reaction is the main contributor of CO_2 conversion, while the influence of direct CO_2 electrolysis is negligible [11]. Schmidt et al. propose a power consumption of SOEL units ranging from 3.2 to 3.7 $kWh_{el.}/Nm^3$ H_2 [5]. As in the previous study, a specific power consumption of 3.37 $kWh_{el.}/Nm^3$ H_2 was chosen [38]. According to Cinti et al., the produced syngas's H_2:CO ratio is primarily defined by the feed's H_2O:CO_2 ratio, which is adjusted to control the H_2:CO ratio at the FT reactor inlet [13]. A detailed elaboration of the presented model has been part of a previous study [2].

$$X_{H_2O} = \frac{\dot{n}_{H_2O,in} - \dot{n}_{H_2O,out}}{\dot{n}_{H_2O,in}} \quad (1)$$

$$X_{CO_2} = \frac{\dot{n}_{CO_2,in} - \dot{n}_{CO_2,out}}{\dot{n}_{CO_2,in}} \quad (2)$$

2.1.2. Fischer-Tropsch synthesis

A low-temperature Fischer-Tropsch synthesis, applying a cobalt-based catalyst system, was assumed for the underlying techno-economic assessment. The FT reactor operates at a temperature of 230 °C and a pressure of 21 bar. Only paraffinic products were considered, as stated in equation (3).

$$n\ CO + (2n+1)\ H_2 \rightarrow H(CH_2)_nH + n\ H_2O \qquad \Delta H_r = -166.4\ kJ/mol \quad (3)$$

The used model is based on the extended Anderson-Schulz-Flory (eASF) distribution, introduced by Förtsch et al., to consider the substantial deviation of real FT product distribution compared with the standard ASF model [39]. The assumed eASF parameters are based on gathered project experience summarized in a previous study [40]. Due to the application of a cobalt-based catalyst, CO_2 is considered to pass the FT reactor as an inert gas [21,41]. A per pass carbon monoxide conversion of $X_{CO,FT}$ = 55 % was assumed. The FT reactor's per pass CO conversion combined with the rate of recirculated tail gas results in the overall system CO conversion. The separation concept of Fischer-Tropsch products is based on studies focusing on the elaboration of Fischer-Tropsch refineries, i.e., introduced by Petersen et al. [23] and de

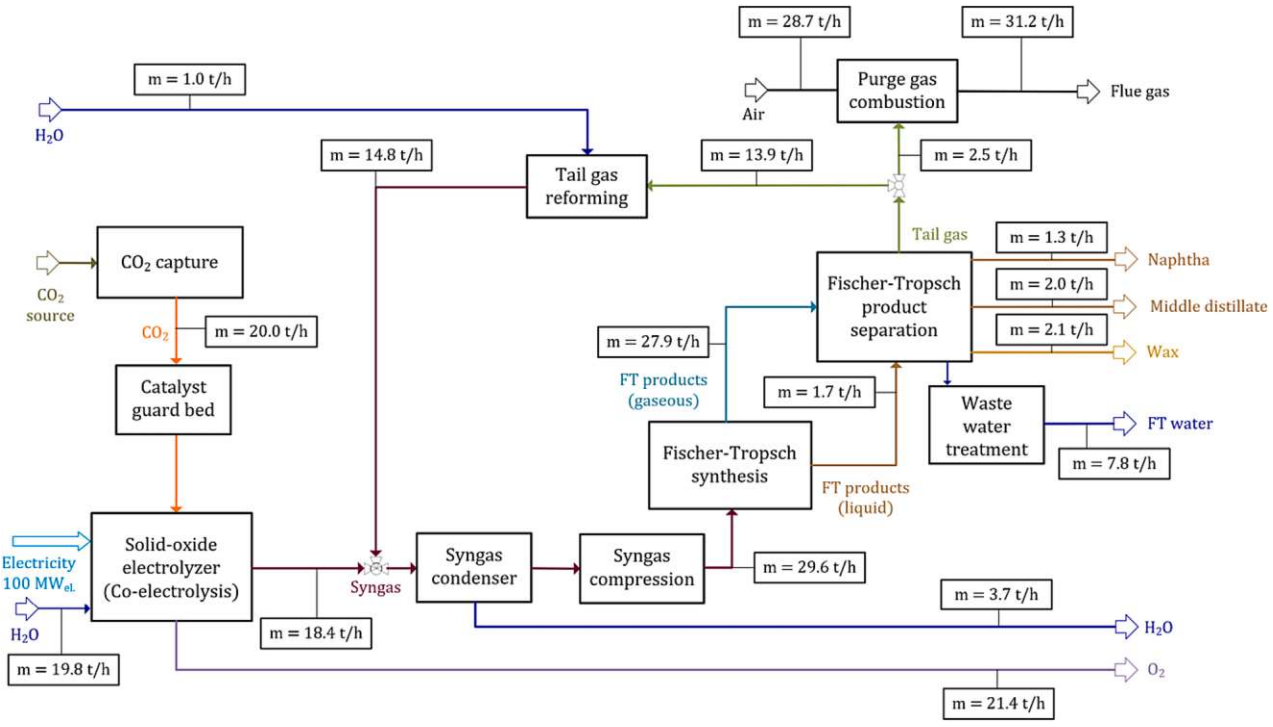

Fig. 1. Simplified process flowchart of the assessed Power-to-Liquid plant (Adapted from [2]) including the mass balance of the reference scenario.

Klerk [18].

Detailed information regarding the assumed Fischer-Tropsch process parameters was provided in a previous study [40].

2.1.3. Additional sub-processes

Besides the SOEL unit and the FT reactor, various sub-processes, e.g., CO_2 capture, multi-stage syngas compression and steam reforming of tail gas, are required to ensure a holistic evaluation of the presented PtL plant concept.

CO_2 capture by MEA absorption is a well-established industrial process. A CO_2 capture efficiency of 90 % [42,43] and a specific heat demand of 3.5 $MJ_{th.}$/kg CO_2 [44–46] was assumed for the presented techno-economic assessment. Additional information is given in a previous study by the authors [2].

A three-stage compression of syngas with intermediate water cooling was designed to realize a pressure in the FT reactor of 21 bar. Table 2 displays the assumed parameters concerning the pressurization of syngas.

The steam reforming of tail gas is based on a stoichiometric model converting CH_4, C_2H_4, C_2H_6, C_3H_8 and CO_2 as introduced by Pratschner et al. [2]. Table 3 summarizes the applied parameters of the steam reformer model.

2.2. Economic modeling and assessment

The presented study aims to provide a preliminary estimate, i.e., a class 4 study adhering to the Association for the Advancement of Cost Engineering International (AACE) classification, of a PtL plant combining SOEL and FT synthesis. AACE class 4 studies are typically based on basic process design and show an expected accuracy range of −15 % to −30 % (lower limit) and +20 % to +50 % (upper limit) [26].

Calculating the net production costs of Fischer-Tropsch products, see equation (4), includes the following steps:

1. Literature research to find the costs of applied equipment
2. Conversion of literature data to the design scale via the cost scaling method
3. Conversion to 2022 levels based on the cost escalation method
4. Conversion to German market levels based on location factors
5. Determination of the required fixed capital investment based on the factorial method
6. Discounting and allocating the total fixed capital investment via the annuity method
7. Determination of fixed OPEX, variable OPEX and by-product revenue
8. Determination of the net production costs based on the annuity, OPEX, revenue and the total mass flow rate of Fischer-Tropsch products

Table 2
Assumed efficiencies of compressors and electric motors.

Parameter	Value
Compressor: Isentropic efficiency	90 %
Compressor: Mechanical efficiency	90 %
Motor: Electric efficiency	96 %
Motor: Mechanical efficiency	90 %
Pressure ratio per stage	2.7–3.0

Table 3
Assumed parameters of the steam tail gas reformer.

Parameter	[47]	[48]	This study
Temperature	850 °C	830 °C	850 °C
Pressure	1.05 bar	10 bar	10 bar
Steam/Carbon ratio	2.2–4	3	2.5
CH_4 conversion	90 %	92 %	90 %
C_2H_4 conversion	90 % [1)]	–	90 % [1)]
C_2H_6 conversion	95 %	–	95 % [2)]
C_3H_8 conversion	99 %	–	99 % [2)]
CO_2 conversion	–	–	Chem. eq.

[1)] Assumption based on ΔH_r.
[2)] Assumption: The conversion of C_2H_6 and C_3H_8 behaves simultaneously at elevated pressure as for CH_4.

$$NPC = \frac{Annuity + OPEX_{Fixed} + OPEX_{Variable} - O_2\ revenue}{Annual\ production\ of\ FT\ products} \quad (4)$$

Corporate overhead charges, i.e., product distribution, R&D as well as selling and marketing, are assumed to be 5 % of the NPC in accordance with Towler and Sinnott [26].

The required FT product selling prices for varying amortization periods were determined by applying the net present value method, see equation (5) [26].

$$NPV = FCI + \sum_{m=1}^{n} \frac{Cash\ flow_m}{(1+i)^m} \quad (5)$$

A detailed explanation of the described steps, including formulas, is given in the following chapters. Table 4 summarizes the assumed economic parameters for the underlying techno-economic assessment of a Power-to-Liquid plant located in central Europe. The average electricity price for non-household consumers in Germany was around 0.2 €/kWh$_{el}$ in 2022 [72] and slightly above 0.1 €/kWh$_{el}$ in the European Union from 2008 to 2019 [78].

2.2.1. Capital expenditure and annuity

Initially, the obtained equipment literature cost data must be converted to the design plant scale and the reference year 2022. Scaling up or down cost data of a unit or process, see equation (6), requires a capacity value, e.g., mass flow rate, volume flow rate or electric performance, and the scaling exponent d. Determining the scaling exponent d of single units or whole chemical processes has been extensively discussed in several studies [26,27,49–51].

$$Costs_{Design} = Costs_{Base}\left(\frac{Scale_{Design}}{Scale_{Base}}\right)^d \quad (6)$$

The effect of cost escalation due to inflation is considered via the Chemical Engineering Plant Cost Index introduced by the Chemical Engineering Magazine. The CEPCI comprises the weighted average of 41 industry and commodity indices as well as twelve labor cost indices and is divided into sub-categories with different weighting factors, e.g., construction labor, heat exchangers, engineering and buildings [52]. Converting cost data to the chosen reference year 2022 is done with equation (7).

$$Costs_{2022} = Costs_{Base\ year} \cdot \left(\frac{CEPCI_{2022}}{CEPCI_{Base\ year}}\right) \quad (7)$$

Regional differences in equipment and plant costs were considered by implementing location factors, as stated in Equation (8) [26].

$$Costs_{Location\ i} = Costs_{USGC} \cdot Location\ factor_{Location\ i} \quad (8)$$

A factorial method was applied to convert equipment costs to the actual fixed capital investment by counting in additional expenditures, e.g., installation, engineering, piping, instrumentations and services, as stated by equation (9). The updated Lang factor of 5.04 for modern industry standards, as proposed by Seider et al. [27], was assumed for the underlying assessment.

$$FCI = 5.04 \cdot \sum Costs_{Equipment} \quad (9)$$

As a next step, the annuity was determined based on the plant's total fixed capital investment FCI, the discount rate i and the plant lifetime n, see equation (10).

$$Annuity = FCI \cdot \frac{(1+i)^n \cdot i}{(1+i)^n - 1} \quad (10)$$

2.2.2. Fixed OPEX, variable OPEX and O_2 revenue

Determining the fixed OPEX, i.e., maintenance, insurance, administration, unforeseen expenses and additional costs, and variable OPEX, e.g., electricity, catalysts and waste water treatment, is critical to ascertaining the net production costs of Fischer-Tropsch products. Electricity is a major cost driver within the presented plant concept and is thus listed as a separate cost center. Various approaches were proposed in previous studies to determine the fixed and variable OPEX of industrial plants, e.g., by Neuling and Kaltschmitt [29], Decker et al. [6] and Herz et al. [9]. Table 5 lists the chosen factors to determine the fixed OPEX as a function of the total CAPEX.

The plant's labor costs were determined by applying a method proposed by Green and Southard [53] by determining the required shift operators based on equipment coefficients and detailed process flowcharts for the CO_2 capture unit [54], SOEL and FT unit [2]. It was assumed that 4.2 operators are necessary for a continuous plant operation. An annual salary of 60,500 €/a per plant operator was considered, adhering to the salaries of industrial operators in Germany in 2022 [79]. In addition, supervision was counted in at 20 % of the operating labor expenses. The payroll charges amount to 30 % of operating labor and supervision expenses [53]. Table 6 provides an overview of the plant's necessary labor costs.

Table 7 displays the specific variable expenses for electricity (grid-based scenarios), operating materials and services. The required catalysts, nickel-based for the steam reformer and cobalt-based for the FT synthesis, are assumed to be replaced every three years, adhering to Neuling and Kaltschmitt [29]. The costs for an entire FT catalyst loading, as proposed by Zang et al., have been converted to the presented study's scale [32]. The specific costs of a Ni-based steam reforming catalyst are based on a report on biofuels conducted by Müller-Langer [55]. A stack replacement period of ten years is assumed for the SOEL unit in accordance with Decker et al. [6].

3. Results

The obtained net production costs of Fischer-Tropsch products produced by grid-based and off-grid Power-to-Liquid plants are presented in the following chapter. Various scenarios for 2022 and 2050 based on different power sources were evaluated. In addition, a sensitivity analysis is presented to highlight the influence of the electricity costs, plant availability, discount rate, plant lifetime and FCI.

3.1. Effect of plant configuration and scale-up

The influence of the different plant configurations and scale-up, i.e.,

Table 4
Assumed economic parameters.

Parameter	Value
Reference year	2022
Plant availability (grid-based)	8000 h/a
Discount rate	6 %
Plant lifetime	20 a
Electricity costs (grid-based)	0.1–0.2 €/kWh$_{el.}$
Lang factor	5.04
Exchange rate	0.95 €/$

Table 5
Factors to determine the fixed OPEX as proposed by Neuling and Kaltschmitt [29].

Cost center	Factor of CAPEX [%]
Maintenance	1.50
Insurance	1.00
Administration	0.50
Unforeseen expenses	1.00
Additional costs	0.75
SUM	4.75

Table 6
Labor costs for a continuous plant operation based on Green and Southard [53].

Sub-process	Required operators per shift
CO_2 capture	1.7
SOEL	1.5
FT synthesis	3.4
Whole PtL plant	6.6
Required operators	28
	Costs [mil. €/a]
Labor	1.69
Incl. supervision	2.03
Incl. payroll charges	2.64

Table 7
Specific factors for variable OPEX and oxygen revenue.

Position	Costs (2022)	Unit	Comment	Source
Electricity	0.1–0.2	€/kWh$_{el.}$	–	[72,78]
Waste water	1.87	€/m^3	–	[29]
Co catalyst (FT)	99.45	€/kg	Changed every 3 years	[32]
Ni catalyst (SR)	70.91	€/kg	Changed every 3 years	[55]
Process water	0.95	€/t	–	[32]
O_2 revenue	81.30	€/t	–	[56]
Stack overhaul	12 % of FCI$_{SOEL}$		Every 10 years	[6]

the SOEL's rated power, on the net production costs of Fischer-Tropsch products is displayed in Figure 2. A grid-based scenario realizing 8000 operating hours per year based on electricity costs of 0.2 €/kWh$_{el.}$ was assumed. The NPC range from 5.2 to 5.9 €/kg for a 1 MW$_{el.}$ pilot-scale plant. Scaling up the plant to 10 MW$_{el.}$ results in a cost reduction of 16 % to values of around 4.6 €/kg. A decrease in NPC of 20 %, compared with a rated power of 1 MW$_{el.}$, can be expected for a PtL plant based on a 100 MW$_{el.}$ electrolyzer. Scaling up by another factor to 1 GW$_{el.}$ does only result in a minor decrease in NPC by another 2 percentage points to values around 4.3 €/kg. Thus, the NPC of Fischer-Tropsch products can be significantly lowered by scaling up the PtL plant. However, the economy of scales' effect diminishes after surpassing a rated power of 100 MW$_{el.}$. A significant difference in NPC for the different plant configurations can be obtained for small-scale pilot plants. Nonetheless, this effect weakens for increased plant scales. Hence, process configuration 2, based on tail gas reforming by a steam reformer, is chosen as a reference scenario for this study due to its realistic technical feasibility.

3.2. CAPEX and OPEX

The costs of required equipment, e.g., compressors, pumps, reactors, solid-oxide electrolyzer and heat exchangers, in combination with fixed OPEX, variable OPEX and revenue for O_2, serve as a groundwork for the presented study.

3.2.1. CAPEX

The fixed capital investment, including base capacity and scaling exponent d, for the reference scenario of the evaluated PtL, process configuration 2, including a short tail gas recirculation and a tail gas reformer at a plant scale of 100 MW$_{el.}$ electrolyzer power input are listed in Table 8. The given data can be converted to different design scales by applying equation (6) in chapter 2.2.1. The solid-oxide electrolyzer unit is the major cost center with a required fixed capital investment of almost 80 mil. € in 2022. However, a significant cost reduction to 30 mil. € can be expected until 2050. Other central cost centers are the CO_2 capture unit, the FT process, steam reforming and the combustion of purge gas. The plant's input and output streams for the base scenario powered with grid electricity are displayed in Table 9.

3.2.2. Fixed OPEX, variable OPEX and oxygen revenue

The annual total fixed OPEX, variable OPEX and O_2 revenue of the reference scenario, process configuration 2, including a tail gas reformer based on a rated electrolyzer power of 100 MW$_{el.}$, is summarized in Table 10.

3.3. Cost allocation of Fischer-Tropsch products

As seen in chapter 3.1, scaling up PtL plants significantly affects the reduction of NPC until a certain threshold is reached. Analyzing the net production costs' respective cost centers and their allocation, displayed in Figure 3, is crucial in understanding Power-to-Liquid plants' ideal economic design parameters.

Figure 3 shows the respective cost centers' share, e.g., electricity, OPEX excluding electricity and CAPEX, as a function of the SOEL unit's rated power. The presented data is based on process configuration 2, including tail gas reforming with a steam reformer, with grid electricity costs of 0.1 and 0.2 €/kWh$_{el.}$.

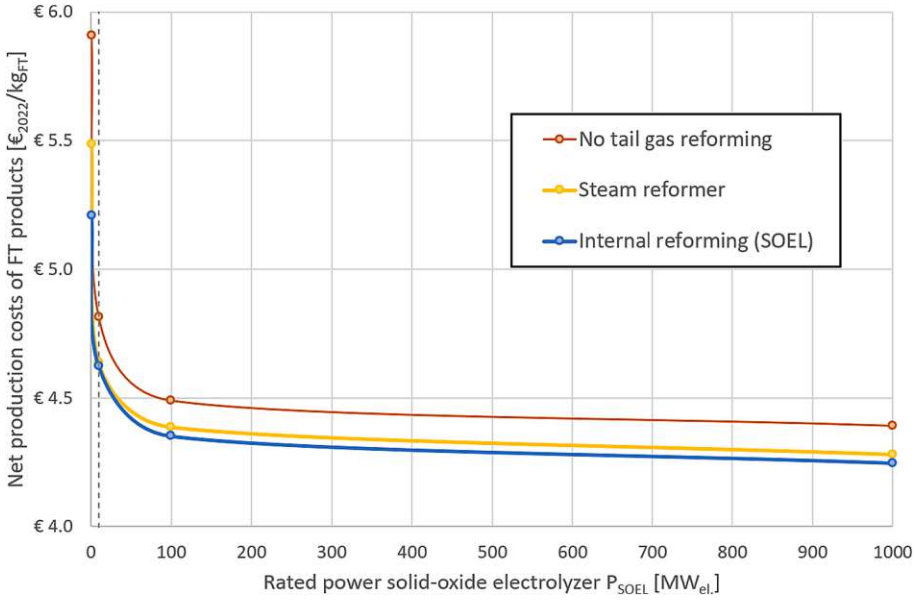

Fig. 2. Effect of plant configuration and scale-up on the net production costs of Fischer-Tropsch products.

Table 8
Fixed capital investment for process configuration 2 at a scale of 100 $MW_{el.}$ rated electrolyzer power.

Equipment	Capacity	Unit	d	FCI [mil. €$_{2022}$] [1)]	Source
MEA CO_2 capture	20	t_{CO2}/h	0.65	23.03 [2)]	[54]
$SOEL_{2022}$	100	$MW_{el.}$	1.00	79.75	[6,7,57]
$SOEL_{2050}$	100	$MW_{el.}$	1.00	30.00	[8]
FT reactor	66.5	MW_{FT}	0.70	19.68	[10,30,32,58,59]
FT product separation [3)]	5,430	kg_{FT}/h	0.65	5.51	[32]
Syngas compressor	6.6	$MW_{el.}$	0.60	7.02 [2)]	[26]
Steam reformer	980	kmol/h	0.65	12.02	[29,32]
Purge gas combustion	11	$MW_{th.}$	0.80	1.28 [2)]	[26]
Add. heat exchangers	–	m^2	–	5.90 [4)]	[26]
Product storage	5,430	kg_{FT}/h	0.65	1.94	[32]
Pumps and blowers	–	kg/h;Nm^3/h	0.65	0.05	[26,30]
Waste water plant	2.2	kg/s	1.00	0.40	[29]
Auxiliaries	–	–	–	1.07	–
SUM_{2022}	–	–	–	157.62	–
SUM_{2050}	–	–	–	107.87	–

1) Lang factor included.
2) Location factors: China = 0.61, U.S. Gulf Coast = 1, Germany = 1.11 [26].
3) Includes gas/liquid separation, wax separation and product drying.
4) Installation factor of 3.5 [26].

Table 9
Input and output streams of process configuration 2 at a scale of 100 $MW_{el.}$.

Input streams		Output streams	
Flue gas	150.0 t/h	Naphtha	1.3 t/h
(of which CO_2	20.0 t/h)	Middle distillate	2.0 t/h
Water	20.8 t/h	Wax	2.1 t/h
Air	28.7 t/h	FT water	7.8 t/h
		Flue gas	31.2 t/h
		(of which CO_2	3.2 t/h)
		Oxygen	21.4 t/h
		Water	3.7 t/h
		MEA off-gas	130.0 t/h
		(of which CO_2	2.2 t/h)
SUM	199.5 t/h	SUM	199.5 t/h

The electricity expenses are the plant's most substantial cost center, with shares of 78 % for a grid electricity price of 0.1 €/$kWh_{el.}$ and 88 % for a grid electricity price of 0.2 €/$kWh_{el.}$. The total NPC can be reduced by 26 % (0.2 €/$kWh_{el.}$) or 40 % (0.1 €/$kWh_{el.}$) when scaling up from 1 to 100 $MW_{el.}$. Responsible for that is the reduction in CAPEX and OPEX due to the benign effect of the economies of scale. The electricity's financial expenditure is directly proportional to the amount of synthesized Fischer-Tropsch products, thus explaining the substantial increase in electricity costs from 50 % to 78 % of the total NPC based on electricity costs of 0.1 €/$kWh_{el.}$. This phenomenon substantially limits the positive effect of plant scale-up on the net production costs of Fischer-Tropsch products after exceeding a SOEL rated power of 100 $MW_{el.}$.

3.4. 2022 and 2050 off-grid scenarios based on renewable electricity

This study aims to determine the economic differences between off-grid and grid-based PtL plants. The net production costs of Fischer-Tropsch products based on five different renewable sources for 2022 and 2050 are displayed in Figure 4. The presented outcomes are all founded on a discount rate of 6 % and a plant lifetime of 20 years. The respective levelized cost of electricity (LCOE) is based on a study by the International Renewable Energy Agency (IRENA) [60]. Expected values for the 2050 scenarios were taken from studies conducted by Sens et al. [61], Tran and Smith [62] and IRENA [60]. The evaluated power sources' expected full load hours were chosen adhering to studies published by Fraunhofer ISE [63], Tramme and Trieb [64], Fuchs [65] and Frick et al. [66]. Data concerning the SOEL unit's fixed capital investment is provided in chapter 3.2.1.

Table 10
Total annual OPEX and O_2 revenue for process configuration 2 at a scale of 100 $MW_{el.}$.

Cost center	Costs/revenue [mil. €$_{2022}$/a]
$OPEX_{Fixed}$	10.85
Electricity	177.68
Waste water	0.21
Process water	0.17
Co catalyst	0.56
Ni catalyst	0.23
Stack overhaul	0.48
O_2 revenue	−13.89
SUM	176.29

The results depicted in Figure 4 stress the plant availability's significant influence on the economic performance of Power-to-Liquid plants. Fischer-Tropsch products derived from a plant powered with geothermal electricity obtain the lowest NPC of 1.52 €/kg (2022) and 0.55 €/kg (2050) due to a plant availability of 7700 h per year. Supplying the presented plant concept with hydropower entails NPC of 1.55 €/kg in 2022 due to a satisfactory availability of 4400 annual operating hours. However, the LCOE of hydropower plants is not expected to decrease until 2050, thus showing limited potential for cost reductions until 2050. Off-grid PtL plants powered with onshore wind parks show promising potential for the 2050 scenario due to a significant decrease in LCOE, obtaining NPC of 1.10 €/kg. Offshore wind park and PV-powered PtL plants obtain the highest NPC of around 2.40 €/kg for the 2022 scenario. However, PV-based systems show the potential to significantly lower their NPC due to a projected significant decrease in LCOE until 2050.

A comparison between the economic performance of grid-based and off-grid Power-to-Liquid plants is given in Figure 5. Applying a grid electricity price of 0.1 €/$kWh_{el.}$ results in potential NPC of 2.42 €/kg. Grid-based PtL plants show a broad distribution in NPC due to their significant dependency on the electricity market. Applying electricity costs of 0.2 €/$kWh_{el.}$ results in NPC of 4.56 €/kg. Off-grid PtL plants powered with an onshore wind park (3500 operating hours and LCOE of 0.038 €/$kWh_{el.}$) can achieve lower NPC than the grid-based scenario of 1.85 €/kg. Implementing hybrid power plants, e.g., combining wind and solar power, has the potential to increase the plant availability, resulting in an enhanced economic performance of PtL plants. Applying additional electricity and syngas storage technologies can potentially result in plant availabilities exceeding 6000 annual operating hours. Based on these assumptions, NPC ranging from 1.08 to 1.28 €/kg can be realized based on the LCOE of onshore wind parks and photovoltaic farms in 2022.

Table 11 shows the differences in obtained NPC of FT products based

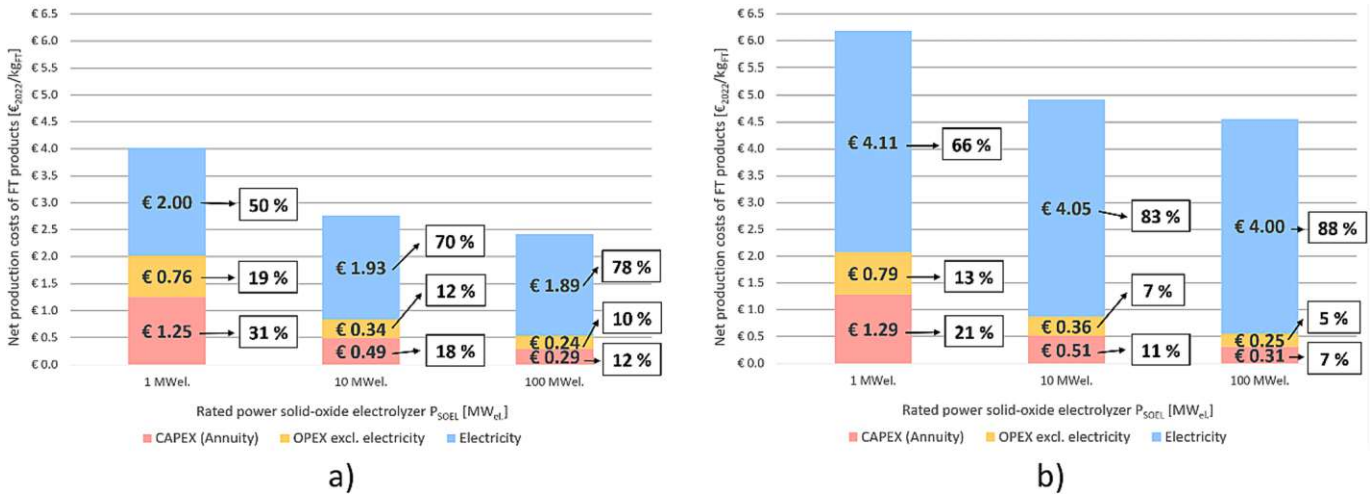

Fig. 3. Cost centers and cost allocation of Fischer-Tropsch products. a) Electricity costs = 0.1 €/kWh$_{el.}$. b) Electricity costs = 0.2 €/kWh$_{el.}$.

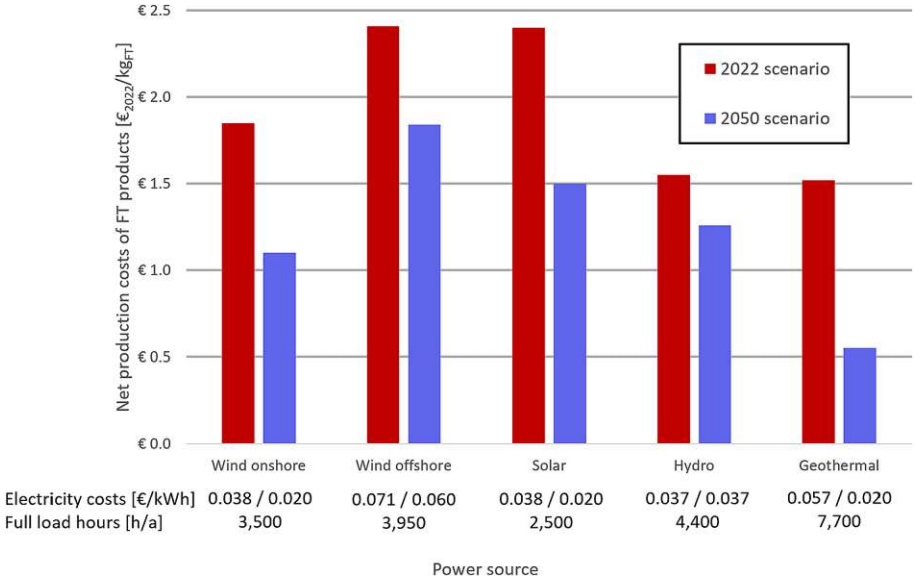

Fig. 4. Net production costs of Fischer-Tropsch products based on off-grid renewable power sources.

on SOEL and PEMEL technology for grid electricity scenarios. An increased electrolyzer scale of 152.8 MW$_{el.}$ is required to process the same mass flow rate of CO_2 based on an assumed specific electricity demand of 5 kWh$_{el.}$/Nm^3 H_2 [67] and a required fixed capital investment of 380 €/kW$_{el.}$ [68]. In addition, an rWGS reactor is necessary to convert CO_2 and H_2 into Syngas. Table 12 summarizes the different assumptions and specifications of the PEMEL process route. Assuming electricity costs of 0.2 €/kWh$_{el.}$ results in NPC of 4.46 €/kg (SOEL) and 6.53 €/kg (PEMEL), an increase of 46 %.

3.5. Required Fischer-Tropsch product selling price to break even

Table 13 summarizes the required FT product prices for amortization periods of 5, 10 and 20 years for scenarios based on grid electricity, an off-grid onshore wind park and a hybrid power plant. The grid electricity scenario requires prices ranging from 4.35 to 4.90 €/kg to break even between 5 and 20 years. A PtL plant based solely on onshore wind power must sell its FT products at prices between 1.77 and 3.02 €/kg. The most promising results of 1.22 to 1.95 €/kg are obtained by an off-grid power plant based on an assumed plant availability of 6000 h/a.

3.6. Sensitivity analysis

A sensitivity analysis, as displayed in Figure 6, has been conducted to evaluate the economic parameters', i.e., discount rate, plant lifetime, plant availability, electricity costs and fixed capital investment, influence on the net production costs of Fischer-Tropsch products. The assumed base values are listed in a separate textbox in Figure 6. An increase in electricity costs of 0.05 €/kWh$_{el.}$ leads to a rise in the NPC of Fischer-Tropsch products of 1.07 €/kg. The NPC decline exponentially for increasing plant availabilities. Power-to-Liquid plants operating below 3000 h per year entail a significant increase in net production costs. Enhancing the plant availability from 3000 to 6000 h/a results in a 15 % reduction in NPC. An additional increase to 8000 h/a reduces the NPC by 18 % compared with a plant availability of 3000 h/a. Compared to the electricity costs and the plant availability, the discount rate and plant lifetime have a negligible influence on the NPC of Fischer-Tropsch products. The impact of the plant's fixed capital investment on its economic performance is not as significant as the electricity costs and plant availability due to the substantial share of annual electricity expenses. Doubling the fixed capital investment from 160 to 320 mil. € results in an increase in NPC of 20 %.

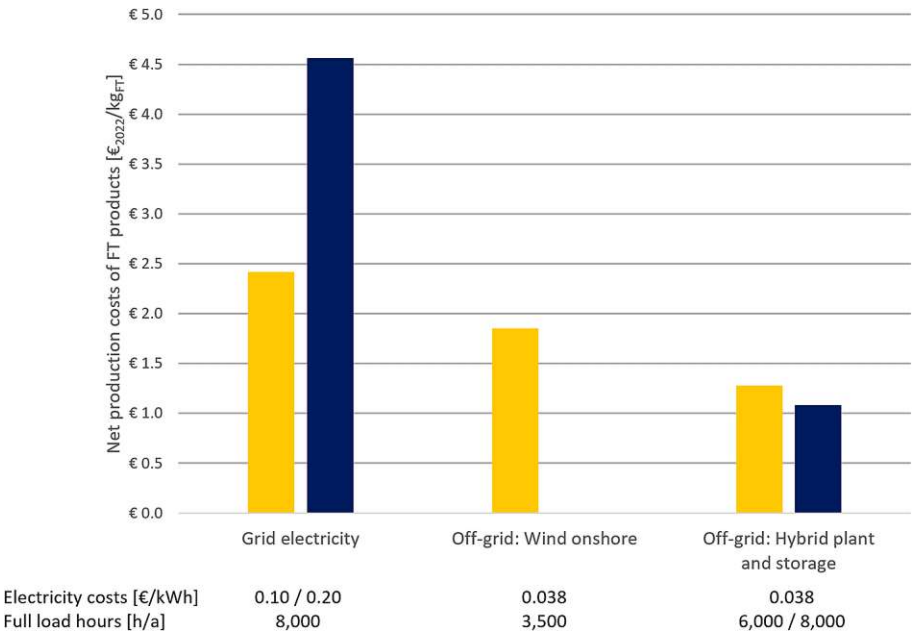

Fig. 5. Comparison of grid-based and off-grid scenarios of a Power-to-Liquid plant.

Table 11
NPC comparison between SOEL and PEMEL for process configuration 2.

Electrolyzer	0.1 €/kWh$_{el.}$	0.2 €/kWh$_{el.}$
SOEL	2.42 €/kg	4.56 €/kg
PEMEL	3.36 €/kg	6.53 €/kg

Table 12
Fixed capital investment of PEMEL and rWGS reactor.

Equipment	Capacity	Unit	d	FCI [mil. €$_{2022}$]	Source
rWGS reactor	22.8	t/h	0.60	8.83	[32]
PEMEL	152.8	MW$_{el.}$	1.00	58.05	[67,68]

Table 13
Required FT product prices for amortization periods of 5,10 and 20 years.

Scenario	5 years	10 years	20 years
Grid electricity [1)]	4.90 €/kg	4.53 €/kg	4.35 €/kg
Wind onshore [2)]	3.02 €/kg	2.17 €/kg	1.77 €/kg
Hybrid plant [3)]	1.95 €/kg	1.46 €/kg	1.22 €/kg

1) 0.2 €/kWh$_{el.}$; 8000 h/a.
2) 0.038 €/kWh$_{el.}$; 3500 h/a.
3) 0.038 €/kWh$_{el.}$; 6000 h/a.

4. Discussion

The economic performance of three different plant configurations, i.e., short tail gas recirculation with and without a tail gas reformer and a long tail gas recirculation cycle to the SOEL unit's inlet, were analyzed within the underlying study. A significant difference in NPC of 12 % was obtained at small-scale plants at a rated electrolyzer power of 1 MW$_{el.}$. However, only a 3 % difference was found at a rated power of 100 MW$_{el.}$. Scaling up PtL plants is necessary to make the technology cost-competitive with conventional fossil-based processes. A scale-up from 1 to 100 MW$_{el.}$ results in a 20 % reduction in NPC of Fischer-Tropsch products. Nonetheless, scaling up the plant by another factor of 10 has only a minor influence due to the increasing relative share of electricity costs per unit of FT product. Thus, the process route based on a short tail gas recirculation, including tail gas reforming at a scale of 100 MW$_{el.}$, was chosen as this study's reference scenario.

Total fixed capital investments of 157.6 and 107.9 mil. € were determined for the 2022 and 2050 scenarios, respectively. Annual fixed OPEX of 10.9 mil. € and annual variable OPEX of 179.3 mil. € are required to operate a grid-based PtL plant at the chosen reference scenario. Electricity costs accounted for the major share of OPEX with 177.7 mil. € per year. Sales for the by-product O_2 amount to 13.9 mil. € per year.

Furthermore, the cost allocation of Fischer-Tropsch products was analyzed for a grid-based scenario assuming electricity costs of 0.1 and 0.2 €/kWh$_{el.}$. CAPEX and fixed OPEX combined obtain significant shares of 34 % and 50 % for small-scale plants at 1 MW$_{el.}$ rated electrolyzer power but have only a minor influence on the NPC of FT products for industrial-scale PtL plants. The relative share of electricity costs increases substantially to shares of 78 % to 88 % at a scale of 100 MW$_{el.}$, thus explaining the limited effect of scale-up when surpassing a rated electrolyzer power of 100 MW$_{el.}$.

Various off-grid scenarios of PtL plants were evaluated in the presented study. Lower electricity costs can be realized by off-grid renewable power sources. However, this comes at the expense of decreased plant availability due to limited full load hours. The NPC of Fischer-Tropsch products based on off-grid scenarios ranged from 1.52 €/kg for a geothermal power plant to 2.40 €/kg for a photovoltaic farm for the 2022 scenario. NPC ranging from 0.55 to 1.84 €/kg were obtained for the 2050 scenario. The inferior economic results based on photovoltaic plants can be explained by its limited full load hours of only 2500 h/a and below. In contrast, geothermal plants provide relatively low electricity costs in combination with beneficial full load hours of up to 7700 h/a. Hybrid power plants, based on solar and wind power, in combination with electricity or syngas storage technologies could be applied to increase the plant availability to industrial levels of around 8000 h/a, potentially realizing NPC based on non-grid scenarios of 1.08 to 1.28 €/kg. Analyzed grid-based scenarios lead to NPC ranging between 2.42 and 4.56 €/kg for assumed electricity costs of 0.1 and 0.2 €/kWh$_{el.}$. A comparison with a grid-based process configuration including a PEMEL unit and an rWGS reactor resulted in NPC ranging from 3.36 to 6.53 €/kg.

In addition, the required FT product selling prices for amortization periods of 5,10 and 20 years were determined for scenarios based on grid electricity, an onshore wind park and a hybrid power plant. The most promising selling prices of 1.22 to 1.95 €/kg were obtained based

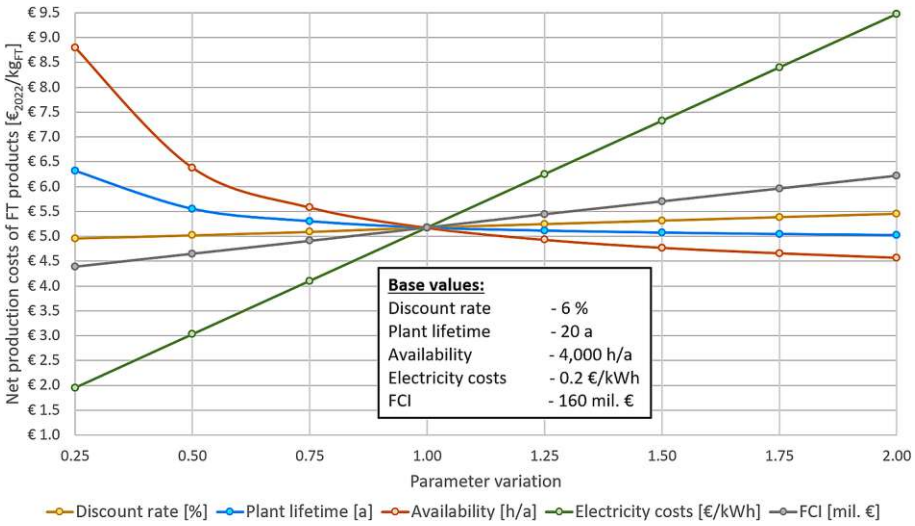

Fig. 6. Sensitivity analysis – influence of economic parameters on the net production costs of Fischer-Tropsch products.

on a hybrid power plant. Significantly higher selling prices between 1.77 and 3.02 €/kg are required to amortize an off-grid PtL plant solely based on onshore wind power compared with the grid electricity-based scenario, obtaining prices ranging from 4.35 to 4.90 €/kg.

The plant availability and electricity costs are the main levers for the economic performance of PtL plants. Off-grid-based plants are unaffected by the electricity market's uncertainty, making them less susceptible to potential future crises, but entail disadvantageous plant availability. As indicated by a sensitivity analysis, the availability of PtL plants should not drop below 3000 h/a. The long-term goal should be the realization of 6000 h/a by implementing hybrid off-grid power plants in combination with electricity and syngas storage technologies.

Table 14 displays a comparison of this study's results, grid-based as well as off-grid scenarios for 2022 and 2050, with previously conducted economic assessments of PtL processes. All values have been converted to 2022 levels based on the CEPCI. The presented study's results lie within the obtained values of previous studies. Compared with BtL plants, PtL plant concepts underlie larger uncertainties due to their high dependency on electricity costs and alternating plant availabilities.

Power-to-liquid plants based on photovoltaic farms and offshore wind parks obtained the highest NPC of 2.40 €/kg regarding the evaluated off-grid scenarios. PtL plants based on onshore wind parks obtained better results than those powered with offshore wind parks by balancing their lower availability with decreased LCOE. Geothermal power plants are tailor-made for PtL plants due to their availability of up to 7700 h/a in combination with LCOE or around 0.05 €/$kWh_{el.}$. The 2050 scenarios based on onshore wind parks and geothermal plants showed the most promising reductions in NPC, which were 41 % and 64 %, respectively. It has to be stated that the assessed 2050 scenarios did not consider technology learning curves for already established industrial processes, i.e., MEA-based CO_2 capture and Fischer-Tropsch technology.

Finding the optimum location for PtL plants is a highly challenging task. Choosing locations with low electricity costs and high availability of renewable power sources seems reasonable but entails additional risk factors due to long supply chains and political and economic dependency. Compelling arguments for implementing PtL plants in Europe are shortened supply chains, regional added-value and jobs as well as an independent supply with sustainable fuels and platform chemicals. The North Sea and Baltic coast, i.e., Denmark, Sweden, The Netherlands and northern Germany, are promising PtL plant locations in Europe due to their high availability of water and wind power as well as their vicinity to CO_2 emitting industries. Viable locations of off-grid PtL plants could be offshore PtX hubs in the North Sea, based on offshore wind power, Iceland, based on geothermal power plants and the North Sea and Baltic coastline, based on onshore wind power.

Recirculating the FT water to the electrolyzer or steam reformer can potentially increase the plant's performance but entails too much risk under current circumstances. Water electrolysis is highly sensitive to impurities. Thus, utilizing the FT water as a feedstock can significantly reduce stack lifetime and, hence, the process's economic performance. A possible alternative is using FT water for tail gas reforming, thus providing the reformer with steam while reforming the FT water's oxygenate content. However, technology providers have strict water purity specifications and might not guarantee liability if those are not met.

The presented study is based on static process simulation; thus, the fluctuating behavior of renewable power sources was not considered. Only limited economic and technical data is available due to the SOEL technology's comparably low TRL. Nonetheless, the TRL is expected to increase significantly within this decade because of the spiking interest in this technology. As a result, the required fixed capital investment is anticipated to drop substantially due to increased production capacities. Another factor of uncertainty is the assumed revenue realized by selling produced O_2. Future industrial sites must be founded on smart sector coupling concepts, bringing together the supply and demand of by-products like oxygen.

Supplying PtL plants with grid electricity ensures an industrial availability of up to 8000 h/a but also entails exposure to possible electricity market disruptions. In addition, the plant's location substantially influences the CO_2 footprint of Fischer-Tropsch products concerning the local electricity mix's emission factor. In contrast, off-grid-based solutions ensure the supply of cheap and clean electricity but have to deal with low full load hours. The presented study adds value to previous techno-economic assessments by providing detailed economic information concerning the most beneficial electricity sources for PtL plants based on 2022 parameters. In addition, this study facilitates the design of future PtL plants by discussing the effects of plant configuration and scale-up from an economic vantage point. An analysis of the FT products' cost allocation underpinned the substantial impact of electricity costs with increasing plant scales. A scale of 100 $MW_{el.}$ rated electrolyzer power emerged as the optimum and is thus recommended for future PtL projects.

5. Conclusions

The presented study's objective was to evaluate the economic performance of a Power-to-Liquid plant combining a solid-oxide electrolyzer and Fischer-Tropsch synthesis. In detail, grid-based and off-grid scenarios for various renewable electricity sources, i.e., wind,

Table 14
Comparison of obtained results with previous PtL and BtL techno-economic assessments.

NPC [1)]	This study: grid-based	This study: off-grid (2022)	This study: off-grid (2050)	[31]	[30]	[36]	[9]	[33]	[30]	[32]	[69]	[29]
Tech.	SOEL + FT	SOEL + FT	SOEL + FT	SOEL + FT	SOEL + FT	SOEL + FT	SOEL + FT	Elec + FT	PEM + FT	rWGS + FT	BtL	BtL
NPC_{Min}	2.42	1.28	0.55	1.38	3.40	1.26	2.24	8.40	4.39	2.59	3.09	1.42
NPC_{Max}	4.56	2.40	1.84	2.72	7.70	1.61	5.38	10.60	7.26	2.84	4.65	3.85

[1)] All values in €/kg and converted to 2022 levels (CEPCI = 816.0).

photovoltaic, hydro and geothermal, were assessed to answer the following research question:

Should off-grid Power-to-Liquid plants powered with renewable electricity be prioritized over the supply with grid electricity?

Three process configurations were evaluated for plant scales ranging from 1 to 1000 $MW_{el.}$ rated electrolyzer power. Scaling up the plant from 1 $MW_{el.}$ to 100 $MW_{el.}$ results in a 20 % reduction in net production costs of Fischer-Tropsch products. However, further scaling up the plant to 1000 $MW_{el.}$ resulted only in an additional decrease of 2 percentage points. No significant differences in net production costs of Fischer-Tropsch products were obtained for the three analyzed process configurations at a plant scale exceeding 100 $MW_{el.}$. Thus, plant configuration 2, based on a short tail gas recycle, including steam reforming of tail gas, was chosen as a reference for further analyses.

Additionally, the Fischer-Tropsch products' cost allocation was assessed in detail for a grid-based scenario. The capital expenditure and the electricity costs are significant cost centers for pilot-scale Power-to-Liquid plants at a rated electrolyzer power of 1 $MW_{el.}$, obtaining shares of 31 % and 50 %. The electricity costs become the main cost driver for industrial-scale Power-to-Liquid plants at 100 $MW_{el.}$ with a share of up to 88 %. This observation explains the diminishing effect of economies of scale for Power-to-Liquid plants.

The most promising results of the analyzed off-grid 2022 scenarios of 1.52 €/kg were obtained based on geothermal electricity, whereas applying offshore wind power or photovoltaic power resulted in the worst outcome of 2.40 €/kg. Using onshore wind power resulted in net production costs of 1.85 €/kg. Net production costs of 1.55 €/kg were obtained for the 2022 off-grid scenario based on hydropower.

In addition, 2050 scenarios were established based on expected reductions in the solid-oxide electrolyzer's fixed capital investment and the renewable power sources' levelized cost of electricity. Reduced net production costs ranging from 0.55 €/kg (geothermal) and 1.84 €/kg (offshore wind) are expected for off-grid scenarios until 2050.

In comparison, the assessed grid-based scenarios for the reference plant configuration resulted in Fischer-Tropsch net production costs ranging from 2.42 to 4.56 €/kg, based on electricity costs of 0.1 and 0.2 €/$kWh_{el.}$, respectively.

Fischer-Tropsch products must be sold at 1.95 €/kg for an off-grid PtL plant powered by a hybrid power plant to realize an amortization period of five years. A substantially higher selling price of 4.90 €/kg is necessary for the grid-based scenario due to significantly higher electricity costs.

The sensitivity analysis underlined the crucial influence of electricity costs and plant availability on the economic feasibility of Power-to-Liquid plants. Increasing the electricity costs by 0.05 €/$kWh_{el.}$ entails an increase in net production costs of 1.07 €/kg. Furthermore, the economic performance of Power-to-Liquid plants sinks substantially when the plant availability falls below 3000 operating hours per year. In general, plant availabilities surpassing 4000 h/a are recommended for future Power-to-Liquid projects.

Uncertain economic parameters regarding the solid-oxide electrolyzer are a potential weakness of the underlying assessment. However, significant reductions in required fixed capital investment are expected within the following years due to a substantial expansion in solid-oxide electrolysis production capacities. Another uncertainty factor is the study's foundation on static process simulation software.

The presented techno-economic assessment of a Power-to-Liquid plant adds value to existing studies showing that off-grid solutions have the potential to be cost-competitive with grid-based plants. Off-grid configurations offer cheap electricity but underlie the significant downfall of inferior full load hours. Thus, hybrid power plants and storage technologies must be established to further increase off-grid Power-to-Liquid concepts' feasibility. In addition, future Power-to-Liquid projects are facilitated by this study's findings concerning the ideal plant configuration and scale of 100 $MW_{el.}$ rated electrolyzer power.

Future research based on this study's findings should implement dynamic simulation tools to analyze the power supply of renewable volatile electricity sources, e.g., wind and solar, for different seasons and plant locations. In addition, hybrid power plants, including electricity or syngas storage technologies, could be designed in combination with the presented plant concept, thus approximating industrial plant availabilities of 7500 annual operating hours or higher. Integrating Fischer-Tropsch waste water as a feedstock for the electrolyzer or reformer can potentially increase the process's performance and hence, should be evaluated in experimental studies. Furthermore, future studies focusing on life cycle assessments of the grid-based and off-grid scenarios established in this work are essential to ensure a holistic evaluation of Power-to-Liquid processes. Conducting economic studies assessing potential business cases of the presented Power-to-Liquid plant is recommended for different plant locations in Europe.

Funding

The underlying work has received funding from the Mobility of the Future program – a research, technology and innovation funding program of the Federal Ministry of Climate Action, Environment, Energy, Mobility, Innovation and Technology, Republic of Austria. The Austrian Research Promotion Agency (FFG) has been authorized for the program management of the project "IFE – Innovation Flüssige Energie" (project #884340). In addition, the authors would like to thank TU Wien Bibliothek for covering article processing charges through its Open Access Funding program.

CRediT authorship contribution statement

Simon Pratschner: Conceptualization, Data curation, Formal analysis, Investigation, Methodology, Software, Validation, Visualization, Writing – original draft, Writing – review & editing. **Martin Hammerschmid:** Methodology, Project administration, Software, Validation, Writing – review & editing. **Stefan Müller:** Funding acquisition, Project administration, Resources, Software, Supervision, Writing – review & editing. **Franz Winter:** Funding acquisition, Project administration, Resources, Supervision, Writing – review & editing.

Declaration of competing interest

The authors declare that they have no known competing financial interests or personal relationships that could have appeared to influence the work reported in this paper.

Data availability

Data will be made available on request.

Acknowledgements

The authors would like to acknowledge the "IFE – Innovation Flüssige Energie" project consortium, the TU Wien doctoral college CO_2Refinery and the open access funding by TU Wien.

References

[1] C. Wulf, P. Zapp, A. Schreiber, Review of power-to-X demonstration projects in Europe, Front. Energy Res. 8 (2020) 191, https://doi.org/10.3389/fenrg.2020.00191.
[2] S. Pratschner, M. Hammerschmid, S. Müller, F. Winter, Evaluation of CO2 sources for power-to-liquid plants producing Fischer-Tropsch products, J. CO2 Util. 72 (2023) 102508, https://doi.org/10.1016/j.jcou.2023.102508.
[3] S. Pratschner, F. Radosits, A. Ajanovic, F. Winter, Techno-economic assessment of a power-to-green methanol plant, J. CO2 Util. 75 (2023) 102563, https://doi.org/10.1016/j.jcou.2023.102563.
[4] A. Kecebas, M. Kayfeci, M. Bayat, Electrochemical hydrogen generation, in: Solar Hydrogen Production - Processes, Systems and Technologies, 2019.
[5] O. Schmidt, A. Gambhir, I. Staffell, A. Hawkes, J. Nelson, S. Few, Future cost and performance of water electrolysis: an expert elicitation study, Int. J. Hydrogen Energy 42 (2017) 30470–30492, https://doi.org/10.1016/j.ijhydene.2017.10.045.
[6] M. Decker, F. Schorn, R.C. Samsun, R. Peters, D. Stolten, Off-grid power-to-fuel systems for a market launch scenario – a techno-economic assessment, Appl. Energy 250 (2019) 1099–1109, https://doi.org/10.1016/j.apenergy.2019.05.085.
[7] D. DeSantis, B. James, G. Saur, H2A: Hydrogen Analysis Production Models - Future Central Hydrogen Production from PEM electrolysis (2019) version 3.2018, (2019). https://www.nrel.gov/hydrogen/h2a-production-models.html (accessed October 4, 2022).
[8] European Commission. Directorate General for Energy., E3 Modelling., Ecofys., Tractebel., Technology pathways in decarbonisation scenarios., Publications Office, LU, 2020. https://data.europa.eu/doi/10.2833/994817 (accessed February 9, 2023)..
[9] G. Herz, E. Reichelt, M. Jahn, Techno-economic analysis of a co-electrolysis-based synthesis process for the production of hydrocarbons, Appl. Energy 215 (2018) 309–320, https://doi.org/10.1016/j.apenergy.2018.02.007.
[10] M. Marchese, E. Giglio, M. Santarelli, A. Lanzini, Energy performance of Power-to-Liquid applications integrating biogas upgrading, reverse water gas shift, solid oxide electrolysis and Fischer-Tropsch technologies, Energy Convers. Manage.: x. 6 (2020) 100041, https://doi.org/10.1016/j.ecmx.2020.100041.
[11] Y. Wang, T. Liu, L. Lei, F. Chen, High temperature solid oxide H2O/CO2 co-electrolysis for syngas production, Fuel Process. Technol. 161 (2017) 248–258, https://doi.org/10.1016/j.fuproc.2016.08.009.
[12] G. Cinti, A. Baldinelli, A. Di Michele, U. Desideri, Integration of Solid Oxide Electrolyzer and Fischer-Tropsch: A sustainable pathway for synthetic fuel, Appl. Energy 162 (2016) 308–320, https://doi.org/10.1016/j.apenergy.2015.10.053.
[13] G. Cinti, G. Discepoli, G. Bidini, A. Lanzini, M. Santarelli, Co-electrolysis of water and CO 2 in a solid oxide electrolyzer (SOE) stack: Study of high-temperature co-electrolysis reactions in SOEC, Int. J. Energy Res. 40 (2016) 207–215, https://doi.org/10.1002/er.3450.
[14] A. Hauch, K. Brodersen, M. Chen, M.B. Mogensen, Ni/YSZ electrodes structures optimized for increased electrolysis performance and durability, Solid State Ion. 293 (2016) 27–36, https://doi.org/10.1016/j.ssi.2016.06.003.
[15] C.M. Stoots, J.E. O'Brien, J.S. Herring, J.J. Hartvigsen, Syngas production via high-temperature coelectrolysis of steam and carbon dioxide, J. Fuel Cell Sci. Technol. 6 (2009) 011014, https://doi.org/10.1115/1.2971061.
[16] H. Xu, B. Chen, J. Irvine, M. Ni, Modeling of CH4-assisted SOEC for H2O/CO2 co-electrolysis, Int. J. Hydrogen Energy 41 (2016) 21839–21849, https://doi.org/10.1016/j.ijhydene.2016.10.026.
[17] H. Becker, J. Murawski, D.V. Shinde, I.E.L. Stephens, G. Hinds, G. Smith, Impact of impurities on water electrolysis: a review, Sustainable Energy Fuels 7 (2023) 1565–1603, https://doi.org/10.1039/D2SE01517J.
[18] A. de Klerk, Fischer-Tropsch Refining, 1st. ed., Wiley-VCH, Weinheim, Germany, 2011.
[19] R. Guettel, U. Kunz, T. Turek, Reactors for Fischer-Tropsch synthesis, Chem. Eng. Technol. 31 (2008) 746–754, https://doi.org/10.1002/ceat.200800023.
[20] J. Guilera, J.A. Díaz-López, A. Berenguer, M. Biset-Peiró, T. Andreu, Fischer-Tropsch synthesis: towards a highly-selective catalyst by lanthanide promotion under relevant CO2 syngas mixtures, Appl. Catal. A 629 (2022) 118423, https://doi.org/10.1016/j.apcata.2021.118423.
[21] M. Martinelli, M.K. Gnanamani, S. LeViness, G. Jacobs, W.D. Shafer, An overview of Fischer-Tropsch Synthesis: XtL processes, catalysts and reactors, Appl. Catal. A 608 (2020) 117740, https://doi.org/10.1016/j.apcata.2020.117740.
[22] C. Bouchy, G. Hastoy, E. Guillon, J.A. Martens, Fischer-Tropsch Waxes Upgrading *via* hydrocracking and selective hydroisomerization, Oil & Gas Science and Technology - Rev IFP. 64 (2009) 91–112, https://doi.org/10.2516/ogst/2008047.
[23] A.M. Petersen, F. Chireshe, O. Okoro, J. Gorgens, J. Van Dyk, Evaluating refinery configurations for deriving sustainable aviation fuel from ethanol or syncrude, Fuel Process. Technol. 219 (2021) 106879, https://doi.org/10.1016/j.fuproc.2021.106879.
[24] N.A. Rahman, C. Jose Jol, A.A. Linus, D.S. Rozellia Kamel Sharif, V. Ismail, Fischer Tropsch water composition study from distillation process in gas to liquid technology with ASPEN simulation, Case Stud. Chem. Environ. Eng. 3 (2021) 100106, https://doi.org/10.1016/j.cscee.2021.100106.
[25] N. Ahad, A. De Klerk, Fischer-Tropsch acid water processing by Kolbe electrolysis, Fuel 211 (2018) 415–419, https://doi.org/10.1016/j.fuel.2017.09.075.
[26] G.P. Towler, R.K. Sinnott, Chemical engineering design: principles, practice and economics of plant and process design, Third edition, Butterworth-Heinemann, Oxford [England] ; Cambridge, MA, 2022.
[27] W.D. Seider, D.R. Lewin, J.D. Seader, S. Widagdo, R. Gani, K.M. Ng, Product and process design principles: synthesis, analysis, and evaluation, fourth ed., John Wiley & Sons Inc., New York, 2017.
[28] K.T. Peters, Plant Design and Economics for Chemical Engineers, 4th ed., McGraw-Hill Book Co., 1991.
[29] U. Neuling, M. Kaltschmitt, Techno-economic and environmental analysis of aviation biofuels, Fuel Process. Technol. 171 (2018) 54–69, https://doi.org/10.1016/j.fuproc.2017.09.022.
[30] G. Herz, C. Rix, E. Jacobasch, N. Müller, E. Reichelt, M. Jahn, A. Michaelis, Economic assessment of Power-to-Liquid processes – Influence of electrolysis technology and operating conditions, Appl. Energy 292 (2021) 116655, https://doi.org/10.1016/j.apenergy.2021.116655.
[31] R. Peters, N. Wegener, R.C. Samsun, F. Schorn, J. Riese, M. Grünewald, D. Stolten, A techno-economic assessment of fischer-tropsch fuels based on syngas from co-electrolysis, Processes. 10 (2022) 699, https://doi.org/10.3390/pr10040699.

[32] G. Zang, P. Sun, A.A. Elgowainy, A. Bafana, M. Wang, Performance and cost analysis of liquid fuel production from H2 and CO2 based on the Fischer-Tropsch process, J. CO2 Util. 46 (2021) 101459, https://doi.org/10.1016/j.jcou.2021.101459.
[33] C. Markowitsch, M. Lehner, M. Maly, Evaluation of process structures and reactor technologies of an integrated power-to-liquid plant at a cement factory, J. CO2 Util. 70 (2023) 102449, https://doi.org/10.1016/j.jcou.2023.102449.
[34] S. Pratschner, M. Hammerschmid, S. Müller, F. Winter, CO2 Footprint of Fischer-Tropsch Products produced by a Power-to-Liquid Plant, in: 15th Mediterranean Congress of Chemical Engineering (MeCCE-15) Abstracts Publication, Grupo Pacífico, 2022. https://doi.org/10.48158/MeCCE-15.T4-O-16.
[35] M. Micheli, D. Moore, V. Bach, M. Finkbeiner, Life-cycle assessment of power-to-liquid kerosene produced from renewable electricity and CO2 from direct air capture in Germany, Sustainability 14 (2022) 10658, https://doi.org/10.3390/su141710658.
[36] M. Fasihi, D. Bogdanov, C. Breyer, Techno-economic assessment of power-to-liquids (PtL) fuels production and global trading based on hybrid PV-wind power plants, Energy Procedia 99 (2016) 243–268, https://doi.org/10.1016/j.egypro.2016.10.115.
[37] J.M. Spurgeon, B. Kumar, A comparative technoeconomic analysis of pathways for commercial electrochemical CO $_2$ reduction to liquid products, Energy Environ. Sci. 11 (2018) 1536–1551, https://doi.org/10.1039/C8EE00097B.
[38] HELMETH, High temperature electrolysis cell (SOEC), (n.d.). http://www.helmeth.eu/index.php/technologies/high-temperature-electrolysis-cell-soec (accessed February 22, 2022).
[39] D. Förtsch, K. Pabst, E. Groß-Hardt, The product distribution in Fischer-Tropsch synthesis: an extension of the ASF model to describe common deviations, Chem. Eng. Sci. 138 (2015) 333–346, https://doi.org/10.1016/j.ces.2015.07.005.
[40] S. Pratschner, M. Hammerschmid, F.J. Müller, S. Müller, F. Winter, Simulation of a pilot scale power-to-liquid plant producing synthetic fuel and wax by combining fischer-tropsch synthesis and SOEC, Energies 15 (2022) 4134, https://doi.org/10.3390/en15114134.
[41] P.M. Maitlis, A. de Klerk (Eds.), Greener Fischer-Tropsch Processes for Fuels and Feedstocks, Wiley-VCH, Weinheim, 2013.
[42] L.-M. Bjerge, P. Brevik, CO2 capture in the cement industry, norcem CO2 capture project (Norway), Energy Procedia 63 (2014) 6455–6463, https://doi.org/10.1016/j.egypro.2014.11.680.
[43] T. Hills, D. Leeson, N. Florin, P. Fennell, Carbon capture in the cement industry: technologies, progress, and retrofitting, Environ. Sci. Technol. 50 (2016) 368–377, https://doi.org/10.1021/acs.est.5b03508.
[44] K. Li, A. Cousins, H. Yu, P. Feron, M. Tade, W. Luo, J. Chen, Systematic study of aqueous monoethanolamine-based CO $_2$ capture process: model development and process improvement, Energy Sci. Eng. 4 (2016) 23–39, https://doi.org/10.1002/ese3.101.
[45] T. Pröll, G. Schöny, G. Sprachmann, H. Hofbauer, Introduction and evaluation of a double loop staged fluidized bed system for post-combustion CO 2 capture using solid sorbents in a continuous temperature swing adsorption process, Chem. Eng. Sci. 141 (2016) 166–174, https://doi.org/10.1016/j.ces.2015.11.005.
[46] Y. Wang, L. Zhao, A. Otto, M. Robinius, D. Stolten, A review of post-combustion CO2 capture technologies from coal-fired power plants, Energy Procedia 114 (2017) 650–665, https://doi.org/10.1016/j.egypro.2017.03.1209.
[47] B.T. Schädel, M. Duisberg, O. Deutschmann, Steam reforming of methane, ethane, propane, butane, and natural gas over a rhodium-based catalyst, Catal. Today 142 (2009) 42–51, https://doi.org/10.1016/j.cattod.2009.01.008.
[48] H.-G. Park, S.-Y. Han, K.-W. Jun, Y. Woo, M.-J. Park, S.K. Kim, Bench-scale steam reforming of methane for hydrogen production, Catalysts 9 (2019) 615, https://doi.org/10.3390/catal9070615.
[49] D.O. Kunysz, Kostenschätzung im chemischen anlagenbau: cost estimation basics, springer fachmedien wiesbaden, Wiesbaden (2020), https://doi.org/10.1007/978-3-658-29251-5.
[50] M.S. Peters, K.D. Timmerhaus, R.E. West, Plant Design and Economics for Chemical Engineers, 5th ed, McGraw-Hill, New York, 2003.
[51] R. Turton (Ed.), Analysis, Synthesis, and Design of Chemical Processes, 4th ed., Prentice Hall, Upper Saddle River, NJ, 2012.
[52] Access Intelligence LLC, Chemical Engineering, April 2023. Volume 130 (4) (2023).
[53] D.W. Green, M.Z. Southard (Eds.), Perry's Chemical Engineers' Handbook, Ninth Edition, 85th, anniversary ed., McGraw Hill Education, New York, 2019.
[54] Y. Yang, T. Du, Y. Li, Q. Yue, H. Wang, L. Liu, S. Che, Y. Wang, Techno-economic assessment and exergy analysis of iron and steel plant coupled MEA-CO2 capture process, J. Clean. Prod. 416 (2023) 137976, https://doi.org/10.1016/j.jclepro.2023.137976.
[55] F. Müller-Langer, Analyse und Bewertung ausgewählter zukünftiger Biokraftstoffoptionen auf Basis fester Biomasse, Deutsches Biomasse Forschungszentrum, Leipzig, GER, 2011.
[56] M. Yousaf, A. Mahmood, A. Elkamel, M. Rizwan, M. Zaman, Techno-economic analysis of integrated hydrogen and methanol production process by CO2 hydrogenation, Int. J. Greenhouse Gas Control 115 (2022) 103615, https://doi.org/10.1016/j.ijggc.2022.103615.
[57] S. Schemme, Techno-economic Assessment of Processes for the Production of Fuels from H2 and CO2, Rheinisch-Westfälische Technische Hochschule Aachen, Institut für Energie- und Klimaforschung, 2020.
[58] R. Swanson, J. Satrio, R. Brown, A. Platon, D. Hsu, Techno-Economic Analysis of Biofuels Production Based on Gasification, National Renewable Energy Laboratory, U.S. Department of Energy, 2010 https://www.nrel.gov/docs/fy11osti/46587.pdf (accessed September 27, 2022.
[59] T.G. Kreutz, E.D. Larson, C. Elsido, E. Martelli, C. Greig, R.H. Williams, Techno-economic prospects for producing Fischer-Tropsch jet fuel and electricity from lignite and woody biomass with CO2 capture for EOR, Appl. Energy 279 (2020) 115841, https://doi.org/10.1016/j.apenergy.2020.115841.
[60] IRENA, Renewable Power Generation Costs in 2021, International Renewable Energy Agency, Abu Dhabi, n.d.
[61] L. Sens, U. Neuling, M. Kaltschmitt, Capital expenditure and levelized cost of electricity of photovoltaic plants and wind turbines – Development by 2050, Renew. Energy 185 (2022) 525–537, https://doi.org/10.1016/j.renene.2021.12.042.
[62] T.T.D. Tran, A.D. Smith, Incorporating performance-based global sensitivity and uncertainty analysis into LCOE calculations for emerging renewable energy technologies, Appl. Energy 216 (2018) 157–171, https://doi.org/10.1016/j.apenergy.2018.02.024.
[63] C. Kost, S. Shivenes, V. Jülch, H.-T. Nguyen, T. Schlegl, Stromgestehungskosten Erneuerbare Energien, Fraunhofer ISE, 2018.
[64] R. Tamme, F. Trieb, DESERTEC - Wüstenstrom für Europa und MENA, German Aerospace Center, 2011. https://elib.dlr.de/71720/1/09-13-2011-BMWi-Trieb.pdf.
[65] M. Fuchs, Hydropower Potential in Austria, Pöyry Austria, Vienna, 2018. https://oesterreichsenergie.at/fileadmin/user_upload/Oesterreichs_Energie/Publikationsdatenbank/Studien/2018/WasserkraftpotenzialOesterreich2018.pdf.
[66] S. Frick, M. Kaltschmitt, G. Schröder, Life cycle assessment of geothermal binary power plants using enhanced low-temperature reservoirs, Energy 35 (2010) 2281–2294, https://doi.org/10.1016/j.energy.2010.02.016.
[67] M. Nasser, T.F. Megahed, S. Ookawara, H. Hassan, A review of water electrolysis–based systems for hydrogen production using hybrid/solar/wind energy systems, Environ. Sci. Pollut. Res. 29 (2022) 86994–87018, https://doi.org/10.1007/s11356-022-23323-y.
[68] A.H. Reksten, M.S. Thomassen, S. Møller-Holst, K. Sundseth, Projecting the future cost of PEM and alkaline water electrolysers; a CAPEX model including electrolyser plant size and technology development, Int. J. Hydrogen Energy 47 (2022) 38106–38113, https://doi.org/10.1016/j.ijhydene.2022.08.306.
[69] F.G. Albrecht, D.H. König, N. Baucks, R.-U. Dietrich, A standardized methodology for the techno-economic evaluation of alternative fuels – a case study, Fuel 194 (2017) 511–526, https://doi.org/10.1016/j.fuel.2016.12.003.

Online references

[70] Danish Ministry of Climate, Energy and Utilities. 2023. The Government's strategy for Power-to-X. Available at: https://ens.dk/sites/ens.dk/files/ptx/strategy_ptx.pdf. [Accessed: 15.12.2023].
[71] Federal Ministry for Economic Cooperation and Development. 2023. Green Hydrogen and Power-to-X. Available at: https://www.bmz.de/de/themen/wasserstoff#:~:text=Ziel%20der%20Strategie%20ist%20es,Ausr%C3%BCster%20modernster%20Wasserstofftechnik%20zu%20machen. [Accessed: 15.12.2023].
[72] Statista. 2023. Prices of electricity for non-household consumers with a consumption of 500 to 2,000 MWh in the European Union from 2008 to 2022. Statista. Available at: https://www.statista.com/statistics/1046630/electricity-prices-for-non-household-european-union/. [Accessed: 13.12.2023].
[73] European Council. 2023. Infographic – Fit for 55: Increasing the uptake of greener fuels in the aviation and maritime sectors. Available at: https://www.consilium.europa.eu/en/infographics/fit-for-55-refueleu-and-fueleu/. [Accessed: 13.12.2023].
[74] Advanced Energy Technology. 2020. Advanced CtL, GtL and BtL Facilities With Fischer-Tropsch System, and Patenting Activity in the World. Advanced Energy Technology. Available at: https://aenert.com/fileadmin/default/templates/images/Technologies/Unconventional_fossil_fuels/Synthetic_fuels/2021_Overview/22_fischer-tropsch-plants-map-2020_font_update.pdf. [Accessed: 7.8.2023].
[75] Parkes, R., 2023. Underestimated? Why solid-oxide electrolysers could be the dark horse of hydrogen industry. Hydrogeninsight. Available at: https://www.hydrogeninsight.com/electrolysers/underestimated-why-solid-oxide-electrolysers-could-be-the-dark-horse-of-the-hydrogen-industry/2-1-1452425. [Accessed: 30.6.2023].
[76] Sunfire. 2023. Renewable hydrogen project "Multiplhy": World's largest high-temperature electrolyzer from Sunfire successfully installed. Available at: https://www.sunfire.de/en/news/detail/renewable-hydrogen-project-multiplhy-worlds-largest-high-temperature-electrolyzer-from-sunfire-successfully-installed. [Accessed: 7.8.2023].
[77] Topsoe. 2023. Press Release - Topsoe celebrates Milestone in Construction of World's first Industrial Scale SOEC Electrolyzer Facility. Topsoe. Available at: https://www.arctictoday.com/arctic_business/topsoe-celebrates-milestone-in-construction-of-worlds-first-industrial-scale-soec-electrolyzer-facility/. [Accessed: 30.6.2023].
[78] Statista. 2023a. Electricity prices for non-household consumers in the European Union in 2022 by country. Available at: https://www.statista.com/statistics/1046605/non-household-electricity-prices-european-union-country/. [Accessed: 15.12.2023].
[79] Salary Expert. 2023. Chemical Plant Operator Average Base Salary. Available at: https://www.salaryexpert.com/salary/job/chemical-plant-operator/germany. [Accessed: 14.12.2023].